STRUCTURAL BASIS OF ANTIBODY BREADTH ELICITED BY COMPUTATIONALLY OPTIMIZED INFLUENZA VACCINES

by

KAITO NAGASHIMA

(Under the Direction of Jarrod Mousa)

ABSTRACT

Influenza A viruses (IAVs) pose a significant challenge worldwide, causing respiratory disease for 9 to 41 million individuals every year within the United States. The current seasonal vaccine targets the hemagglutinin (HA) glycoprotein to elicit an antibody response, and is the current countermeasure against this pathogen. However, the antibody response elicited by seasonal vaccination is only protective for a single season due to viral antigenic variation through mechanisms of antigenic drift and antigenic shift. Therefore, to expand antibody protection, a universal influenza vaccine called COBRA, for computationally optimized broadly reactive antigen, has been investigated. This approach combines wild-type HAs into a single COBRA HA immunogen through computational consensus building to expand antibody breadth to multiple strains.

Despite multiple reports showing the efficacy of the COBRA approach, the epitopes targeted by this vaccine have not been fully characterized in humans or animal models. This gap in knowledge could inform further vaccine optimization efforts to elicit antibodies against highly conserved epitopes. Therefore, to characterize this aspect of the COBRA approach, we evaluated the pre-existing monoclonal antibody (mAb) response to COBRA HA immunogens after seasonal

vaccination. We further assessed the epitopes targeted by adjuvanted and multimeric COBRA HA vaccination. Finally, we also defined the structural features of historic as well as lead COBRA vaccine candidates in the context of epitope elucidation. Through these studies, we found novel mAb epitopes which could then be used to characterize vaccine-elicited antibody breadth in animal models. In summary, this work provides a foundation to further advance the COBRA vaccine from an epitope-focused perspective.

INDEX WORDS: Influenza, COBRA, antibody, monoclonal antibody, mAb, epitope, hemagglutinin, vaccine

STRUCTURAL AND FUNCTIONAL CHARACTERIZATION OF ANTIBODIES TARGETING COMPUTATIONALLY OPTIMIZED INFLUENZA HEMAGGLUTININS

by

KAITO NAGASHIMA

B.S., University of Georgia

A Dissertation Submitted to the Graduate Faculty of The University of Georgia in Partial Fulfillment of the Requirements for the Degree

DOCTOR OF PHILOSOPHY

ATHENS, GEORGIA

2023

STRUCTURAL AND FUNCTIONAL CHARACTERIZATION OF ANTIBODIES TARGETING COMPUTATIONALLY OPTIMIZED BROADLY REACTIVE INFLUENZA HEMAGGLUTININS

by

KAITO NAGASHIMA

Major Professor:	Jarrod Mousa
Committee:	Mark Tompkins
	Daniela Rajao
	Eva Strauch
	Jeff Hogan

Electronic Version Approved:

Ron Walcott
Vice Provost for Graduate Education and Dean of the Graduate School
The University of Georgia
December 2023

ACKNOWLEDGEMENTS

I would like to thank, first and foremost, my mentor Dr. Jarrod Mousa for his supervision. His guidance has been immensely useful in my graduate career, and I would not have been able to complete this work without his support. I would also like to thank my committee members, Dr. Eva Strauch, Dr. Jeff Hogan, Dr. Mark Tompkins, and Dr. Daniela Rajao for advising me over the past several years.

I am also extremely thankful to everyone in the Mousa lab who I have been fortunate enough to meet during my Ph.D. program for troubleshooting and advice with experiments—Aaron Gingerich, Anna McCormick, Rose Miller, Nada Abbadi, Giobensky Vildor, Jiachen Huang, Ian Durie, Avik Banerjee, Lauren Mahoney, Fredejah Royer, and many others. I would also like to give a special thanks to my undergraduate mentees, Abigail Roegner and Ved Vyas, for their eagerness to learn about, and contribute to, the work presented here.

I also would like to thank my many collaborators for their many suggestions in sharing various materials and reagents, guiding the writing of manuscripts, as well as in sharing invaluable data and analyses. I would specifically like to acknowledge Dr. Rebecca DuBois, Dr. Andrew Ward, Dr. Thomas Edwards, Dr. Ted Ross, John Dzimianski, Julianna Han, Jan Abendroth, Meng Yang, Giuseppe Sautto, and Spencer Pierce.

Much of this work also could not have been completed without the support of many of the facilities at UGA and at other institutions. I would like to thank the Georgia Genomics and Bioinformatics Core (GGBC) and Dr. Magdy Alabady, Georgia Electron Microscopy (GEM) and Mary Ard, the CTEGD Flow Cytometry Core and Julie Nelson and Juan Bustamante, the Georgia

Advanced Computing Resource Center (GACRC) for access to a workstation for cryo-EM analysis, and University Research Animal Resources for their care of the research animals used in these projects.

I would also like to thank my undergraduate mentor, Dr. Biao He, and his lab for first introducing me to the bench and to the many opportunities in scientific research. I would also like to finally thank my family and friends for their unwavering support over the course of my Ph.D.

TABLE OF CONTENTS

Page

ACKNOWLEDGEMENTS iv

LIST OF TABLES ix

LIST OF FIGURES x

CHAPTER

1 INTRODUCTION 1

2 LITERATURE REVIEW 4

Abstract 5

Introduction 6

Humoral immune responses to influenza 7

Challenges with current seasonal vaccines 8

Alteration of glycosylation sites in HA immunogens 10

HA head-targeting vaccine designs 11

HA stem-targeting vaccine designs 13

Headless HA vaccines 13

Chimeric HA vaccines 14

HA head- and stem-targeting vaccine designs 16

Mosaic HA vaccines 16

Adjuvant effects on vaccine responses 17

Conclusions 23

3 CHARACTERIZATION OF PRE-EXISTING HUMAN ANTIBODIES AND B CELLS TO COMPUTATIONALLY OPTIMIZED HEMAGGLUTININS 28
Abstract 29
Introduction 30
Methods 33
Results 42
Discussion 49
4 ADJUVANT-DEPENDENT ANTIBODY RESPONSES TO A COMPUTATIONALLY OPTIMIZED HEMAGGLUTININ 63
Abstract 64
Introduction 65
Methods 67
Results 73
Discussion 78
5 ANTIBODY BREADTH MEDIATED BY NANOPARTICLE PRESENTATION OF COMPUTATIONALLY OPTIMIZED HEMAGGLUTININS 91
Abstract 92
Introduction 93
Methods 94
Results 99
Discussion 102
6 STRUCTURAL AND ANTIGENIC CHARACTERIZATION OF A COMPUTATIONALLY OPTIMIZED H1 SUBTYPE HEMAGGLUTININ 110

Abstract.....111
Introduction.....112
Methods.....114
Results.....124
Discussion.....131
7 STRUCTURAL CHARACTERIZATION OF A COMPUTATIONALLY OPTIMIZED H3 SUBTYPE HEMAGGLUTININ.....151
Abstract.....152
Introduction.....153
Methods.....155
Results.....157
Discussion.....161
8 SUMMARY.....170
REFERENCES.....174

LIST OF TABLES

Page

Table 3.1: mAb and B cell receptor V(D)J gene usage characteristics.....62

Table 6.S1: X6 X-ray crystallography data collection and refinement statistics.....144

Table 6.S2: CA09-26 Fab:X6 cryo-EM data collection and refinement statistics 145

Table 6.S3: #58 Fab:X6 cryo-EM data collection and refinement statistics.....146

Table 6.S4: BE1 Fab:X6 cryo-EM data collection and refinement statistics.....147

Table 6.S5: CR6261 Fab:X6 cryo-EM data collection and refinement statistics.....149

LIST OF FIGURES

Page

Figure 2.1: Antigenic sites and epitopes on H1 and H3 HAs 25

Figure 2.2: HA-based universal influenza vaccine designs 27

Figure 3.1: Binding titers of oligoclonal B cell supernatants pre-vaccination (d0) and 21 days post-vaccination (d21) from four representative subjects 53

Figure 3.2: Gene usage and CDR3 lengths of isolated mAbs 54

Figure 3.3: Models of H1 COBRAs used in this study 56

Figure 3.4: Reactivity and functional activities of mAbs isolated from 2017-2018 QIV-vaccinated subjects 57

Figure 3.5: Epitope binning identifies five epitopes from human antibodies isolated at 21 days post-vaccination 59

Figure 3.6: Structural characterization of P1-05 binding to Y2 COBRA 60

Figure 3.7: Sequence characteristics of Y2 COBRA-specific B cells from a human subject receiving the 2019-2020 seasonal vaccine 61

Figure 4.1: H1 HA immunization schedule and serum IgG titers after adjuvanted vaccination with Y2 and CA09 HAs 83

Figure 4.2: Th1/Th2 ELISAs at d56 after adjuvanted vaccination with Y2 and CA09 HAs 85

Figure 4.3: cH6/1 HA IgG titers at d56 after adjuvanted vaccination with Y2 and CA09 HAs 86

Figure 4.4: Epitope mapping of d56 sera against the CA09 HA from Y2- and CA09 HA-immunized mice 87

Figure 4.5: HAI titers of d56 sera against the CA09 HA from Y2- and CA09 HA-immunized mice 89

Figure 4.6: N1-I NA immunization schedule, serum IgG titers, and NAI titers after vaccination 90

Figure 5.1: Formulation and biochemical validation of the H1 subtype COBRA Y2 and H3 subtype COBRA NG2 on the I53_dn5 NP system 105

Figure 5.2: Mouse immunization studies to evaluate antibody breadth and reactivity from the Y2 and NG2 NP vaccination 106

Figure 5.3: Murine serum responses to the NP core scaffold following NG2 rHA, NG2 NP, and NP core vaccination after the prime-boost-boost regimen 108

Figure 5.4: Terminal HAI titers elicited by NP and rHA COBRA vaccination against a panel of H1N1 and H3N2 IAVs 109

Figure 6.1: Sequence and structural comparisons of wild-type HAs to X6 135

Figure 6.2: Crystal structure and glycosylation features of the X6 COBRA HA 136

Figure 6.3: Cryo-EM structures of HA RBS-binding antibody Fabs with X6 137

Figure 6.4: Cryo-EM structure of the HA lateral patch-binding antibody BE1 Fab with X6 138

Figure 6.5: Cryo-EM structure of the broadly reactive antibody CR6261 with X6 139

Figure 6.S1: Sequence alignment of X6 and wild-type pre-2009 and post-2009 HAs 140

Figure 6.S2: Binding and functional characteristics of serum from subject D160 and mAb #58 141

Figure 6.S3: Density fit of Fab:X6 complexes to cryo-EM maps 142

Figure 6.S4: Binding and HAI activities of BE1 and other X6-specific mAbs 143

Figure 7.1: Sequence comparison of the NG2 COBRA HA to wild-type H3 HAs 164

Figure 7.2: Cryo-EM structures of broadly HAI-active antibody Fabs with COBRA NG2 reveal an intact RBS 165

Figure 7.3: Cryo-EM structure of broadly reactive antibody TJ5-1 with NG2 reveals an intact stem 167

Figure 7.4: TJ5-1 can inhibit cleavage of NG2 HA0 as assessed by SDS-PAGE 169

CHAPTER 1

INTRODUCTION

Influenza A viruses (IAVs) cause significant burden both within the United States as well as worldwide every year due to annual epidemics and occasional pandemics. The current countermeasure against IAVs, the seasonal vaccine, targets the predominant surface glycoprotein, hemagglutinin (HA) to elicit an antibody response for H1 and H3 subtypes [1]. The seasonal vaccine provides only strain-specific protection [2] and is based on predictions of circulating strains [3]. The high rates of antigenic variation within IAVs obfuscate long-term protection mediated by seasonal vaccine antibodies, and vaccine strains may deviate from circulating strains, further limiting antibody-based protection. Therefore, a universal influenza vaccine candidate called COBRA, for computationally optimized broadly reactive antigen, has been developed to enhance antibody breadth to multiple influenza strains through a consensus layering approach of wild-type HAs to generate COBRA HA immunogens [4]. This approach has been validated in several animal models such as mice and ferrets, eliciting antibodies against several virus strains of a single subtype, thereby affording greater antibody breadth in comparison to the seasonal vaccine. However, whether the COBRA methodology might elicit broadly reactive antibodies and B cells in human populations has not been characterized, and aspects of vaccine and immunogen formulation on antibody breadth have yet to be explored. The structural correlates of the COBRA HA that drive the expanded antibody response also have not been characterized.

The scientific premise of this work is that broadly reactive epitopes of the influenza HA can be characterized and optimally targeted through studying the antibody response to COBRA

HAs, either through vaccination or with correlative studies using B cells and antibodies seasonally vaccinated human subjects. This work will characterize conserved and broadly neutralizing COBRA HA antibody epitopes, advancing the field through informing the optimal epitopes in COBRA vaccine design. The primary hypothesis is that antibody breadth depends on targeting of conserved HA epitopes by optimally formulated COBRA HA vaccines.

To evaluate this hypothesis, three aims are proposed:

Specific Aim 1: Determine the extent of pre-existing, functional antibody immunity to H1 subtype COBRA immunogens from seasonal vaccination. Most individuals possess pre-existing immunity to the influenza HA from seasonal vaccination. We hypothesize that there will be a COBRA-reactive population due to overlapping seasonal vaccine and COBRA vaccine epitopes. To determine if the B cell repertoire of these individuals possesses cross-reactivity to COBRA HA immunogens, reactivity and functionality of the antibody and B cell responses to these HAs after seasonal vaccination to these immunogens will be evaluated.

Specific Aim 2: Determine the role of adjuvant and antigen formulation on the breadth of COBRA-elicited antibodies. Adjuvants can alter the antibody response to wild-type HA vaccination, enhancing antibody breadth and changing the targeted epitopes [5]. This effect will be evaluated for the COBRA HA through assessing serum responses from mice who have been vaccinated with the COBRA HA when paired with four different adjuvants. We hypothesize that differentially expanded antibody breadth will be observed for the COBRA HA immunogen based on the use of different adjuvants.

Multimeric nanoparticle presentation of seasonal vaccine HAs can enhance B cell activation through cross-linking of B cell receptors and can select for conserved epitopes on non-seasonal vaccine subtype HAs [6]. Sera from vaccinated with COBRA-presenting nanoparticles

will be evaluated for reactivity and functional breadth to H1 and H3 IAV subtypes. The hypothesis for this sub-aim is that multimeric presentation of H1 and H3 COBRA HAs on homotypic nanoparticles can augment antibody breadth to non-vaccine subtypes.

Specific Aim 3: Determine the structural correlates of COBRA-induced antibody breadth. The HA possesses variable and conserved regions that can elicit strain-specific or broadly reactive antibodies. The COBRA methodology is expected to capture more conserved features across virus strains within an antigenic space, including monoclonal antibody (mAb) epitopes, which will be evaluated through cryo-electron microscopy (cryo-EM) and X-ray crystallography of mAbs obtained in Specific Aim 1. We hypothesize that COBRA HAs possess mAb epitopes that are intact on the immunodominant head domain and the immunosubdominant stem domain.

Altogether, these studies will inform the epitopes to COBRA HAs in seasonally vaccinated human populations, and will assess aspects of vaccine formulation in the context of eliciting an optimal antibody response. This work will provide structural insights for how COBRA HA vaccines may be further optimized to elicit a long-lived antibody response against IAV strains, improving the longevity of the response to influenza vaccination.

CHAPTER 2

LITERATURE REVIEW[1]

[1]A part of this chapter was accepted by *Viruses*. Reprinted here with the permission of the publisher. (This is an open-access article distributed under the terms of the Creative Commons Attributions License – CC BY). Nagashima, K.A.; Mousa, J.J. Next-Generation Influenza HA Immunogens and Adjuvants in Pursuit of a Broadly Protective Vaccine. *Viruses* **2021**, *13*, 546, doi:10.3390/v13040546.

Abstract

Influenza virus, a highly mutable respiratory pathogen, causes significant disease nearly every year. Current vaccines are designed to protect against circulating influenza strains of a given season. However, mismatches between vaccine strains and circulating strains, as well as inferior vaccine effectiveness in immunodeficient populations, represent major obstacles. In an effort to expand the breadth of protection elicited by influenza vaccination, the major surface glycoprotein, hemagglutinin (HA), has been modified to develop immunogens that display conserved regions from multiple viruses. These approaches, which target either the head or the stalk domain of HA, or both domains, have shown promise in recent preclinical and clinical studies. Furthermore, the role of adjuvants in bolstering the robustness of the humoral response has been studied, and their effects on the vaccine-elicited antibody repertoire are currently being investigated. This review will discuss the progress made in the universal influenza vaccine field with respect to influenza A viruses from the perspectives of both antigen and adjuvant, with the focus of broadly neutralizing antibody elicitation.

Introduction

Influenza virus is a major cause of respiratory disease, causing significant morbidity and mortality in the United States and across the globe. Influenza epidemics typically occur annually, with estimates attributing between 9.3 and 38 million illnesses, and between 140,000 and 810,000 hospitalizations in the United States to the disease each year [7]. Importantly, the detection incidence of influenza virus has diminished since the implementation of community mitigation strategies to prevent the spread of SARS-CoV-2, although external factors including viral interference may play a role [8]. Influenza virus is a negative-sense, segmented, single-stranded RNA virus of the family *Orthomyxoviridae*, and is categorized into four genera: A, B, C, and D [9]. The predominant influenza genera, influenza A and B, are further stratified into phylogenetic groups and lineages. Influenza A viruses (IAVs) are categorized into two broad groups based on the relative differences of the hemagglutinin protein (and the neuraminidase protein, NA): group 1 and group 2; group 1 consists of subtypes H1, H2, H5, H6, H8, H9, H11, H12, H13, H16, H17, and H18, and group 2 of subtypes H3, H4, H7, H10, H14, and H15 [10]. Influenza B viruses consist of virus strains of the Victoria and Yamagata lineages, which co-circulate and demonstrate plasticity in the HA and NA proteins due to immune pressure [11]. Vaccination is effective at reducing the incidence of influenza virus, but annual vaccination is required for inducing protection due to constant antigenic drift. In efforts to obviate the necessity for yearly vaccines, and to increase their effectiveness against circulating strains, several approaches towards 'universal' influenza vaccines, those that elicit an immune response against the majority of encountered influenza viruses, have been pursued. Furthermore, the mechanisms of adjuvants have garnered attention in an effort to improve the immune response induced by such influenza immunogens. In this review, hemagglutinin (HA)-based approaches to universal influenza

vaccines will be discussed, with a focus on influenza A viruses (IAVs) due to their higher diversity. Given that adjuvants have been recognized as a key component of influenza vaccines by conferring a robust immune response, a number of adjuvants under study will also be discussed.

Humoral immune responses to influenza

The humoral immune response to influenza infection and vaccination comprises an essential part of host defense. Antibodies targeting the two predominant viral surface glycoproteins, HA and neuraminidase (NA), neutralize influenza virus by inhibiting viral attachment/fusion and release, respectively. Moreover, hemagglutination/HA inhibiting (HAI) titers and NA inhibition (NAI) titers are important correlates of protection [12]. HA is responsible for viral attachment to sialylated host cell receptors, as well as entry through fusion with the endosomal membrane during the course of infection. The HA protein of human-tropic strains preferentially recognizes α(2,6)-linked sialic acid, while avian-tropic strains utilize α(2,3)-linked sialic acid [13]. Expression of α(2,3)-linked sialic acid differs across avian species [14]. Within a species, tissues within the respiratory and gastrointestinal tracts exhibit differential sialic acid expression that permit viral attachment [14]. Species with avian and human receptors, such as quail, turkey, and pigs, may permit host switching [14]. HA evolution mediates the adaptation of avian-origin strains to replicate in humans. The amino acid residues within the receptor-binding site (RBS) of HA favor either human or avian tropism. In H9N2 avian influenza virus (AIV) isolates, a glutamine at position 226 within the RBS is known to favor human-type α(2,6)-linked sialic acid receptors [15]. Furthermore, a non-RBS residue at position 190, which affects viral binding affinity to murine and human lung-expressed sialic acid, is implicated in the initial stages of viral replication [15].

The attachment and fusion functions of the HA glycoprotein are mediated by two domains: the globular head domain and the stem/stalk domain, respectively [13]. HA is cleaved from a HA0 precursor into the HA1 and HA2 subunits, which is required for membrane fusion activity [16]. During influenza attachment, the RBS of the head domain attaches to sialic acid receptors, followed by endosomal uptake of the virus particle [16]. Low pH within the endosome triggers membrane fusion, involving insertion of the fusion peptide into the endosomal membrane and uncoating of viral genome segments [16,17]. As the predominant surface glycoprotein, HA is targeted extensively by B cells; likewise, HA-specific antibodies predominate the humoral immune response. Whereas antibodies binding the RBS or other antigenic sites/epitopes in the immunodominant, variable head domain comprise most of the response, a subset of antibodies bind to the more conserved, albeit immunosubdominant, stalk domain [18,19]. The major epitopes on the HA head for the H1 subtype are the Sa, Sb, Ca1, Ca2, and Cb antigenic sites, which were determined through mutagenesis studies in the presence of anti-HA antibodies [20]. Similar work using competition assays was also performed for the H3 subtype to characterize antigenic sites A, B, C, D, and E [21–23]. These antigenic sites comprise the apical, membrane-distal region of the HA1 head domain, including the RBS, as well as the region near the head-stem interface [20–23] **(Figure 2.1)**.

Challenges with current seasonal vaccines

An individual's history of influenza exposure plays an essential role in the extent of protection to currently circulating viruses. The idea of original antigenic sin (OAS) posits that the initial exposure to a given strain imprints antibodies against certain epitopes that then dominate subsequent exposures to secondary strains [24]. Since the doctrine of OAS, related ideas of antigenic seniority and serological imprinting, where secondary exposures to antigenically drifted

strains generate novel antibodies, have been proposed [25,26]. Annual vaccination is required due to variation in circulating strains and the relatively short protective effects of the antibody response post-vaccination, particularly among older individuals and those with underlying medical conditions [27,28]. Trivalent or quadrivalent vaccines, which contain two influenza A viruses (IAVs): one H1N1, one H3N2, and one or two influenza B viruses (IBVs), exhibit roughly 50 to 60% vaccine coverage globally [28,29]. At present, seasonal vaccines are comprised of a combination of influenza virus strains that are predicted to be antigenically similar to those circulating at the time of vaccination [3]. As six months are typically needed from the selection of vaccine strains through vaccine production, release, and distribution, vaccine mismatch may occur due to the emergence of novel strains [29]. Moreover, differences in glycosylation between HA proteins in vaccines and those in circulating viruses can exacerbate vaccine mismatch [30,31]. Variation in the effectiveness of the current influenza vaccine can also be attributed to the rate at which influenza viruses undergo antigenic drift [32]. Antigenic drift results from the error-prone nature of the viral RNA-dependent RNA polymerase, resulting in the accumulation of mutations within the viral genome with successive rounds of replication [32].

Avian and swine transmission events also contribute to the emergence of novel viruses within the human population [32], and both natural and immune pressures on the HA select for drift variants [33]. In general, H1N1 viruses undergo antigenic drift to a lesser extent than H3N2 viruses, with approximately 2.45 amino acids substituted in the HA per year for H1N1 viruses, compared to 3.6 amino acid substitutions per year for H3N2 viruses, possibly due to the antigenically novel nature of the pandemic-like H1N1 virus [34,35]. Antigenic shift can result from reassortment events of HA genes between genome segments, such as between human and avian viruses [36]. Alternatively, zoonotic spillover events from antigenically exotic viruses can

also lead to antigenic shift [36]. The population to be immunized with the seasonal vaccine also plays a role in vaccine effectiveness and efficacy. For instance, vaccine uptake in immunocompromised and pediatric populations varies widely. For this population, adjuvanted vaccines containing MF59, and high-dose inactivated virus vaccines are available but nonetheless present an obstacle to vaccine-based protection [27,37]. To circumvent these issues, several HA-based vaccine designs have been developed and studied in pre-clinical studies and clinical trials **(Figure 2.2).**

Alteration of glycosylation sites in HA immunogens

It has been well-documented that glycosylation patterns in the HA immunogen can greatly alter the reactivity of antibodies. One study showed that the addition of glycosylation sites to the H5N1 virus A/duck/Niger/2090/2006 altered viral growth properties, enhancing viral diffusion due to reduced HA activity and enhanced NA activity, and also decreased neutralizing activity of sera from vaccinated mice, thereby contributing to immune escape [38]. Similarly, H1N1 subtype influenza virus containing a glycosylation site at position 144, corresponding to antigenic site Sa, effectively masked a highly targeted site by HAI antibodies in mice [39].

It could be inferred that such glycan masking of HA epitopes, as well as the presence of non-native glycosylation sites from egg-based vaccine production, could restrict the breadth of antibody protection. Likewise, removal of these glycans, either through enzymatic means or through the use of alternative cell culture systems, to generate less-glycosylated HAs could be effective in affording enhanced breadth of protection. Studies investigating this hypothesis have demonstrated success in achieving wider protection and cross-reactivity by utilizing monoglycosylated and alternatively deglycosylated HA immunogens [39–42]. Specifically, treatment of embryonated chicken eggs with kifunensine, an inhibitor of α-mannosidase I-

mediated glycosylation, in embryonated egg-based vaccine production, and virions with endoglycosidase H to trim their glycans to a monoglycosylated form, produced vaccines with superior HAI and neutralizing titers in mice [42]. Moreover, the same treatment afforded improved stem-specific antibody titers as well as antibody-dependent cellular cytotoxicity [42].

More subtle alterations to the glycosylation landscape of HA can alter the inter-group specificity and breadth of antibodies resulting from vaccination. Utilizing a stem nanoparticle vaccine, it was shown that the introduction of an glycosylation site at position 38 in the HA1 subunit in a group 1 stem to mimic a group 2-specific stem glycosylation site changed its antigenicity, preventing the binding of group 1-specific antibodies [43]. This alteration also mediated cross-group reactivity after assaying mice sera receiving this modified HA stem nanoparticle vaccine, with appreciable heterosubtypic neutralization against group 2 viruses and provided passive protection from a group 2 virus, A/Anhui/1/13 [43].

HA head-targeting vaccine designs

During the course of infection or vaccination, antibodies against the immunodominant globular head domain are predominantly elicited. Although the head is antigenically variable, there are nonetheless regions that remain fairly conserved; notably, cross-strain-, as well as cross-group-reactive antibodies targeting the receptor-binding site have been well-characterized [44]. Other conserved head epitopes have also been discovered, including the 'lateral patch' on the lower side of the head domain [45], as well as within the HA trimer interface [46–49]. Antibodies binding at the intratrimeric epitope are protective but non-neutralizing. It is thought that they elicit protection through Fc receptor- and complement-dependent mechanisms [46,49], as well as by dissociating the HA trimer [46,47]. Notably, an intratrimeric epitope has recently been discovered for another type I fusion protein, the human metapneumovirus fusion protein, and an antibody

targeting this epitope was neutralizing [50]. Recent strategies to target these head epitopes have gained traction and have primarily involved immunization with a 'consensus' HA immunogen representing multiple viruses from distinct antigenic spaces.

Computationally optimized broadly reactive antigens (COBRAs), which utilize merged sequences from divergent virus strains, represent promising vaccine candidates that are now in the late pre-clinical stage of development [51]. The COBRA platform is also highly amenable to several formulations, and protective effects have been noted for nanoparticle, live-attenuated, virus-like particle (VLP), and split-inactivated vaccines [52–54]. Each COBRA antigen represents a single viral subtype encompassing several time periods in multiple antigenic spaces using a layered consensus-building approach. Consequently, the resulting COBRA immunogens represent both the sequence and structural conformations of its constituent HAs [55]. For instance, H3N2-based COBRAs have been developed that retain the structural characteristics of its constituent sequences, including antigenic sites and glycosylation sequences [53]. Moreover, the period of time in which a set of HA sequences is selected for a given COBRA design alters the breadth of the resulting antibody response. For example, COBRAs representing a particular subset of H3N2 sequences between 1968 and 2013 were shown to elicit significantly broader HAI responses than for those where all H3N2 HAs from this period were represented [53].

A primary correlate of protection that COBRA vaccines aim to elicit is HAI activity from antibodies that bind the head domain. In this respect, COBRA vaccines have shown notable success, where leading COBRA antigens elicit significant HAI antibody titers. This has been shown for several subtypes, including H5N1 [4], H3N2 [53,54], and H1N1 [54] viruses, where such HAI antibodies likely provide protection. It is likely that COBRA vaccines target conserved regions within the head domain, and COBRA-reactive antibodies block HA attachment to sialic

acid receptors through binding the RBS and nearby epitopes. In a preimmune model where ferrets were pre-infected with historical H1N1 viruses, then immunized with a H1 COBRA VLP, stem antibodies did not consistently ameliorate viral replication following challenge with A/California/07/2009 [56]. This finding suggests that stem-based antibodies are not a major mode of the protective efficacy of this vaccine design. Similar findings were shown in H3N2-based COBRAs on the basis that neutralization and HAI titers correlated with one another well following vaccination [53].

HA stem-targeting vaccine designs

The stem domain of HA is highly conserved and has shown promise as an effective immunogen. Broadly reactive stem-binding antibodies are prevalent within human sera for group 1 viruses, and stem-targeting B cells can be expanded upon exposure to the antigen [57]. Furthermore, because of its relatively conserved nature, the stem epitope elicits broad, heterosubtypic antibody protection, even across diverse phylogenetic groups of influenza virus [58–60]. Since the discovery of the stem epitope, many groups have engineered a number of HA stem immunogens to redirect the antibody response away from the more variable head domain to this conserved region of HA. These include headless HAs that completely remove the head domain and chimeric HAs which replace the native head domain with an antigenically distant head from another influenza subtype.

Headless HA vaccines

Headless HA vaccines are comprised solely of the HA stem domain while lacking the globular head domain. Such vaccines overcome immunodominance of the head domain by retaining only the stem domain. Such vaccines were initially shown to be protective in mice, where a stem-truncated HA construct protected 70% of vaccinated mice from lethal challenge of H2N2

subtype virus A/Okuda/57 [61]. Further modifications to optimize and stabilize the immunogen through the inclusion of a linker between the N- and C-termini of the HA1 subunit, and incorporation into virus-like particles, were successful in reducing morbidity in challenged mice and conferring cross-reactivity to viral subtypes H1, H2, and H5 [62]. However, in the same study, mouse antibody responses were limited in their cross-reactivity to intra-group subtypes [62]. In another study, Tni insect cells were used to generate VLPs co-expressing headless HA and the influenza M1 protein from H1N1 PR8 [63]. Vaccination of mice in a prime-boost-boost regimen led to increased antibody-dependent cellular cytotoxicity (ADCC), lung and nasal IgG and IgA endpoint titers, and IgG-producing antibody-secreting cells (ASCs), suggesting that stem-binding antibodies were indeed being produced; however, the breadth of the immune response was not tested in this study [63].

Chimeric HA vaccines

Chimeric HAs (cHAs) utilize a similar approach in obscuring antibody responses to the HA head domain; however, in this strategy, an antigenically novel globular head domain from one IAV is grafted onto the stem domain of interest from another IAV subtype. Multiple immunizations with cHA constructs containing similar stems but distinct head domains restrict the elicitation of novel head-directed antibodies, focusing the response to conserved stem epitopes. The rationale behind cHAs is based on observations involving primary infection with one subtype of a group 1 or 2 virus, followed by a secondary infection with a different strain of the same group with a substantially distinct head domain [64]. Sera from patients that were seropositive with H3N2 showed significant increases in neutralizing activity against a cH7/3N3 influenza virus (with the H7 head and H3 stem) following infection, illustrating functional, neutralizing stem-directed antibodies against the conserved group 2 stem [64].

To further study the efficacy of the cHA approach, mice were primed with a cHA construct containing a H4 head and a H3 stalk (cH4/3 HA), followed by a first boost with a cH5/3 HA, then with cH7/3 HA, and then challenged with a heterologous H3N2 virus [65]. These animals were protected from mortality following challenge [65]. Similar experiments with initially sublethal infections of virus, followed by priming with similar chimeric constructs to simulate subclinical infections in humans, enhanced levels of broadly protective antibodies against heterosubtypic viruses [65]. Protection has been established using these cHAs in ferrets with group 1 viruses, as shown by stem-specific antibodies that confer heterologous and heterosubtypic protection [66]. Most recently, cHAs were approved for a phase I clinical trial, where participants were primed with live-attenuated or inactivated cH8/1N1 virus, then boosted with cH5/1N1 IIV [67]. Encouragingly, some potentially protective HAI and neutralizing antibodies appeared to be elicited, alongside broadly reactive, stalk-directed antibodies [67]. Interestingly, structural analysis of a cH5/1 cHA (containing a H5 head and a H1 stalk) showed that, compared to the native HAs of the constituent head and stem subtypes, the head of the cHA is misplaced on the stem by 60 degrees, while still retaining functionality in viral entry and antigenicity in the stem and head epitopes [68]. The fact that these properties are retained despite structural differences in the cHA conformation suggests that HA is relatively plastic and can accommodate such differences while retaining robust immunogenicity.

Chimeric HA immunogens have also been shown to be protective in mice when combined with stem-only immunogens. In an immunization regimen involving priming with a cH9/1 (containing a H9 subtype head and a H1 subtype stem) DNA vaccine, followed by two boosts with a PR8-based H1 headless HA, complete protection from homologous H1N1 virus and moderate protection from heterosubtypic H5N1 and H6N1 viruses were achieved [69]. Notably, headless

stem immunogens from this study did not appear to induce traditional neutralizing activity as the conformations of neutralizing epitopes differ from those of full-length HA [69]. To overcome this issue, 'mini-HAs' were engineered in a study based on the HA of the H1N1 A/Brisbane/59/2007 virus, now aiming to maintain its native trimeric conformation [70]. These constructs were quite immunogenic in mice, and the resulting antibodies bound the full-length HA of the homologous virus [70]. Moreover, these antibodies also showed virus-neutralizing activity unlike previous studies, as well as ADCC activity [70]. Non-human primate (NHP) models also showed neutralizing stem-directed antibodies following immunization with these constructs [70]. These antibodies also demonstrated broad cross-group binding and heterosubtypic neutralization [70]. Similar heterosubtypic protection has also been found in a nanoparticle-based platform, in a mechanism that may rely on Fc effector functions rather than neutralization [71].

HA head- and stem-targeting vaccine designs

Both neutralizing head-targeting antibodies and broadly reactive stem antibodies are likely necessary for an optimal immune response to influenza. Likewise, approaches that elicit both types of antibodies would be ideal in conferring robust protection.

Mosaic HA vaccines

Mosaic HAs (mHAs) utilize a HA immunogen that is a composite of several HA sequences. In one approach, the whole stem domain and head domain of one subtype is merged with the major antigenic sites of another subtype or genus to overcome strain-specific responses while retaining conserved and neutralizing epitopes [72,73]. In one study, mice were primed with the H4 subtype HA in a DNA vaccine, followed by two boosts, one with a mH10/3 HA, then a mH14/3 HA, comprising antigenic sites A through E of either the H10 or the H14 subtype, respectively, and the remaining head and stem residues from the H3 subtype [72]. When tested in mice, this approach

elicited antibodies with Fc-mediated effector functions targeting the stem domain, in addition to neutralizing, head-directed antibodies [72]. These results suggest that the mosaic HA approach can elicit both effective anti-head antibodies like those produced by the current vaccine, as well as broader anti-stalk antibodies similar to those produced from chimeric and headless HAs.

Another mosaic HA approach, utilizing an immunogen representing the H1 subtype from 1918 to 2018 viruses, employs combined sections of full-length HA sequences to generate a novel HA while retaining conformationally important features predicted to be necessary for antibody binding [74]. Originally derived from HIV vaccinology approaches to broaden the immune response against mismatched strains, this mosaic HA was effective in eliciting antibodies against divergent H1 strains [74,75]. One mosaic immunogen showed close sequence similarity with pre-pandemic strains, including A/Brisbane/59/2007 [74]. *In vivo* studies of vaccination using an Ad5-vectored antigen confirmed the presence of antibodies with broader HAI activity against pre-pandemic H1 viruses [74]. High antibody titers were detected by ELISA, but only a fraction of these had HAI activity, suggesting the presence of stalk antibodies [74]. Studies on the extent to which such stem antibodies are produced from mosaic HA immunization are warranted. Other groups utilized the same approach, showing its efficacy in eliciting neutralizing, homosubtypic protection through DNA and recombinant protein formulations, as well as heterologous protection in modified vaccinia Ankara (MVA) formulations, illustrating versatility in the formulation method while retaining protectiveness [76,77].

Adjuvant effects on vaccine responses

Adjuvants are commonly used in inactivated and recombinant vaccines to stimulate a more robust immune response akin to that of live-attenuated vaccines. Adjuvants also provide other beneficial effects, including antigen dose-sparing [78], the induction of a preferentially biased

immune response, and enhancing antigen immunogenicity [79]. Some currently licensed influenza vaccines already include adjuvants, such as MF59, a squalene-based oil-in-water emulsion, which is present in the Fluad vaccine aimed at individuals aged 65 and older; AS03, another oil-in-water adjuvant, is also used in licensed influenza vaccines in Europe, such as Pandemrix [79–81]. The ongoing discovery and design of several adjuvants, along with the elucidation of their mechanisms of action, are particularly relevant for the influenza vaccine where a robust humoral response is now known to be essential for protection. Adjuvants are especially useful for inducing robust antibody responses in high-risk populations, such as the elderly and those with pre-existing conditions such as HIV and obesity. Below we summarize the properties of commonly used adjuvants and their impacts on the influenza vaccine response.

Aluminum salts and alum: Alum, the oldest adjuvant in use, includes a range of aluminum salts such as aluminum hydroxide, and is also the most widely used adjuvant in humans. It is currently included in several vaccines, such as the DTaP and hepatitis A and B vaccines [81], and is known to provide a strong, Th2-skewed response characterized by IgG1 antibodies [82,83]. Moreover, HAI titers were significantly increased in its presence compared to no adjuvant during subcutaneous influenza immunization with subunit vaccine HA antigen [82]. Although alum induces a strong Th2-biased immune response and HAI titers, this may not necessarily correlate with virus clearance. In mice vaccinated with PR8 H1N1 whole inactivated virus (WIV), IgG1 antibodies increased while IgG2a antibodies decreased, typical of a Th2 response [83]. In addition, the lung viral titers in alum-adjuvanted WIV mice were nearly two logs higher than in WIV only-vaccinated mice [83]. This may illustrate the necessity of stimulating a less Th2-polarized, more mixed Th1/Th2, or Th1-polarized response to gain a more protective IgG1/IgG2a ratio that alum alone cannot provide, at least with a WIV subunit vaccine.

Oil-in-water emulsions: MF59 has been used in current influenza vaccines and elicits a broadly reactive B cell response, dependent in part on the induction of strong immune memory [84,85]. This adjuvant can stimulate both cellular and humoral responses, and when compared to alum, can induce similar, if not higher, HAI and antibody titers [82,86]. Furthermore, a major advantage of MF59 is in inducing a protective immune response from vaccination for at-risk populations, including young children and in the elderly, eliciting higher HA titers when adjuvanted [87–89]. The mechanism by which MF59 provides superior antibody protection has yet to be fully characterized, although one study suggested the elicitation of cross-reactive antibodies in a prime-boost regimen for H5N3 viruses [84]. In another study, the antibody repertoire in both adults and children was found to be diversified for those receiving a MF59-adjuvanted, inactivated 2009 pandemic vaccine compared to a non-adjuvanted control [90]. Serum antibodies binding the H1 HA1 subunit were significantly increased, had higher affinity, and correlated with higher virus neutralization in individuals vaccinated with the MF59-adjuvanted vaccine [90]. Interestingly, MF59 appeared to shift the pool of antibody epitopes towards the head domain, away from the HA2 stem domain, and also increased affinity maturation against a novel H5N1 strain following initial H1N1 exposure [90]. More recently, the role of antibody effector functions has been implicated in the mechanism of MF59. In one study, it was found to enhance complement deposition and neutrophil phagocytosis, but not antibody-dependent monocyte or NK cell effector functions, suggesting a more complex role of Fc receptors and complement beyond the traditionally accepted roles of Fcγ receptors [91].

AS03, a similar squalene-based adjuvant, has been used in current influenza vaccines for its capacity to produce high antibody titers and increase breadth of protection [92]. Similar to MF59, AS03-adjuvanted animals receiving a split-inactivated H5N1 vaccine produced high levels

of neutralizing antibodies against homologous and heterologous H5N1 viruses in ferrets [93]. Individuals receiving TIV followed by AS03-adjuvanted pandemic H1N1 (pH1N1) HA showed enrichment for plasma cells with mutated BCRs that cross-react with pH1N1 HA; furthermore, naïve B cells were also more strongly activated when adjuvanted, and had increased isotype switching to IgG1 and IgG3 [94]. Adjuvanted vaccines also altered the proportion of V gene alleles that were utilized and mutated in BCRs; notably, mutations in the *V_H1-69* allele, associated with stem-binding antibodies, comprised a higher part of the total repertoire when the pandemic vaccine was adjuvanted with AS03 [94]. Although these results suggest a similar mechanism of AS03 to that of MF59, further studies to confirm correlations between BCR sequences and antibody epitopes are warranted. Also similar to MF59, AS03 appeared to play some role in stimulating complement-dependent lysis (CDL) for individuals receiving the 2009 pandemic H1N1 vaccine [95]. Furthermore, this CDL activity extended to a small extent to a heterologous, pre-pandemic influenza virus strain [95].

TLR agonists: Toll-like receptors (TLRs) are proteins present ubiquitously on external and internal membranes of certain immune cells, including B cells, and recognize pathogen-associated molecular patterns (PAMPs). Downstream signaling pathways transduce ligand binding, producing immune activation phenotypes that can be modulated based on the ligand (and thereby the TLR) [96]. A number of TLR agonists have been engineered for potential use in influenza vaccines. One such TLR agonist, 3M-052, an imidazoquinoline that binds TLR7/8, has been shown to broaden the antibody response in pandemic H5N1 HA antigen vaccination in ferret and mouse models [97]. This adjuvant provided protection from homologous and heterologous drifted strains, which may be due to an increase in V gene diversity that was previously observed for co-administration of the adjuvant with malarial antigen [97]. Further studies are necessary to

determine whether heterosubtypic neutralization is observed. In another study, the A/California/7/2009 HA globular head domain was fused to bacterial flagellin, a TLR5 agonist [98]. Increases in HAI titer and seroconversion were seen for both young (18-49 years old) and old (65 years or older) populations, showing appreciable seroprotection and seroconversion in the older population [98]. The fact that a robust immune response was elicited in older individuals may be attributed to the innate stimulation of TLR5 by the flagellin component/adjuvant of the vaccine antigen, showing a proof-of-principle where antigen and adjuvant are covalently linked. Other TLR agonists target TLR9, which is specific for DNA analogs, predominantly CpG. When CpG was conjugated to nanoparticles comprising the A/New Caledonia/20/1999 HA, ELISA binding and HAI titers were significantly increased, higher than when CpG was mixed with HA nanoparticles [99]. Another notable TLR9 agonist, CpG 1018, formulated by Dynavax Technologies, was recently shown to elicit neutralizing antibodies against SARS-CoV-2 when paired with the pre-fusion spike protein and alum, eliciting a Th1-type response [100], and has also been approved for use in a hepatitis B virus VLP vaccine (HEPLISAV-B) [100]. This CpG agonist in the influenza vaccine may be useful in amplifying similar neutralization-based protection.

Advax: Advax has shown promising safety when used in split-virion and recombinant influenza vaccines [101,102]. As a delta inulin microparticle-based polysaccharide adjuvant, Advax is comprised of 1-2 μm particles, and has also been investigated for intranasal vaccinations and as a mucosal adjuvant [103]. Immunization of mice with whole-inactivated virus (WIV) and Advax adjuvant increased lung IgG antibody titers, as well as IgG and IgA antibody-secreting cell (ASC) populations compared to the non-adjuvanted group; Advax also increased the memory B cell response [103]. A single high dose of Advax has been shown to improve B cell responses in

neonatal mice, leading to increased class-switching from the IgM to the IgG1 isotype following vaccination with inactivated H1N1 and Advax [104]. Therefore, Advax may be an effective adjuvant to include in pediatric populations that receive the influenza vaccine to improve memory and class-switching responses for inactivated formulations. Whether the adaptive response to an Advax-adjuvanted vaccine is Th2- or Th1-biased appears to depend on the antigen used, where the split-inactivated vaccine and Advax induces a Th2-type response, whereas WIV and Advax induces a Th1-type response [105].

Iscomatrix: Iscomatrix adjuvant consists of cage-like structures made of phospholipid, saponin, and cholesterol; these structures promote a balanced Th1/Th2 response and antigen trafficking into the lymph nodes, as well as the production of intracellular antigen depots within dendritic cells for sustained presentation [106]. When used with H7N9 VLPs to immunize mice, homologous protection from a lethal challenge was achieved, in addition to protective HAI titers against both homologous H7N9 and heterologous H7N3 [107]. Similar to the MF59 adjuvant, epitope spreading with higher-affinity antibodies against the HA1 subunit was also observed for individuals receiving a H7N9 VLP vaccine with Iscomatrix adjuvant, possibly resulting from increased germinal center reactions of HA-specific T cells with B cells [108]. The interaction of T and B cells may drive increased receptor affinity as well as novel stimulation of clones reactive against HA1 [108]. Furthermore, the off-rates of antibodies binding HA1 were significantly lower when the VLP vaccine was adjuvanted, and a negative correlation was seen between the heterologous binding activities of serum antibodies to vaccine strain H7 HA1 and the neutralizing titers to a heterologous H7 virus [108].

Conclusions

HA head- and stem-directed vaccine designs are currently under investigation to improve upon current influenza vaccines. Despite the variability of influenza virus, conserved epitopes have nonetheless been identified through antibody epitope analysis. The COBRA approach has proven the ability to elicit potent antibodies with HAI and neutralizing activities that target a diverse number of epitopes on the globular head domain. This consensus layering approach aims to target sequences that will be present in future pandemic and seasonal HA sequences. In contrast, stem-directed designs have shown success in narrowing the antibody response to the relatively conserved stem domain, now having elicited stem antibodies in a phase I trial utilizing the chimeric HA approach. Headless HA designs have also been refined greatly, preserving the natural conformation of native HAs and its associated epitopes. Mosaic vaccines appear to elicit antibodies against both the HA head and stem domains, potentially optimizing the antibody response to maintain a neutralizing and broadened epitope repertoire. Further studies into the impact of pre-existing immunity in these vaccine approaches may inform the role of original antigenic sin in adopting a universal influenza vaccine. Considering that vaccine immunogen design efforts have been historically biased towards HA, recent studies into next-generation NA immunogens, the more conserved surface glycoprotein, have also shown promise, and optimal, broad protection may only be achieved through combination of next-generation HA immunogens and next-generation NA immunogens [109–111]. Adjuvants that have also been employed for use in current and next-generation influenza vaccines, such as alum, AS03, and MF59, and more novel systems like TLR agonists, Advax, and Iscomatrix, are only now beginning to be understood for how they might alter the antibody response. The discovery that they broaden the antibody repertoire may be key to optimizing the elicitation of broadly neutralizing antibodies during vaccination, and further

studies to illuminate this aspect are certainly needed. Overall, continued studies into these two components will be essential to develop a universal influenza vaccine.

Figures

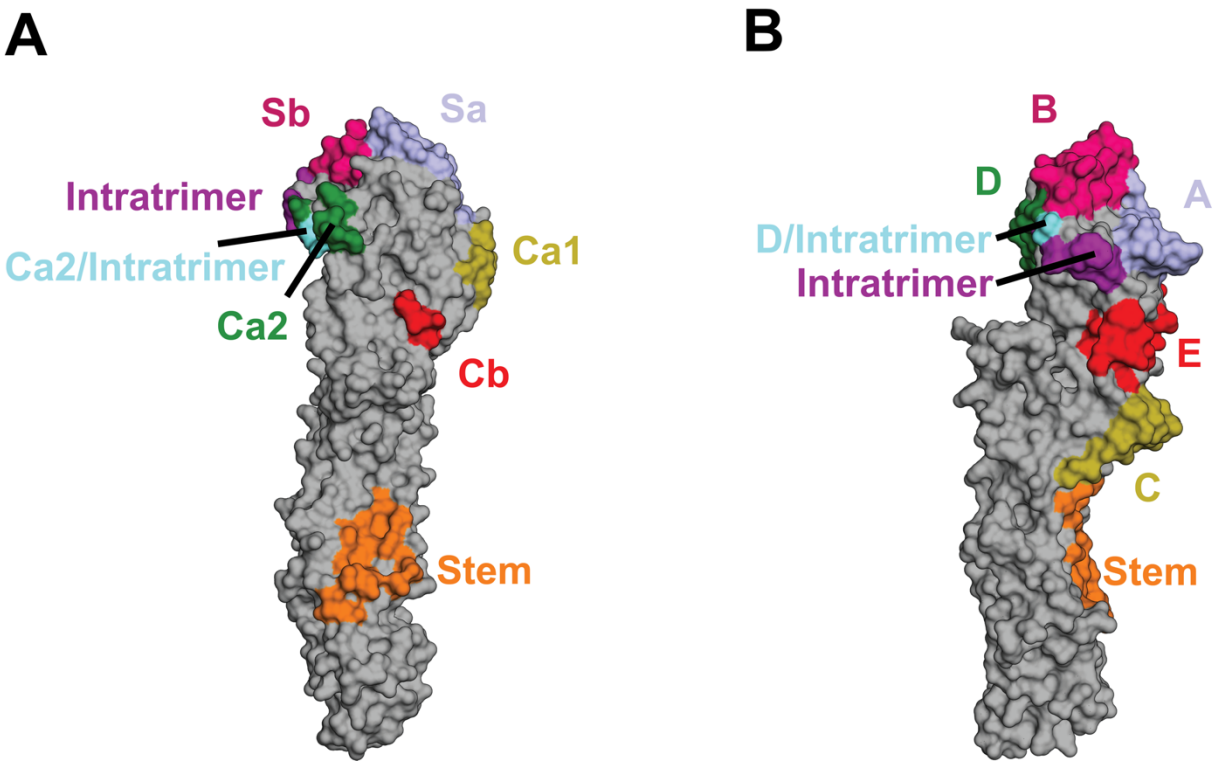

Figure 2.1. Antigenic sites and epitopes on H1 and H3 HAs. (A) H1 antigenic sites and antibody epitopes labeled on the A/California/04/2009 HA (gray). Antigenic sites Sa (light blue), Sb (magenta), Ca1 (dark yellow), Ca2 (green), and Cb (red) are located on the globular head domain. The intratrimer epitope, represented by the FluA-20 antibody epitope (purple), is present on the interface between HA protomers in the trimer. Residues overlapping the intratrimer epitope and the Ca2 antigenic site are in sky blue. Sa, Sb, and Ca2 comprise the periphery of the RBS. The epitope of a H1 stem-reactive antibody, CR6261, is shown in orange. (B) H3 antigenic sites and antibody epitopes on the A/Hong Kong/1/1968 HA (gray). Antigenic sites A (light blue), B (magenta), C (dark yellow), D (green), and E (red) are present on the head, as is the intratrimer epitope (purple), shown as the epitope of FluA-20. Residues in both antigenic site D and the

intratrimer epitope are shown in sky blue. Antigenic sites A, B, and D comprise the receptor-binding site. The epitope of a stem antibody reactive to H3 viruses, CR9114, is labeled in orange. A/California/04/2009 HA taken from PDB structure 5GJS. A/Hong Kong/1/1968 HA taken from PDB structure 4FQY. Epitopes were labeled based on the interacting residues of monoclonal antibodies (mAbs) CR6261, CR9114, and FluA-20 with HA.

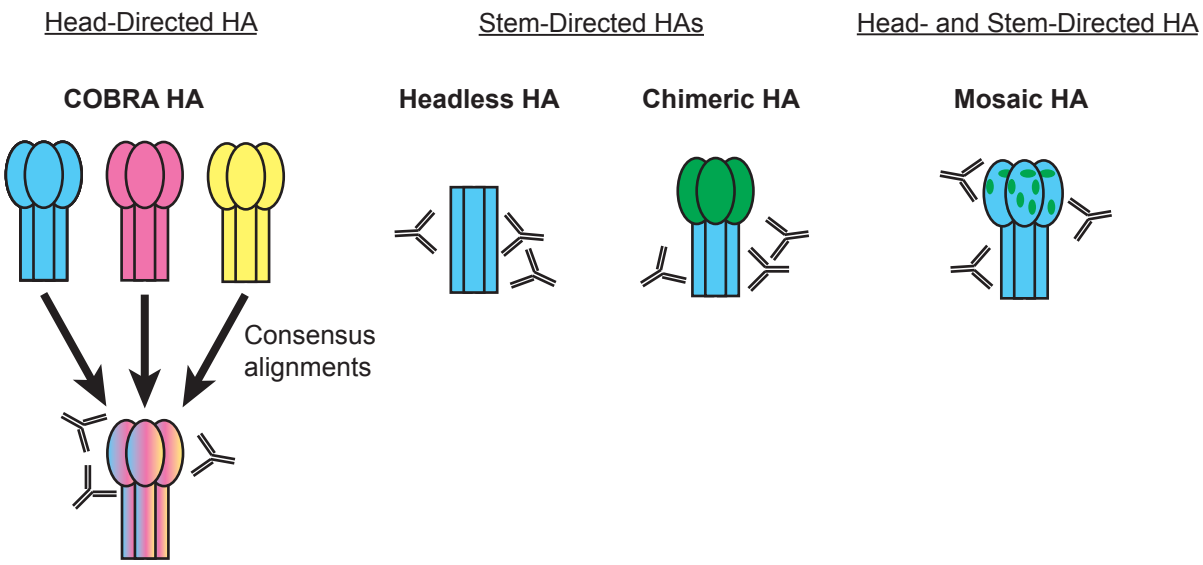

Figure 2.2. HA-based universal influenza vaccine designs. COBRA (computationally optimized broadly reactive antigen)-based HAs are head-focused HA immunogens incorporating multiple sequences (shown in HAs of different colors) of a particular subtype into a consensus HA (shown as a HA of multiple colors) that elicit mainly head-targeting antibodies. Headless HAs lack the globular head domain and are comprised solely of the stem domain to focus antibody responses to the otherwise immunosubdominant, but conserved, stem. Chimeric HAs (cHAs) consist of the globular head domain of one subtype (shown in green) and the stem domain of another subtype (shown in cyan) to be targeted, more closely mimicking a native HA molecule while focusing antibody responses to the conserved stem through exposure to multiple cHA immunogens. Mosaic HAs (mHAs), which can be seen as a refinement of cHAs, consist of the majority of the head domain and the entire stem domain of one subtype (shown as a blue HA trimer), but the head antigenic sites of another subtype (shown as green regions in the HA head), eliciting both head- and stem-directed antibodies.

CHAPTER 3

CHARACTERIZATION OF PRE-EXISTING HUMAN ANTIBODIES AND B CELLS TO COMPUTATIONALLY OPTIMIZED HEMAGGLUTININS[2]

[2]A part of this chapter was accepted by *The Journal of Immunology*. Reprinted here with the permission of the publisher.
Nagashima, K.; Dzimianski, J. V.; Han, J.; Abbadi, N.; Gingerich, A.D.; Royer, F.; O'Rourke, S.; Sautto, G.A.; Ross, T.M.; Ward, A.B.; et al. The Pre-Existing Human Antibody Repertoire to Computationally Optimized Influenza H1 Hemagglutinin Vaccines. *J. Immunol.* **2022**, *209*, 5–15, doi:10.4049/jimmunol.2101171.

Abstract

Computationally optimized broadly reactive antigen (COBRA) hemagglutinin (HA) immunogens have previously been generated for several influenza subtypes to improve vaccine-elicited antibody breadth. As nearly all individuals have pre-existing immunity to influenza viruses, influenza-specific memory B cells will likely be recalled upon COBRA HA vaccination. We determined the epitope specificity and repertoire characteristics of pre-existing human B cells to H1 COBRA HA antigens. Cross-reactivity between wild type HA and H1 COBRA HA proteins P1, X6, and Y2 were observed for isolated monoclonal antibodies (mAbs). The mAbs bound five distinct epitopes on the pandemic A/California/04/2009 HA head and stem domains, and the majority of the mAbs had HAI and neutralizing activity against 2009 pandemic H1 strains. Two head-directed mAbs, CA09-26 and CA09-45, had HAI and neutralizing activity against a pre-pandemic H1 strain. One mAb, P1-05, targeted the stem region of H1 HA, but did not compete with a known stem-targeting H1 mAb. We determined that mAb P1-05 recognizes a recently discovered HA epitope, the anchor epitope, and we identified similar mAbs using B cell repertoire sequencing. In addition, the trimerization domain distance from HA was critical to recognition of this epitope by mAb P1-05, suggesting the importance of protein design for vaccine formulations. Overall, these data indicate that seasonally vaccinated individuals possess a population of functional H1 COBRA HA-reactive B cells that target head, central stalk, and anchor epitopes, and demonstrate the importance of structure-based assessment of subunit protein vaccine candidates to ensure accessibility of optimal protein epitopes.

Introduction

Influenza viruses are a major cause of morbidity and mortality worldwide each year [112]. In particular, influenza A viruses (IAVs) and influenza B viruses cause annual epidemics in humans, and IAVs have caused multiple pandemics over the past century [113]. Currently, H1N1 and H3N2 IAVs cause epidemic disease [114,115]. Long-term protection to influenza viruses remains a challenge due to high mutation rates caused by a low-fidelity RNA polymerase, which leads to antigenic drift, as well as reassortment events of HA and NA with avian influenza viruses, which is termed antigenic shift [116]. Current seasonal influenza vaccines provide protection against matched circulating viral strains. However, vaccine efficacy varies year to year due to mismatches between circulating strains and vaccine strains, as well as differences in hemagglutinin (HA) protein glycosylation patterns between vaccine and circulating strains [29–31]. This variability in vaccine efficacy highlights the importance of developing an improved influenza vaccine, which would elicit an immune response to most circulating influenza A and/or B viruses [117]. Current vaccines typically elicit strain-specific antibodies, and only a minority show cross-reactivity to other viral subtypes. The antibody response to influenza virus infection and vaccination focuses predominantly on HA. Within HA-targeting antibodies, those targeting the variable globular head domain dominate the response, whereas those that bind the more conserved stem domain are elicited less frequently [19].

H1N1 IAVs have caused two known pandemics, including the Spanish influenza pandemic of 1918-1919, which caused an estimated 40-50 million deaths, and the 2009 swine influenza pandemic, which caused an estimated 575,000 deaths [118]. Circulating 2009 pandemic pH1N1/09-like viruses have replaced pre-2009 seasonal H1N1 influenza viruses in the human population [118]. Antigenic sites defined on the H1 subtype HA have been characterized through

mutagenesis studies in the presence of neutralizing antibodies [20]. These highly variable sites are present on the immunodominant head domain, and include the Sa, Sb, Ca1, Ca2, and Cb sites [20]. More recently discovered antibody epitopes include the receptor-binding site (RBS), the lateral patch, and the intratrimeric epitope, which exhibit broader reactivities [45,49,117,119].

Computationally optimized broadly reactive antigen (COBRA) HA immunogens aim to elicit a broader antibody response compared to current seasonal vaccines [52,54]. In this approach, multiple-layered consensus building alignments of HA sequences are used to generate an immunogen encompassing multiple epitopes for a single subtype [54]. The resulting constellation of consensus epitopes, focused primarily in the antigenic sites of the head domain, represent diverse sequences that elicit broadly reactive antibodies in several animal models, including in mice and ferrets [52,54]. Structural analysis of COBRA HA immunogens has shown that these antigens resemble wild type HA proteins [55]. The primary mechanism of COBRA HA-induced antibodies are through hemagglutination inhibition (HAI) and neutralization via HA head domain-binding antibodies [54]. In contrast, stem-directed antibodies do not appear to be a major component of COBRA HA vaccine-induced immunity [56,120]. Some H1 subtype-based COBRA HAs have been previously described that incorporate both seasonal (pre-2009) and pandemic-like (post-2009) influenza virus HA sequences. These include P1, which incorporates human sequences from 1933 to 1957 and 2009 to 2011 as well as swine sequences from 1931 to 1998, and X6, which incorporates human sequences from 1999 to 2012 [121]. The Y2 COBRA HA, encompassing sequences from 2014 to 2016, represents the most recent set of H1 subtype viruses that are antigenically similar to the 2009 pandemic H1N1 virus. Importantly, the Y2 COBRA HA has been shown previously to elicit broadly HAI-active antibodies against recent 2018 and 2019 H1N1

pandemic-like viruses in a mouse model, whereas the P1 and X6 COBRA HAs elicit a less broad response against these isolates [122].

An individual's immune history to influenza also plays a major role in the antibody response to vaccination. For example, the idea of original antigenic sin (OAS) describes the dominant nature of the antibody response to the first influenza virus strain compared to exposures to subsequent strains [24]. While COBRA HAs have been shown to be efficacious in naïve as well as pre-immune mouse and ferret models of influenza infection, pre-existing immunity to COBRA HAs in humans has not been investigated. This is important to understand as these antigens move toward clinical trials. Here, we identify epitope and repertoire characteristics of the pre-existing antibody response from previous infection and vaccination that is recognized by H1 COBRA HA antigens. We show that human antibodies and B cells that cross-react with COBRA HAs, predominantly with the Y2 COBRA HA and a minority with the P1 and X6 COBRA HAs, are present in individuals vaccinated with the 2017-2018 and 2019-2020 quadrivalent influenza vaccine (QIV). A panel of 26 monoclonal antibodies (mAbs) was isolated, and these mAbs bind five distinct epitopes on the A/California/04/2009 HA protein, including an epitope near the viral membrane, termed the anchor epitope. Moreover, a subset of these antibodies bind both pre- and post-2009 pandemic strains with demonstrable HAI and neutralization activity. Overall, our data identify the major epitopes and repertoire characteristics of pre-existing human antibodies that recognize COBRA HA antigens.

Methods

Human subject samples

All human studies were approved by the University of Georgia Institutional Review Board. mAb isolation was conducted from subjects aged 22 to 51 years vaccinated with the 2017-2018 seasonal influenza vaccine (Fluzone) from peripheral blood mononuclear cells (PBMCs) isolated from blood draws 21-28 days following vaccination. 80% (4/5) of these subjects showed HAI titers >40 to at least one pre-2009 H1 virus before vaccination. Repertoire sequencing was completed from a single human subject vaccinated with the 2019-2020 influenza vaccine (Fluzone) from blood obtained 28 days following vaccination.

B cell expansion of human subject PBMCs

PBMCs were plated at a density of 25,000 cells/well in a 96-well plate on a layer of gamma-irradiated NIH 3T3 cells (20,000 cells/well) expressing hCD40L, hIL-21, and hBAFF in the presence of CpG and cyclosporine A as previously described [50,123]. B cell supernatants were screened by enzyme-linked immunosorbent assay (ELISA) at 7 days post-plating of PBMCs.

Expression and purification of recombinant influenza HA proteins

Trimeric wild-type HA or COBRA HA ectodomains were expressed and purified in Expi293F cells following the manufacturer's protocol and as previously described [124]. Collected supernatants containing the HA antigens were purified on a HisTrap Excel column following the manufacturer's recommended protocol. Eluted fractions were pooled and purified proteins were verified for integrity by probing with an anti-HIS tag antibody (Biolegend) as well as with subtype-specific mAbs via SDS-PAGE and Western blot.

ELISA screening of B cells, hybridoma supernatants, mAbs, and rAbs

Untreated 384-well plates (VWR) were coated with recombinant HA proteins diluted to 2 μg/mL in PBS at 4 °C overnight. Plates were washed once with water, then blocked with 2% blocking buffer (PBS + 2% non-fat dry milk (Bio-Rad) + 2% goat serum + 0.05% Tween-20) for 1 hr at room temperature. Plates were washed three times with water, and 25 μL of B cell supernatants, hybridoma supernatants, mAbs, or recombinant antibodies (rAbs) were added. mAbs and rAbs were serially diluted three-fold in PBS from 20 μg/mL prior to addition for twelve total dilutions. Plates were incubated at 37 °C for 1 hr, then washed three times with water. Goat anti-human IgG Fc-AP secondary antibody (Southern Biotech), diluted 1:4000 in 1% blocking buffer (1:1 dilution of PBS and 2% blocking buffer), was added and plates were incubated at room temperature for 1 hr. Plates were then washed five times with PBS-T (PBS + 0.05% Tween-20). *p*-Nitrophenyl phosphate (PNPP) substrate, diluted in substrate buffer (1.0 M Tris + 0.5 mM $MgCl_2$, pH=9.8) to 1 mg/mL, was added, and plates were incubated for 1 hr and read at 405 nm on a BioTek plate reader. To quantify HA-reactive IgG from each subject, plates were coated overnight with eight two-fold serial dilutions of human plasma IgG standard (Athens Biotechnology) starting at 10 μg/mL. All steps were followed as for antigen, except PBS was used in the primary antibody step. GraphPad Prism was used to interpolate antigen-reactive IgGs from the human plasma IgG standard curve. The EC_{50} value for each mAb was determined by using the four-parameter logistic curve fitting function in GraphPad Prism software.

Generation of HA-reactive mAbs

Eight days following plating of PBMCs, wells identified to contain positive B cells by ELISA were selected for electrofusion to generate hybridomas as previously described [50,123]. Hybridomas were plated in 384-well plates for HAT selection, and grown for 14 days at 37°C, 5%

CO_2. Following screening by ELISA, hybridomas were single-cell sorted using a MoFlo Astrios cell sorter using live/dead staining by propidium iodide. The sorted hybridomas were cultured in 25% Media E (StemCell) + 75% Media A (StemCell) for two weeks, then subjected to another round of screening by ELISA. Hybridomas with the highest signal were grown in 250 mL serum-free media (Gibco) for approximately one month. Secreted mAbs were purified using a Protein G column (GE Healthcare) and concentrated for use in downstream assays.

Hybridoma sequencing

Hybridoma cell lines encoding each mAb were sequenced utilizing the primers described by Guthmiller *et al.* [125]. Briefly, RNA was extracted from each hybridoma and cDNA was generated using the SuperScript IV First-Strand cDNA Synthesis Kit (Invitrogen). A nested PCR protocol was used to generate sequencing products. In the first nested PCR step, a primer mix specific to the heavy, kappa, or lambda chain *V* gene and the constant region were used to amplify the variable region using the cDNA as template. In the second PCR step, the first PCR product was used as a template with a nested primer mix to improve product specificity and yield. The second nested PCR products were sequenced using the constant region primer and the *V, D,* and *J* alleles were identified by IMGT/V-QUEST [126]. Percent identity of mAb variable regions to germline were calculated as the similarity to the germline allele at the nucleotide level using IMGT/V-QUEST [126].

Hemagglutination inhibition assay

The HAI titer for each mAb was determined as previously described [120]. Influenza viruses were titered to eight HAUs (hemagglutination units). 50 μL of mAbs or rAbs diluted to 20 μg/mL in PBS were added to the first well of a 96-well U-bottom plate (VWR), and diluted two-fold in PBS for 25 μL mAb total per dilution. Eight HAUs of virus were added in a 1:1 ratio to

each mAb dilution, and each well was mixed and incubated for 20 min at room temperature. Following this, 50 μL of 1.0% turkey red blood cells (Lampire) were added per well. Plates were read 45 min after the addition of 1.0% turkey red blood cells.

Focal reduction assay

Focal reduction assays (FRAs) were completed for each mAb as previously described [120]. MDCK cells were plated in 96-well plates overnight to achieve >95% confluency the next day. Cells were washed twice with PBS, and 50 μL of virus growth media (VGM: DMEM + 2 μg/mL TPCK-trypsin + 7.5% BSA) were added and the plates were returned to the incubator at 37°C, 5% CO_2. mAbs at 20, 8, or 1 μg/mL were serially diluted two-fold in VGM, and virus was diluted to a concentration of $1.2x10^4$ FFU/mL in VGM. MDCK cells were washed with PBS and 25 μL serially diluted mAbs were added, followed by 25 μL of $1.2x10^4$ FFU/mL of virus. Plates were incubated at 37 °C, 5% CO_2 for 2 hr, and then 100 μL/well of overlay media (1.2% Avicel + modified Eagle media (MEM)) were added and incubated overnight. The overlay was removed and wells were washed twice with PBS. Ice-cold fixative (20% formaldehyde + 80% methanol) was added and plates were incubated at 4 °C for 30 min. Plates were washed twice with PBS and permeabilization buffer (PBS + 0.15% glycine + 0.5% Triton-X 100) was added, followed by a 30 min incubation. Plates were washed three times with PBS-T and primary IAV anti-NP mouse antibody (IRR), diluted 1:2000 in ELISA buffer (PBS + 10% goat serum + 0.1% Tween-20), was added. Plates were incubated at room temperature for 1 hr. Plates were then washed three times with PBS-T and secondary goat anti-mouse IgG-HRP antibody (Southern Biotech), diluted 1:4000 in ELISA buffer, was added. Plates were incubated at room temperature for 1 hr and then washed with PBS-T. KPL TrueBlue Peroxidase substrate was added per well and plates were incubated for 10-20 min. Plates were washed, dried, and foci were enumerated using an ImmunoSpot S6

ULTIMATE reader with ImmunoSpot 7.0.28.5 software (Cellular Technology Limited). Neutralizing IC_{50}s were calculated using the GraphPad Prism four-parameter logistic curve fitting function.

Epitope binning by biolayer interferometry

The panel of mAbs isolated from human subjects were competed for binding using the A/California/04/2009 HA protein on the OctetRED384 system as previously described [123]. Anti-penta-HIS biosensors (Sartorius) were immersed in kinetics buffer (PBS + 0.5% BSA + 0.05% Tween-20) for 60 s to obtain a baseline reading. Biosensors were then loaded with 100 μg/mL of A/California/04/2009 HA protein diluted in kinetics buffer for 60 secs. Biosensors were returned to kinetics buffer for a baseline of 60 s. Following this, biosensors were immersed in the first mAb (100 μg/mL in kinetics buffer) for 300 s for the association step. The biosensors were then immersed in the competing, second mAb (100 μg/mL in kinetics buffer) for 300 s. The biosensors were then regenerated in 0.1 M glycine, pH = 2.7 and PBS alternately for three cycles before proceeding to the next mAb competition set. The extent of competition was calculated as the percentage of the signal from the second mAb in the second association step in the presence of the first mAb to that of the second mAb alone in the first association step for all biosensors. A ratio of <=33% was considered complete competition, >33 and <=67% moderate competition, and >67% no competition.

Antibody-dependent phagocytic activity of mAbs

To measure antibody-dependent phagocytic activity, 2×10^9 1-μm Neutravidin-coated yellow-green FluoSpheres (Invitrogen #F8776) were resuspended in 1 mL of 0.1% PBS. The FluoSpheres were then centrifuged at 5000 rpm for 15 minutes, 900 μL supernatant was removed, and the FluoSpheres were resuspended with 900 μL of 0.1% PBS. This process was repeated for

a second wash, then the FluoSpheres were resuspended with 20 µg of biotinylated Y2 protein. The FluoSpheres were then incubated overnight at 4 °C, protected from light, with end-to-end rocking. Next, HA-specific antibodies were diluted in complete RPMI media (cRPMI, RPMI + 10% FBS) to a final concentration of 1 µg/mL in a U-bottom 96-well plate. Then, 20 µL of antibody dilution was transferred into a clean F-bottom 96-well plate, and 10 µL of FluoSpheres were added with the antibody followed by a 2 hr incubation at 37 °C for opsonization. After 1.5 hr, THP-1 cells were centrifuged at 200 × g for 5 min, washed once with PBS, then resuspended in culture medium (RPMI & 10% FBS) at a concentration of 5×10^5 cells/mL. Then, 200 µL of cells were added to each well and incubated at 37 °C with 5% CO_2 while shaking for 6 hr. Once the incubation finished, the plate was then centrifuged at 2000 rpm for 5 min. Then, 100 µL was pipetted out of each well and replaced with 100 µL of cold 4% paraformaldehyde to fix the cells. The plate was then left at room temperature for 20 min, protected from light. The plate was then stored at 4 °C in the dark. Cells were then analyzed with a NovoCyte Quanteon flow cytometer.

Expression and purification of recombinant proteins for electron microscopy

For EM studies, Y2 HA COBRA was cloned using Gibson assembly into a derivative of pcDNA3.1+ [127]. Plasmids for the P1-05 heavy and light chain were synthesized (Genscript) and cloned into pcDNA3.1+. Cells and media were purchased from Thermo Fisher Life Technologies unless stated otherwise. Y2 HA protein expression was initiated by transfection of endotoxin free DNA into CHO-S cells using flow electroporation technology (MaxCyte). Transfected cells were suspended in CD OptiCHO supplemented with 2 mM GlutaMAX, HT, 0.1% pluronic acid, and incubated at 37 ºC, 8% CO_2, 85% humidity in an orbital shaker (Kuhner). After 24 hrs, cultures were supplemented with 1 mM sodium butyrate, and the culture temperature was dropped to 32ºC. Cultures were supplemented daily with MaxCyte CHO A Feed (0.5% yeastolate, 2.5% CHO-CD

Efficient Feed A, 2 g/L glucose, 0.25 mM GlutaMAX). The media was harvested 8-12 days post-transfection and filtered. For purification of Y2, media was diluted with an equal volume of Buffer A (500 mM NaCl, 20 mM sodium NaH_2PO_4, 20 mM imidazole) and loaded onto a 1 mL HisTrap column (GE Healthcare). The column was washed with Buffer A and the protein eluted with a gradient to Buffer B (500 mM NaCl, 20 mM NaH_2PO_4, 500 mM imidazole) on an ÄKTA Pure chromatography system (GE Healthcare). Fractions containing the protein were pooled, concentrated, and further purified and buffer exchanged on a Superdex 200 10/300 column (GE Healthcare) equilibrated in PBS (Sigma). Fractions were pooled and concentrated, then flash frozen in liquid N_2 and stored at -80ºC until use. For P1-05, the mAb was purified using a 1 mL HiTrap Protein A HP column (GE Healthcare). The media was diluted with an equal volume of Protein A IgG Binding Buffer (Thermo Scientific) and loaded onto the column. The column was washed with binding buffer, then eluted with a gradient to Protein A IgG Elution Buffer (Thermo Scientific). To adjust the pH, 55 µl of 1.89 M Tris pH 8 was added per 1 mL fraction. Fab was generated and purified using the Pierce™ Fab Preparation Kit according to the manufacturer's instructions (Thermo Scientific). The Fab product in PBS was flash frozen in liquid N_2 and stored at -80 ºC until use.

Cloning and expression of Y2 COBRA with a thrombin cleavage site

Y2 COBRA was cloned into the pBacPAK8 vector in frame with an N-terminal gp67 signal sequence and C-terminal thrombin cleavage site, T4 fibritin domain, and hexahistidine/StrepTag II tags. The construct design results in predicted vector supplied sequences of AATNA and LVPRGSPGSGYIPEAPRDGQAYVRKDGEWVLLSTFLGHHHHHHGGSWSHPQFEK at the N- and C-termini, respectively. Baculovirus was generated using the *flash*Bac™ kit according to the manufacturer's instructions (Mirus Bio). The protein was expressed in 2 L of Sf9 cells at 2×10^6

cells/mL maintained in ESF921 media (Expression Systems) by adding 25 mL virus per liter of culture. The media was harvested after 3 days, pH adjusted with NaCl and Tris pH 8, and stored at -20ºC. Prior to purification, the thawed media was filtered and concentrated to 150-200 mL by tangential flow with a Vivaflow® 200 (Sartorius). The resulting sample was diluted with an equal volume of Buffer A, filtered, and loaded onto a 5 mL HisTrap column (GE Healthcare). The column was washed with Buffer A and the protein eluted with a gradient to Buffer B. The protein was pooled, concentrated, and supplemented with 5% glycerol prior to flash freezing and storage at -80 ºC.

Kinetic assays by biolayer interferometry

Biolayer interferometry kinetic assays were performed in triplicate on the Octet® Red384 system (Sartorius) with a buffer containing PBS, 1% BSA, and 0.05% Tween. Anti-penta-HIS biosensors were immersed in buffer for 120 s, then loaded with 10 μg/mL Y2 for 300 s. The biosensors were then dipped into buffer for 120 s to obtain a baseline, dipped into buffer containing P1-05 Fab in a dilution series ranging from 54 nM to 0.67 nM for 300 s, and buffer for 600 s to measure dissociation. The data were processed in the Octet Data Analysis HT software v7 (Sartorius). Each curve was reference subtracted, aligned to the baseline, and aligned for inter-step correction through the dissociation step for each curve. Each replicate was fit globally for well-resolved curves in the dilution series using a 1:1 binding model. Parameters were optimized based on the R^2, χ^2, and individual K_D error values to maximize the goodness of fit. The final reported K_D value (98.5±32.3 pM) represents the mean ± standard deviation of three independent experiments.

Electron microscopy of the Y2+P1-05 complex

The protein samples were thawed on ice. To generate the immune complex, P1-05 Fab and Y2 COBRA produced in CHO cells were combined in a 3:1 Fab:HA trimer ratio and incubated at room temperature for 1 hr. For negative stain analysis, the immune complex was deposited at 15 μg/mL onto carbon-coated, glow-discharged, 400 mesh copper grids (EMS) and stained with 2% w/v uranyl formate. The sample was imaged on an Arctica Talos 200C electron microscope (FEI) operating at 73,000x nominal magnification with a Falcon II direct electron detector and a CETA 4k camera (FEI). Micrographs were collected with Leginon and particles were picked using a difference of Gaussians particle picker and processed with Appion [128–130]. Particles were classified in 2D and 3D in Relion 3.0 and Cryosparc2 and reconstructed in 3D in Cryosparc2 [131,132]. Figures were made in UCSF Chimera [133].

Single-cell V(D)J sequencing and analysis

PBMCs were stained with the following antibodies and proteins for flow sorting: anti-CD19-APC (1:10 dilution, clone HIB19, cat. no. 982406, BioLegend), anti-IgD-FITC (1:20 dilution, clone IA6-2, cat. no. 348206, BioLegend), anti-IgM-FITC (1:20 dilution, clone MHM-88, cat. no. 314506, BioLegend), Ghost Dye Red (1:1000), Y2-PE (1:20 dilution), and Y2-BV605 (1:20). AviTagged Y2 COBRA HA proteins containing the Y98F mutation to reduce sialic acid binding were biotinylated using the BirA biotin-protein ligase in the BirA500 kit (Avidity) and complexed to streptavidin-fluorophores SA-PE (1:500 dilution, cat. no. S866, Thermo Fisher) and SA-BV605 (1:250 dilution, cat. no. 405229, BioLegend). $CD19^{+}IgM/IgD^{-}PE^{+}BV605^{+}$ double-positive, antigen-specific B cells were flow sorted on the MoFlo Astrios and resuspended in PBS+0.04% BSA. These cells were then used to generate Single Cell 5’ v2 Dual Index V(D)J libraries using the 10X Chromium Next GEM Single Cell 5’ Reagent Kit v2 (10X Genomics).

Libraries were then sequenced using a NextSeq 550 sequencer (Illumina). Single-cell V(D)J FASTQ files were generated and demultiplexed using Cell Ranger v4.0.0 and data were visualized using the Loupe VDJ v3.0.0 browser. Only B cells with complete, ungapped variable regions and singly paired heavy and light chains were considered for downstream analysis. Six B cell receptor sequences were expressed as recombinant IgGs in 293 cells and used for ELISAs and HAIs.

Results

COBRA HA-specific B cell responses

To determine the size of the H1 COBRA HA-reactive B cell population within seasonally vaccinated individuals, total B cells from four vaccinated subjects (2017-2018 cohort) were stimulated on an irradiated feeder layer as previously described [123]. B cell supernatants were assayed for activity against A/California/04/2009 HA, P1 COBRA HA, and X6 COBRA HA recombinant proteins by ELISA. As expected, HA- and COBRA HA-reactive IgG titers were higher in day 21 post-vaccination samples compared to those obtained pre-vaccination **(Figure 3.1).** Comparisons of A/California/04/2009 HA-reactive IgG titers to those of P1 HA- and X6 HA-reactive IgGs indicated that binding to A/California/04/2009 HA protein was consistently higher. The majority of subjects demonstrated significant P1 HA-reactive IgG titers that, while lower than A/California/04/2009 HA-reactive IgG titers, were higher than or equivalent to X6 HA-reactive IgG titers in three of four subjects. The disparity in antibody titers between wild-type A/California/04/2009 HA- and COBRA HA-reactive proteins may be attributed to the relatively high abundance of pandemic strain-specific antibodies, and the absence of these potential binding epitopes on the P1 and X6 H1 COBRA HA proteins. Moreover, the degree of similarity of each COBRA HA to the A/California/04/2009 HA appeared to be reflected in the degree to which

reactive IgG titers were elicited. Namely, the P1 COBRA HA, representing pandemic-like human and swine H1 HA sequences, demonstrates 84.63% identity to A/California/04/2009 HA, whereas the X6 HA, representing seasonal-like H1 HA sequences, demonstrated a lower 80.53% identity to A/California/04/2009 HA.

Lineage analysis of pre-existing COBRA HA-specific mAbs

To further probe the pre-existing B cell response to COBRA HA antigens, we isolated 26 mAbs from five additional human subjects vaccinated with the 2017-2018 quadrivalent influenza vaccine within the same cohort, using A/California/04/2009 HA and P1 COBRA HA as screening antigens. The antibody-encoding genes were sequenced, and the results indicated the usage of several different immunoglobulin *V* genes across the entire panel **(Figure 3.2, Table 3.1)**. When comparing usage of heavy chain genes, V_H*1*, V_H*3*, V_H*4*, and V_H*5* gene families were represented **(Figure 3.2A)**. Approximately 50% of all mAbs utilized a gene from the V_H*3* family, and approximately another 50% utilized a gene from the V_H*4* family. In the light chain, for those mAbs utilizing the kappa chain, many utilized genes V_K*3-11* and V_K*3-15*. The remainder used *V* genes V_K*3-20* or those from V_K*1* or V_K*2* families. mAbs utilizing the lambda chain used predominantly V_L*3-21* and V_L*2-14*. Paired heavy and light chain *V* genes showed variation across the antibody panel, with the V_H*3-7*:V_K*3-15* and V_H*4-39*:V_L*2-14* pairings being the most abundant for kappa- and lambda chain-utilizing mAbs, respectively **(Figure 3.2B)**. The CDR3 regions ranged in length from 10-22 amino acids for the heavy chain, 8-10 amino acids for the kappa chain, and 10-12 amino acids for the lambda chain **(Figure 3.2C).** The percent identities of the variable genes to the germline sequence had averages of 93% for both the heavy and kappa chains, and 96% for the lambda chain at the nucleotide level **(Figure 3.2C)**.

Binding analysis of COBRA HA-specific human mAbs

P1 and X6 COBRA HA proteins incorporate historical epitopes from both pre- and post-2009 viruses, while Y2 COBRA HA incorporates more recent 2009 pandemic-like sequences from 2014 to 2016, representing the HA epitopes from more recent H1 isolates [122] **(Figure 3.3)**. The majority of isolated mAbs demonstrated high binding to A/California/04/2009 HA protein by ELISA, with an average EC_{50} of 30 ng/mL **(Figure 3.4A)**. Of these A/California/04/2009 HA protein-reactive mAbs, only a subset demonstrated binding to the divergent P1 and X6 COBRA HA proteins. mAbs P1-02, P1-05, and 163-20 showed reactivity against the P1 COBRA protein, and mAbs CA09-26, CA09-30, CA09-45, P1-02, and P1-05 demonstrated binding to the X6 COBRA protein. The limited mAb binding to P1 and X6 COBRA proteins correlated with the lower reactive B cell frequencies to these respective HAs in **Figure 3.1.** All mAbs had similar EC_{50} values and reactivities to the Y2 COBRA HA compared to A/California/04/2009 HA **(Figure 3.4A)**. We also determined whether mAbs were broadly reactive by utilizing a chimeric HA protein bearing a H6 HA head and a H1 HA stem (cH6/1) **(Figure 3.4A)**. mAb P1-05 bound to the chimeric protein with high avidity, suggesting this mAb may bind the stem region of the H1 HA protein, or some other conserved epitope present in both H1 and H6 HAs. These results indicate that 2017-2018 QIV-vaccinated subjects possessed mAbs with potent binding to the 2009 pandemic-like Y2 COBRA HA protein. Moreover, mAbs from different subjects with reactivity against the divergent P1 and/or X6 COBRA HAs were found, although these represented a small part of the total antibody response. Based on these data and the B cell screening data, COBRA HA-reactive B cells constitute part of the human B cell response to influenza vaccination, and COBRA HA antigens can likely recall such B cells targeting both the head and stem regions.

Functional analysis of COBRA HA-specific mAbs

To characterize the functional activities of the isolated mAbs, HAI and neutralizing activities were assessed **(Figure 3.4B, 4C)**. The majority of mAbs showed HAI activity against the pandemic-like A/Michigan/45/2015 virus **(Figure 3.4B)**. These data are consistent with the fact that most mAbs bound the head domain of A/California/04/2009 HA **(Figure 3.4A)**. Of those mAbs with the highest HAI activity of the panel against the recent pandemic-like A/Michigan/45/2015 virus, CA09-26 and CA09-45 were tested for HAI against two pre-pandemic H1 viruses as these mAbs bind the X6 HA COBRA, which incorporates pre-pandemic sequences, and both target the HA head domain. CA09-26 had HAI activity against A/New Caledonia/20/1999 and A/Brisbane/59/2007 viruses, while CA09-45 had HAI activity against A/New Caledonia/20/1999, and no activity against A/Brisbane/59/2007 **(Figure 3.4B)**. We next assessed neutralizing activity against A/California/07/2009 **(Figure 3.4C)**. Approximately 60% of mAbs (16/26 mAbs) neutralized the pandemic A/California/07/2009 virus (A/CA/09). Notably, mAbs CA09-26 and CA09-45 were among the most potent mAbs in the panel with half-maximal inhibitory concentrations (IC_{50}s) of 0.013 μg/mL and 0.032 μg/mL, respectively. These two mAbs were also tested for neutralizing activity against A/New Caledonia/20/1999 and A/Brisbane/59/2007 **(Figure 3.4C)**. They had IC_{50} values of 0.081 μg/mL and 0.286 μg/mL, respectively, against A/New Caledonia/20/1999, indicating potent neutralization activity. However, these two mAbs did not demonstrate neutralizing activity against the A/Brisbane/59/2007 virus, in accordance with the observation that little to no HAI activity was observed for the same strain.

Neutralization-independent, Fc-dependent activities are an important aspect of anti-influenza antibodies that bind both the head and stem domains [46,48,134]. Stem-binding

antibodies elicited by P1 HA vaccination also demonstrate Fc activity by inducing cellular cytotoxicity [120]. To determine the extent of one such Fc effector function, antibody-dependent phagocytosis (ADP) activity was measured by assessing the capacity for the monocytic THP-1 cell line to phagocytose Y2 COBRA HA-coated beads through mAb binding **(Figure 3.4D)**. The entire mAb panel demonstrated ADP activity relative to a negative mAb control. These included both neutralization/HAI-positive mAbs as well as mAbs that did not demonstrate significant HAI or neutralization activity.

Multiple distinct epitopes on the A/California/04/2009 HA are bound by isolated mAbs

To determine the epitopes bound by the panel of 26 mAbs isolated from these vaccinated subjects, biolayer interferometry-based epitope binning was performed as previously described [123,135]. Biosensors were loaded with A/California/04/2009 HA, associated with one mAb, and then exposed to a second mAb to determine mAb competition **(Figure 3.5)**. Control mAbs Ab6649, 5J8, and CR6261 were utilized to determine the relative locations of each epitope. Ab6649 binds the lateral patch, proximal to the Sa antigenic site; 5J8 binds the receptor-binding site (RBS), comprising antigenic sites Sb and Ca2; CR6261 binds a conserved portion of the stem region found for all group 1 viruses **(Figure 3.5A)**. Five distinct epitopes on A/California/04/2009 HA protein were distinguished **(Figure 3.5B)**. Of the epitopes on the globular head domain, two known major epitopes, termed epitope 1 and epitope 3, corresponding to those of mAbs Ab6649 and 5J8, respectively, were identified. MAbs competing with Ab6649 were comprised in part of those using the heavy chain gene V_H*3-23*, including mAbs CA09-19 and CA09-29, similar to those described recently that bind the lateral patch, although these mAbs did not contain the characteristic YXR motif within the heavy chain CDR3 [136]. The position of one predominantly bound epitope, epitope 2, could not be identified by epitope binning with the control mAbs used.

Two other epitopes, characterized only by the competition of a single mAb to itself, were epitopes 4 and 5, which correspond to mAbs CA09-38 and P1-05, respectively. No mAbs competed with CR6261, indicating that although mAb P1-05 may target the stem, as evidenced by binding to the cH6/1 protein **(Figure 3.3),** this mAb might target a different epitope on the stem of the H1 HA protein. Overall, these data suggest that the epitopes bound by mAbs from vaccinated subjects are likely comprised, in part, of regions within or around conserved sites on the head domain, such as those involving the RBS and the lateral patch, in addition to portions of the stem.

Epitope 5, characterized by binding by mAb P1-05, was likely located on the stem of the H1 HA protein yet did not overlap with other antibody epitopes **(Figure 3.5)**. To determine the epitope of mAb P1-05, we generated a complex of Y2 HA bound to P1-05 Fab fragments and evaluated its structure by negative-stain electron microscopy (EM) **(Figure 3.6A, 6B)**. The 2D class averages revealed that P1-05 binds to the base of the HA stem in an upward angle **(Figure 3.6B)**. We also observed that insertion of residues between the Y2 C-terminus and the Foldon trimerization domain disrupted mAb P1-05 binding, potentially due to trimer splaying and disruption of this membrane proximal epitope **(Figure 3.6C)**. Recently, a similar class of mAbs targeting this region on HA, termed the "anchor" epitope, was discovered, and such mAbs protect against H1N1 infection in mice [137,138]. Anchor mAbs do not compete with known stem mAbs and utilize *V_K3-11* or *V_K3-15* kappa V genes that encode a germline encoded NWP motif in the CDR3 region [138]. The restricted light chains can pair with *V_H3-23*, *V_H3-30/V_H3-30-3*, or *V_H3-48 V* genes. mAb P1-05 utilizes *V_K3-11* paired with *V_H3-23* and also possesses the NWP motif. Furthermore, it was also recently reported that binding of anchor mAbs is disrupted by the use of a GCN4 trimerization domain [138], which has different spacing than the Foldon domain, which matches our data with the disruption of binding observed in **Figure 3.6C.** These data affirmed that

P1-05 binds to the anchor epitope in the stem, consistent with data from **Figure 3.3A**, rather than another conserved HA epitope in the head domain. These observations are critical for subunit HA protein vaccine development as they indicate the importance of antigen design, stability, and the incorporation of mAb binding avidity studies to ensure that important epitopes are properly displayed on candidate vaccine antigens.

Repertoire analysis of Y2-specific B cells

To further probe the repertoire of pre-existing COBRA HA-specific B cells in a more recent vaccine season, we conducted a single-cell RNA sequencing experiment using B cells from a single subject vaccinated with the 2019-2020 seasonal influenza vaccine. Approximately 3000 $CD19^{+}IgM^{-}IgD^{-}$ B cells positive for the Y2 COBRA HA were sorted and subjected to 10X barcoding **(Figure 3.7)**. Prior to loading onto the 10X controller, sorted Y2-specific cells were supplemented with the CA09-26 hybridoma clone as a loading control. 119 unique paired heavy and light chains were obtained following data demultiplexing and analysis compared to the human genome database. Similar to the mAb sequencing, the V_H*1* and V_H*4* gene families were highly prevalent in the B cell repertoire. In particular, V_H*4-39* and V_H*4-59* were prevalent in both mAb sequencing and B cell sequencing results. We also identified several additional mAbs utilizing the V_H*3-23* gene, with one in particular (clone 70) having an NWP motif in a paired V_K*3-15* light chain, although this clone utilized a J_K*2* gene, rather than the J_K*4* or J_K*5* gene, which were previously used to identify anchor epitope-specific mAbs [138] **(Table 3.1)**. A fraction of clones using the V_H*1-69* gene were also identified, which is utilized by mAbs targeting the stalk epitope. Hence, pre-existing mAbs binding Y2 utilize a relatively diverse repertoire.

To identify whether these B cell clones were reactive against the baiting Y2 antigen, we recombinantly expressed six selected clones, 32, 58, 60, 70, 73, and 86, as recombinant antibodies

(rAbs). We then evaluated binding to the Y2 and cH6/1 HAs, as well as HAI activity against the more recent 2019 H1N1 strain A/Guandong-Maonan-SWL-1536/2019 (A/GM/19) **(Figure 3.7E, 7F)**. All rAbs bound the Y2 COBRA HA with high affinity **(Figure 3.7E)** but had no significant activity against the H1 HA stem as assessed by cH6/1 HA binding, including clone 70, which possessed the NWP motif but used the J_K2 gene. To evaluate functionality, we performed HAI assays against the recent A/GM/19 virus. All but one rAb, 70, possessed HAI activity against this strain **(Figure 3.7F)**. These data suggest that Y2-reactive antibodies isolated from PBMCs from a 2019-2020 seasonally vaccinated subject generally possess functionality against recent 2009 pandemic-like H1N1 strains, including a drifted 2019 virus. Importantly, this virus represents a strain not included in the original design period of the Y2 COBRA HA (2014-2016), yet rAbs derived from Y2-reactive B cells possessed HAI activity, indicating functionality against a future H1N1 strain with the COBRA HA platform.

Discussion

H1 COBRA HA antigens have been successful at broadening the antibody response compared to wild-type HA sequences in naïve and pre-immune mouse and ferret models of influenza infection [121,122]. However, pre-existing immunity to influenza in humans remains a major challenge to overcome due to repeated previous exposure to the influenza HA protein during infection and vaccination events. In this study, we sought to determine the extent of the H1 subtype COBRA HA-reactive pre-existing B cell repertoire in human subjects to predict recall responses as COBRA HA antigens move toward clinical trials. At the oligoclonal B cell level, pre-existing B cell responses were observed for P1 and X6 COBRA antigens in individuals vaccinated with the 2017-2018 seasonal influenza vaccine, which incorporated the pandemic-like

A/Michigan/45/2015 vaccine strain. COBRA HA-reactive B cell responses were lower than those observed for A/California/04/2009 HA protein, likely due to the loss of strain-specific variable head epitopes and incorporation of seasonal pre-pandemic and swine HA sequences in the X6 and P1 antigens, respectively. While it is likely that seasonal vaccination induced these COBRA HA-reactive B cells, it is possible that prior exposures to H1 viruses before vaccination may also have induced these HA-reactive B cell subsets. Moreover, we examined antibody responses to COBRA HAs in a small cohort of five vaccinated subjects, which may limit our conclusions on the extent of pre-existing antibodies to H1 COBRA HAs in the general population. Only a small subset of mAbs isolated against A/California/04/2009 HA reacted with P1 and X6 COBRA antigens. In contrast, the mAb binding profile to the recently described Y2 COBRA HA, which incorporates more recent 2009 pandemic-like H1 sequences from 2014-2016, was similar to that observed for the A/California/04/2009 HA protein. The presence of such Y2-reactive mAbs may indicate specificities against common epitopes present only in more recent 2009 pandemic-like strains but not in historical pre-2009 viruses, which could be more relevant for immunity against future H1 virus exposures. The majority of the mAbs had HAI activity and neutralizing activity against A/Michigan/45/2015 and A/California/07/2009, and two head-binding mAbs that bind the X6 protein, CA09-26 and CA09-45, had HAI activity and neutralizing activity against the pre-pandemic strain A/New Caledonia/20/1999. These data suggest that X6 HA-reactive mAbs are mainly endowed with functional activity against both pre-pandemic and pandemic-like H1 viruses. Overall, the amino acid similarity of COBRA HA antigens to A/California/04/2009 HA correlated with high B cell and mAb reactivity. In addition to binding, neutralization, and HAI activity, we also assessed if COBRA HA-reactive mAbs had Fc-mediated functions, namely ADP, and all mAbs were able to induce THP-1 phagocytosis of Y2-coated beads.

Several epitopes on the H1 HA protein have been previously defined [117], and we determined mAb epitopes on the A/California/04/2009 HA protein using biolayer interferometry. The majority of the mAbs targeted three head-binding epitopes on the Sa and Sb/Ca2 sites, and an undefined epitope, epitope 2, which is currently under structural characterization. One limitation of the BLI-based binning assay is that it does not definitively characterize antibody breadth and functionality, only providing data on the relative positions of epitopes. For instance, we observed a significant number of mAbs competing with the widely reactive 5J8 and Ab6649 antibodies, yet most isolated mAbs competing with 5J8 and Ab6649 did not bind as widely, with most lacking reactivity to the divergent P1 and X6 COBRA HAs. mAb CA09-38 did not exhibit HAI or neutralizing activity, nor did it bind the cH6/1 HA, suggesting that this mAb may target an undefined, non-neutralizing epitope on the head. We discovered that P1-05 targets a unique epitope on the H1 HA stem region, and this epitope is similar to the recently described anchor epitope [138]. Based on these data, while COBRA antigens were primarily designed to induce broadly reactive antibodies to the head domain, these antigens will likely also recall broadly reactive anchor mAbs in humans in addition to head-based recall and *de novo* antibody responses. Further repertoire analysis in a subject vaccinated with the 2019-2020 seasonal influenza vaccine identified similar sequences to our mAbs targeting the head domain from the 2017-2018 season which possessed HAI activity against a drifted 2019 H1N1 virus, A/Guangdong-Maonan/SWL-1536/2019, indicating that the COBRA-reactive B cell population may be similar across subjects and influenza vaccine seasons.

These data provide evidence that a pre-immune population with exposure to the seasonal influenza virus vaccine exhibits B cell reactivity towards conserved epitopes present on COBRA HA antigens. As the COBRA HA platform enters clinical trials, it is likely that head-specific and

some stem-specific antibodies will be elicited as part of a recall response. Moreover, the antibody epitopes identified in this work overlap in part with those previously identified on the head domain near the RBS and the lateral patch, in addition to those on the stem. These epitopes are the focus of future structural studies, particularly for those mAbs that cross-react with the X6 COBRA HA as well as with the HA stem domain. Our data also exemplify the importance of structural analysis of protein epitopes to ensure epitopes that elicit broadly neutralizing antibodies, such as the anchor epitope, remain intact following design optimization for subunit HA vaccines.

Figures

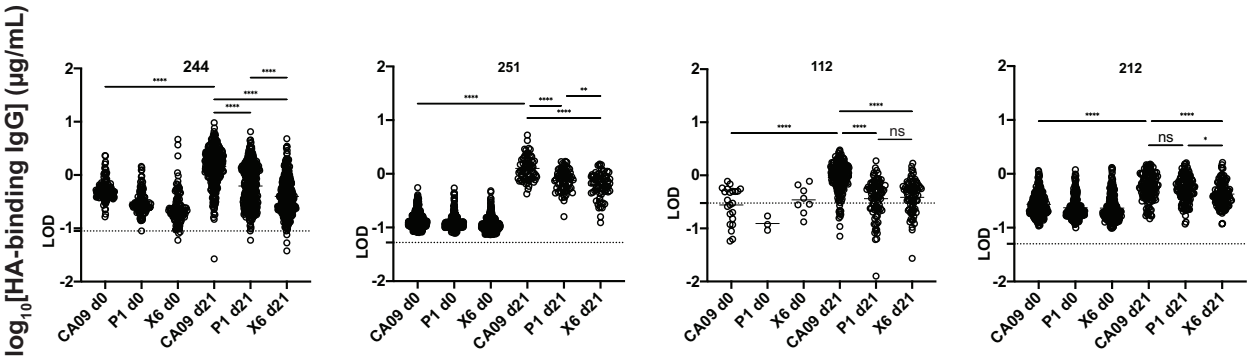

Figure 3.1. Binding titers of oligoclonal B cell supernatants pre-vaccination (d0) and 21 days post-vaccination (d21) from four representative subjects. IgG titers against CA09 HA (CA09), P1 COBRA (P1), and X6 COBRA (X6), are shown for representative subjects receiving the 2017-2018 QIV. Supernatants from stimulated PBMCs were screened by ELISA using plates coated with the indicated antigen. PBMCs were standardized to 25,000 cells per well. Each circle indicates one well, the mean is shown as a bar, and the limit of detection (LOD) is indicated by a dotted line. LOD was calculated as three times the standard deviation of the lowest concentration divided by the slope of the standard curve for each sample, interpolated to its corresponding log concentration. Results represent one experiment. ****P<0.0001, **P=0.0062, *P=0.0216, ns=not significant.

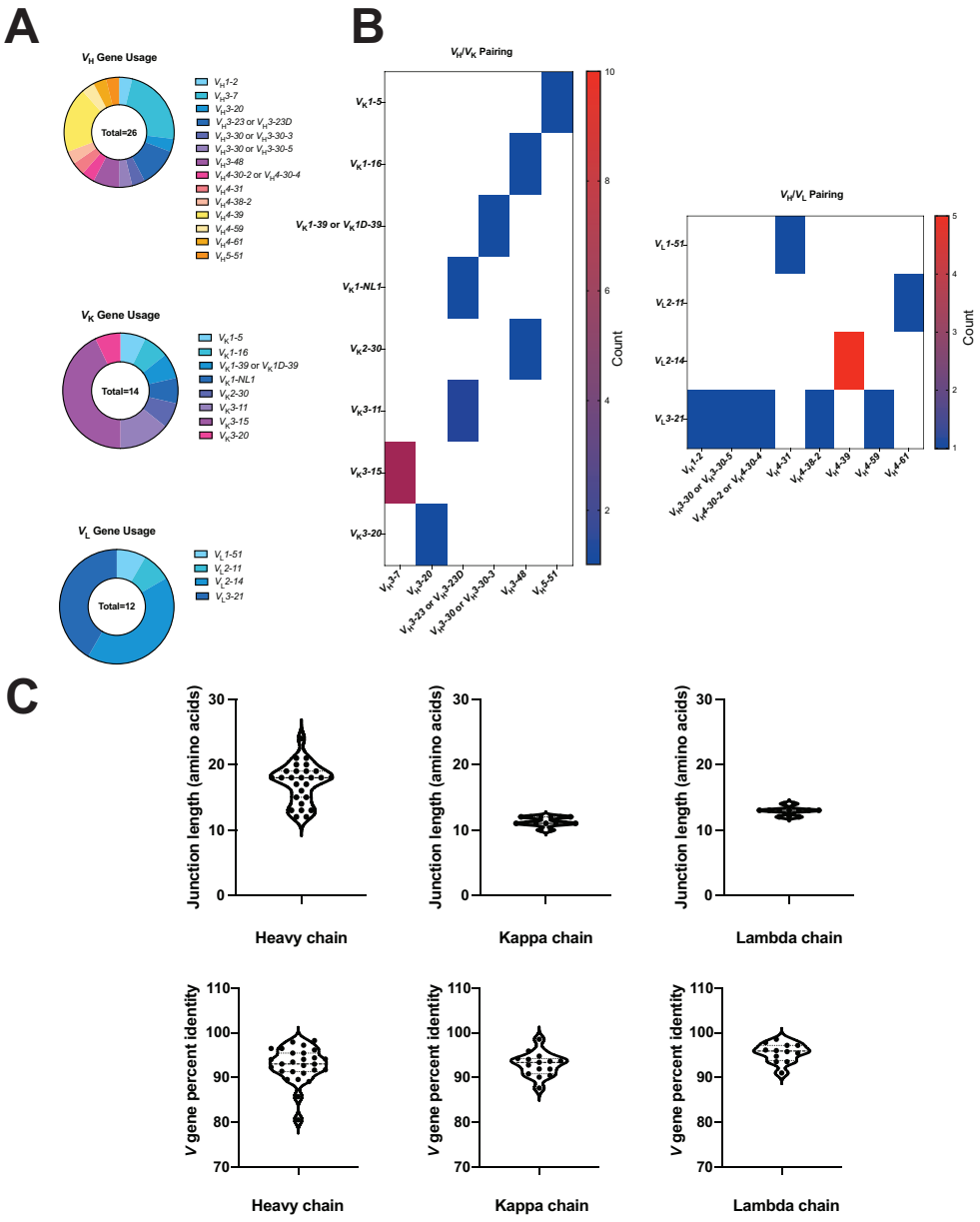

Figure 3.2. Gene usage and CDR3 lengths of isolated mAbs. (A) The usage of heavy, kappa, and lambda chain genes are shown as a proportion of all respective genes from the panel of isolated mAbs by sequencing the hybridoma line for each clone. The pairing of heavy and light chains is shown in (B), with the number of antibodies corresponding to each pairing shown as a heat map. (C) The amino acid lengths of the heavy and light chain CDR3 regions are shown (top) alongside

the nucleotide percent identity of the *V* gene to the germline sequences determined by IMGT/V-QUEST (bottom).

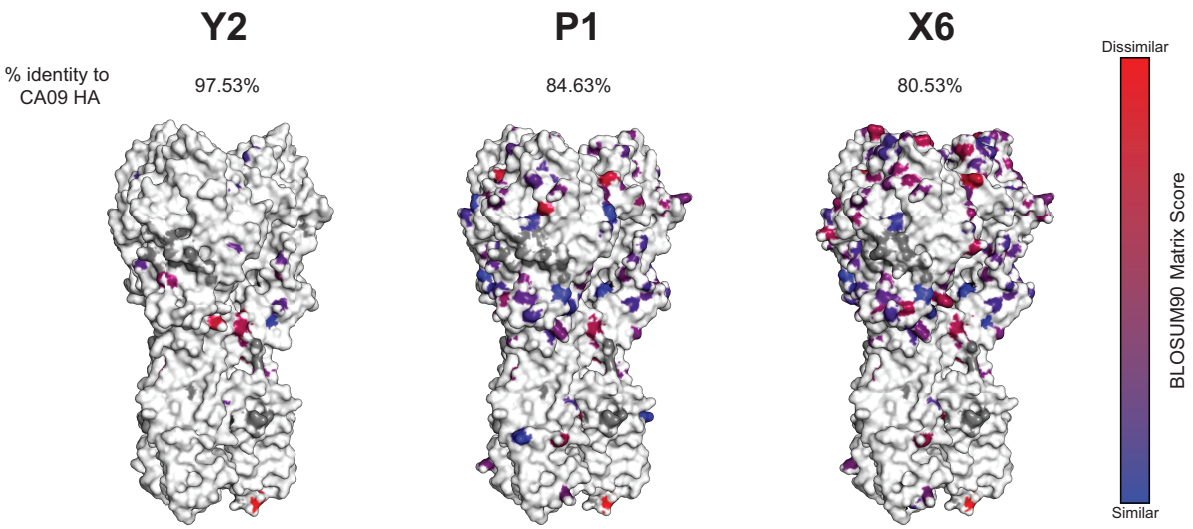

Figure 3.3. Models of H1 COBRAs used in this study. The models of the H1 subtype COBRAs used are shown alongside the percent identity to the A/California/04/2009 HA. Substitution mutations are indicated in colors corresponding to the BLOSUM90 matrix score, a measure of the likelihood of a given amino acid mutation. White residues indicate an identical amino acid as the A/California/04/2009 HA, blue a substitution with a highly similar amino acid, and red a substitution with a highly dissimilar amino acid. Models were generated using SWISS-MODEL.

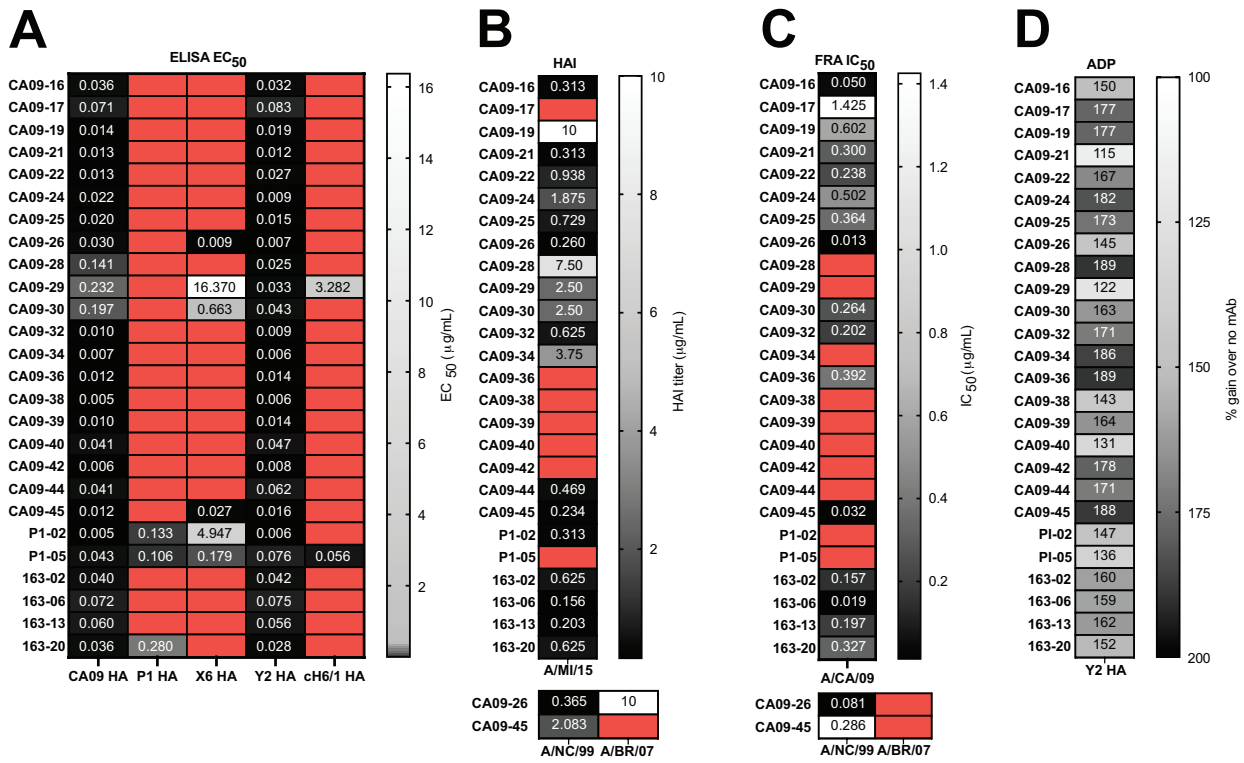

Figure 3.4. Reactivity and functional activities of mAbs isolated from 2017-2018 QIV-vaccinated subjects. (A) Half-maximal effective concentrations (EC_{50}s) are represented for each mAb. ELISAs were completed with each mAb serially diluted three-fold. Shown are the EC_{50} values against CA09 HA, P1 COBRA HA, X6 COBRA HA, Y2 COBRA HA, and cH6/1 HA. For the EC_{50} heat map, boxes in red indicate the signal at 20 µg/mL did not reach 1.5 units at 405 nm, or the calculated EC_{50} was outside the tested concentration range due to an overall low signal. Results represent two independent experiments performed in quadruplicate. (B) HAI titers of each mAb are shown for the indicated viruses. The experiment was performed in duplicate for two independent experiments. Boxes in red indicate no HAI activity was observed at 10 µg/mL. (C) Half-maximal inhibitory concentrations (IC_{50}s) are shown for the indicated mAbs against the viruses shown. Results represent the average of triplicate measurements for one experiment. Boxes in red indicate less than 50% neutralization at the highest concentration tested or the calculated IC_{50} was outside the tested concentration range due to overall low neutralization activity. (D) ADP

activities measured using Y2 HA-coated beads for each mAb are shown as the percentage gain over the no mAb control. Results represent one experiment performed in triplicate.

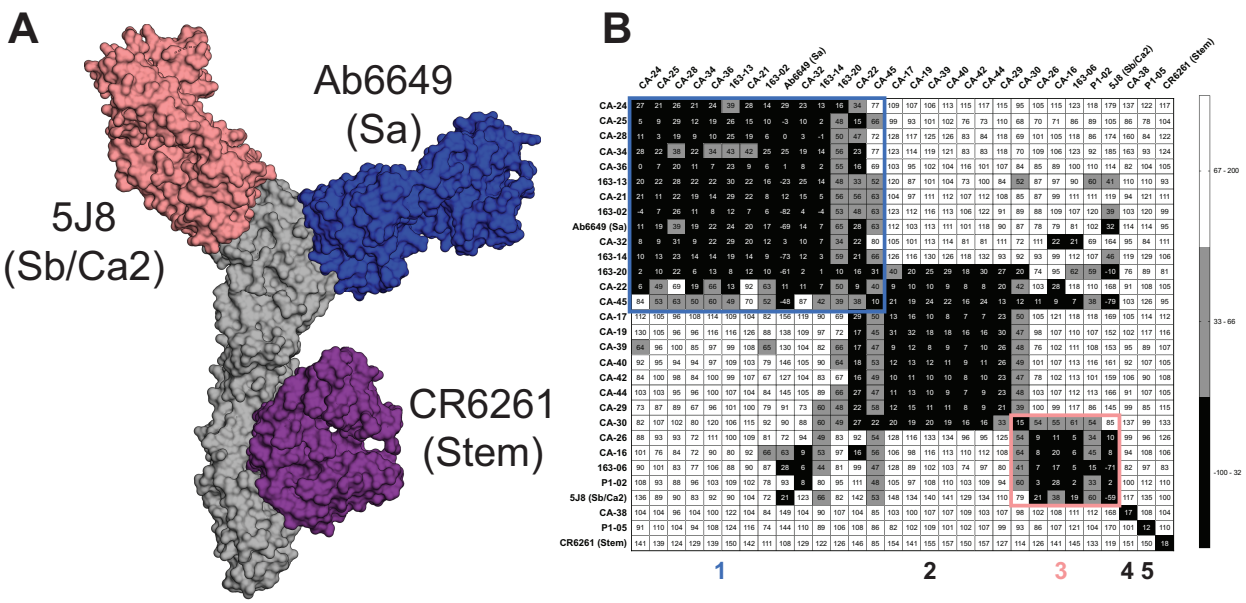

Figure 3.5. Epitope binning identifies five epitopes from human antibodies isolated at 21 days post-vaccination. (A) Model of A/California/04/2009 HA in complex with Fabs of three control antibodies used for epitope binning. 5J8 and Ab6649 bind the head domain at the conserved RBS and lateral patch epitopes, respectively. CR6261 binds the stem domain at a site conserved for group 1 viruses. (B) Epitope binning was performed against A/California/04/2009 HA using full-length mAbs. Competition was measured as the percentage of the response from the association of the second antibody (horizontal axis) in the presence of the first antibody (vertical axis) as compared to the second antibody alone. Black indicates complete competition, gray moderate competition, and white no competition. Results represent one experiment with one measurement taken per competition set. Identified epitopes that have been previously characterized are outlined in blue (for the lateral patch) and pink (for the RBS). The antigenic sites of the epitopes of control mAbs Ab6649 and 5J8 are shown in parentheses.

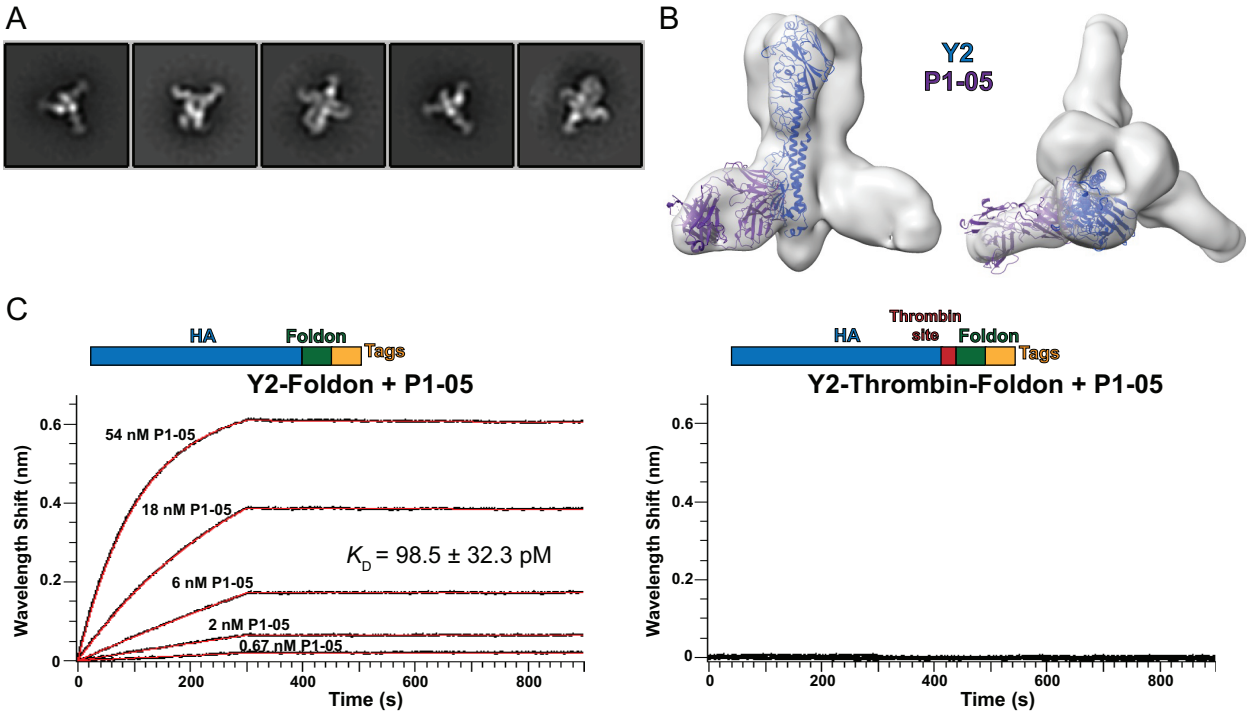

Figure 3.6. Structural characterization of P1-05 binding to Y2 COBRA. (A) 2D class averages and (B) 3D reconstruction of the Y2+P1-05 complex. (C) Comparison of P1-05 binding with Y2 in the presence or absence of a thrombin cleavage site by biolayer interferometry. Representative runs are shown. The K_D represents the mean ± standard deviation of three independent experiments.

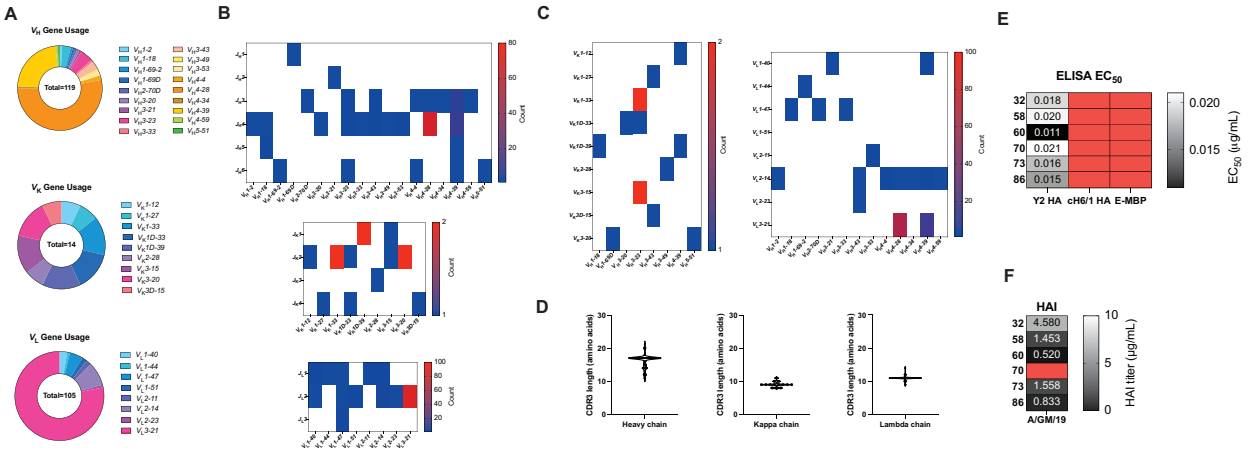

Figure 3.7. Sequence characteristics of Y2 COBRA-specific B cells from a human subject receiving the 2019-2020 seasonal vaccine. (A) The usage of heavy, kappa, and lambda chain genes are shown as a proportion of all respective genes for all B cells with paired heavy and light chains. (B) The pairing of *V* and *J* genes are shown, with the number of B cells contributing to each pairing for each chain, as heat maps. (C) The pairing of heavy and light chain *V* genes is shown for heavy-kappa chain pairings (left) and heavy-lambda chain pairings (right) as heat maps. (D) The amino acid lengths of the CDR3 regions for the heavy and light chains are shown. (E) Six B cell receptor sequences were expressed as rAbs and tested for binding to the indicated antigens by ELISA. E-MBP, negative control. The experiment was performed twice, and measurements taken in quadruplicate. (F) HAI activity of these six rAbs against A/Guangdong-Maonan/SWL-1536/2019. Results represent the average of two independent experiments with measurements taken in duplicate. Red indicates no activity for either assay in (E) and (F).

Tables

Table 3.1. mAb and B cell receptor V(D)J gene usage characteristics. The mAbs elicited by 2017-2018 seasonal vaccination and B cell clonotypes elicited by 2019-2020 seasonal vaccination are shown. The variable (*V*), joining (*J*), and diversity (*D*) genes for the heavy chain (HC) and light chain (LC) are shown, alongside the heavy and light chain isotypes and junction/CDR3 sequences. The junctions include the terminal C and W (heavy chain) or C and F residues (light chain) before and after the CDR3 sequences.

mAb isolation

mAb	Subject	Frequency	Antigen	HC *V* Gene	HC *J* Gene	HC AA Junction	LC *V* Gene	LC *J* Gene	LC AA Junction
163-02	163 d21	1	CA09/Y2	VH3-7	JH2	CAREKPYRFGSEWYFDLW	VK3-15	JK1	CQQYNNRRTF
163-13	163 d21	1	CA09/Y2	VH4-31	JH4	CARATIPYYSSGRRYYFDNW	VL1-51	JL3	CGTWDSSLSGWVF
163-20	163 d21	1	CA09/Y2/P1	VH3-48	JH3	CARGDYEYWSGYDAFDMW	VK2-30	JK2	CMQATHWPYTF
CA09-21	229 d21	1	CA09/Y2	VH3-7	JH4	CATDSPYAYSYGWYFDYW	VK3-15	JK2	CQQYNIWPRSF
CA09-22	255 d21	1	CA09/Y2	VH1-2	JH4	CAREGNWHREFDSW	VL3-21	JL3	CQVYDSSSDVWVF
CA09-24	255 d21	1	CA09/Y2	VH3-48	JH4	CATYLDILTGYPDFDYW	VK1-16	JK4	CQQYDSYPHTF
CA09-25	255 d21	1	CA09/Y2	VH3-7	JH2	CARGSQYVFSSPWYFGLW	VK3-15	JK1	CQQYNNGRTF
CA09-28	255 d21	1	CA09/Y2	VH3-7	JH2	CVRDHYFVGHSYWYFDLW	VK3-15	JK1	CQQYNRWPRTF
CA09-32	255 d21	1	CA09/Y2	VH3-30	JH4	CARERDVWSGASYPFFDYW	VK1-39	JK1	CQQSYNTPWWTF
CA09-34	255 d21	1	CA09/Y2	VH3-7	JH6	CARGHCSGSTCNYYYYGMDVW	VK3-15	JK5	CQQYNKWPSITF
CA09-36	255 d21	1	CA09/Y2	VH3-7	JH4	CARDTPYVNSFGWYFDLW	VK3-15	JK1	CQQYNRWPPGTF
CA09-17	229 d21	1	CA09/Y2	VH4-39	JH4	CATGASFEAFDYW	VL2-14	JL2	CNSYKFSSPPYVLF
CA09-19	229 d21	1	CA09/Y2	VH3-23	JH4	CAKDTGTYCGVDCYLGGDYYFDFW	VK1-NL1	JK1	CQQYYSIPLTF
CA09-29	255 d21	1	CA09/Y2	VH3-23	JH4	CARWIEKWLPSFDYW	VK3-11	JK2	CQQRYNWPGYTF
CA09-30	255 d21	1	CA09/Y2/X6	VH4-38-2	JH4	CARALRSTTVDRNFSFDQW	VL3-21	JL2	CQVWDISSDHVVF
CA09-39	241 d21	1	CA09/Y2	VH4-39	JH3	CSSGGSFDAFDVW	VL2-14	JL1	CSSYTSSITYVF
CA09-40	241 d21	1	CA09/Y2	VH4-61	JH3	CARKPGFCSGGSCYSGAFDIW	VL2-11	JL2	CCSYAGSYIFEVF
CA09-42	241 d21	1	CA09/Y2	VH4-39	JH4	CVSPKRLTIEYFDYW	VL2-14	JL2	CSSYTTSTTPHVVF
CA09-44	241 d21	1	CA09/Y2	VH4-39	JH3	CAGGRNVDDFPDW	VL2-14	JL2	CSSFTSSTTVVF
CA09-45	241 d21	1	CA09/Y2/X6	VH4-39	JH3	CAVFEERTMIDAFDIW	VL2-14	JL3	CSSYSTTSTLLF
163-06	163 d21	1	CA09/Y2	VH3-30	JH4	CARQLPGYGSGWYSGGLDYW	VL3-21	JL2	CQVWDSSSDHVVF
CA09-16	229 d21	1	CA09/Y2	VH5-51	JH6	CARQKDDTIFVGGMDVW	VK1-5	JK1	CQQYNSYSRTF
CA09-26	255 d21	1	CA09/Y2/X6	VH4-30-2	JH4	CARGLRSTTVDRNYYFDNW	VL3-21	JL2	CQVWDISSDHVVF
P1-02	156 d21	1	CA09/Y2/P1	VH4-59	JH5	CARTAVVRDLDTFNYFDPW	VL3-21	JL1	CQVWDRSSDHYVF
CA09-38	241 d21	1	CA09/Y2	VH3-20	JH5	CARGTNGLFDSW	VK3-20	JK2	CQQYGRASYTF
P1-05	241 d21	1	CA09/Y2/P1/X6	VH3-23	JH4	CAKDWVRAVSQQGYFDSW	VK3-11	JK5	CQQRSNWPPITF

10X

Clonotype	Subject	Frequency	Antigen	HC *V* Gene	HC *J* Gene	HC AA Junction	LC *V* Gene	LC *J* Gene	LC AA Junction
3	MOUFLU1-003C d28	13	Y2	VH4-28	JH4	CARGLRSTTVDRNYYFDNW	VL3-21	JL2	CQVWDISSDHVVF
4	MOUFLU1-003C d28	9	Y2	VH4-28	JH4	CARGLRATTVDRNYYFDNW	VL3-21	JL2	CQVWDISSDHVVF
5	MOUFLU1-003C d28	7	Y2	VH4-28	JH4	CARGLRSTTGDRNYYFDNW	VL3-21	JL2	CQVWDISSDHVVF
7	MOUFLU1-003C d28	5	Y2	VH4-28	JH4	CARCLRSTTVDRNYYFDNW	VL3-21	JL2	CQVWDISSDHVVF
9	MOUFLU1-003C d28	5	Y2	VH4-39	JH3	CARGYGEYLFDAFGLW	VL3-21	JL2	CQVWDISSDHVVF
8	MOUFLU1-003C d28	5	Y2	VH4-39	JH3	CASIYGQIDAFDIW	VL3-21	JL2	CQVWDISSDHVVF
11	MOUFLU1-003C d28	4	Y2	VH4-28	JH4	CARGLRSTTVDHNYYFDNW	VL3-21	JL2	CQVWDISSDHVVF
10	MOUFLU1-003C d28	4	Y2	VH4-39	JH4	CARGLRSTTVDRNYYFDNW	VL3-21	JL2	CQVWDISSDHVVF
20	MOUFLU1-003C d28	2	Y2	VH1-18	JH5	CARVDVGEGADWFDPW	VL1-47	JL3	CASWDDTVWLF
14	MOUFLU1-003C d28	2	Y2	VH3-53	JH4	CARGNLGSDFWSGYYFDYW	VL2-11	JL1	CCSYAGSYFFGVF
16	MOUFLU1-003C d28	2	Y2	VH4-28	JH4	CARGLRSTTVDRNYYFDNC	VL3-21	JL2	CQVWDISSDHVVF
18	MOUFLU1-003C d28	2	Y2	VH4-28	JH4	CARGLRSTTLDRNYYFDNW	VL3-21	JL2	CQVWDISSDHVVF
12	MOUFLU1-003C d28	2	Y2	VH4-28	JH4	CARGLRSTTEDRNYYFDNW	VL3-21	JL2	CQVWDISSDHVVF
19	MOUFLU1-003C d28	2	Y2	VH4-39	JH4	CARGLRSSTVDRNYYFDNW	VL3-21	JL2	CQVWDISSDHVVF
69	MOUFLU1-003C d28	1	Y2	VH1-18	JH4	CARVEYTDGYSSRWPDFDYW	VK1D-39	JK1	CQQSYSTLWTF
75	MOUFLU1-003C d28	1	Y2	VH1-18	JH5	CARVDVGEGADWFDPW	VL1-47	JL3	CASWDDSVWVF
53	MOUFLU1-003C d28	1	Y2	VH1-2	JH4	CAREPTLYHAPSFDYW	VL2-14	JL1	CSSFSSSSTPYVF
37	MOUFLU1-003C d28	1	Y2	VH1-69-2	JH6	CATGIFGVVTASPDYYYDVW	VL1-44	JL1	CAVWDDSLHVVVF
100	MOUFLU1-003C d28	1	Y2	VH1-69D	JH1	CARDPRGTVWPGTEYFQDW	VK3-20	JK2	CQQYGSSPATF
44	MOUFLU1-003C d28	1	Y2	VH2-70D	JH3	CARIFEGWAFDIW	VL1-47	JL2	CAAWDDSLSGVVF
76	MOUFLU1-003C d28	1	Y2	VH3-20	JH4	CTRGYCSGGSCFSGDYW	VK1D-33	JK4	CQQYRDPFTF
56	MOUFLU1-003C d28	1	Y2	VH3-21	JH2	CAREEGGSSLWLGYFDLW	VL1-40	JL2	CQSYDRSLSAHVVF
80	MOUFLU1-003C d28	1	Y2	VH3-23	JH3	CAKGGYGDYGLDVFDIW	VK1D-33	JK2	CQQYGNLPYTF
60	MOUFLU1-003C d28	1	Y2	VH3-23	JH3	CAKGGFGDYGLDVFDIW	VK1-33	JK2	CQQYGNLPYTF
41	MOUFLU1-003C d28	1	Y2	VH3-23	JH3	CAKGGHNDYGLDAFDIW	VK1-33	JK2	CQQYKNLPYTF
33	MOUFLU1-003C d28	1	Y2	VH3-23	JH4	CAKDPAAGFGGGNVFEYW	VK3-15	JK1	CQQYDNWQTF
70	MOUFLU1-003C d28	1	Y2	VH3-23	JH4	CAKDWEPVVDATLFEYW	VK3-15	JK2	CQQYDNWPPYTF
58	MOUFLU1-003C d28	1	Y2	VH3-23	JH6	CSKGDEFWSGYSPSYSYYMDVW	VL1-51	JL1	CGTWDSSLSTGGYYVF
86	MOUFLU1-003C d28	1	Y2	VH3-33	JH4	CARDRYYQYIWGSFQLDQW	VL1-47	JL1	CAAWDDSLSLYVF
34	MOUFLU1-003C d28	1	Y2	VH3-43	JH3	CAAYSGSLDGLEIW	VL2-14	JL1	CSSYTRSRIFVF
64	MOUFLU1-003C d28	1	Y2	VH3-43	JH3	CAKGNGYSYALDAFDIW	VL2-23	JL2	CCSFAGSDTLVF
49	MOUFLU1-003C d28	1	Y2	VH3-43	JH4	CAKDSGFYSNYLDSW	VK1-27	JK4	CQKYNNAPLTF
85	MOUFLU1-003C d28	1	Y2	VH3-43	JH4	CVKGSLLYGDPYSAFDYW	VK3D-15	JK4	CQEYISWPPALTF
54	MOUFLU1-003C d28	1	Y2	VH3-49	JH4	CSRVVKGSGYYTSSSDYW	VK2-28	JK3	CMQALQTPVTF
88	MOUFLU1-003C d28	1	Y2	VH4-28	JH3	CATAAPRVAIDDFNIW	VL2-14	JL2	CSSYTSSISVIF
26	MOUFLU1-003C d28	1	Y2	VH4-28	JH4	CARGLRSTTVDRIYYFDNW	VL3-21	JL2	CQVWDISSDHVVF
103	MOUFLU1-003C d28	1	Y2	VH4-28	JH4	CARGLWSTTVDRNYYFDNW	VL3-21	JL2	CQVWDISSDHVVF
89	MOUFLU1-003C d28	1	Y2	VH4-28	JH4	CARGLRSTSVDRNYYFDNW	VL3-21	JL2	CQVWDISSDHVVF
67	MOUFLU1-003C d28	1	Y2	VH4-28	JH4	CARGLRSTTVDRNYYFDNW	VL3-21	JL2	CQVWDISSDHVVF
24	MOUFLU1-003C d28	1	Y2	VH4-28	JH4	CARGLRSTTVDRNYYFDKW	VL3-21	JL2	CQVWDISSDHVVF
72	MOUFLU1-003C d28	1	Y2	VH4-28	JH4	CASGLRSTTVDRNYYFDNW	VL3-21	JL2	CQVWDISSDHVVF
93	MOUFLU1-003C d28	1	Y2	VH4-28	JH4	CARGMRTTTVDRNYYFDNW	VL3-21	JL2	CQVWDISSDHVVF
21	MOUFLU1-003C d28	1	Y2	VH4-28	JH4	CARGLRSTTVDRNYYFDNW	VL3-21	JL2	CQVWDISSDHVVF
102	MOUFLU1-003C d28	1	Y2	VH4-28	JH4	CARGLRSTTVDRNYYFDNW	VL3-21	JL2	CQVWDISSHHVVF
84	MOUFLU1-003C d28	1	Y2	VH4-28	JH4	CARGLRSTTVDRNYYFDNW	VL3-21	JL2	CQVWDISSDHVVF
94	MOUFLU1-003C d28	1	Y2	VH4-28	JH4	CARGLRSTTVDRNSYFDNW	VL3-21	JL2	CQVWDISSDHVVF
101	MOUFLU1-003C d28	1	Y2	VH4-28	JH4	CARGLRSTTVDRNHYFDNW	VL3-21	JL2	CQVWDISSDHVVF
97	MOUFLU1-003C d28	1	Y2	VH4-28	JH4	CARGLRSTTVDRHYYFDNW	VL3-21	JL2	CQVWDISSDHVVF
65	MOUFLU1-003C d28	1	Y2	VH4-28	JH4	CARGLWATTVDRNYYFDNW	VL3-21	JL2	CQVWDISSDHVVF
31	MOUFLU1-003C d28	1	Y2	VH4-28	JH4	CARGLRSTTVDRYYYFDNW	VL3-21	JL2	CQVWDISSDHVVF
81	MOUFLU1-003C d28	1	Y2	VH4-28	JH4	CARGPRSTTVDRNYYFDNW	VL3-21	JL2	CQVWDISSDHVVF
96	MOUFLU1-003C d28	1	Y2	VH4-28	JH4	CARGLRSTTVDLNYYFDNW	VL3-21	JL2	CQVWDISSDHVVF
43	MOUFLU1-003C d28	1	Y2	VH4-28	JH4	CARGLRWTTVDRNYYFDNW	VL3-21	JL2	CQVWDISSDHVVF
50	MOUFLU1-003C d28	1	Y2	VH4-34	JH3	CARGERGNFDAFDVW	VL2-14	JL2	CSSYTTSTTFGVLF
73	MOUFLU1-003C d28	1	Y2	VH4-39	JH3	CATAAPAVAIDAFVW	VL2-14	JL2	CSSYTDTISVIF
91	MOUFLU1-003C d28	1	Y2	VH4-39	JH4	CARGLRSTTVDRNYYFDDW	VL3-21	JL2	CQVWDISSDHVVF
68	MOUFLU1-003C d28	1	Y2	VH4-39	JH4	CARLANSGDFWSGYYFDYW	VL1-51	JL1	CGTWDSSLHYVF
32	MOUFLU1-003C d28	1	Y2	VH4-39	JH4	CAHSDRRLVDDVDSAIVFFDYW	VK1D-39	JK1	CQQGYSTPWTF
48	MOUFLU1-003C d28	1	Y2	VH4-39	JH4	CARGLMSTTVDRNYYFDNW	VL3-21	JL2	CQVWDISSDHVVF
52	MOUFLU1-003C d28	1	Y2	VH4-39	JH4	CARGLRSTTVDRNYYFDNW	VL3-21	JL2	CQVWDISSDHVVF
39	MOUFLU1-003C d28	1	Y2	VH4-39	JH4	CARHGLLDCSGGRCSYYYFDYW	VL1-40	JL1	CQSYDTSLSGHVF
38	MOUFLU1-003C d28	1	Y2	VH4-39	JH4	CARHLYYCGGDCTYYLDHW	VL3-21	JL2	CQVWVGGSDPHVVF
51	MOUFLU1-003C d28	1	Y2	VH4-39	JH4	CARTLHQQLEALDYW	VL2-14	JL1	CSSYTSGTTLYVF
79	MOUFLU1-003C d28	1	Y2	VH4-39	JH5	CVRSYSSTWNNRFDPW	VL1-40	JL1	CQSYDISLSADYVF
66	MOUFLU1-003C d28	1	Y2	VH4-39	JH6	CARDRYPRGYSSGFPQYGLDVW	VK1-12	JK2	CQQAKNIPHYTF
27	MOUFLU1-003C d28	1	Y2	VH4-4	JH3	CARGKLFEAFDIW	VL2-14	JL2	CSSYTTSSTPSVIF
90	MOUFLU1-003C d28	1	Y2	VH4-4	JH6	CARSMDWLSVDDPYYHYYYMDVW	VL2-14	JL2	CSSYTSSSIVIF
77	MOUFLU1-003C d28	1	Y2	VH4-59	JH3	CTSDINSDAYHIW	VL2-14	JL2	CASYSTSGTLVIF
59	MOUFLU1-003C d28	1	Y2	VH5-51	JH6	CVRLGGDPYNFYYYMDVW	VK3-20	JK2	CQLYGSPYTF

CHAPTER 4

ADJUVANT-DEPENDENT ANTIBODY RESPONSES TO A COMPUTATIONALLY OPTIMIZED HEMAGGLUTININ[3]

[3]A part of this chapter was accepted by *Viruses*. Reprinted here with the permission of the publisher. (This is an open-access article distributed under the terms of the Creative Commons Attributions License – CC BY). Nagashima, K.; Abbadi, N.; Vyas, V.; Roegner, A.; Ross, T.M.; Mousa, J.J. Adjuvant-Mediated Differences in Antibody Responses to Computationally Optimized Hemagglutinin and Neuraminidase Vaccines. *Viruses* **2023**, *15*, 347, doi:10.3390/v15020347.

Abstract

Computationally optimized broadly reactive antigens (COBRAs) are a next-generation universal influenza vaccine candidate. However, how these COBRAs induce antibody responses when combined with different adjuvants has not previously been well-characterized. Therefore, we performed *in vivo* studies with an HA-based H1 COBRA, Y2, and an NA-based N1 COBRA, N1-I, to assess this effect for the H1N1 subtype. We tested the adjuvants AddaVax, AddaS03, CpG, and Alhydrogel. AddaS03 performed the best, eliciting high IgG titers and hemagglutination inhibition (HAI) activity for Y2 immunizations. Interestingly, serum antibody epitopes were relatively similar across adjuvant groups. Moreover, following N1-I immunization with these adjuvants, AddaS03 also elicited the highest IgG and neuraminidase inhibition (NAI) titers against the 2009 pandemic virus, A/California/07/2009 (A/CA/09). These results inform adjuvant selection efforts for H1 and N1 COBRA HA and NA antigens in a mouse model.

Introduction

Influenza poses a significant health burden worldwide [112]. It is responsible for annual epidemics, for which the only major countermeasure is the seasonal influenza vaccine. However, due to the highly mutable nature of influenza virus, seasonal influenza vaccines have variable and short-lived effectiveness, requiring annual vaccination. In an effort to provide broadened and longer-lasting protection, a next-generation vaccine design platform, termed COBRA (computationally optimized broadly reactive antigen), has been developed [52,54,139]. COBRAs can broaden the antibody response against the surface glycoproteins, hemagglutinin (HA) and neuraminidase (NA). This platform incorporates wild-type HA or NA sequences from selected time periods and antigenic spaces to produce a COBRA immunogen that elicits enhanced antibody breadth. These COBRA vaccines have been designed for the influenza viruses that cause disease in humans, influenza A viruses (IAVs) and influenza B viruses (IBVs). In both naïve and pre-immune animal models, immunization with COBRA HAs and NAs typically produces protective and broadly-acting antibody responses against a wide range of viruses [4,56,139].

H1N1 subtype viruses circulate every year and comprise one component of the seasonal influenza vaccine, alongside H3N2 and IBVs [140]. Viruses of this subtype were in circulation from 1918 to 1957, disappearing from 1957 to 1977, then re-emerging and remaining for every season since [118]. The 2009 swine influenza pandemic, resulting from a reassortment event between avian, swine, and human influenza viruses, led to an antigenic shift, after which antigenically similar viruses have been in circulation [118]. Several HA antibody epitopes have also been characterized in the immunodominant head domain and the immunosubdominant stem domain. The receptor-binding site (RBS) is a conserved target of certain head-binding antibodies that prevent sialic acid binding and host cell attachment [141]. In addition, the lateral patch epitope

is another conserved region on the head domain [45,136]. Within the more conserved stem domain, the central stem epitope is a target of group 1-specific, broadly reactive antibodies including CR6261 [59]. Antibodies that bind the membrane-proximal region of the HA at the anchor epitope have been identified as well [138,142]. Whereas the HA component of each virus varies substantially across strains, the NA component remains relatively stable, accruing mutations only occasionally [143]. Current seasonal vaccines are standardized by HA content but not by NA content, despite the more conserved nature of this glycoprotein. Furthermore, anti-NA titers have been observed to be a useful correlate of protection [144,145]. Likewise, employing a NA-based universal vaccine to supplement a HA-based vaccine may afford longer-term protection.

Adjuvants are critical components of several licensed vaccines and drive enhanced immune responses, particularly for subunit vaccines [146]. Adjuvants can act through several pathways to exert their effects, which include polarization of the overall immune response and skewing of antibody epitopes [146]. Moreover, they can alter B cell receptor affinity and diversity, as has been shown for MF59 [147]. In this study, we aimed to characterize the effect of adjuvant on the antibody response to vaccinations with COBRA immunogens. This involved analysis of HA antibody epitopes, Th1 versus Th2 responses, and antibody functionality for the H1 subtype HA. We also assessed total and functional antibody titers elicited by the N1 subtype of NA of H1N1 viruses for the following adjuvants: AddaVax, AddaS03, CpG ODN 2395, and Alhydrogel. AddaVax and AddaS03, analogs of MF59 and AS03, respectively, are oil-in-water emulsions that enhance somatic hypermutation and affinity maturation [90,92]. In contrast, CpG is a TLR9 agonist [96], and Alhydrogel is an analog for alum [79], which may operate through the depot effect and adsorption of antigen, eliciting a Th2-skewed response. We found that adjuvants differentially alter total serum titers against the leading H1 COBRA HA candidate Y2 [122],

designed from human HA sequences from 2014 to 2016, and N1 COBRA NA candidate N1-I [139], designed from human, avian, and swine sequences from 1990 to 2015. Moreover, the epitope profiles on the A/California/04/2009 pandemic HA were similar across these adjuvants when used in immunizations with Y2. AddaS03 elicited high and broadly functional antibodies when combined with COBRAs in immunizations, suggesting that it may be an ideal adjuvant to supplement with the Y2 and N1-I antigens. Overall, these data suggest that the choice of adjuvant plays a significant role on antibody titers and functional potency following immunization with next-generation influenza vaccines.

Methods

Protein production.

Trimeric wild-type CA09 HA, Y2 COBRA HA, chimeric HA cH6/1, composed of the globular head region from H6N1 isolate A/mallard/Sweden/81/2002 and the HA stem region of the 2009 pandemic H1N1 isolate [148], and tetrameric N1-I NA ectodomains were expressed and purified in Expi293F cells following the manufacturer's protocol and as previously described [124]. Collected supernatants containing the HA or NA antigens were purified on a HisTrap Excel column following the manufacturer's recommended protocol. Eluted fractions were pooled and purified proteins were verified for integrity by probing with an anti-HIS tag antibody (Biolegend) as well as with subtype-specific mAbs via SDS-PAGE and Western blot.

Viruses

The viruses used, A/California/07/2009 (A/CA/09), A/Brisbane/02/2018 (A/BR/18), and A/Guangdong-Maonan/SWL1536/2019 (A/GM/19) were grown for two passages in MDCK

London (ATCC) cells. Viruses were titered by hemagglutination (HA) assays using 1% turkey blood.

Animals and vaccinations

All procedures were reviewed and approved by the University of Georgia Institutional Animal Care and Use Committee (IACUC). For the H1 HA study, ten six-to-eight week old male and female BALB/c mice (Charles River Laboratories) per group were immunized subcutaneously with 20 μg of Y2 COBRA HA, CA09 HA, or PBS adjuvanted with AddaVax, AddaS03, CpG ODN 2395, Alhydrogel (Invivogen), or PBS as a no adjuvant control. Mice were bled at 27 days post-prime for d27 serum, then immunized at 28 days post-prime with 20 μg of the antigen. At 56 days post-prime, animals were bled for d56 serum, then euthanized with Avertin.

For the N1-I NA study, five six-to-eight week old female BALB/c mice (Charles River Laboratories) per group were immunized intramuscularly with 6 μg of N1-I COBRA HA or PBS adjuvanted with AddaVax, AddaS03, CpG ODN 2395, Alhydrogel (Invivogen), or PBS as a no adjuvant control. Mice were bled at 27 days post-prime for d27 serum, then immunized at 28 days post-prime with 6 μg of the antigen. At 56 days post-prime, animals were bled for d56 serum, then euthanized with Avertin.

Enzyme-linked immunosorbent assays (ELISAs)

For total and chimeric H6/1 (cH6/1) IgG ELISAs, 384-well plates (Greiner Bio-One) were coated with antigen diluted to 2 μg/mL in phosphate-buffered saline (PBS) at 4 °C overnight. The plates were washed once with water and then blocked with 2% blocking buffer (PBS + 2% nonfat dry milk [Bio-Rad] + 2% goat serum + 0.05% Tween 20) for 1h at room temperature. The plates were washed three times with water, and 25 μL of diluted mouse serum was added. Sera were serially diluted three-fold in 1% blocking buffer from a 1:50 initial dilution for 12 total dilutions.

The plates were incubated at 37°C for 1h and then washed three times with water. Goat anti-mouse IgG Fc-AP secondary antibody (Southern Biotech), diluted 1:4000 in 1% blocking buffer (1:1 dilution of PBS and 2% blocking buffer), was added, and the plates were incubated at room temperature for 1h. The plates were then washed five times with PBS-T (PBS + 0.05% Tween 20). p-Nitrophenyl phosphate (PNPP) substrate, diluted in substrate buffer (1.0 M Tris + 0.5 mM MgCl2, pH 9.8) to 1 mg/mL, was added, and the plates were incubated for 1h and read at 405 nm on a BioTek plate reader. The area under the curve (AUC) value for each mouse group was determined using GraphPad Prism software using a baseline of 0.3 absorbance units at 405 nm and $\log_{10}$-transformed serum dilutions.

For Th1/Th2 ELISAs to determine the relative abundance of IgG subclasses to Y2 or CA09 HAs, a similar protocol was used for coating and blocking steps. After these steps, plates were washed three times with water, and serum was pooled across male or female mice for each group. Pooled serum was then serially diluted three-fold in 1% blocking buffer from a 1:50 dilution for 12 dilutions, and added to the ELISA plate and incubated at 37□C for 1h. Plates were washed three times with water, and goat anti-mouse IgG1, IgG2a, IgG2b, IgG2c, or IgG3 Fc-AP secondary antibody (Southern Biotech) diluted 1:4000 in 1% blocking buffer were added in separate wells and incubated for 1h at room temperature. The plates were then washed five times with PBS-T. PNPP substrate, diluted in substrate buffer to 1 mg/mL, was added and the plates were incubated for 1h and read at 405 nm on a BioTek plate reader. The AUC value for each mouse group was determined using GraphPad Prism software using a baseline of 0.3 absorbance units at 405 nm and $\log_{10}$-transformed serum dilutions.

Competition ELISAs

mAbs used in competition ELISAs were isolated and characterized previously [142]. 384-well plates (Greiner Bio-One) were coated with CA09 HA diluted to 2 μg/mL in PBS at 4°C overnight. Plates were washed once with water and blocked with 2% blocking buffer for 1h at room temperature. Plates were washed three times with water. Pooled mouse serum was three-fold serially diluted from a 1:10 dilution in 1% blocking buffer, then human monoclonal Abs (mAbs) specific for head and stem domain epitopes diluted in 1% blocking buffer were added in a 1:1 ratio. Alternatively, 1% blocking buffer was added to mAbs in a 1:1 ratio for the mAb only control. 25 μL of the serum/mAb or the 1% block/mAb mixture were added to the plate and incubated at 37°C for 1h. Plates were then washed three times with water, and 25 μL of goat anti-human IgG Fc, multi species SP ads-AP (Southern Biotech) diluted to 1:4000 in 1% blocking buffer was added, and then incubated for 1h. Plates were washed five times with PBS-T, then PNPP substrate diluted to 1 mg/mL in substrate buffer was added, incubated for 1 hr, and read at 405 nm on a BioTek plate reader. Competition was calculated as the ratio of signal from a given serum dilution with mAb to the signal of the corresponding dilution in the mAb only control. Low competition was defined as a ratio between 0 and <0.330, intermediate competition >=0.330 and <0.660, and high competition between >=0.660 and 1.

Hemagglutination assays (HAs)

50 μL of virus was diluted two-fold in PBS from a 1:2 dilution for 50 □L total for eleven dilutions. Turkey whole blood in Alsevers' solution (Lampire) was washed three times with PBS and diluted to a 1.0% concentration in PBS. 50 μL of these 1.0% turkey red blood cells were added per well. Plates were tilted for 30 sec and read 45 min after the addition of 1.0% turkey red

blood cells. The well with the highest virus dilution that did not drip was determined to be the HA titer.

Hemagglutination inhibition assays (HAIs)

Serum was treated with receptor-destroying enzyme II (RDE II, Denka Seiken) to remove background hemagglutination activity. Briefly, one volume of serum was added to three volumes of RDE II in PBS and incubated at 37 °C overnight. The following day, the treated serum was heat-inactivated at 56 °C for 45 min, allowed to cool to room temperature, then six volumes of PBS were added. Influenza viruses were titered to eight HAUs (hemagglutination units) per mL. 50 μL of RDE-treated serum were added to the first well of a 96-well V-bottom plate (Thermo Scientific) and diluted two-fold in PBS for 25 μL total for eleven dilutions. The virus, titered to eight HAUs per mL, was added in a 1:1 ratio to each serum dilution, and each well was mixed and incubated for 20 min at room temperature. Following this, 50 μL of 1.0% turkey red blood cells (Lampire) were added per well. Plates were read 45 min after the addition of 1.0% turkey red blood cells. The last well with the highest serum dilution that dripped was determined to be the HAI titer. Although the WHO and the European Committee for Medicinal Products have defined a 1:40 titer to be seroprotective in humans [149], a more stringent 1:80 titer was defined to be seroprotective, similar to the cutoff determined previously [53].

Enzyme-linked lectin assays (ELLAs)

To determine A/California/07/2009 NA activity, high binding flat-bottom 96-well plates (Greiner Bio-One) were coated with 100 μL of 25 μg/ml fetuin (Sigma-Aldrich) at 4 °C overnight. Influenza virus A/California/07/2009 was diluted in sample diluent (PBS, 1% BSA, 0.5% Tween 20) to an initial dilution of 1:10 and then serially diluted 2-fold for 11 dilutions. A negative-control column was included containing 100 μL of only sample diluent. Fetuin plates were washed three

times with PBS-T (PBS + 0.05% Tween 20). 50 µL of serially diluted virus were added to the fetuin-coated plate containing 50 µL of sample diluent in duplicate. Plates were incubated for 18 hrs at 37 °C and 5% CO_2. After incubation, plates were washed six times in PBS-T, and 100 µL of peanut agglutinin-HRPO (Sigma-Aldrich) diluted 1,000-fold in conjugate diluent (PBS, 1% BSA) was added. Plates were incubated at RT for 2 hrs. Plates were washed three times in PBS-T, and 100 µL (500 µg/ml) of o-phenylenediamine dihydrochloride (OPD) (Sigma-Aldrich) in phosphate-citrate buffer (Sigma-Aldrich) was added to the plates. Plates were incubated in the dark for 10 min at RT. The reaction was stopped with 100 µL of 1 N sulfuric acid. The absorbance was read at 490 nm on a BioTek plate reader. The dilution of the virus needed to achieve 90 to 95% NA activity was determined and used for subsequent NA inhibition ELLAs.

Neuraminidase inhibition assays (NAIs)

Mouse sera was heat inactivated at 56 °C for 1 hr. Serum was serially diluted 5-fold in sample diluent from 1:100 initial dilution for 10 dilutions. A negative-control column (no serum or virus) was included containing 100 µL of only sample diluent. A virus only column was also included. 50 µL of duplicate dilutions were added to fetuin plates. 50 µL of the virus diluted to 90 to 95% NA activity in sample diluent was added to the plate. Plates were incubated for 18h at 37°C and 5% CO_2, after which they were processed as described above with the ELLAs. Endpoint titers were identified as the highest serum dilution that resulted in at least 50% inhibition of the maximum signal.

Quantification and statistical analysis

One-way ANOVA was used to compare between vaccination groups using GraphPad Prism 9 software (GraphPad, San Diego, CA, USA). Statistical significance was defined as follows: *, p<=0.05; **, p<=0.01; ***, p<=0.001; ****, p<=0.0001.

Results

Adjuvanted vaccination with Y2 alters serum antibody titers to the Y2 COBRA HA

To determine the serum IgG response to adjuvanted wild-type 2009 pandemic A/California/04/2009 (CA09) HA or COBRA HA vaccination, we used a prime-boost regimen in mice **(Figure 4.1A)**. Animals were immunized with either the Y2 COBRA HA or the CA09 HA. Four adjuvants were used: AddaVax, AddaS03, CpG ODN 2395, Alhydrogel, or no adjuvant as a control. We then evaluated titers against the homologous immunizing antigen by ELISA. At 27 days post-vaccination, we found that AddaS03 elicited the highest antibody titers to their respective immunizing antigens, followed by Alhydrogel, AddaVax, and CpG **(Figure 4.1B)**. This pattern was consistent across both Y2 and CA09 immunizations. This trend was conserved at 56 days post-vaccination after a single boost, where AddaS03 and Alhydrogel elicited the highest titers. Notably, we found that the no adjuvant control elicited minimal titers for the CA09 HA after two immunizations whereas all adjuvanted groups showed detectable serum IgG titers. In comparison, the no adjuvant control for the Y2-immunized animals elicited significant titers after a prime and a boost, suggesting Y2 is more immunogenic in the BALB/c mouse background. As expected, adjuvanted groups generally showed improved titers relative to the no adjuvant control, and no titers were observed for PBS-immunized animals. Therefore, we found that formulation of the HA antigen with various adjuvants elicited elevated levels of serum IgG relative to the no adjuvant control, and AddaS03 was superior in this respect.

Adjuvants can alter the overall immune profile following immunization, biasing it towards a Th1, Th2, or a balanced Th1/Th2 response [117]. To evaluate this effect in mice, we measured the relative concentrations of IgG subclasses within the serum **(Figure 4.2)**. We pooled male and

female mouse serum from each group, and evaluated terminal titers against the homologous HA for subclasses IgG1, IgG2a, IgG2b, IgG2c, and IgG3. We found that the choice of adjuvant alters the Th1/Th2 ratio, suggesting changes within the overall immune profile, with most adjuvants eliciting primarily a Th2-skewed response. Overall, trends were similar between Y2 and CA09 HA immunizations across adjuvants. AddaVax elicited a Th2-biased response, where most serum IgG antibodies were of the IgG1 subclass, and a minority were of the IgG2b subclass. AddaS03 also elicited both IgG1 and IgG2b antibodies, but IgG1 titers were nonetheless elevated compared to IgG2b. CpG was associated with a balanced response, with both IgG1 and IgG2 antibodies observed in similar ratios, albeit at lower overall titers. Expectedly, Alhydrogel, a known Th2-skewing adjuvant, elicited a Th2-biased response with most antibodies being of the IgG1 subclass. For the Y2 no adjuvant control, we detected IgG1 antibodies only, which is consistent with the inherent Th2-skewed response seen with the BALB/c background.

Serum antibody epitopes are similar between adjuvants following Y2 immunization

In addition to total serum IgG responses to the immunizing HA, we also determined the serum IgG response to the H1 HA stem domain **(Figure 4.3)**. The stem domain is more conserved than the head domain across influenza strains, and serves as a target for some universal vaccine candidates, such as the chimeric HA (cHA) approach [67]. To evaluate antibodies against this domain, we evaluated binding to the cH6/1 cHA construct [148,150]. The cH6/1 cHA contains an exotic H6 subtype head genetically fused to the H1 subtype CA09 HA stem. Four weeks after boost, we found that there were significant titers for all adjuvanted groups for both Y2 and CA09 HA immunizations. The differences between adjuvants closely mirrored those for serum IgG titers against the Y2 and CA09 HA antigens. AddaS03 elicited the highest cH6/1-binding IgG responses, followed by Alhydrogel and AddaVax, with CpG eliciting the lowest titers of all adjuvanted

groups. For Y2 immunizations, we detected antibodies against the cH6/1 HA as well, potentially suggesting that stem antibodies may be elicited. We also compared titers between Y2- and CA09 HA-immunized animals against the cH6/1, finding statistically increased titers for Y2 relative to CA09 HA for the CpG-adjuvanted and no adjuvant groups. This implied that to some extent, Y2 is more immunogenic than the CA09 HA. Of note, it is possible that antibodies targeting non-HA-specific regions, such as the trimerization domain or the His-tag, could be contributing to this antibody response. Nonetheless, the observation of cH6/1 HA-specific serum antibodies may suggest that the adjuvants evaluated here may amplify stem-specific responses to some extent.

To assess the specific epitopes targeted by serum from adjuvanted Y2 immunizations, we performed competition ELISAs against the wild-type CA09 HA **(Figure 4.4)**. We assessed the competition of pooled terminal serum against a panel of previously characterized human monoclonal antibodies (mAbs) that bind both the head and stem domains, including the recently characterized anchor epitope [142]. We did not see any competition for the CA09 HA-immunized no adjuvant control, as expected due to minimal serum titers after a prime and boost. Otherwise, however, we found similar trends between Y2- **(Figure 4.4A)** and CA09 HA-immunized groups **(Figure 4.4B)**. For most adjuvanted groups, a large proportion of head domain-binding antibodies competed with human mAb CA09-16, which binds near the RBS. This was most pronounced in AddaS03- and Alhydrogel-adjuvanted mice. For the Y2 no adjuvant control, we also saw moderate competition of serum with this antibody. In addition, we saw some competition from the sera of all groups with CA09-40, which also binds near the RBS. Lateral patch-binding serum antibodies were also detected in Y2- and CA09 HA-immunized mouse sera as seen by competition with mAb CA09-28, again being most pronounced for AddaS03- and Alhydrogel-adjuvanted groups. Only low amounts of these antibodies appeared in the no adjuvant Y2 only control. In addition to head-

specific serum antibodies, those targeting the stem were also seen for both the central stem and anchor epitopes. Overall, for CA09 HA-immunized groups, all adjuvanted groups showed low to intermediate competition with the central stem-binding antibody CR6261, and either similar or slightly higher levels of competition with the P1-05 anchor epitope-binding antibody. Similar results were seen with Y2 HA-immunized mice, where stem-binding antibodies appeared to be immunosubdominant to head-binding antibodies. Again, the extent of anchor-binding antibodies were either similar to, or slightly higher than, those of central stem-binding antibodies, as seen for the AddaS03- and AddaVax-adjuvanted groups. The Y2 no adjuvant group showed similar, if not slightly lower, competition with these stem epitopes than adjuvanted groups. In general, the epitopes targeted between the head and stem domains were similar across all adjuvanted groups, despite differences in total serum titers. In addition, RBS-binding antibodies, and to a lower extent, anchor epitope-binding antibodies, were generally enhanced by the addition of adjuvant.

Adjuvants confer altered HAI antibody breadth following Y2 immunization

To determine whether the addition of adjuvant could alter the functionality of serum antibodies, we performed HAI assays against a panel of recent 2009 pandemic-like H1N1 viruses **(Figure 4.5)**. We saw similar trends between HAI titers and ELISA serum IgG titers across adjuvants, where AddaS03 elicited the highest titers, followed by AddaVax and Alhydrogel, with CpG generally inducing the lowest titers of adjuvanted groups. All groups developed seroprotective titers (HAI titer >1:80) against the A/California/07/2009 (A/CA/09) virus for Y2-immunized animals **(Figure 4.5A)**. In the Y2 no adjuvant control, some individuals developed higher HAI titers against A/CA/09 than in adjuvanted groups, which may reflect the relatively high immunogenicity of Y2. In contrast, lower but seroprotective titers were observed only with adjuvanted groups for the CA09-immunized mice, but not with the non-adjuvanted CA09-

immunized animals against A/CA/09 **(Figure 4.5D)**. With respect to antibody breadth, it appeared that Y2 immunization with AddaS03 elicited the highest HAI breadth against all three viruses, where titers significantly above 1:80 were observed against A/Brisbane/02/2018 (A/BR/18) and A/Guangdong-Maonan/SWL1536/2019 (A/GM/19) **(Figure 4.5B, C)**. Y2 immunization adjuvanted with Alhydrogel also appeared to elicit statistically significantly increased titers against A/BR/18 relative to the no adjuvant control **(Figure 4.5B)**. Y2+CpG and Y2+AddaVax, while eliciting HAI titers above the threshold for seroprotection against A/GM/19, overall showed lower titers compared to the Y2+AddaS03 adjuvant group for this virus **(Figure 4.5C)**. Of CA09-immunized mice, those receiving AddaS03 adjuvant developed the highest HAI titers against the A/BR/18 and A/GM/19 viruses **(Figure 4.5E, F)**. In addition, Alhydrogel-adjuvanted CA09 immunization appeared to confer broad HAI activity against all of the H1N1 viruses relative to the no adjuvant control **(Figure 4.5D-F)**.

Adjuvanted vaccination with the N1-I COBRA elicits differential serum IgG titers and NAI titers against a 2009 pandemic virus

Although HA has been the primary focus of universal influenza vaccines, neuraminidase (NA) has been shown to elicit protection as well [151]. Likewise, we assessed the effect of adjuvant on serum IgG titers against the N1-I COBRA, an NA-based universal vaccine candidate [139] **(Figure 4.6A)**. The same panel of adjuvants were used in a prime-boost regimen with N1-I. At 27 days following prime, minimal titers were observed for N1-I-immunized mice, and none for the PBS control group. Following a boost, however, serum IgG titers mirrored those seen with Y2 immunizations, although differences between adjuvants were less pronounced **(Figure 4.6B)**. AddaS03 elicited the highest serum IgG titers, whereas AddaVax, Alhydrogel, and CpG-elicited titers were somewhat lower. N1-I vaccination without adjuvant elicited notably lower titers than

those with adjuvant, as expected. Overall, these data suggest that general trends between these adjuvants may be similar regardless of whether the HA or NA COBRA is used during immunization. Again, supplementing with AddaS03 adjuvant elicited the highest titers of all adjuvanted groups.

NAI assays were performed to assess the functionality of serum antibodies following N1-I vaccination against the A/CA/09 virus **(Figure 4.6C)**. We found that NAI titers were highest for AddaS03 and AddaVax, followed by Alhydrogel and CpG. Again, these trends are similar to those seen in ELISAs. These results imply that serum antibodies elicited by N1-I are functional and can decrease NA enzymatic activity. Oil-in-water emulsion adjuvants appeared to be more effective than CpG or Alhydrogel in inducing these NA-inhibitory antibodies.

Discussion

In this study, we assessed the effect of adjuvant on serum antibody responses against both a HA COBRA, Y2, and a NA COBRA, N1-I, against H1N1 viruses. We found that there exists a general trend in total serum titers across both of these antigens for the panel of adjuvants tested. Overall, AddaS03 appeared to elicit the highest IgG titers against both Y2 and N1-I, as well as the broadest and highest functional serum antibody titers as assessed by HAI and NAI, respectively.

Y2 has been shown to elicit robust humoral responses in several animal models and is protective against challenges with recent H1N1 isolates [122]. In our study, we found that the addition of adjuvant was able to increase overall serum IgG titers against this COBRA HA, as expected. However, the degree to which this increased varied based on the adjuvant used. Y2, when combined with AddaS03 and Alhydrogel, appeared to elicit the highest titers, which were apparent following a single vaccination. AddaVax and CpG also elicited significant titers, but

differences between these groups and the no adjuvant control did not reach statistical significance. We saw similar trends when the wild-type CA09 HA was adjuvanted, again being highest for the AddaS03 and Alhydrogel groups, followed by AddaVax and CpG. We did not see significant titers at d56 for the non-adjuvanted CA09 HA control in contrast to the Y2 non-adjuvanted control, which may suggest that COBRA HAs possess enhanced immunogenicity relative to wild-type HAs.

We also observed the induction of potential stem domain-specific antibodies, as significant serum IgG titers against the cH6/1 HA were seen following Y2 immunization. Trends between adjuvants were relatively similar to those observed with the homologous immunizing HA, where the addition of AddaS03 enhanced serum titers the most of all adjuvanted groups. We also tested individual serum antibody epitopes by competition ELISAs with human mAbs. These experiments suggested that the addition of adjuvant may skew serum epitopes primarily towards head domain epitopes and somewhat to stem domain epitopes. We observed significant competition with the RBS-specific CA09-16 mAb for all adjuvant groups, as well as to the CA09-28 lateral patch epitope, albeit to a lower extent. Additionally, AddaVax- and CpG-adjuvanted groups showed somewhat similar epitope profiles to one another, characterized by moderate competition with another RBS-proximal head-binding mAb, CA09-40, and CA09-16. All adjuvanted groups showed some competition with CA09-38, a previously uncharacterized, non-neutralizing head domain-specific antibody. For most adjuvanted groups, some competition was seen with the P1-05 anchor epitope mAb, which was either similar to or somewhat higher than that seen with the CR6261 central stem mAb. These might reflect the frequency of stem-binding antibodies, where anchor epitope mAbs generally are more frequent than central stem mAbs, although this has been shown for human but not mouse models [138]. The Y2+no adjuvant group, however, did appear

to differ from all adjuvanted groups, showing no competition with CA09-38, and moderate competition with head-binding mAbs. The overall similarity in targeted epitopes across adjuvant groups may suggest a more general mode of enhancing the antibody response between them without much change to the overall frequencies of serum epitopes.

The functionality of serum antibodies following Y2 vaccination were assessed by HAI against a panel of recent H1N1 viruses. Whereas those against A/CA/09 were relatively high for all groups, they generally decreased somewhat against the A/BR/18 and A/GM/19 viruses. AddaS03 elicited the highest and broadest HAI activity, followed by Alhydrogel, and AddaVax and CpG. Median titers remained above 1:80, our defined threshold for seroprotection, for all adjuvanted groups with Y2 against all viruses, whereas it dropped slightly below this threshold for the non-adjuvanted Y2 group for A/GM/19. The gradual decrease in relative HAI titers with more recent H1N1 viruses might reflect the effects of antigenic drift that permit some escape from antibodies against earlier 2009 pandemic-like viruses. Overall, with the addition of adjuvant, however, the degree of functional HAI-active antibodies appears to be able to overcome this effect.

The NA protein is more conserved than the HA protein across influenza viruses, making it an attractive candidate for a universal vaccine. Likewise, we assessed antibody responses to an N1 subtype NA COBRA, N1-I, when combined with adjuvant. Following a prime-boost regimen, titers followed the same general trend as for Y2, where AddaS03 elicited the highest titers against N1-I, followed by AddaVax, then Alhydrogel and CpG. Differences between adjuvant groups, however, were not as pronounced as those seen with Y2, possibly because of the immunosubdominant nature of NA to HA [19]. Nonetheless, the trends observed between adjuvants persisted in NAI assays against the A/CA/09 2009 pandemic virus, with animals immunized with N1-I+AddaS03 showing significantly increased activity relative to the non-

adjuvanted control. Interestingly, these trends between adjuvants were consistent between subcutaneous and intramuscular immunization between the H1 and N1 studies. It may be of interest to perform NAIs against more recent H1N1 isolates following N1-I immunization and assess whether activity decreases like that seen for HAIs against the A/BR/18 and A/GM/19 viruses. In general, these suggest that AddaS03 is the most efficacious adjuvant with respect to total IgG titers and NAI-based functionality.

Adjuvants are an integral component of several vaccines, including currently approved influenza vaccines like FluAd and Pandemrix [79]. These are tailored towards higher-risk populations, where the action of adjuvant is needed to induce a sufficiently protective immune response. In the development of universal COBRA vaccines, the use of adjuvant is likely needed to enhance the immune response. The selection of adjuvant has been known to alter antibody titers and the corresponding protection that is afforded. Therefore, in this study, we assayed a number of adjuvants that act through distinct mechanisms. We found that AddaS03 affords both the highest binding and functional antibody titers following Y2 and N1-I immunization. In addition, it elicited significant serum antibodies against the RBS epitope and the stem anchor epitope relative to other adjuvants. AddaS03, an analog of AS03, contains a number of immune-stimulating components that might prime the increased antibody response observed in this study. This includes DL-α-tocopherol, which has been shown to strengthen the innate immune response, and, consequently, the cell-mediated and humoral responses [152]. This adjuvant has also been associated with enhanced somatic hypermutation and affinity maturation that could account for the enhanced functional breadth following Y2 or N1-I immunization [153]. Importantly, in our study we did not combine the Y2 and N1-I COBRAs in a single immunization, which may be of interest to investigate the effects of adjuvant in the context of HA and NA immunodominance. Nevertheless,

our studies provide data on polyclonal antibody breadth, epitopes, and functionality that can inform adjuvant selection for COBRA candidates as they enter clinical studies.

Figures

A

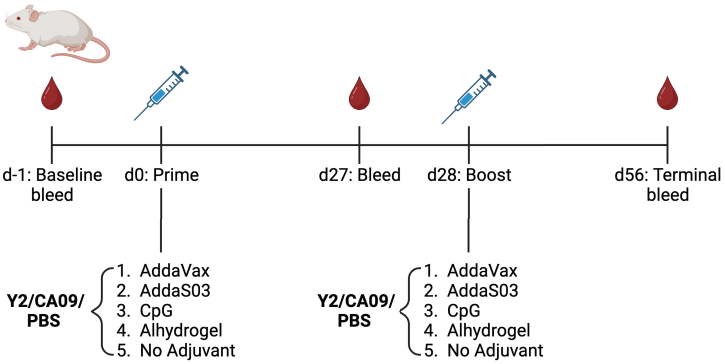

B

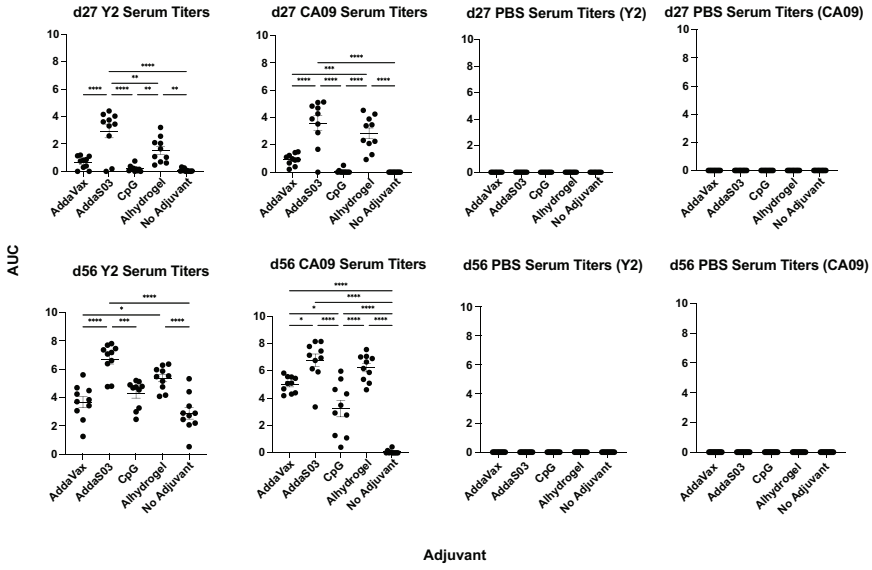

Figure 4.1. H1 HA immunization schedule and serum IgG titers after adjuvanted vaccination with Y2 and CA09 HAs. (A) Overall immunization scheme of the H1 HA study. Time points for bleeds and vaccinations are shown. (B) Titers of IgG antibodies in sera from vaccinated mice, determined by ELISA, are shown for 27 days post-prime after one immunization (d27, top) for all groups against the homologous immunizing HA. Titers for both HAs are shown for the PBS immunization control. Those at 56 days post-prime (28 days post-boost) are shown on the bottom. Titers are represented as area under the curve (AUC) values, where a minimum baseline

absorbance at 405 nm of 0.3 was considered a positive binding signal. *, p<=0.05; **, p<=0.01; ***, p<=0.001; ****, p<=0.0001. One-way ANOVA was used for statistical comparisons between groups.

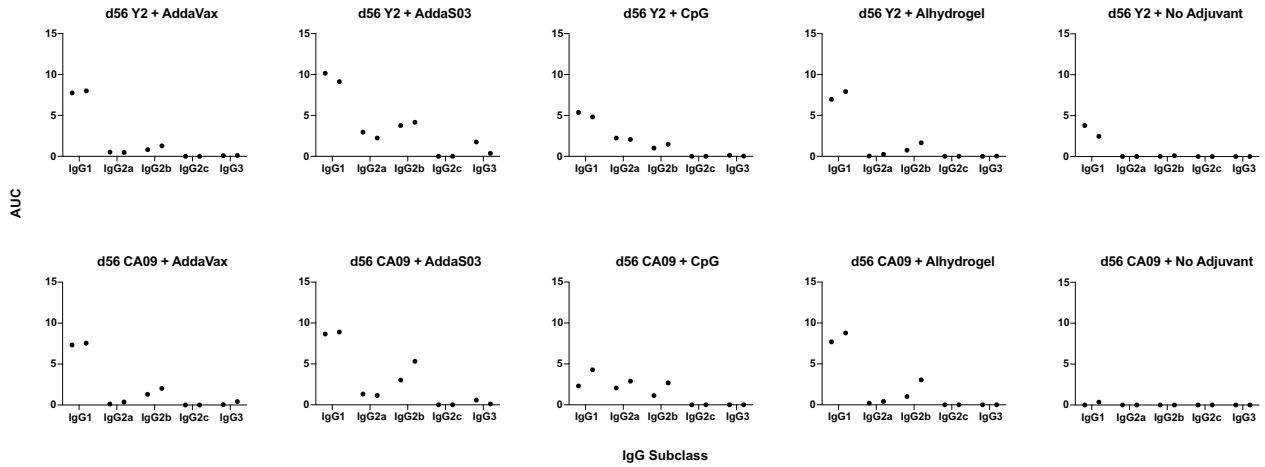

Figure 4.2. Th1/Th2 ELISAs at d56 after adjuvanted vaccination with Y2 and CA09 HAs. IgG subclass-specific serum titers, determined by ELISA, against the homologous Y2 or CA09 HA used for vaccination are shown. Pooled serum titers for male and female mice are shown. The left point for each IgG subclass corresponds to male mice serum titers and the right point to female mouse serum titers. A minimum baseline absorbance at 405 nm of 0.3 was considered a positive binding signal. *, p<=0.05; **, p<=0.01; ***, p<=0.001; ****, p<=0.0001. One-way ANOVA was used for statistical comparisons between groups.

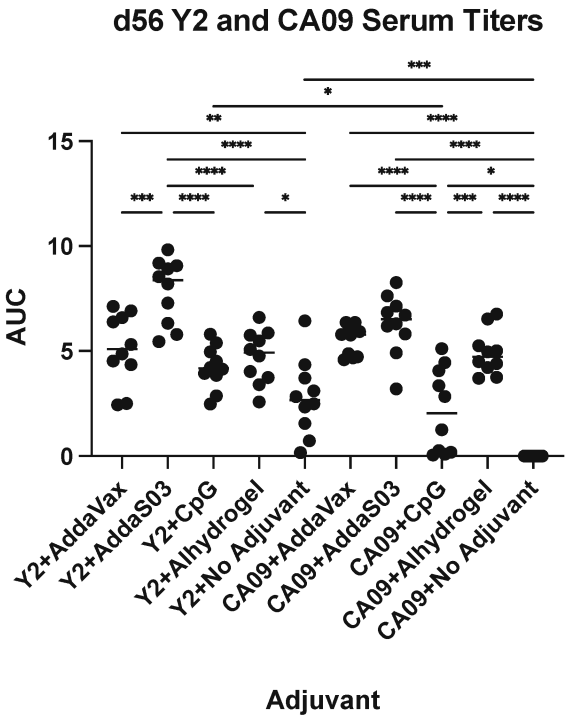

Figure 4.3. cH6/1 HA IgG titers at d56 after adjuvanted vaccination with Y2 and CA09 HAs. Serum IgG titers, determined by ELISA, are shown as AUC values for both Y2- and CA09 HA-immunized mouse groups. A minimum baseline absorbance at 405 nm of 0.3 was considered a positive binding signal. *, $p \leq 0.05$; **, $p \leq 0.01$; ***, $p \leq 0.001$; ****, $p \leq 0.0001$. One-way ANOVA was used for statistical comparisons between groups.

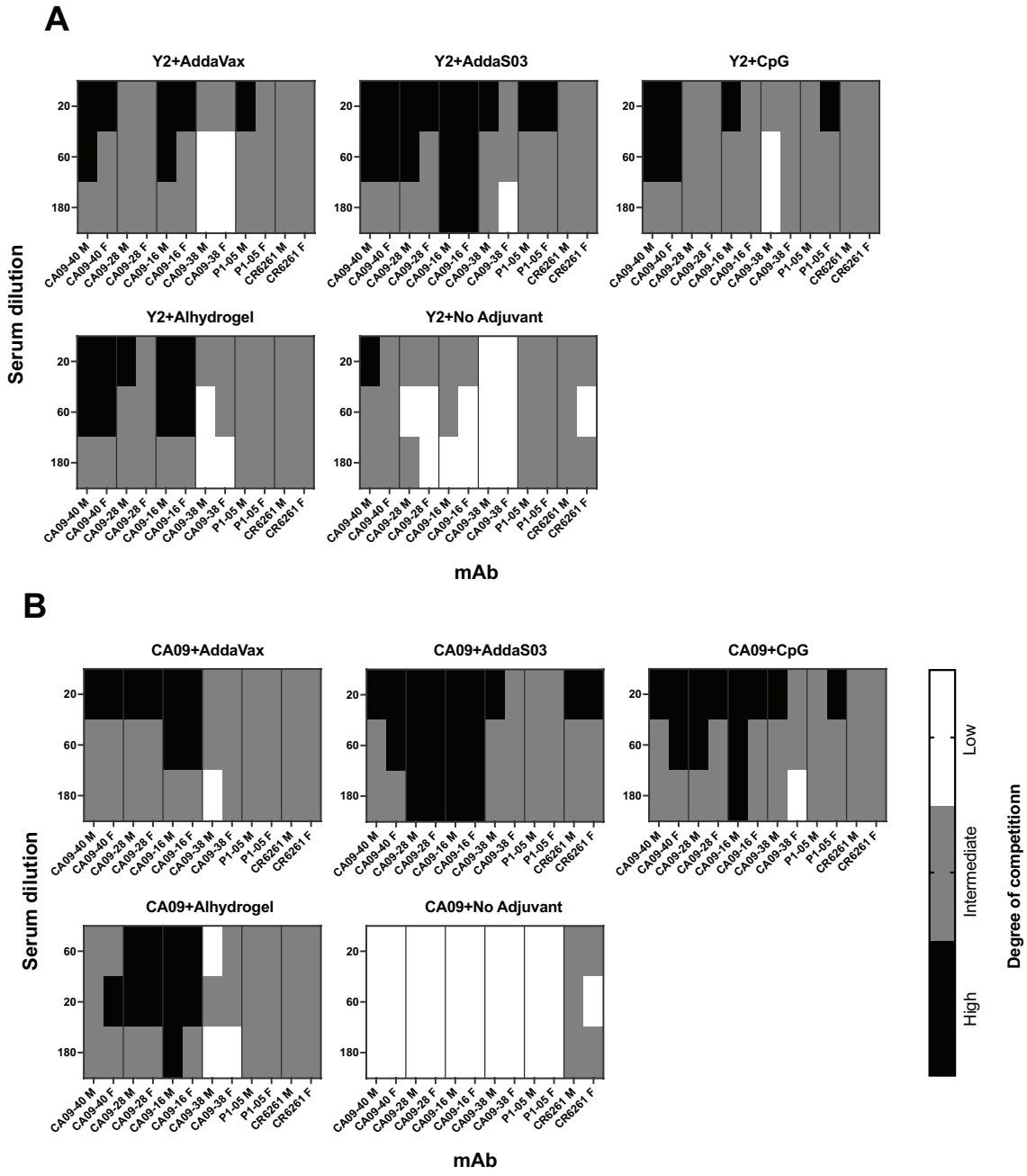

Figure 4.4. Epitope mapping of d56 sera against the CA09 HA from Y2- and CA09 HA-immunized mice. Competition ELISAs were used to determine the HA epitopes bound by mouse serum for Y2- and CA09 HA-immunized mice. Sera from pooled mice were competed with human mAbs specific against distinct HA head and stem epitopes. The degree of competition for serially diluted mouse sera with the indicated human mAbs is shown as a heat map for final serum dilutions

of 1:20, 1:60, and 1:180 for these groups for (A) Y2-immunized mice and (B) CA09-immunized mice. M, male pooled serum; F, female pooled serum.

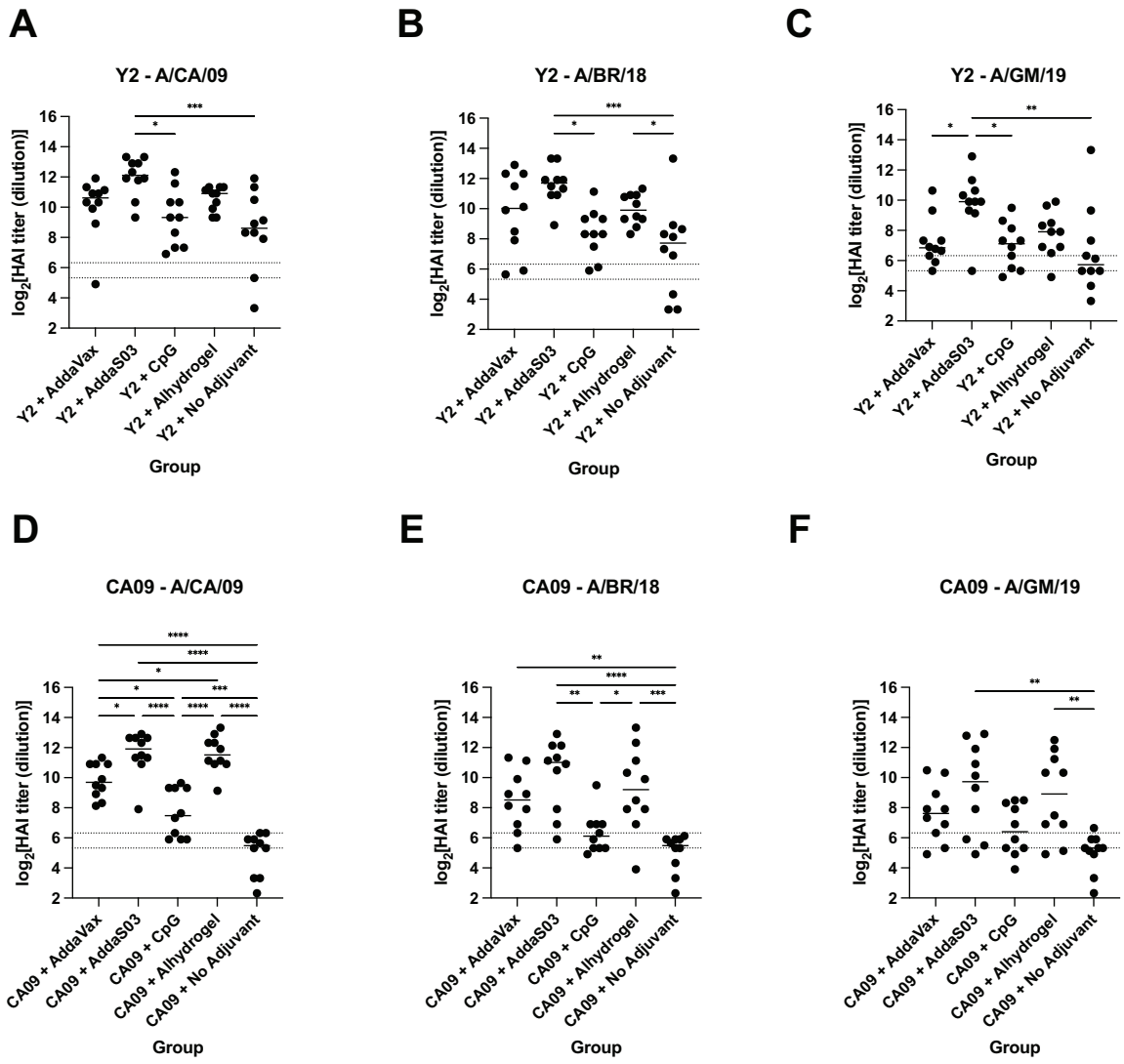

Figure 4.5. HAI titers of d56 sera from Y2- and CA09 HA-immunized mice. HAI titers against a panel of recent H1N1 viruses are shown for (A-C) Y2- and (D-F) CA09-immunized animals. Titers are represented as log_2-transformed reciprocal dilutions. The lower dotted line represents a titer of 1:40 and the upper line a titer of 1:80, which has been correlated with seroprotection in humans. A/CA/09, A/California/07/2009; A/BR/18, A/Brisbane/02/2018; A/GM/19, A/Guangdong-Maonan/SWL1536/2019.

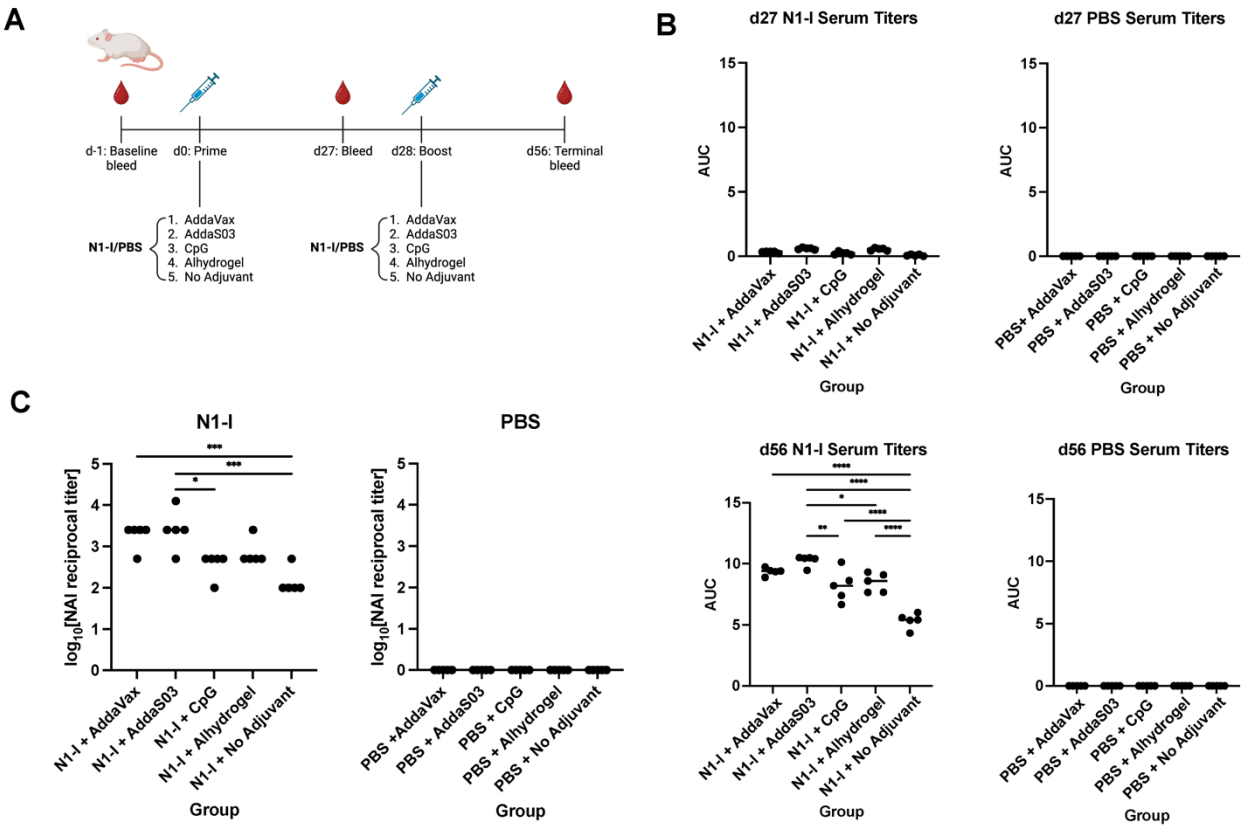

Figure 4.6. N1-I NA immunization schedule, serum IgG titers, and NAI titers after vaccination. (A) Immunization scheme of the N1-I NA study. (B) d27 and d56 serum IgG titers, determined by ELISA, against the N1-I NA COBRA. Titers are shown as AUC. (C) Terminal NAI titers after vaccination against A/CA/09, shown as log_{10}-transformed reciprocal dilutions. NAI titers were determined as the serum dilution that provided 50% inhibition of NA activity. A minimum baseline absorbance at 405 nm of 0.3 was considered a positive binding signal. *, p<=0.05; **, p<=0.01; ***, p<=0.001; ****, p<=0.0001. One-way ANOVA was used for statistical comparisons between groups.

CHAPTER 5

ANTIBODY BREADTH MEDIATED BY NANOPARTICLE PRESENTATION OF COMPUTATIONALLY OPTIMIZED HEMAGGLUTININS[4]

[4]Nagashima, Kaito. To be submitted to *Journal of Virology*.

Abstract

Influenza A viruses (IAVs) pose a significant health burden every year. The current countermeasure against influenza infection, the seasonal vaccine, only offers strain-specific antibody protection for a given season through targeting of the predominant hemagglutinin (HA) glycoprotein. To enhance antibody-based breadth to multiple strains and protection across multiple years, several vaccine approaches have been developed. One approach, termed COBRA, for computationally optimized broadly reactive antigen, employs consensus building of wild-type HAs from a given antigenic space to generate a novel COBRA HA antigen that captures the antigenic features of these HAs to multiple strains of the same subtype. Another approach has involved the use of a two-component protein nanoparticle (NP) to present the HA protein based on the mixture of HA-I53_dn5B and I53_dn5A protein components to generate NPs presenting 20 HA trimers in a multimeric manner, which could expand antibody breadth to non-seasonal vaccine subtypes. To investigate if antibody breadth from a single COBRA HA could be expanded to multiple subtypes with the use of this two-component NP platform, we presented the lead H1 and H3 subtype COBRA vaccine candidates Y2 and NG2 on this system in a homotypic format. We found that doing so could elicit functional breadth against H1 subtype IAVs for the H3 COBRA NG2, but not for the H1 COBRA Y2, suggesting that this combination of next-generation vaccine immunogens and platforms could enhance targeting towards cross-group epitopes.

Introduction

Influenza A viruses pose a major health burden worldwide [1]. Current seasonal vaccines offer only limited protection through targeting of antibody responses against the major surface glycoprotein, hemagglutinin (HA) using predictions of circulating strains [1,3]. Due to significant antigenic variation in the HA protein across multiple viral strains, antibody-mediated protection from the seasonal vaccine is typically strain-specific. Antibody responses can generally be targeted to two domains of HA, the relatively variable head domain and the conserved stem domain [117]. Within the head domain, the strain-specific antigenic sites Sa, Sb, Ca1, Ca2, and Cb for the H1 subtype and A, B, C, D, and E for the H3 subtype have been characterized [20,21,117]. In addition, a number of conserved epitopes have been also identified such as the receptor-binding site (RBS), the lateral patch, and the intratrimer epitope which are the targets of broadly reactive monoclonal antibodies (mAbs) [45,46,136,154]. The stem domain contains the central stem and anchor epitopes on the middle and bottom of the HA [59,138,155]. The strain-specific response elicited by the seasonal vaccine is due to targeting primarily against the variable head domain and away from the conserved stem.

Nanoparticle (NP) presentation of viral antigens has been previously shown to enhance the antibody response against viral fusion proteins including the HA protein. Several NP platforms have been used, such as the protein-based *Helicobacter pylori* ferritin-based system to present the influenza HA [156,157], the SpyTag-SpyCatcher system [158], as well as computationally designed protein scaffolds [6]. A report demonstrating the use of a computationally designed protein platform involved the use of a two-component scaffold to present the influenza HA protein from the 2017-2018 seasonal vaccine for the H1, H3, influenza B virus (IBV) Victoria and Yamagata lineage HAs, consisting of components HA-I53_dn5B and I53_dn5A which self-

assemble into nanoparticles presenting 20 HA trimers when mixed. In mouse, ferret, and non-human primate animal models, this NP immunogen could elicit breadth to non-vaccine subtype H5, H6, H7, and H10 subtypes [6].

Given that this approach could provide heterosubtypic antibody breadth non-vaccine subtypes after multivalent presentation with H1, H3, and influenza B HAs, we reasoned that the use of COBRA HAs with this system could similarly induce broad antibody breadth [6]. Therefore, in this work we generated homotypic nanoparticle constructs presenting a single subtype H1 COBRA, Y2 [122], or a H3 COBRA HA, NG2 [159], based on this two-component scaffold and assessed their immunogenicity and capacity to enhance antibody breadth relative to a soluble COBRA recombinant HA trimer (rHA) control. We found that for the Y2 NP vaccination, no increase in antibody breadth to the H3 subtype was found. In contrast, a NG2 H3 NP could elicit cross-group, hemagglutination inhibition (HAI)-active antibodies against the H1 subtype of influenza A viruses, likely targeting conserved epitopes on the head domain and receptor-binding site (RBS) of the HA protein that are conserved across group 1 and group 2 viruses. Overall, this work suggests that the use of a nanoparticle platform to present a next-generation influenza vaccine candidate can further augment antibody breadth.

Methods

Nanoparticle generation

Plasmids encoding the Y2 and NG2 COBRA HA sequences possessing a Y98F mutation were fused to the I53_dn5B scaffold protein to generate the Y2-I53_dn5B and NG2-I53_dn5B components in the pcDNA3.1(+) vector. In addition, a plasmid encoding the I53_dn5B protein, lacking a HA fusion, was also generated in the pET-28a(+) vector. Expi293F cell cultures were

transfected with each of the HA-I53_dn5B (Y2-I53_dn5B or NG2-I53_dn5B) plasmids for protein expression, followed by protein purification at 5-7 days post-transfection on a HisTrap Excel column (GE Healthcare). The I53_dn5A-encoding plasmid was transformed into competent BL21 cells, which were then grown in LB+kanamycin medium at 37°C until the OD_{600} reached a value between 0.5 and 0.8. Protein expression was then induced following the addition of 100 μM IPTG, and BL21 cells were allowed to grow overnight at 25°C. The following day, BL21 cells were centrifuged and resuspended in lysis buffer (20 mM Tris, pH=8.0, 200 mM NaCl), followed by sonication to lyse cells. The cell lysate was centrifuged to remove cell debris and the clarified supernatant was run through a HisTrap Excel column (GE Healthcare) to purify the I53_dn5A protein.

Following HA-I53_dn5B, I53_dn5B, and I53_dn5A protein purification, the components were mixed in a 1:1 molar ratio and incubated at 25°C for 30 min to allow for nanoparticle assembly. The mixture was then run on the Superdex 200 10/300 GL or the Superose 6 Increase 10/30 GL size exclusion column (GE Healthcare) to separate intact nanoparticles from unassembled components using 20 mM Tris, pH=7.5/100 mM NaCl buffer. The nanoparticle constructs were then used in ELISAs to validate their antigenicity.

Negative-stain electron microscopy (nsEM)

To evaluate the structural features of the Y2 NP, NG2 NP, and the NP core, 5 μL of 50 μg/mL of purified NPs from SEC were added to glow-discharged, carbon-coated copper grids (Electron Microscopy Sciences) for 3 min. The grid was then blotted, and washed in water twice prior to staining with Nano-W (Nanoprobes) once, blotting, then staining with Nano-W (Nanoprobes) for 1.5 min. Micrographs were acquired using a JEOL JEM1011 transmission electron microscope equipped with a high-contrast 2K-2K AMT midmount digital camera.

Animal experiments

4 female mice/group of DBA/2J mice (Jackson Laboratories) were used for immunizations with the Y2 NP in a prime-boost-boost regimen. Briefly, mice were immunized with 3 μg equivalents of the HA protein every four weeks, either in the Y2 rHA soluble format, the Y2 NP, and the NP core through intramuscular vaccination in the left hind leg. Blood was obtained from the submandibular vein at four weeks following each vaccination. All vaccinations were adjuvanted with the AddaS03 adjuvant (Invivogen).

2 male and 3 female mice/group of DBA/2J mice (Jackson Laboratories) were used for immunizations with the NG2 rHA, 3 male and 2 female mice/group for the NG2 NP, and 1 male and 1 female mice/group for the NP core group, respectively, in a prime-boost-boost regimen. Mice were immunized with 3 μg equivalents of the HA protein every four weeks, either in the NG2 rHA soluble format, the NG2 NP, or the NP core through intramuscular vaccination in the left hind leg. Blood was obtained from the submandibular vein at four weeks following each vaccination. All vaccinations were adjuvanted with the AddaS03 adjuvant (Invivogen).

Enzyme-linked immunosorbent assay (ELISA)

To validate the antigenicity of the Y2 NP, NG2 NP, and NP core, 384-well plates (Greiner Bio-One) were coated with these NPs diluted to 2 μg/mL in phosphate-buffered saline (PBS) at 4°C overnight. The plates were washed once with water and then blocked with 2% blocking buffer (PBS + 2% nonfat dry milk [Bio-Rad] + 2% goat serum + 0.05% Tween 20) for 1 h at room temperature. The plates were washed three times with water, and 25 μL of mAb dilutions were added. MAbs CA09-30 (against the H1 HA), TJ5-4 and TJ5-13 (against the H3 HA), and 46 (against the IBV HA) were serially diluted three-fold in PBS from a 20 μg/mL initial dilution for 12 total dilutions. The plates were incubated at 25°C for 1 h, then washed three times with water.

25 μL of goat anti-human IgG Fc-AP secondary antibody (Southern Biotech), diluted 1:4000 in 1% blocking buffer (1:1 dilution of PBS and 2% blocking buffer), were added, and the plates were incubated at 25°C for 1 h. The plates were then washed five times with PBS-T (PBS + 0.05% Tween 20). p-Nitrophenyl phosphate (PNPP) substrate, diluted in substrate buffer (1.0 M Tris + 0.5 mM MgCl2, pH 9.8) to 1 mg/mL, was added, and the plates were incubated for 1 h and read at 405 nm on a BioTek plate reader. The EC_{50} for each mAb was determined using GraphPad Prism software using the four-parameter nonlinear regression.

For Y2, NG2, and NP core serum IgG ELISAs, 384-well plates (Greiner Bio-One) were coated with Y2, NG2, or NP core antigen diluted to 2 μg/mL in phosphate-buffered saline (PBS) at 4°C overnight. The plates were washed once with water and then blocked with 2% blocking buffer (PBS + 2% nonfat dry milk [Bio-Rad] + 2% goat serum + 0.05% Tween 20) for 1 h at room temperature. The plates were washed three times with water, and 25 μL of diluted mouse serum were added. Sera were serially diluted three-fold in 1% blocking buffer from a 1:50 initial dilution for 12 total dilutions. The plates were incubated at 37°C for 1 h and then washed three times with water. 25 μL of goat anti-mouse IgG Fc-AP secondary antibody (Southern Biotech), diluted 1:4000 in 1% blocking buffer (1:1 dilution of PBS and 2% blocking buffer), were added, and the plates were incubated at room temperature for 1 h. The plates were then washed five times with PBS-T (PBS + 0.05% Tween 20). p-Nitrophenyl phosphate (PNPP) substrate, diluted in substrate buffer (1.0 M Tris + 0.5 mM $MgCl_2$, pH 9.8) to 1 mg/mL, was added, and the plates were incubated for 1 h and read at 405 nm on a BioTek plate reader. The area under the curve (AUC) value for each mouse group was determined using GraphPad Prism software using a baseline of 0.3 absorbance units at 405 nm and log_{10}-transformed serum dilutions.

Hemagglutination inhibition assay (HAI)

The HAI titer of mouse serum was determined as previously described [160]. Serum was treated with receptor-destroying enzyme II (RDE II, Denka Seiken) to remove background hemagglutination activity. Briefly, one volume of serum was added to three volumes of RDE II in PBS and incubated at 37 °C overnight. The following day, the treated serum was heat-inactivated at 56 °C for 45 min, allowed to cool to room temperature, then six volumes of PBS were added.

For HAIs against H1 viruses, influenza viruses were titered to eight HAUs (hemagglutination units) per mL. 50 μL of RDE-treated serum were added to the first well of a 96-well V-bottom plate (VWR) and diluted two-fold in PBS for 25 μL total for eleven dilutions. The virus, titered to eight HAUs per mL, was added in a 1:1 ratio to each serum dilution, and each well was mixed and incubated for 20 min at room temperature. Following this, 50 μL of 1.0% turkey red blood cells (Lampire) were added per well. Plates were read 45 min after the addition of 1.0% turkey red blood cells.

For HAIs against H3 viruses, influenza viruses were titered to eight HAUs. 50 μL of RDE-treated serum were added to the first well of a 96-well V-bottom plate (VWR) and diluted two-fold in PBS. Eight HAUs of virus with 40 nM oseltamivir were added in a 1:1 ratio to each serum dilution, and each well was mixed and incubated for 30 min at room temperature. Following this, 50 μL of 0.8% guinea pig red blood cells (Lampire) were added per well. The plates were read 1 h after the addition of 0.8% guinea pig red blood cells.

Results

Nanoparticles presenting the COBRA HA are intact and retain the expected antigenicity

We first generated NP constructs using the I53_dn5A/I53_dn5B platform described previously that presented either the Y2 COBRA HA, the NG2 COBRA HA, or lacked the HA component [6] **(Figure 5.1A)**. To generate the Y2 NP, the NG2 NP, or the NP core, the Y2-I53_dnB, the NG2-I53_dn5B, or the I53_dn5B component, containing a Y98F mutation to reduce HA binding to sialic acid and enhance yield, was purified and mixed with bacterially expressed I53_dn5A. Subsequently, size exclusion chromatography (SEC) was used to purify the intact Y2 NP (called Y2_I53_dn5), the NG2 NP (called NG2_I53_dn5), or the NP core (called I53_dn5) from unassembled Y2-I53_dn5B, NG2-I53_dn5B, I53_dn5B, or I53_dn5A **(Figure 5.1B)**. The Y2 NP and the NG2 NP eluted at 10 mL, whereas the NP core eluted at 12 mL. Following nanoparticle purification, we evaluated their structural integrity and purity by negative-stain electron microscopy (nsEM) **(Figure 5.1C)**. We found that the Y2 NP, the NG2 NP, and the NP core formed the expected structures, consisting of a central, circular core. Spikes of the HA trimer were only visible on the Y2 NP and the NG2 NP constructs but not for the NP core, as expected. Furthermore, we assessed the antigenicity of these constructs by enzyme-linked immunosorbent assay (ELISA) **(Figure 5.1D)**. We found that the Y2 NP only bound H1 HA-specific monoclonal antibody (mAs) CA09-30, the NG2 NP bound only H3 HA-specific mAbs TJ5-4 and TJ5-13, and the NP core demonstrated no binding to any of the mAbs within this panel. Therefore, we found that this nanoparticle platform could reliably present the Y2 H1 COBRA HA or the NG2 H3 COBRA HA in a multimeric array while maintaining the COBRA HAs' overall antigenicity.

Y2 and NG2 NPs elicit differential antibody breadth based on the COBRA immunogen

To evaluate the immunogenicity and antibody breadth of the Y2 and NG2 NP constructs *in vivo*, we immunized DBA2/J mice in a prime-boost-boost regimen, using the NP core as a negative control **(Figure 5.2A)**. After immunization with the Y2 NP construct, we observed significant titers against the homologous Y2 H1 COBRA but not against the NG2 H3 COBRA **(Figure 5.2B)**. In comparison to the Y2 rHA group, however, titers were lower for the Y2 NP-immunized group after the full vaccination regimen. Evaluation of the serum antibody titers elicited by NG2 NP vaccination, in contrast, showed a significant response against not only the homologous NG2 H3 COBRA HA, but also against the Y2 H1 COBRA HA after just one immunization **(Figure 5.2C)**. NG2 NP titers were generally lower compared to the NG2 rHA group when evaluating heterosubtypic H1 Y2 COBRA HA-reactive titers, whereas those for the homosubtypic H3 NG2 COBRA HA appeared to be comparable **(Figure 5.2C)**. Cross-reactive titers between the H1 and H3 COBRA HAs were also seen for NG2 rHA-immunized groups. These may be due to antibodies targeting non-HA ectodomain epitopes on the HA construct used, such as the Foldon trimerization domain and the His tag. In contrast, these sequences are absent on the NG2 NP construct, where the HA sequence is directly fused to the I53_dn5B scaffold, which naturally forms trimers in the nanoparticle structure. These binding titers increased after each boost for both the Y2 and NG2 COBRA HAs, showing that the NG2 NP, but not the Y2 NP, can elicit significant serum antibodies against both homologous and heterologous IAV HAs.

Antibody responses to the NP protein scaffold are limited compared to the HA for NG2 NP- and NP core-immunized mice

We also evaluated the extent to which scaffold-directed antibody responses were elicited after NP vaccination for the NG2 NP-, the NG2 rHA-, and the NP core-vaccinated mice at the

terminal timepoint **(Figure 5.3)**. We found significant titers only for groups that received either the NG2 NP and the NP core, but not for the rHA-immunized group, as expected. Moreover, in comparison to the total binding AUC values obtained against the NG2 rHA itself, the scaffold-directed responses were lower, suggesting that the NG2 HA itself, and not the protein scaffold component, is the major immunodominant component of the NP vaccine **(Figure 5.2C)**. These results were similar to those observed previously, where the presented influenza HA immunogen on this NP platform generally elicited greater antibody responses than to the protein NP scaffold [161].

The NG2 NP, but not the Y2 NP, can enhance functional, HAI-active antibody breadth to the HA head domain of H1 viruses

We also evaluated the functionality of the serum antibodies elicited following vaccination in this regimen using HAI assays for a panel of both H1N1 and H3N2 viruses **(Figure 5.4)**. For all animals immunized with the Y2 NP and the Y2 rHA, titers were comparable between these two formulations for the 2009 swine influenza pandemic H1N1 A/California/07/2009 (A/CA/09) strain **(Figure 5.4A)**. In contrast, we saw reduced HAI titers to the more recent A/Guangdong-Maonan/SWL1536/2019 (A/GM/19) virus relative to the Y2 rHA control. Furthermore, we found no HAI titers whatsoever against the H3N2 strains tested, even with the use of the NP platform to present the Y2 H1 COBRA HA. For NG2 rHA-immunized animals, we found that, as expected, titers were only observed against H3N2 strains but not for any H1N1 strains **(Figure 5.4B)**. In contrast to the limited HAI breadth seen with Y2 NP vaccination, however, we observed that all animals in the NG2 NP-immunized group possessed serum with seroprotective HAI titers (above a 1:80 dilution) against the A/CA/09 and A/GM/19 viruses. Furthermore, HAI titers to H3N2 viruses were comparable to the NG2 rHA group. As expected, the animals from the NP core control

group displayed no HAI activity for neither H1N1 nor H3N2 viruses. This suggested that for the H3 COBRA HA NG2, the NP platform could enhance antibody breadth to H1 IAV viruses, in contrast to the H1 COBRA HA Y2.

Discussion

In this study, we evaluated the effect on antibody breadth of presenting COBRA HA immunogens on a computationally designed, two-component protein NP platform. We found overall that the use of this platform with the H1 COBRA, Y2, could not expand antibody breadth to H3 viruses, whereas the use of this system with the H3 COBRA, NG2, could expand breadth to H1 viruses. These COBRA HA constructs are the current lead vaccine candidates for this methodology as they capture the antigenic features of recent H1 and H3 subtype viruses, respectively [122,159]. Y2 captures H1 HA sequences from 2014 to 2016 from after the 2009 H1N1 swine influenza pandemic, whereas NG2 captures H3 HA sequences from 2016 to 2018 [122,159]. Individually, these COBRA HAs have been shown to elicit expanded, functional HAI breadth to recent H1 strains from 2009 to 2019 for Y2, and from 2012 to 2019 for H3 strains for NG2. However, the antibody breadth from these COBRA HAs is limited to their respective subtype designs. To assess whether a COBRA HA presented on a NP platform could expand breadth to multiple IAV subtypes, we generated homotypic NPs presenting either the Y2 or NG2 HAs.

We verified that the Y2 and NG2 NPs could be successfully assembled using the previously established I53_dn5 two-component NP platform [6]. Structural analyses verified the expected structures of each NP construct, where a central protein scaffold core was surrounded by HA trimer spikes of either Y2 or NG2. We noted, however, that individual Y2 NPs were prone to clustering

compared to NG2 NPs **(Figure 5.1C).** This may be due to lower general stability of H1 subtype HAs. In contrast, the NG2 NP generally appeared as being more monodisperse through nsEM analysis, which presents a more structurally stable H3 subtype HA. Nonetheless, both NP constructs were found in an early peak by SEC that suggested a uniform particle size **(Figure 5.1B)**. Moreover, the antigenic integrity of the Y2 NP and NG2 NP was also verified through binding to previously characterized H1 HA-reactive and H3 HA-reactive mAbs, CA09-30 [142] and TJ5-4 and TJ5-13 [162], respectively **(Figure 5.1D)**.

Differences in NP immunogenicity were also observed between the Y2 NP and NG2 NP vaccination groups, wherein the NG2 NP elicited higher serum binding titers against the homologous NG2 HA compared to Y2 NP against the homologous Y2 HA after fewer vaccinations. Three vaccinations were needed to observe any significant titers against either Y2 or NG2 HAs for the Y2 NP group, whereas reactive titers were seen after just a single vaccination with the NG2 NP **(Figure 5.2)**. This difference may also be due to reduced H1 HA stability relative to the H3 HA. This subtype-dependent difference in immunogenicity also carried over into HAI analyses of RBS-directed antibodies against the HA head domain of H1N1 and H3N2 viruses **(Figure 5.4)**, where no cross-group H3 virus HAI titers were observed with the Y2 NP, whereas animals immunized with the NG2 H3 NP exhibited cross-group H1 HAI titers.

We also found that for NG2 NP-vaccinated animals, scaffold-specific responses were elicited to some extent, but not to the degree of outcompeting antigen-specific responses **(Figure 5.3)**. These results were consistent with a previous report that showed that nanoparticles presenting the influenza HA could still elicit significant HA responses that outcompeted I53_dn5-specific responses even without shielding of the NP scaffold with either glycans or PEG moieties [161].

Given that the NG2 NP could elicit cross-group antibody breadth to H1 viruses, future efforts will be focused on characterizing the antibody response from NP vaccination from splenic antigen-specific B cells that can cross-react with both H1 and H3 Y2 and NG2 HAs. We expect that the expanded accessibility of multiple HA head domains on the NG2 NP might augment B cell activation by cross-linking B cell receptor binding to multiple HAs on the NP construct, potentially activating B cells that bind conserved head domain epitopes on the NG2 COBRA HA that could cross-react with H1 HAs.

Figures

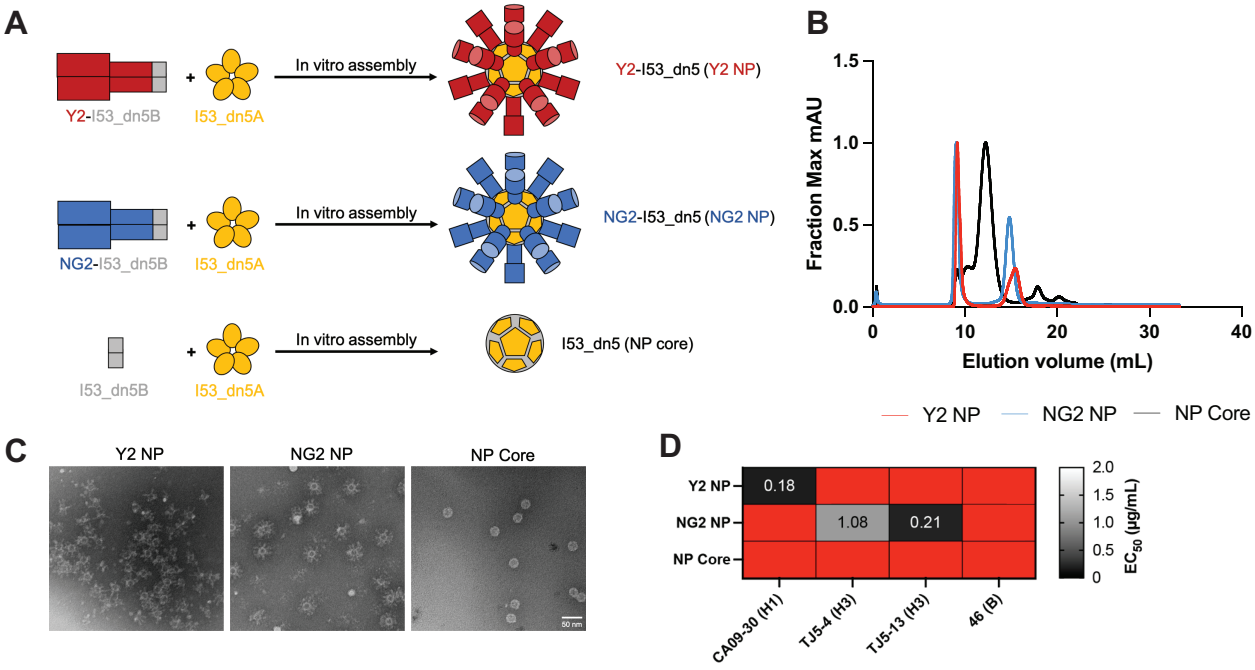

Figure 5.1. Formulation and biochemical validation of the H1 subtype COBRA Y2 and H3 subtype COBRA NG2 on the I53_dn5 NP system. (A) Left, schematic of the assembly and steps of the Y2 NP, the NG2 NP, and the NP core. The HA-I53_dn5B or I53_dn5B alone trimerizes and is then mixed with pentameric I53_dn5A to form the nanoparticles shown on the right. (B) SEC traces of purified Y2 NP, NG2 NP, and NP core from the Superose 6 Increase 10/30 GL column with the absorbance normalized to the maximum value for each elution. The Y2 NP and NG2 NP elute at about 10 mL whereas the NP core elutes at about 12 mL. (C) nsEM analysis of purified NP. Scale bar, 100 nm. (D) ELISA-based validation of NP antigenicity. NPs were assessed for binding to a panel of H1, H3, and influenza B HA-reactive mAbs CA09-30, TJ5-4 and TJ5-13, and 46, respectively. The EC_{50} of each mAb to the NP constructs, in µg/mL, is shown as a heat map. A red color indicates an AUC value of less than 1.5 absorbance units at 405 nm for the highest mAb dilution of 20 µg/mL, the threshold to define a mAb as binding to a NP.

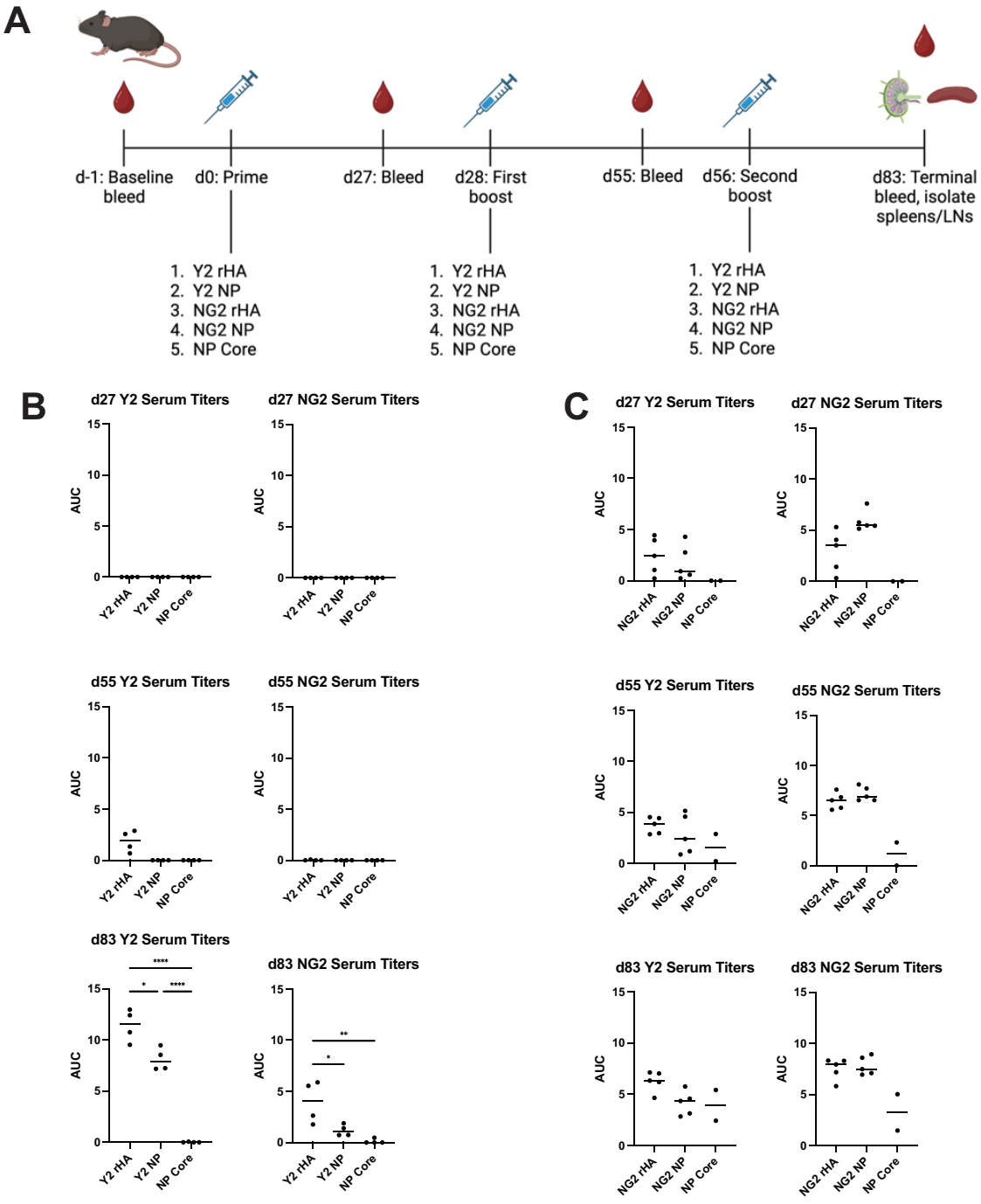

Figure 5.2. Mouse immunization studies to evaluate antibody breadth and reactivity from the Y2 and NG2 NP vaccination. (A) General immunization regimen for Y2 and NG2 NP groups. 3 μg equivalents of the HA protein, standardized either for the trimeric, soluble rHA or the NP,

were used to intramuscularly immunize DBA/2J mice in a prime-boost-boost regimen using intramuscular vaccinations. Blood was taken for serum antibody titer measurements at 4 weeks after each vaccination. (B) ELISA binding titers against the H1 COBRA Y2 or the H3 COBRA NG2, shown as area under the curve (AUC) titers, for Y2-vaccinated mice at d27, d55, and d83. (C) ELISA binding titers against Y2 or NG2 for NG2-vaccinated mice at d27, d55, and d83. *, p<=0.05; **, p<=0.01; ***, p<=0.001; ****, p<=0.0001. One-way ANOVA was used for statistical comparisons between groups.

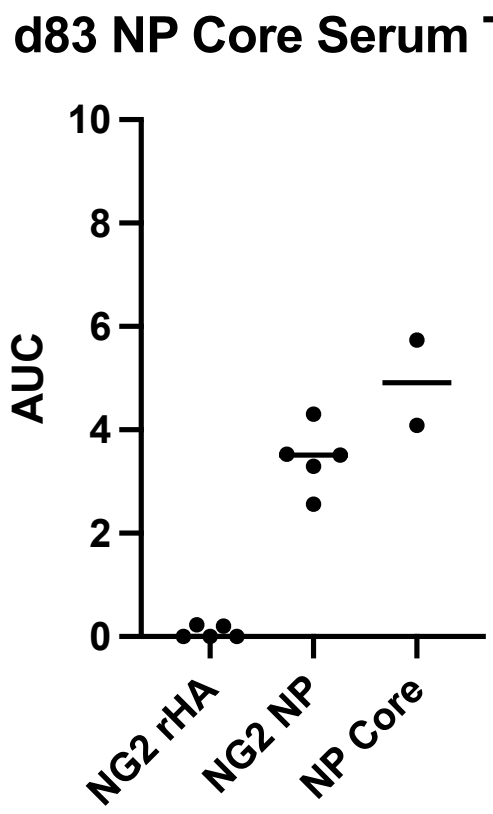

Figure 5.3. Murine serum responses to the NP core scaffold following NG2 rHA, NG2 NP, and NP core vaccination after the prime-boost-boost regimen. AUC binding titers against the assembled NP core at the terminal d83 timepoint are shown, determined by ELISA.

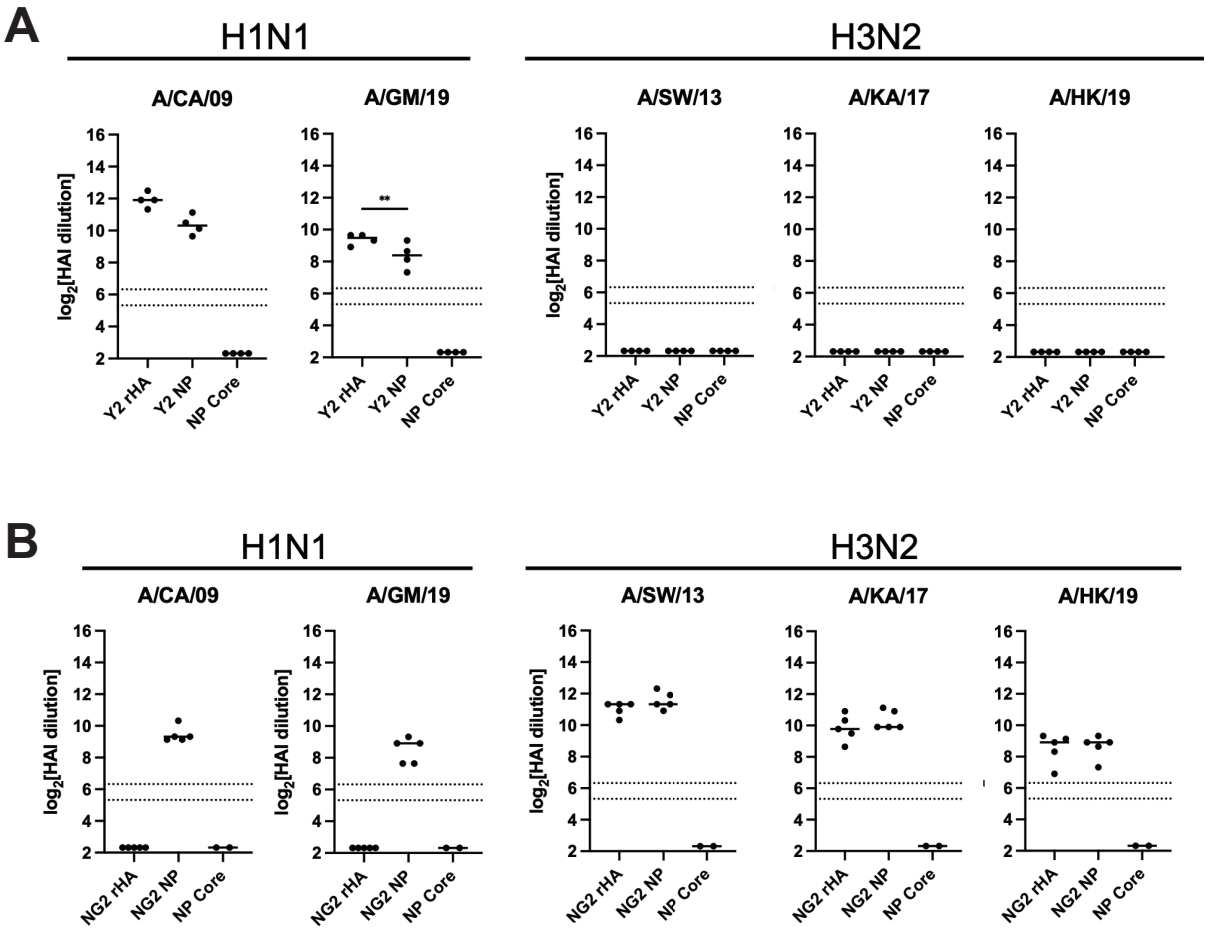

Figure 5.4. Terminal HAI titers elicited by NP and rHA COBRA vaccination against a panel of H1N1 and H3N2 IAVs. Serum HAI titers at d83 were determined for the H1N1 subtype A/California/07/2009 (A/CA/09) and the A/Guangdong-Maonan/SWL1536/2019 (A/GM/19) viruses, and the H3N2 subtype A/Switzerland/9715293/2013 (A/SW/13), the A/Kansas/14/2017 (A/KA/17), and the A/Hong Kong/45/2019 (A/HK/19) viruses for (A) Y2 rHA- and Y2 NP-immunized animals or for (B) NG2 rHA- and NG2 NP-immunized animals. The lower dotted line corresponds to a 1:40 serum dilution and the upper dotted line to the 1:80 serum dilution as a correlate of protection.

CHAPTER 6

STRUCTURAL AND ANTIGENIC CHARACTERIZATION OF A COMPUTATIONALLY OPTIMIZED H1 SUBTYPE HEMAGGLUTININ[5]

[5]A part of this chapter was submitted to *Structure* on 04/26/23.
Nagashima, K.A.; Dzimianski, J.V.; Yang, M.; Abendroth, J.; Sautto, G.A.; Ross, T.M.; DuBois, R.M.; Edwards, T.E.; Mousa, J.J. Structural basis for the broad antigenicity of the computationally optimized influenza hemagglutinin X6.

Abstract

Influenza remains a major infectious burden, causing significant morbidity and mortality. As an alternative approach to current seasonal vaccines, the computationally optimized broadly reactive antigen (COBRA) platform has been previously applied to hemagglutinin (HA). This approach integrates wild-type HA sequences into a single immunogen to expand the breadth of accessible antibody epitopes. Adding to previous studies of H1, H3, and H5 COBRA HAs, we define the structural features of another H1 subtype COBRA, X6, that incorporates human HA sequences from before and after the 2009 H1N1 influenza pandemic. We determined both X-ray and cryo-EM structures of this antigen alone and in complex with COBRA-specific as well as broadly reactive and functional antibody Fab fragments, and we analyzed its glycosylation profile and antigenicity. We found that X6 possesses features that reflect both historic and recent H1 HA strains, enabling binding to both head- and stem-reactive antibodies. Overall, these data confirm the integrity of the broadly reactive antibody epitopes of X6, and contribute to vaccine design efforts for a next-generation influenza vaccine.

Introduction

Influenza virus poses a major health concern worldwide. It is estimated that within the United States, between 140,000 and 810,000 hospitalizations due to the virus occur each year [7]. Seasonal influenza vaccines provide only limited effectiveness against circulating strains due to antigenic drift within the hemagglutinin (HA) glycoprotein, the major viral surface antigen [9]. Moreover, the protective antibody response elicited by the vaccine is short-lived. Therefore, the seasonal vaccine is sensitive to viral immune evasion and must be reformulated every year based on predictions of circulating viruses. Timelines for manufacturing the current vaccine can take up to six months [3] and accurate strain prediction remains a challenge. Delaying strain selection may enable more accurate strain prediction, but usually does not occur, as this reduces vaccine yield and availability.

Several next-generation influenza vaccines have been investigated to elicit enhanced breadth against a wider range of virus strains [117]. One approach, termed COBRA (computationally optimized broadly reactive antigen), employs a layered consensus building strategy to combine wild-type viral sequences into a single antigen [54]. This methodology has been applied to the HA protein for influenza A and B viruses [54,121,122,150,163]. The resulting COBRA HA possesses enhanced effectiveness as a vaccine antigen, whereby studies in mouse and ferret animal models have shown increased functional antibody breadth following COBRA HA vaccination [52,54]. The primary mechanism by which these COBRA HAs elicit protection is through inducing broadly HAI-active, HA head domain-targeting antibodies that block receptor binding [4,53,54]. While it was hypothesized that stem domain-binding antibodies did not contribute significantly to the COBRA HA response [56], we have previously shown that the COBRA HA stem is intact for an H1 HA COBRA, Y2, which both retains binding to anchor

epitope-specific antibodies and induces central stem-binding antibodies [160,164]. Similar stem antibodies have been isolated from H1 COBRA-vaccinated mice [120]. Furthermore, seasonally vaccinated subjects possess antibodies that can bind an H3 COBRA HA [165]. This suggests that COBRA HAs possess the potential to elicit antibodies that bind both the HA head and stem domains.

The 2009 H1N1 influenza pandemic marked a significant antigenic shift in circulating H1N1 viruses. As a reassortant virus resulting from swine, avian, and human strains, the 2009 pandemic virus HA possessed a novel head domain and a more conserved stem relative to circulating pre-2009 seasonal strains [166]. Infection with this 2009 virus elicited stem-reactive antibodies that are thought to have led to the disappearance of pre-2009 seasonal H1N1 viruses and the subsequent dominance of the pandemic-like strains [167]. The X6 COBRA HA has been previously characterized in animal models to elicit broadly reactive serum antibodies against viruses of the H1 subtype [168]. This antigen incorporates sequence elements from both pre-2009 pandemic and post-2009 pandemic viruses from 1999 to 2012 [168]. Immunization with X6 has been shown to elicit polyclonal antibodies with broad reactivity against several H1 viruses [121]. Seasonal vaccination can elicit monoclonal antibodies (mAbs) in human subjects that recognize the X6 COBRA HA, indicating the conservation of epitopes between the seasonal vaccine H1 HA and the X6 COBRA HA [164]. One such mAb, CA09-26, has neutralization activity against both pre-2009 and 2009 pandemic H1 viruses through binding to the receptor-binding site (RBS) [164]. In this study, we demonstrate that other human and murine mAbs, #58 and BE1, show similarly broad H1 reactivity and HAI activity as a consequence of binding the RBS [119] and lateral patch epitopes [45,136]. In addition, we show that conserved H1 HA epitopes are also present within the X6 stem domain by solving the structure of the Fab fragment of a group 1 broadly reactive central

stem-binding mAb, CR6261 [59], in complex with X6. Altogether, these data indicate that the COBRA X6 vaccine incorporates conserved and intact antibody epitopes on the HA protein. These structural analyses provide insights into the mechanism by which COBRA HAs induce enhanced antibody breadth.

Methods

Vaccinations to generate X6-specific murine mAbs

BALB/c mice (female, 8–10 week of age), antibody negative for circulating influenza A (H1N1 and H3N2) and influenza B viruses, were purchased from Envigo (Indianapolis, IN) and housed in microisolator units and fed ad libitum. Mice were handled in accordance with protocols approved by the University of Georgia Institutional Animal Care and Use Committee and were cared under U.S. Department of Agriculture guidelines for laboratory animals. Mice that showed signs of severe morbidity or lost 20% of their original weight were humanely euthanized. The vaccination regimen was identical to that used previously [120,172].

Expression and purification of H1 rHAs for mAb binding studies

Truncated rHA encoding HAs from H1N1 A/Chile/1/1983 (Chile/83), A/Singapore/6/1986 (Sing/86), A/New Caledonia/20/1999 (NC/99), A/Brisbane/59/2007 (Brisb/07), A/California/04/2009 (CA/09), A/Michigan/45/2015 (Mich/15), A/Brisbane/02/2018 (Brisb/18), A/Guangdong-Maonan/SWL1536/2019 (GM/19), A/Wisconsin/588/2019 (Wisc/19), cH6/1 and COBRA X3, X6, P1 and Y2 were cloned, expressed and purified as previously described [173] and used for all the binding experiments. In brief, the different HA proteins were expressed through a transient transfection of the EXPI293F cells (Thermo Fisher Scientific) with the different COBRA and H1N1 HA pcDNA3.1/Zeo(+) encoding vectors following the instruction provided

by the manufacturer. Alternatively, HA proteins were expressed through the generation of stable transfected cells supplemented with 100 µg/mL of Zeocin (Invivogen). rHA proteins were then purified through the ÄKTA Pure system using HisTrap columns (GE Healthcare) according to the manufacturer's instructions. The H1N1 A/Texas/36/1991 rHA protein was kindly provided by F. Krammer (Ichan School of Medicine at Mount Sinai, New York, NY) while A/Puerto Rico/8/1934 (PR/34) and A/Solomon Island/3/2006 were provided by BEI Resources.

Influenza viruses and virus-like particles (VLPs)

All the 7:1 recombinant PR/34 reassortant COBRA (P1, X3 and X6) and PR/34, Chile/83, NC/99, SI/06, Brisb/07 viruses and wild-type Sing/86, TX/91, CA/09, Mich/15, Brisb/18, GM/19, A/Victoria/2570/2019 (Vic/19) viruses were propagated in embryonated chicken eggs as previously described [56]. The A/Philadelphia/1/2013 (Phil/13) was kindly provided by Scott Hensley (Department of Microbiology, Perelman School of Medicine, University of Pennsylvania, Philadelphia, PA). These viruses were titrated and used for immunization, HAI, and focus reduction assay (FRA) experiments described below. The pandemic A/South Carolina/1/1918 (SC/18) HA-expressing VLP were generated as previously described [121] and used for HAI assays.

Enzyme-linked immunosorbent assay (ELISA) of mAbs

ELISA was used to assess mAb reactivity against different H1N1 HA strains. ELISA were performed as previously described [172]. In brief, Immulon 4HBX plates (Thermo Fisher Scientific) were coated overnight at 4℃ with 50 µL per well of a PBS solution containing 1 µg/mL of the different rHA in a humidified chamber. The mAbs were 3-fold serially diluted in blocking buffer starting from 20 µg/mL, and plates were incubated for 1 h at 37℃. Plates were washed five times with PBS, 100 µL per well of HRP-conjugated goat anti-mouse or anti-human IgG (Southern

Biotech) diluted 1:4,000 in blocking buffer was added, and plates were incubated at 37℃ for 1 h. Finally, plates were washed five times with PBS and ABTS substrate (VWR International, Radnor, PA) was added, and plates were incubated at 37℃ for 15-20 min. Colorimetric conversion was terminated by addition of 1% SDS (50 µl per well), and OD was measured at 414 nm (OD414) using a spectrophotometer (PowerWave XS; BioTek).

Hemagglutination inhibition (HAI) assay

The HAI assay was performed as previously described [120]. In brief, mAbs were diluted in a series of 2-fold serial dilutions in v-bottom microtiter plates (Greiner Bio-One) starting from 20 µg/mL. An equal volume of each H1N1 virus, adjusted to 8 hemagglutination units per 50 µL, was added to each well. The plates were covered and incubated at room temperature for 20 min, and then 0.8% of turkey red blood cells (RBCs) (Lampire Biologicals, Pipersville, PA) in PBS was added. RBCs were stored at 4℃ and used within 72 h of preparation. The plates were mixed by agitation and covered, and the RBCs were settled for 30 min at room temperature. The HAI titer was determined by the reciprocal dilution of the last well that contained non-agglutinated RBCs. Positive and negative controls were included for each plate.

Focus reduction assay

The FRA was performed similarly to previously described protocols [120]. In brief, MDCK-SIAT1 cells were seeded at a density of 2.5-3 x 10^5 cells/mL in a 96-well plate (Greiner Bio-One) the day before the assay was run. The following day, the cell monolayers were rinsed with PBS (Thermo Fisher Scientific), followed by the addition of 2-fold serially diluted mAbs at 50 µL per well starting with 20 µg/ml dilution in virus growth medium containing 1 µg/mL of L-(tosylamido-2-phenyl) ethyl chloromethyl ketone (TPCK)–treated trypsin. Afterwards, 50 µL of virus (CA/09) standardized to 1.2 x 10^4 focus forming units per milliliter, and corresponding to

600 focus forming units per 50 µL, was added to each well, including control wells. Following a 2 h incubation period at 37℃ with 5% CO_2, the cells in each well were then overlaid with 100 µL of equal volumes of 1.2% Avicel RC/CL (Type RC581 NF; FMC Health and Nutrition, Philadelphia, PA) in 2X MEM (Thermo Fisher Scientific) containing 1 µg/mL TPCK-treated trypsin, 0.1% BSA, and antibiotics. Plates were incubated for 18-22 h at 37℃, 5% CO_2. The overlays were then removed from each well and the monolayer was washed once with PBS to remove any residual Avicel. The plates were fixed with ice-cold 4% formalin in PBS for 30 min at 4℃, followed by a PBS wash and permeabilization using 0.5% Triton X-100 in PBS/glycine at room temperature for 20 min. Plates were washed three times with PBS supplemented with 0.1% Tween-20 (PBS-T) and incubated for 1 h with a mAb against influenza A nucleoprotein (IRR) in ELISA buffer (PBS containing 10% horse serum and 0.1% Tween-80 [Thermo Fisher Scientific]). Following washing three times with PBS-T, the cells were incubated with goat anti-mouse peroxidase-labeled IgG (SeraCare, Milford, MA) in ELISA buffer for 1 h at room temperature. Plates were washed three times with PBST, and infectious foci (spots) were visualized using TrueBlue substrate (SeraCare) containing 0.03% H_2O_2 incubated at room temperature for 10-15 min. The reaction was stopped by washing five times with distilled water. Plates were dried and foci were enumerated using an ImmunoSpot® S6 Ultimate Analyzer and the CTL ImmunoSpot SC Studio software (Version 1.6.2, Shaker Heights, OH, USA). The FRA IC_{50} titer was reported as the mAb concentration corresponding to 50% foci reduction compared with the virus control minus the cell control.

Expression and purification of X6 for crystallographic studies

The X6 gene was synthesized and cloned into the pBacPAK8 vector (GenScript). The X6 construct consisted of a GP67 secretion signal, the COBRA X6 HA ectodomain, fused to a C-

terminal thrombin cleavage site, T4 fibritin foldon, His-tag, and Strep-tag [174]. Recombinant baculovirus containing the X6 gene was generated using the *flash*BAC™ system (Mirus Bio). Protein expression was performed in Sf9 cells cultured in ESF921 medium (Expression Systems) by infecting with ~23 mL of virus per liter of culture. After 3 days, the supernatant was harvested by centrifugation and stored at -20°C.

The medium containing the X6 protein was thawed at 4°C. It was then subjected to filtering through glass microfiber filter, followed by buffering with concentrated NaCl and Tris pH 8. This solution was then sequentially filtered through 0.45 μm, and 0.22 μm filters and concentrated by tangential flow using VivaFlow 200® cassettes (Sartorius). BioLock (IBA Life Sciences) was added to bind free biotin, then the sample was filtered and loaded onto a 5 mL StrepTrap column (GE Healthcare). The column was washed with 150 mM NaCl, 50 mM Tris [pH 8], 1 mM EDTA, and the protein eluted with 150 mM NaCl, 50 mM Tris [pH 8], 1 mM EDTA, 2.5 mM desthiobiotin. The fractions were pooled, concentrated, and supplemented with glycerol (5%) prior to snap freezing in liquid nitrogen and storage at -80°C.

Crystallization and structural solution of X6

Aliquots of X6 protein were thawed on ice, supplemented with 2 mM $CaCl_2$, and digested with ~7 μg of trypsin per 1 mg of protein to remove the Foldon trimerization domain and cleave the furin site to generate active HA. The trypsin-activated X6 HA was further purified by size exclusion chromatography (SEC) using a Superdex 200 column (GE Healthcare) equilibrated with 50 mM NaCl, 10 mM Tris [pH 7.5]. The fractions containing HA based on an SDS-PAGE gel were pooled and concentrated to 9.8 mg/mL. The protein was crystallized in 2 μL hanging drops with a 1:1 ratio of well solution to protein in a condition consisting of 0.1 M Tris pH 8.4, 22% PEG 3350. Crystals were cryoprotected in a solution consisting of 0.1 M Tris pH 8.4, 22% PEG

3350, 6% ethylene glycol, 6% DMSO, 6% glycerol and flash-cooled in liquid nitrogen. Data collection was performed at the GM/CA beamline 23ID-D at the Advanced Photon Source (APS). Data from a single crystal was indexed and integrated using XDS [175,176], followed by scaling and merging in Aimless [177,178]. The structure was phased using Phaser [179] in the PHENIX suite using a homology model generated by SWISS-MODEL [180]. Three monomer copies were placed in the asymmetric unit to form a single trimer. Refinement and model building were performed in PHENIX [181] and COOT [182]. The final model was validated with MolProbity [183] and Privateer [184].

Fab generation

The CA09-26 mAb, isolated from a subject who received the 2017-2018 Fluzone seasonal vaccine, was purified from hybridoma culture on a Protein GE column as described previously [142] (GE Healthcare). The #58 mAb was generated by single-cell sequencing of the plasmablast repertoire of a Fluzone-vaccinated individual using a previously described strategy [185,186]. Heavy and light chains of mAb #58 were synthesized and cloned in the pcDNA3.4 vector (Thermo Fisher Scientific) by GenScript (Piscataway, NJ, USA) and expressed in human embryonic kidney (HEK) 293F cells and purified as previously described [187]. These mAbs were then digested to Fab fragments using the Fab Preparation Kit (Thermo Fisher Scientific) according to the manufacturer's instructions. Fab was purified from the digestion reaction on a MabSelect column (GE Healthcare) and buffer exchanged into 20 mM Tris, pH=7.5, 100 mM NaCl for generation of the complex.

For the isolation of BE1 and other X6-specific murine mAbs, splenocytes from X6-immunized mice were used to generate B cell hybridoma cell lines, from which the mAbs were purified using previously described methods [120,172]. The BE1 Fab was prepared in a similar

manner as the CA09-26 and #58 Fabs but a final buffer of 1x PBS pH=7.4, 300 mM NaCl and a final concentration of 7.5 mg/mL were used.

The CR6261 antibody Fab fragment was expressed in HEK293 cells as a secreted protein with a C-terminal His_6 tag on the heavy chain and harvested 5 days post-induction. The secreted mammalian media was buffer-exchanged and concentrated by passing over a 10 kDa filter using hollow fiber tangential flow filtration with 20 mM Tris pH=7.4, 250 mM NaCl. The protein was purified by nickel affinity chromatography followed by size exclusion chromatography, then concentrated to 9.8 mg/mL in 25 mM Tris pH 7.4, 150 mM. The Fab was then flash frozen in liquid nitrogen in 100 μL aliquots and stored at -80□C until used in cryo-EM.

Cryo-EM sample preparation

For the CA09-26 Fab:X6 and #58 Fab:X6 structures, the X6 COBRA HA was purified from 293 cells as described previously [121]. X6 COBRA HA, in 20 mM Tris, pH=7.5, 100 mM NaCl, was mixed with CA09-26 or #58 Fab in a molar excess of CA09-26 or #58 Fab. Following incubation of the components at 4°C overnight, the mixture was subjected to size exclusion chromatography on a Superdex 200 column (GE Healthcare) to isolate the Fab:X6 complex from excess Fab.

For the BE1:X6 structure, the complex was prepared in a ratio of 1:1.2 theoretical equivalents of Sf9 cell-expressed X6 HA to Fab. After incubation on ice for 30 minutes, the mixture was subjected to size exclusion chromatography to remove extra BE1 Fab. The peaks that corresponded to the X6 COBRA HA-BE1 Fab complexes were kept for cryo-EM grid preparation. We did not have the BE1 Fab protein sequence at the time and used a generic protein molar extinction coefficient for the BE1 Fab, which resulted in a sub-stoichiometric ratio and a 3:2 HA:Fab complex in the cryo-EM structure.

For the CR6261:X6 structure, Sf9 cell-expressed X6 COBRA HA and CR6261 antibody Fab were mixed in a 1:1.2 molar ratio. Again, after incubation on ice for 30 minutes, the mixture was subjected to size exclusion chromatography to remove extra CR6261 Fab. The peaks that corresponded to the X6 COBRA HA-CR6261 Fab complexes were kept for cryo-EM grid preparation.

Cryo-EM grid preparation and data collection

For CA09-26 Fab:X6 and #58 Fab:X6, Fab:X6 complex at concentrations of 1.47 mg/mL and 1.0 mg/mL, respectively, were applied to Quantifoil 1.2/1.3 (400 mesh) grids previously glow-discharged for 45 s at 25 mAmp current on the carbon side. For CA09-26 Fab:X6, grids were blotted for 10 s with 100% humidity and plunge-frozen in liquid ethane using a FEI Vitrobot Mark IV instrument. For #58 Fab:X6, grids were blotted for 8 and 10 s with 100% humidity using a FEI Vitrobot Mark IV instrument. Cryo-EM data were collected on a Glacios (Thermo Fisher) equipped with a Falcon 4 camera. Cryo-EM movies were acquired using a nominal magnification of 190,000x, with a pixel size of 0.526 Å. Movies were recorded as 30-frame videos in counting mode, with a defocus range from -0.9 to -2.0 µm.

For the BE1 Fab:X6 complex, 4 µL of HA-Fab complex directly purified from SEC were applied to a C-flat R 2/1 (300 mesh) grid after glow discharging. Grids were blotted for 2.5 s with approximately 90% humidity and plunge-frozen in liquid ethane using a FEI Vitrobot Mark IV instrument. Cryo-EM data were collected at liquid nitrogen temperature on a Titan Krios at 300 kV equipped with a K3 summit direct electron detector (Gatan) at McGill University. All cryo-EM movies were recorded using SerialEM software. Specifically, images were acquired at a nominal magnification 135,000x, corresponding to a pixel size of 0.675 Å. Movies were recorded

as 40-frame videos using 2-w exposures in counting mode with a defocus range from -1.0 μm to -2.5 μm.

For CR6261 Fab:X6, 4 μL of HA-Fab complex at a concentration of 0.5 mg/ml were applied to a lacey carbon grid (300 mesh) coated by a layer of graphene oxide (SPI supplies). Grid blotting conditions were the same as the BE1 Fab:X6 complex.

Cryo-EM image processing and model building/refinement

For the CA09-26 Fab:X6 map and the #58 Fab:X6 structure, the data were processed in CryoSPARC for patch motion correction, patch CTF correction, particle picking, and particle extraction. This was followed by multiple rounds of 2D/3D class averaging and refinement. The #58 Fab:X6 structure was manually built in COOT and refined in Phenix.

For the BE1 Fab:X6 cryo-EM dataset, raw movies were directly imported into CryoSPARC 3.2.0 for the analysis. In CryoSPARC, motions were corrected by batch motion correction. Contrast transfer function (CTF) parameters were estimated using patch CTF estimation. Movies with CTF Fit resolution (Å) worse than 8 Å were removed. Blob picker was applied for automatic particle picking. Particles were extracted using a box size 558 pixels and Fourier-cropped to 140 pixels in order to save computation resources. Two rounds of 2D classification were applied to clean the particles, which yielded about 794,000 particles. Ab-initio 3D reconstruction was done by asking for three ab-initio models. The class that contains the greatest number of particles contained two copies of Fabs. The particles in this class were selected and used for Topaz training and particle picking in order to pick more particles. The newly picked particles were cleaned by additional rounds of 2D classification. Then, homogeneous refinement and non-uniform refinement were applied to refine the particles. Lastly, per-particle based CTF refinement was applied to further polish the particles, which were used for local refinement by using a focused

mask covering the two Fab regions and the well resolved HA region. No symmetry was applied during the refinements as there are only two copies of Fab bound. The final map was achieved to 3.47 Å. The sharpened map was obtained using the sharpening tool in CryoSPARC. The CR6261 structure described below was divided into a HA part and a Fab part, after which each of them was then individually docked into the density using ChimeraX. The HA trimer could be placed, along with two copies of the Fab, associated with chains A and B of the HA trimer. The density for Fab bound to chain C was too weak to model. The initial model was then improved by iterative cycles of manual model building in Coot and real-space refinement in Phenix. Cryo-EM data collection, reconstruction and model statistics are summarized in supplemental table 6.S4.

For the CR6261 Fab:X6 structure, movie frames were corrected for their motions using MotionCor2 in Relion 3.1. The motion-corrected movies were imported into CryoSPARC 2.2.0 for downstream analysis. In CryoSPARC, CTF parameters were estimated using patch CTF estimation. Movies with CTF Fit resolution (Å) worse than 8 Å were removed. The blob picker was applied for automatic particle picking. Particles were extracted using a box size of 558 pixels and Fourier-cropped to 140 pixels in order to save computation resources. Three rounds of 2D classification were applied to clean the particles, which yielded about 500,000 particles. Ab-initio 3D reconstruction was done by asking for five ab-initio models. The initial model containing three Fab molecules was selected for further 3D refinement using C1 symmetry. The refined model confirmed the identity of the expected HA-Fab complex. These selected particles were re-retracted using their original pixel size. After per-particle CTF refinement, and non-uniform refinement using C3 symmetry, the final map was refined to 2.64 Å. The sharpened map was obtained using the sharpening tool in CryoSPARC. A sequence alignment was performed between X6 COBRA HA and influenza A virus hemagglutinin from A/Ohio/09/2015 (PDB code: 6UYN) first, then the

side chains of X6 COBRA HA were truncated and aligned on the monomeric crystal structure of the influenza A virus hemagglutinin from A/Ohio/09/2015 using Chainsaw from CCP4. Three copies of the generated monomeric X6 COBRA HA were manually fit into the cryo-EM map. The structure of a single heterodimeric CR6261 Fab was extracted from PDB code 6UYN and then three copies of the molecules were manually fit into the corresponding EM densities. All the glycosylation sites were modeled in coot using a blurred map, which was generated by the sharpen/blur tool under cryo-EM module in coot. The initial model was then subjected to rounds of model building in coot and real-space refinement in Phenix. The final model was validated with statistics from MolProbity and EMRinger. Cryo-EM data collection, reconstruction, and model statistics are summarized in supplemental table 6.S5.

Results

Sequence and Structural Features of the X6 COBRA HA

The design of COBRA X6 includes human-tropic H1 viruses from 1999 to 2012, spanning both pre-2009 and post-2009 HAs in its design. Sequence alignments to wild-type HAs revealed that X6 is more similar to pre-2009 influenza HA sequences compared to post-2009 sequences **(Figure 6.1A)**. X6 possesses ~97% similarity to pre-2009 HAs, and ~80% identity to post-2009 pandemic-like HAs. Moreover, its antigenic sites were generally more similar to pre-2009 HAs (**Figure 6.S1)**. We mapped differences between the A/New Caledonia/20/1999 (NC99) and A/Michigan/45/2015 (MI15) HAs, finding most differences to be in the head domain and a minority in the stem **(Figure 6.1B)**. We also structurally mapped individual sequence differences between X6 and NC99, as well as between X6 and MI15 **(Figure 6.1C)**. We found that the higher divergence of X6 from MI15 was attributable to differences localized predominantly within the

head domain, whereas minimal differences in the head or stem domain were found when structurally aligning X6 to NC99. This comparison affirmed that X6 possesses greater sequence similarity to pre-2009 H1 HAs compared to post-2009 H1 HAs.

To characterize the structural features of X6, we determined the crystal structure of X6 to a resolution of 3.25 Å. As expected, the X6 HA formed a trimer similar to wild-type HAs **(Figure 6.2A)**. Structural alignments of X6 to wild-type HAs revealed that it was also similar to natural HAs, with RMSDs of 0.914 for X6 to NC99, and 0.679 for X6 to MI15. X6 also retained glycosylation sites similar to those found on the pre-2009 NC99 and the post-2009 MI15 HAs **(Figure 6.2B, 2C)**. Seven *N*-linked glycosylation sites in X6 were predicted in the NetNGlyc server [169]. Within the crystal structure, all of these glycosylation sites were observed at residues N11, N23, N54, N87, N125, N159, and N286. Of these sites, four were found on both NC99 and MI15, found primarily on the stem domain and the side of the HA head. Two glycosylation sites, at residue N159 on the top of the globular head domain and at N54 by the bottom of the head domain, were shared only with NC99 but not with MI15. While glycans were present at N480 in NC99 and MI15, no glycan was found at this position for X6. This difference may allow for more stem-directed responses following vaccination with X6. It may be possible that X6 glycans could allow for redirection of the antibody response towards more conserved epitopes found on both pre-2009 and post-2009 pandemic-like HAs. Overall, these data suggest that the glycosylation profile of X6 represents HAs within its design period and is skewed towards pre-2009 HAs.

Structures and Characteristics of X6-Binding Broadly Reactive Head-Binding Antibodies

X6 contains epitopes of monoclonal antibodies (mAbs) isolated from humans, including from seasonally vaccinated populations [142]. These include epitopes near the RBS, which are often associated with broad hemagglutination inhibition (HAI) and neutralizing activities. These

overlap with some of the classically defined antigenic sites, including Sa, Sb, and Ca2, within the HA head domain. To characterize the head-dependent antigenicity of X6, we determined cryo-EM structures of X6 bound to the Fab fragment of human mAb CA09-26 at 4.2 Å resolution, bound to the human #58 Fab fragment to 3.8 Å resolution, and bound to the mouse BE1 Fab fragment at 3.45 Å resolution **(Figure 6.3, Figure 6.4)**.

CA09-26 was isolated previously from a seasonally vaccinated subject who received the 2017-2018 vaccine [142]. It possesses both HAI and neutralizing activities against recent 2009 H1N1-like strains such as A/Michigan/45/2015 (A/MI/15) and A/California/07/2009 (A/CA/09), in addition to a seasonal pre-2009 H1N1 strain, A/New Caledonia/20/1999 (A/NC/99). Although the cryo-EM map was not of sufficient resolution to permit modeling, general fitting of the X6 structure and a generic Fab suggested that its epitope overlaps with the RBS **(Figure 6.3A)**. This corroborated previous biolayer interferometry-based epitope binning observations suggesting competition between 5J8, a known RBS-binding antibody [119], and CA09-26 [142].

mAb #58 was also isolated previously from a human subject, D160, who was vaccinated in 2013 and 2014 with the Fluzone seasonal vaccine. Serum from this subject possessed binding and HAI activity to H1 HAs and H1N1 viruses **(Figure 6.S2A,B)**. #58 was isolated following the 2014 vaccination, and possesses binding activity against some pre-2009 and post-2009 HAs, significant HAI activities for A/NC/99 and A/MI/15, and neutralizes the A/CA/09 2009 pandemic strain **(Figure 6.S2C,D,E)**. Similar to CA09-26, mAb #58 also appeared to bind to the X6 head domain at the RBS **(Figure 6.3B)**. While both mAbs CA09-26 and #58 bound the RBS, mAb #58 bound at a more vertical angle relative to CA09-26, implying distinct contacts within this epitope **(Figure 6.3C)**. mAb #58 also bound the X6 head domain and used both heavy and light chain residues to contact the RBS **(Figure 6.3D, S3A)**. These contacts are located in both the 190-helix

and the 220-loop of the RBS. Specifically, R188 of X6 may interact through polar interactions with the side chain of Y38 in HCDR1. D112.3 of HCDR3 may also participate in electrostatic interactions with X6, making contacts with the side chain of Q222. Moreover, H109 of the mAb #58 LCDR3 loop participates in hydrogen bonding with the side chain of D186.

Residues in the epitope of mAb #58 appeared to be conserved in both the pre-2009 NC99 and post-2009 MI15 HAs, permitting binding **(Figure 6.3E)**. In NC99, the residue at position 186 is an asparagine, mutated from D186 in X6. This D186N mutation may still permit hydrogen bonding interactions with the light chain H109 as both are similarly polar residues. In contrast, NC99 retains both R188 and Q222, permitting electrostatic interactions with Y38 and D112.3 of #58, respectively. MI15 possesses a glutamine at position 188, mutated from R188, which may still permit polar interactions with Y38 of the heavy chain. However, both D186 and Q222 are conserved as well in the #58 epitope of this more recent 2009 pandemic-like strain. Overall, despite some sequence flexibility in the #58 epitope between pre-2009 and post-2009 viruses, the overall set of interactions appears to be conserved.

We isolated mAbs from X6-vaccinated mice and characterized their binding and HAI activity to H1 HAs and H1 viruses **(Figure 6.S4)**. We found other mAbs possessing broad binding to pre-2009 seasonal H1 HAs. These mAbs, 1G8 and 5CA9, did not bind the chimeric H6/1 (cH6/1) HA, which possesses the H6N1 (isolate A/mallard/Sweden/81/2002) head and the HA stem of 2009 pandemic H1N1 (isolate CA/09), suggesting binding to a head epitope. They also lacked HAI activity except for A/Phil/13 for mAb 5CA9, suggesting binding to a conserved, non-RBS head domain epitope. Another mAb, BE1, was also isolated, which similarly possessed binding activity against HAs from before the 2009 H1N1 pandemic and did not bind the cH6/1 HA **(Figure 6.S4A)**. Moreover, BE1 did not show significant HAI activity for most H1N1 viruses

except for A/SI/06, suggesting that it bound a non-RBS epitope **(Figure 6.S4B)**. Therefore, to elucidate the epitope of this class of antibodies, we determined the structure of the BE1 Fab fragment in complex with X6, resulting in an HA trimer bound to two Fabs. From the cryo-EM map, we found that it bound nearly horizontally to a non-RBS epitope on the side of the head domain distal to the RBS **(Figure 6.4A)**. BE1 uses both heavy and light chain residues to interact with its epitope **(Figure 6.4B)**. Heavy chain interactions with the epitope involved Y111 and Y112.1 in HCDR3. Y111 participates in polar interactions with the side chain of N166 in X6, as well as with the main chain carbonyl oxygen of K170. Y112.1 also participates in a polar interaction through its side chain with the main chain of E115. Light chain interactions were more extensive than heavy chain interactions for this antibody. The side chain of S65 is involved in hydrogen bonding with that of S121. K66 participates in a salt bridge with the side chain of E115, and Y56 is involved in hydrogen bonding with the main chain of I116. Y38 also participates in a hydrogen bond with the side chain of N167.

We also compared the BE1 epitope in X6 with those found in pre-2009 and post-2009 H1 HAs **(Figure 6.4C,D)**. We found that all participating residues were conserved in the NC99 HA, consistent with the binding activity observed with pre-2009 H1 HAs **(Figures 6.S4A, 6.4C)**. In that of the post-pandemic MI15 HA, most residues were conserved relative to that of X6 **(Figure 6.4D)**. The only mutation found in this epitope relative to X6 was a N167D mutation. It is likely, however, that this change alone may not significantly impact binding of BE1, as this still places a polar side chain in close proximity to the side chain of Y38. Other structural features may be responsible for the abrogation of BE1 binding to post-2009 H1 HAs. For instance, we found that in MI15 and other post-2009-like HAs, a clash with BE1 was predicted at position 165 in antigenic site Ca1, close to other residues in the BE1 epitope, which was not found for the NC99 pre-2009

HA **(Figure 6.4E-G)**. Specifically, MI15 possesses a bulky isoleucine residue that might clash mainly with Y36 and slightly with Y108 of the light chain, interfering with binding. In X6, the residue at this position is an alanine, and corresponds to a valine for NC99, which both possess sufficiently small side chains to accommodate BE1. This epitope appeared to overlap with the previously described lateral patch, which is conserved across both pre-2009 pandemic and the 2009 pandemic H1 HAs [45,136]. We also compared the binding orientation of the BE1 Fab to those of the Fab fragment of Ab6649, isolated from a subject who received a monovalent A/California/07/2009 vaccine [45], and 045-09 2B05, isolated from another subject who received a 2009 monovalent influenza vaccine [136] **(Figure 6.4H)**. Structural alignment of the BE1 Fab to those of mAbs Ab6649 [45] and 045-09 2B05 [136] indeed confirmed some overlap with the lateral patch, binding at an angle between these Ab6649 and 045-09 2B05 Fabs to the head domain. Overall, these data suggest that X6 contains the RBS epitope in addition to the non-RBS lateral patch epitope, contributing to its broad reactivity.

Structure and Characteristics of X6-Binding Broadly Reactive Stem-Binding Antibodies

Stem-binding antibodies generally possess greater breadth than head-binding antibodies, which could contribute to long-lasting protection [1]. To determine the integrity of potential X6 stem domain epitopes, we obtained a cryo-EM structure of X6 bound to the Fab fragment of CR6261, a known group 1-reactive antibody [59]. The CR6261 Fab:X6 structure was solved to 2.64 Å resolution **(Figure 6.5, S3C)**. The cryo-EM structure revealed that the CR6261 Fab bound X6 at the expected central stem epitope near the middle of the stem similar to previously characterized HAs [59] **(Figure 6.5A)**. We also investigated the structural features of the CR6261 Fab:X6 interaction in comparison to that of previously determined structures of the CR6261 Fab with historic, seasonal pre-2009, and recent swine-origin post-2009 H1 HAs **(Figure 6.5B)**. The

CR6261 Fab interacted with X6 using only its heavy chain. Significant contacts included polar interactions of the side chain of N379 in X6 with the backbone of F30 on CR6261. Q368 of X6 also interacts through polar interactions with the main chain atoms of CR6261 S36 and Y110. The side chain of Y110 also undergoes hydrogen bonding with the backbone oxygen of X6 D345. We further assessed whether CR6261 binding to X6 used similar contacts to historic, seasonal, and recent H1 HAs. When comparing the CR6261 epitope of X6 to those of the historic A/South Carolina/1/1918 (SC18), the seasonal pre-2009 A/Bayern/07/1995 (BA95), and the recentH1n1 variant (H1N1v) swine-origin A/Ohio/09/2015 (OH15) [170] HAs, most of these interactions appeared to be conserved. The hydrogen bond made from T375 of X6 with S36 of CR6261 HCDR1 appeared to be a novel contact not found in wild-type HAs. Additionally, the electrostatic interaction between Q111 of CR6261 to Q364 of SC18 was not found in other CR6261 epitopes analyzed here. In the SC18, BA95, and OH15 structures, S36 appeared to interact through its side chain to the main chain of D372 in the SC18 and OH15 HAs or to the main chain of N372 in BA95 using hydrogen bonding. Nonetheless, all other contacts were found in the SC18, BA96, and OH15 HAs, indicating that overall, the CR6261:X6 interaction occurs through similar residue interactions as for historic, seasonal, and recent HAs.

From a mouse immunized with X6, we also isolated a murine mAb, B3, that bound the cH6/1 HA and all wild-type H1 HAs. This mAb further lacked HAI activity against pre-2009 or post-2009 H1 viruses **(Figure 6.S4)**. These data implied that B3 bound the H1 stem domain, further corroborating the antigenic integrity of the stem in a mouse model. Overall, these data suggest that although X6, and COBRA HAs in general, were previously thought to elicit broadened immunity through head-binding antibodies, they may still elicit broadly reactive stem-binding antibodies.

Discussion

Here we show that the X6 COBRA HA possesses conserved antibody epitopes of HAs from both pre-2009 and post-2009 strains. This is similar to previously characterized COBRA HAs of the H3 and H5 subtypes [55,165]. This observation implies that it could stimulate broadly reactive B cell clones in human populations. From sequence alignments to wild-type HAs, X6 possesses greater identity to pre-2009 HA strains than post-2009 HAs both overall and at the variable antigenic sites. Structurally, these sequence differences were expectedly found to be in the more variable head domain, rather than in the conserved stem domain **(Figure 6.1C)**. The observation that it can bind several antibodies reactive to more recent virus strains, however, suggests that other features, such as glycosylation sites, could additionally be responsible for this enhanced breadth.

X6 is structurally similar to wild-type HAs NC99 and MI15, forming trimers with glycosylation sites that recapitulate both seasonal and pandemic-like HAs. As the majority of these sites are shared across both NC99 and MI15, one potential mechanism of eliciting broadly reactive antibodies could be the redirection of antibody responses to conserved epitopes found across both pre-2009 and post-2009 HAs and away from strain-specific sites. One glycosylation site found on the top of the X6 head domain, at N159, was shared only with NC99 but not with MI15. It is possible that this glycan could block antibodies that bind nearby antigenic sites, such as Sa, in which this glycan is located. This has been seen for other COBRA HAs, such as P1, where removal of a glycosylation site enhanced antibody binding [171].

COBRA HAs are thought primarily to elicit head-binding antibodies [117]. To investigate whether X6 possessed broadly reactive head epitopes, we determined the cryo-EM fits and structures of three mAbs, CA09-26, #58, and BE1 with X6. We found that mAbs CA09-26 and

#58 bound residues in the RBS, consistent with their enhanced HAI breadth against pre-2009 and post-2009 H1N1 strains. In addition, it appeared that the epitope of mAb #58 was relatively conserved both in NC99 and MI15. The approach angles of CA09-26 and mAb #58 also differed from each other, despite appearing to target somewhat similar epitopes on X6, where CA09-26 bound at roughly 45 degrees to X6 whereas mAb #58 bound at a fairly vertical angle. mAb #58 used both heavy and light chain residues to contact the RBS of X6. In addition, we found that mAb BE1 binds to a distinct, non-RBS epitope on the head domain, instead binding to residues that are part of the previously described lateral patch at a near-horizontal angle [45,136]. Although BE1 only binds pre-2009 HAs, the lateral patch epitope with which it overlaps is conserved across both pre- and post-2009 pandemic HAs [45]. Structural comparisons to previously characterized lateral patch antibodies revealed that BE1 binds at an intermediate angle between that of Ab6649 and 045-09 2B05. We found that immunization with X6 elicited other broadly reactive, pre-2009 HA-binding mAbs with minimal HAI activity in mice, possessing similar binding and HAI profiles to mAb BE1 **(Figure 6.S4)**. This may indicate that the lateral patch may be another significant epitope in X6. Therefore, the antibody epitopes found on X6 can likely accommodate a wide range of broadly reactive RBS- and lateral patch-targeting antibodies.

We also structurally characterized the stem of X6 through determining the structure of the Fab of CR6261 with this COBRA HA. CR6261 is a group 1-reactive antibody that possesses neutralizing activity against several subtypes, including H1 and H5 [59]. It has also been used previously to guide vaccine design of stem-based HAs [70]. Here we show that X6 possesses an intact central stem epitope that can bind CR6261 using conserved residues found across wild-type HAs. These CR6261:HA interactions span residues across the historic 1918 Spanish influenza pandemic, the seasonal pre-2009 A/Bayern/07/1995, and the recent swine-origin A/Ohio/09/2015

HAs. While it has been established that immunization with COBRA HAs elicits high amounts of HAI-active, head-focused neutralizing antibodies, the stem-based antibody response has been less characterized. We also showed here that X6 immunization also induces stem antibodies in mice, as observed for mAb B3, which bound all tested H1 HAs and the cH6/1 HA construct while lacking HAI activity against H1 viruses **(Figure 6.S4)**. Structural confirmation of the integrity of this epitope implies that COBRA HAs may indeed elicit stem-reactive antibodies. This was shown previously for another H1 subtype COBRA, Y2, where immunization in mice elicited serum antibodies that competed with CR6261 [160]. In addition, the Y2 COBRA also possesses the recently described anchor epitope, and the H3 COBRA TJ5 binds wild-type H3 HA cross-reactive stem antibodies [164,165].

These data provide structural insights into a next-generation influenza vaccine, providing evidence that COBRA HAs are similar to wild-type HAs from the standpoints of glycosylation and antigenic integrity. Previously we have shown that COBRA HAs cross-react with functional antibodies isolated from seasonally vaccinated human populations [164,165]. From the studies described here, we define the structural basis for this expanded antibody breadth which likely depends on glycan-dependent redirection of antibody responses and broadly reactive head and stem epitopes. COBRA HAs could mediate expanded antibody breadth through (1) eliciting a wide range of antibodies that synergistically expand virus breadth, or by (2) focusing antibody responses to narrow but highly conserved epitopes. Our data presented here, in addition to other structural studies on COBRA HAs [164,165,171], lend credence to this second mechanism. In addition, the broad binding of murine mAbs to wild-type H1 HAs further suggests that, at least in part, monoclonal breadth contributes to the polyclonal breadth to COBRA HAs [150] **(Figure 6.S4).** As the COBRA HA methodology moves into late preclinical and early clinical studies, further

structural characterization will be needed to probe correlates of an effective and long-lasting antibody response.

Figures

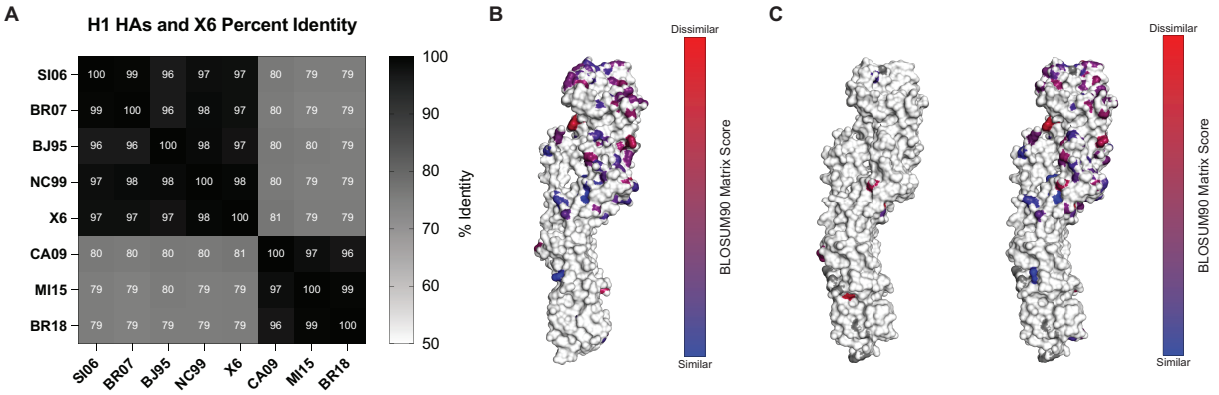

Figure 6.1. Sequence and structural comparisons of wild-type HAs to X6. (A) Heat map of overall percent identity of pre-2009 and post-2009 HAs to X6. (B-C) Structural comparisons between HAs, with mutated residues colored from blue to red based on low to high amino acid similarity as measured by the BLOSUM90 matrix. (B) Structural comparison of the A/New Caledonia/20/1999 (NC99) and A/Michigan/45/2015 (MI15) HAs, mapped to the NC99 HA (PDB 7MFG). (C) Structural differences between X6 and NC99 (left) and X6 and MI15 (right) mapped to X6.

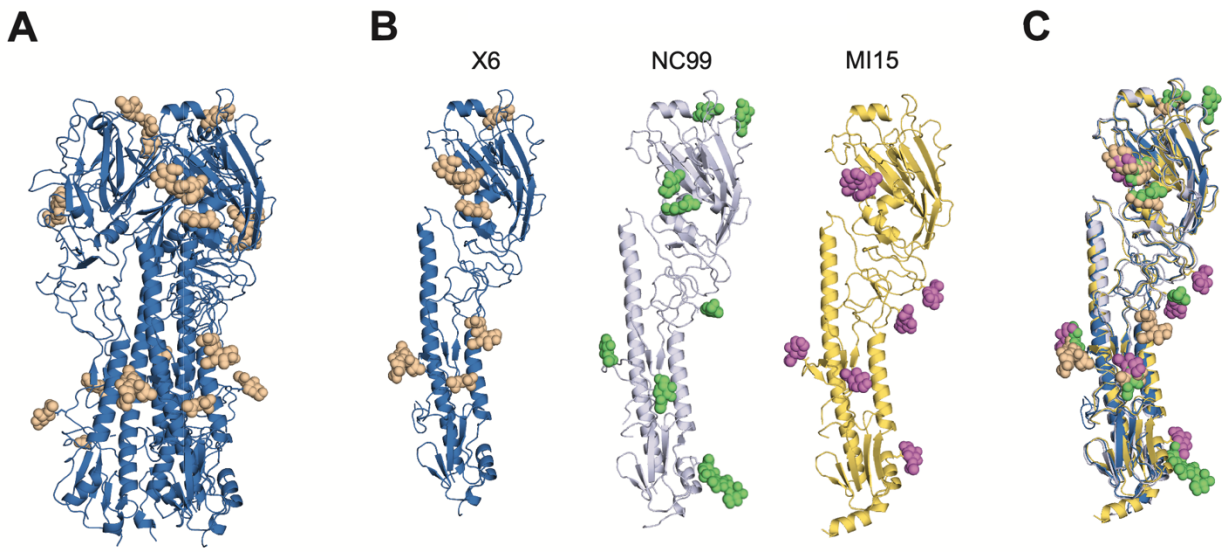

Figure 6.2. Crystal structure and glycosylation features of the X6 COBRA HA. (A) The X6 structure is shown as a trimer, with glycans indicated as light orange spheres. (B) Individual HA monomers for X6, NC99 (PDB 7MFG), and MI15 (PDB 6XGC) are shown. Glycans for NC99 are shown in green, and those for MI15 are shown in pink. (C) Overlay of the X6, NC99, and MI15 HA structures.

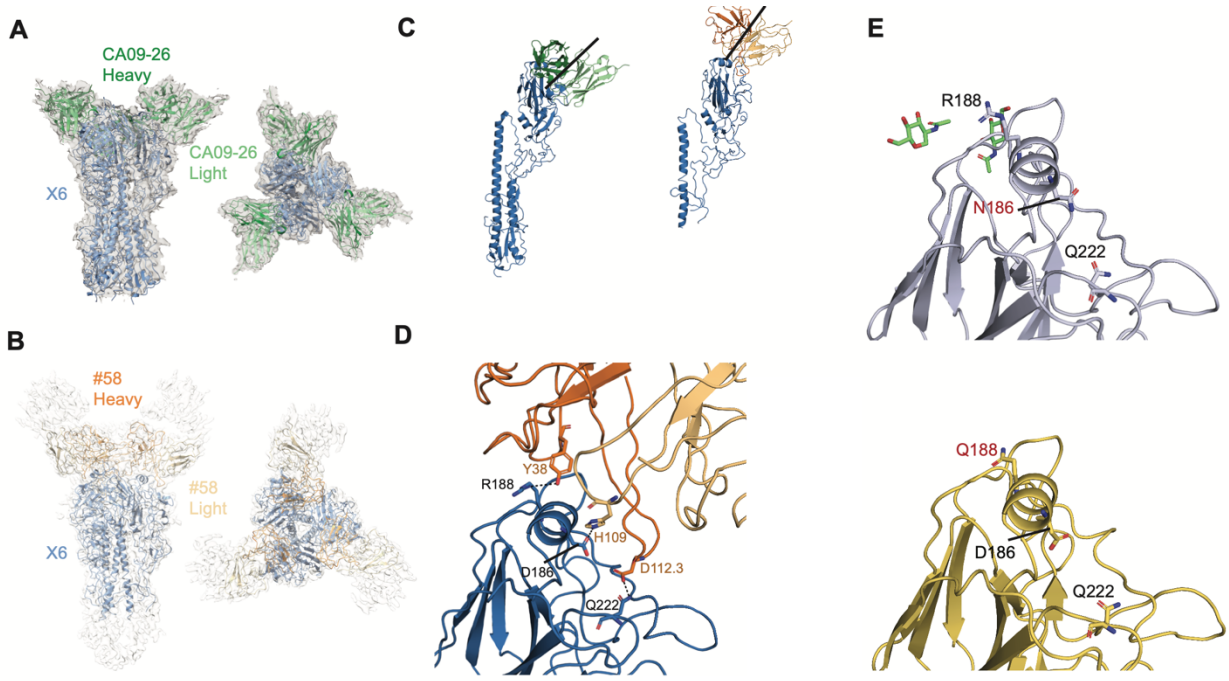

Figure 6.3. Cryo-EM structures of HA RBS-binding antibody Fabs with X6. (A) The fit of a Fab variable fragment extracted from PDB ID 4Q9Q and the X6 trimer HA is shown in the cryo-EM map density of CA09-26 Fab:X6. Left: side view, right: top view. (B) The structure of the #58 Fab with X6 is shown in the cryo-EM density. Left: side view, right: top view. (C) Comparison of binding angles of CA09-26 (left) and #58 (right) with X6. (D) The interface between the #58 Fab and X6. (E) Residue comparisons in the epitope of #58 are shown for the NC99 (top) and MI15 (bottom) HAs. Mutated residues relative to X6 are shown in red.

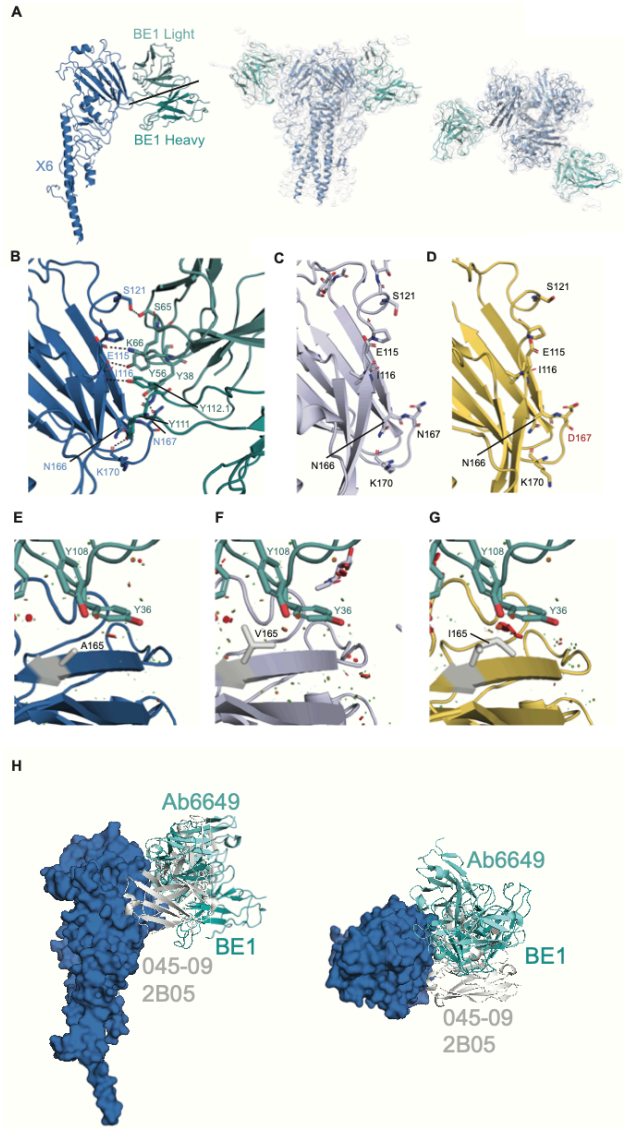

Figure 6.4. Cryo-EM structure of the HA lateral patch-binding antibody BE1 Fab with X6. (A) The binding angle of the BE1 Fab to X6, as well as the structure fit to the cryo-EM map. (B) The interface between the BE1 Fab and X6 with interacting residues shown. (C-D) Residue comparisons in the BE1 epitope for (C) NC99 and (D) MI15, respectively. Mutated residues relative to X6 are shown in red. (E-G) Residue comparisons and steric clashes at position 165, shown in white, for (E) X6, (F) NC99, and (G) MI15, respectively. Clashes are shown in red with more significant clashes shown as larger discs. (H) Structural comparisons of BE1 to other lateral patch antibodies, Ab6649 and 045-09 2B05.

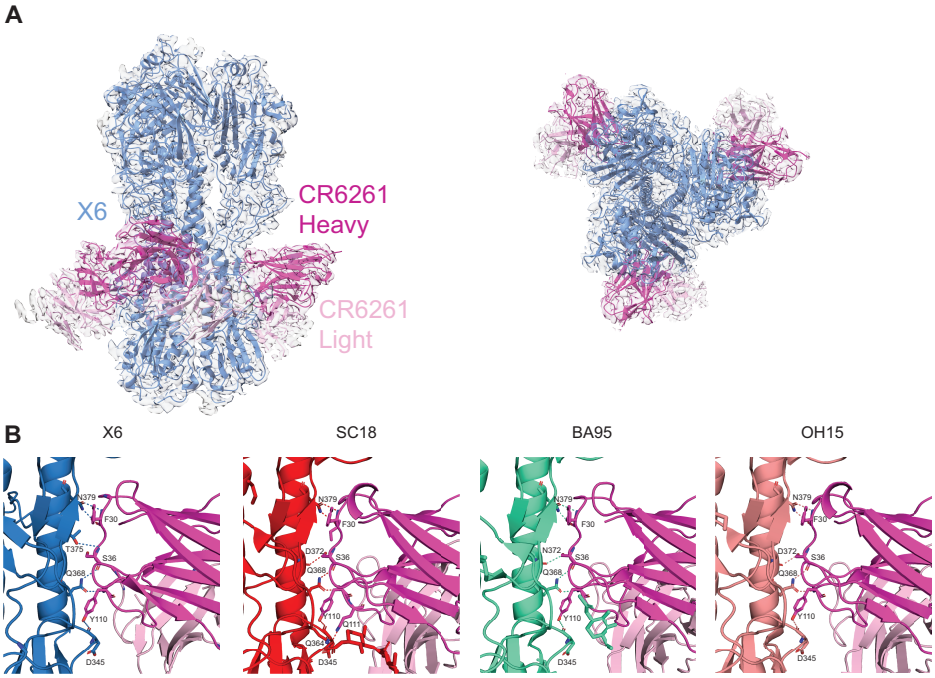

Figure 6.5. Cryo-EM structure of the broadly reactive antibody CR6261 with X6. (A) Fit of the CR6261 Fab:X6 structure to the cryo-EM density for side (left) and top (right) views. (B) Interacting residues between CR6261 and X6, the A/South Carolina/1/1918 HA (SC18, PDB 3GBN), the A/Bayern/07/1995 HA (BA95, PDB 8DIU), and the A/Ohio/09/2015 HA (OH15, PDB 6UYN).

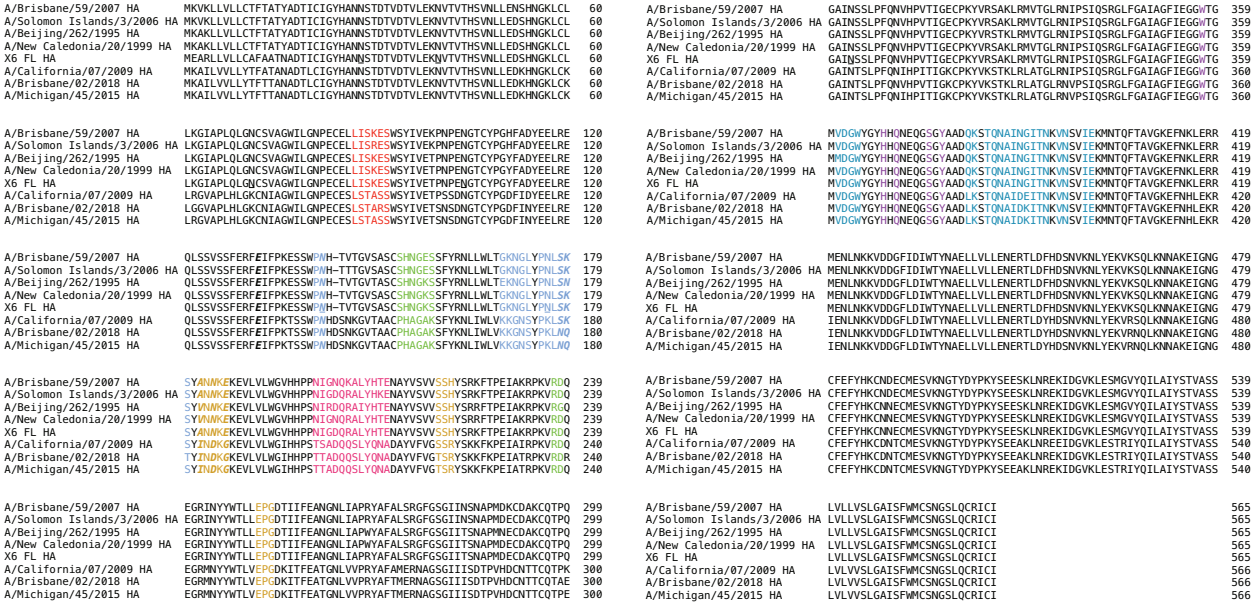

Figure 6.S1. Sequence alignment of X6 and wild-type pre-2009 and post-2009 HAs. The indicated HAs were aligned to the X6 COBRA HA sequence using MUSCLE alignment. The antigenic sites are indicated in colors: Sa is shown in blue, Sb in pink, Ca1 in yellow, Ca2 in green, and Cb in red. The lateral patch epitope is shown in bold italics, the central stem epitope is shown in teal, the anchor epitope is shown in violet, and glycosylation sites are shown as underlined residues for X6.

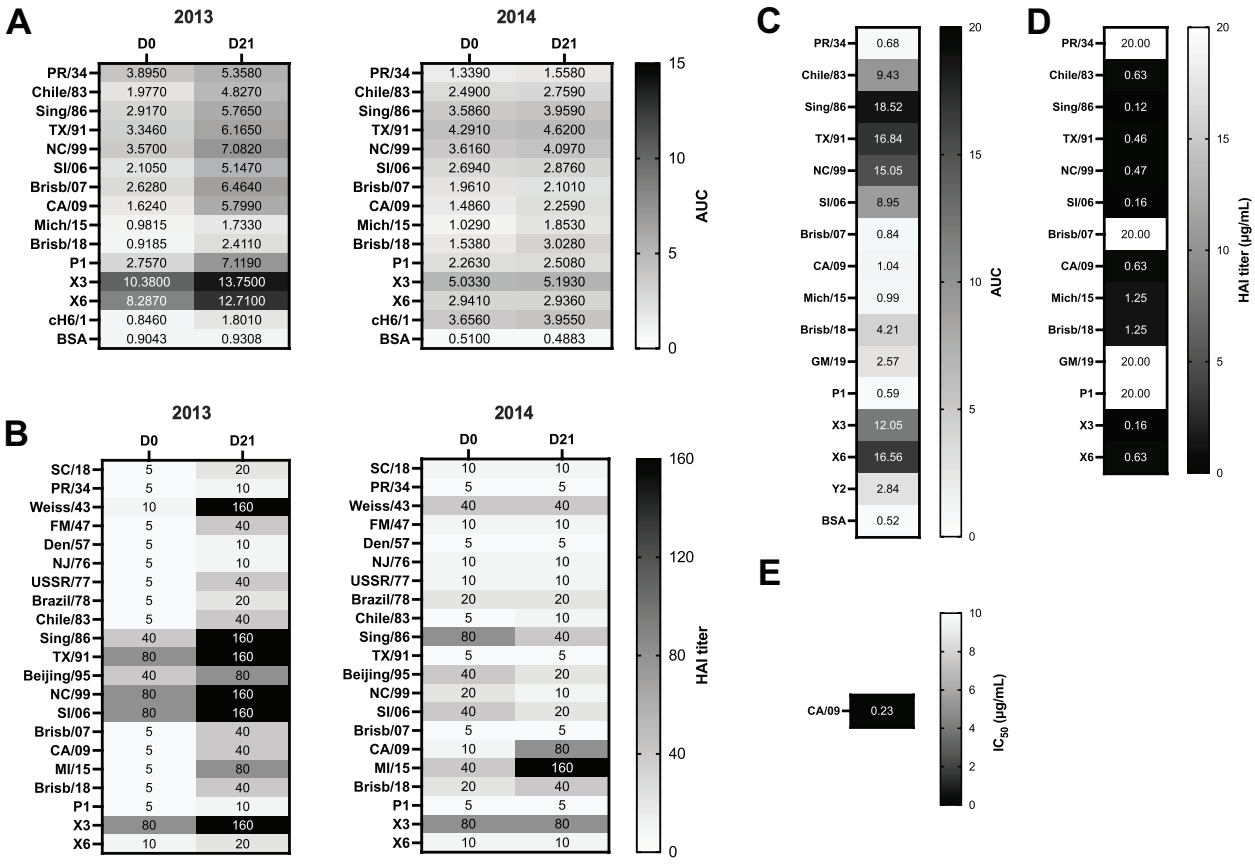

Figure 6.S2. Binding and functional characteristics of serum from subject D160 and mAb #58. (A) Area under the curve (AUC) values of serum against wild-type H1 HAs, COBRA HAs, including X6, and the cH6/1 HA shown as a heat map, determined by ELISA following vaccination with the Fluzone seasonal vaccine in 2013 and 2014. The cH6/1 HA is a chimeric HA with a H6 subtype head attached to a H1 subtype stem. (B) HAI titers of serum against wild-type H1N1 and X6 viruses. HAI titers are shown as a heat map. (C) ELISA binding titers of the #58 mAb to the indicated H1 HAs, shown as AUC values. (D) HAI titers of the #58 mAb to the indicated viruses, shown as a heat map in µg/mL. (E) The IC_{50} of #58 to the A/CA/09 virus, determined by FRA. For (A) and (B), values for D0 indicate those measured at the time of vaccination, and D21 those measured 21 days post-vaccination. Activities against P1 and X3 COBRA HAs and viruses, which have been previously characterized [168], are also shown.

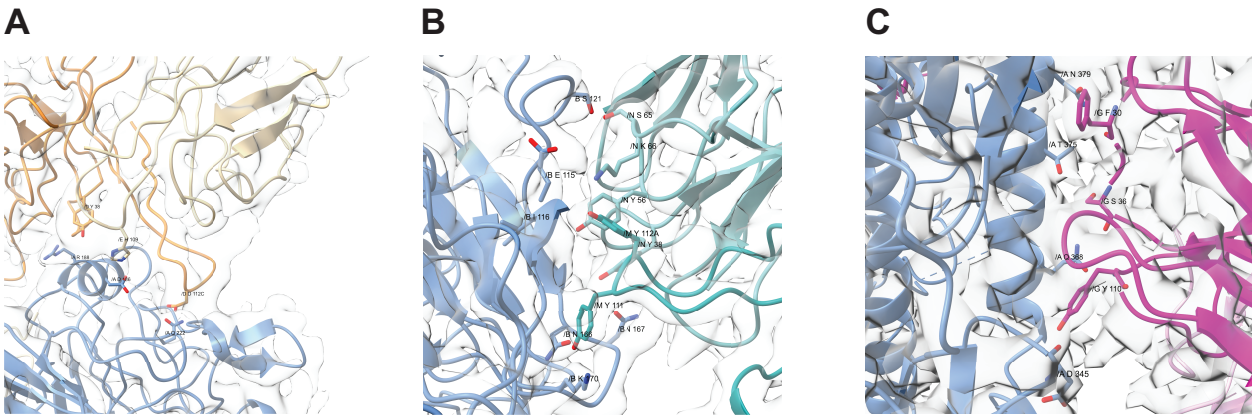

Figure 6.S3. Density fit of Fab:X6 complexes to cryo-EM maps. Fits of the (A) #58 Fab with X6, (B) BE1 Fab with X6, and (C) CR6261 Fab with X6 to the respective electron potential maps.

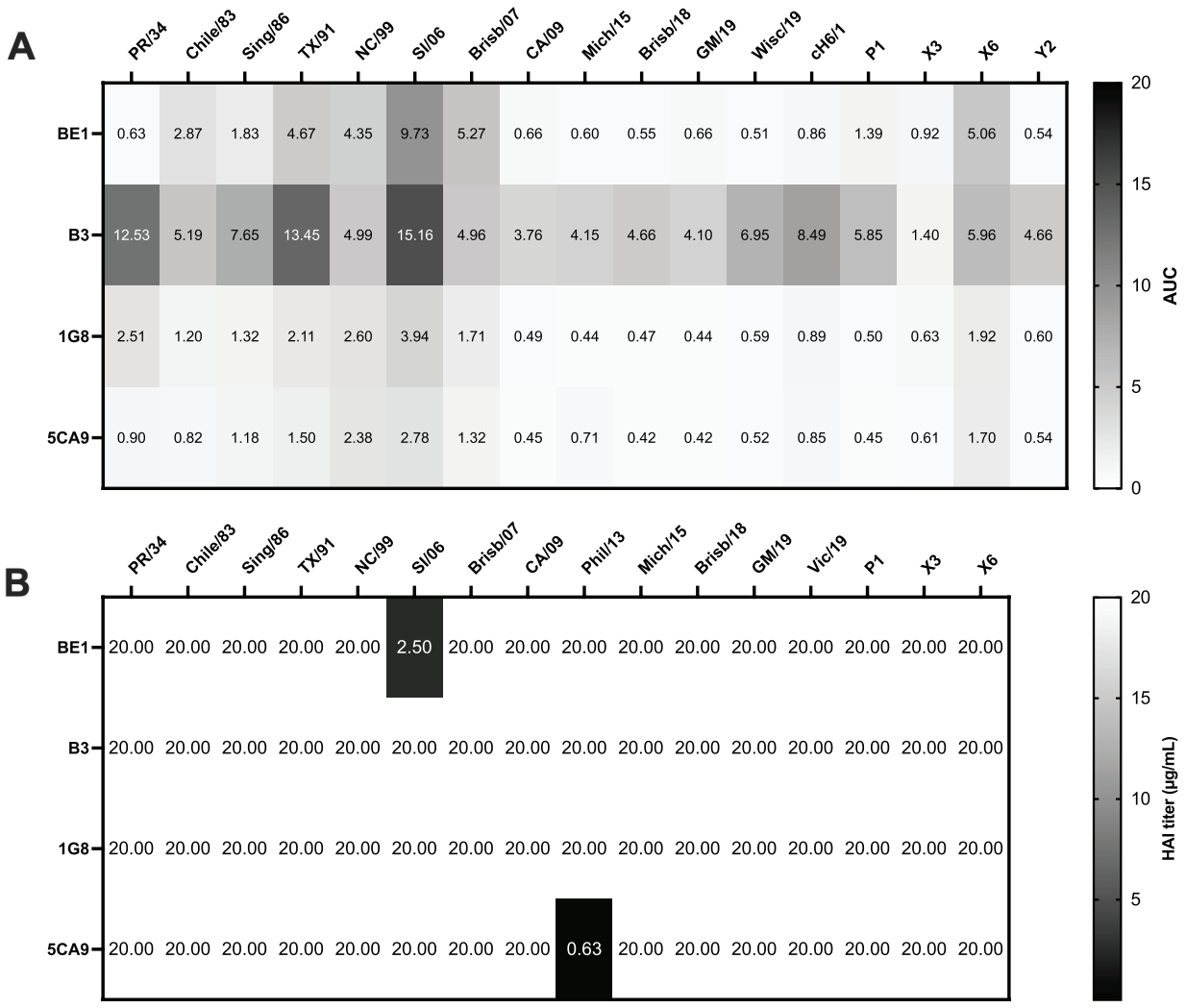

Figure 6.S4. Binding and HAI activities of BE1 and other X6-specific mAbs. (A) AUC values of mAb binding to wild-type H1 HAs, cH6/1 HA, and COBRA HAs, determined by ELISA, shown as a heat map. (B) HAI titers, in µg/mL, to the indicated viruses, shown as a heat map. A value of 20 indicates the absence of HAI activity. Activities against P1, X3, and Y2 COBRA HAs and viruses, which have been previously characterized [122,168], are also shown.

Tables

Table 6.S1: X6 X-ray crystallography data collection and refinement statistics.

	COBRA X6 (PDB 8SJ9)
Data collection	
Space group	$P2_1$
Cell dimensions	
a, *b*, *c* (Å)	68.50, 218.73, 68.57
α, β, γ (°)	90.00, 109.68, 90.00
Resolution (Å)	48.34-3.25 (3.45-3.25)*
R_{merge}	0.143 (1.268)
I / σI	6.0 (1.0)
CC(1/2)	0.995 (0.312)
Completeness (%)	98.3 (98.3)
Redundancy	3.5 (3.5)
Refinement	
Resolution (Å)	44.43-3.25 (3.37-3.25)
No. reflections	29,272 (2917)
R_{work} / R_{free}	0.221 (0.277)
No. atoms	
Protein	11,518
Ligand/ion	327
B-factors	
Protein	121.70
Ligand/ion	172.89
R.m.s. deviations	
Bond lengths (Å)	0.002
Bond angles (°)	0.46
Ramachandran plot statistics (%)	
Outliers	0.00
Allowed	2.91
Favored	97.09

*Values in parentheses are for highest-resolution shell.

Table 6.S2. CA09-26 Fab:X6 cryo-EM data collection and refinement statistics.

CA09-26 Fab complexed with X6	
EMDB ID	***
PDB ID	***
Data collection	
Microscope	Glacios
Detector	Falcon 4
Voltage (kV)	200
Magnification	190,000
Defocus range (μm)	-0.9 to -2.0 (interval 0.3)
Pixel size (Å)	0.526
Number of Frames	30
Dose rate	57.22 e/Å^2/s
No. of Images collected	10,870
Reconstruction	
Software	CryoSPARC
Number of used particles	60,400
Symmetry	C3
Final Resolution (Å) ($FSC_{0.143}$)	4.2 Å
Map sharpening B-factor (Å^2)	-174.4

Table 6.S3. #58 Fab:X6 cryo-EM data collection and refinement statistics.

#58 Fab complexed with X6	
EMDB ID	***
PDB ID	***
Data collection	
Microscope	Glacios
Detector	Falcon 4
Voltage (kV)	200
Magnification	190,000
Defocus range (μm)	-0.9 to -2.0 (interval 0.3)
Pixel size (Å)	0.526
Number of Frames	30
Dose rate	57.22 e/Å^2/s
No. of Images collected	11,361
Reconstruction	
Software	CryoSPARC
Number of used particles	134,751
Symmetry	C3
Final Resolution (Å) ($FSC_{0.143}$)	3.8 Å
Map sharpening B-factor (Å^2)	-160.6
Model building and Refinement	
Model building software	Coot
Refinement software	Phenix
Number of chains	9
Atoms	13611
Residues	Proteins: 1758; Nucleotide: 0
Validation	
R.m.s deviations	
Bonds length (Å)	0.005 (0)
Bonds Angle (°)	0.958 (3)
Ramachandran plot statistics (%)	
Outliers	0.00
Allowed	14.19
Favored	85.81
MolProbity score	2.61
Clash score	29.93
Rotamer outliers (%)	0.00
CaBLAM outliers (%)	7.19
CC(volume)	0.76

Table 6.S4. BE1 Fab:X6 cryo-EM data collection and refinement statistics.

Influenza A virus hemagglutinin (InvcI.18715.a.K1; X6-COBRA) in complex with BE1 Fab	
EMDB ID	EMD-40046
PDB ID	8GHK
Data collection	
Microscope	Titan Krios
Detector	Gatan K3
Voltage (kV)	300
Magnification	130, 000
Defocus range (μm)	-1.0 to -2.5 (interval 0.25)
Pixel size (Å)	0.675
Number of Frames	40
Dose rate	34.85 e/Å^2/s
Dose per frame (e$^-$)	2.00
Exposure time (s)	2.29
No. of Images collected	7031
Reconstruction	
Software	CryoSPARC V3.2
Number of used particles	100708
Symmetry	C1
Box size (pix)	558
Final Resolution (Å) ($FSC_{0.143}$)	3.47 Å
Map sharpening B-factor (Å^2)	-72.4
Model building and Refinement	
Model building software	Coot
Refinement software	Phenix
Number of chains	14
Atoms	11671
Residues	Proteins: 1556; Nucleotide: 0
Ligands	BMA:2; NAG:15
EMRinger Score	2.63
Validation	
R.m.s deviations	
Bonds length (Å)	0.002 (0)
Bonds Angle (°)	0.488 (1)
Ramachandran plot statistics (%)	
Outliers	0.0

Allowed	3.85
Favored	96.15
MolProbity score	1.62
Clash score	6.48
Rotamer outliers (%)	0.63
CaBLAM outliers (%)	3.64
CC(volume)	0.81

Table 6.S5. CR6261 Fab:X6 cryo-EM data collection and refinement statistics.

Influenza A virus hemagglutinin (InvcI.18715.a.K1; X6-COBRA) in complex with CR6261 Fab	
EMDB ID	EMD-28833
PDB ID	8F38
Data collection	
Microscope	Titan Krios
Detector	Gatan K3
Voltage (kV)	300
Magnification	130, 000
Defocus range (μm)	-1.0 to -2.5 (interval 0.25)
Pixel size (Å)	0.675
Number of Frames	40
Dose rate	34.67 e/Å^2/s
Dose per frame (e$^-$)	2.00
Exposure time (s)	2.397
No. of Images collected	8973
Reconstruction	
Software	Relion 3.1.2; CryoSPARC V3.2.0
Number of used particles	385474
Symmetry	C3
Box size (pix)	558
Final Resolution (Å) ($FSC_{0.143}$)	2.64 Å
Map sharpening B-factor (Å^2)	-115.1
Model building and Refinement	
Model building software	Coot
Refinement software	Phenix
Number of chains	14
Atoms	16941
Residues	Proteins: 2122; Nucleotide: 0
Ligands	BMA:3; NAG:30
EMRinger Score	4.09
Validation	
R.m.s deviations	
Bonds length (Å)	0.004 (0)
Bonds Angle (°)	0.699 (4)
Ramachandran plot statistics (%)	
Outliers	0.14
Allowed	3.24

Favored	96.62
MolProbity score	1.79
Clash score	3.81
Rotamer outliers (%)	3.36
CaBLAM outliers (%)	1.78
CC(volume)	0.82

CHAPTER 7

STRUCTURAL CHARACTERIZATION OF A COMPUTATIONALLY OPTIMIZED H3 SUBTYPE HEMAGGLUTININ[6]

[6]Nagashima, Kaito. To be submitted to *Journal of Virology*.

Abstract

H3 subtype influenza viruses circulate every year and cause disease in a significant proportion of the human population. Current seasonal vaccines only offer short-term protection against these viruses due to viral evolution and antigenic variation. The consensus-based computationally optimized broadly reactive antigen (COBRA) vaccine approach has been previously developed to elicit extended antibody breadth to multiple strains of influenza viruses. This has been correlated with a broader antibody response to the hemagglutinin (HA) glycoprotein. However, studies on the structural correlates of how the COBRA HA mediates expanded antibody breadth have been limited. Here, we identified antibody epitopes on the NG2 COBRA HA that were highly conserved across multiple H3 subtype strains on the variable head domain and the conserved stem domain using cryo-electron microscopy (cryo-EM). These analyses suggest that the NG2 COBRA HA, similar to previously characterized COBRA HAs, possess intact epitopes that might be targeted by B cells to induce a broadly reactive antibody clones.

Introduction

Influenza viruses are responsible for significant morbidity and mortality ever year [188]. Influenza A viruses (IAVs) and influenza B viruses (IBVs) comprise the major circulating strains and are targeted by the current seasonal vaccine, which is the major countermeasure against this pathogen [3]. The seasonal vaccine offers protection through targeting of antibody responses to the predominant hemagglutinin (HA) glycoprotein, which is needed for the viral entry step [117]. These vaccines are usually trivalent or quadrivalent, consisting of H1N1 and H3N2 IAV strains in combination with one or two lineages of IBVs [117], although it appears that the Yamagata lineage has not been detected more recently since the COVID-19 pandemic [189]. Antibodies that are induced by the vaccine often target strain-specific epitopes that do not confer significant cross-season reactivity [117]. Therefore, the current vaccine only induces short-lived protection for a single season, due to the high mutability of influenza and its capacity to undergo significant antigenic variation through mechanisms of antigenic shift and antigenic drift [9].

H3N2 subtype influenza viruses circulate every year, and have been in circulation since the 1968 Hong Kong pandemic [114]. The HAs of H3 subtype viruses have undergone significant antigenic evolution since the 1968 pandemic [35]. The sites targeted by antibodies on the HA protein include the immunodominant but variable head domain as well as the immunosubdominant but conserved stem domain [117]. Currently characterized epitopes for H3 subtype HAs on the head domain include the variable antigenic sites A, B, C, D, and E, the receptor-binding site (RBS) [190], needed for viral attachment to sialic receptors on host cells, and the intratrimer epitope between HA monomers in the trimer [46]. The stem domain contains a central stem epitope that can be bound by group 2 broadly neutralizing antibodies (bNAbs) such as CR9114 [191], as well

as a membrane-proximal stem epitope that is targeted by other group 2 bNAbs CR8020 and CR8043 [192,193].

In an effort to improve antibody breadth to multiple seasons, next-generation or universal influenza vaccines approaches have been investigated, either through the design of immunogens that re-focus antibody responses to conserved parts or domains of the HA protein such as the stem domain or less variable regions of the head domain [117]. One such approach, the COBRA (computationally optimized broadly reactive antigen) methodology, uses a consensus building strategy to combine wild-type viral HA sequences from a selected design period into a single antigen [54]. This strategy has been employed for the H3 subtype of IAVs for more recent strains with the NG2 COBRA HA, which incorporates sequences from 2016 to 2018, and could reduce burden from challenge with a H3N2 virus from 2017 in a mouse model [159]. This was also correlated with the induction of hemagglutination inhibition (HAI)-active antibodies that prevent attachment of virus to sialic acid receptors [159]. More recent studies have also underscored the potential importance of stem domain-directed antibodies in the COBRA HA approach as well, namely through the discovery that seasonally vaccinated subjects possess antibodies that can bind an H3 COBRA HA [162].

Broadly reactive mAbs elicited by seasonal vaccination with COBRA HA cross-reactivity have been previously isolated for the H3 subtype COBRA NG2, and were found through epitope binning studies to target the RBS of the head domain and the stem domain, two major conserved epitopes [162]. In this study, we demonstrate that three such human mAbs characterized previously, #1664 [186], TJ5-1 [162], and TJ5-13 [162], show broad H3 HA reactivity, HAI activity, and neutralization capabilities through divergent mechanisms involving blocking of receptor binding as well as binding of residues within the HA1/HA2 cleavage site and fusion

peptide by biochemical and cryo-electron microscopy (cryo-EM) analyses. Altogether, these data indicate that the COBRA NG2 vaccine incorporates conserved and intact antibody epitopes on the HA protein. These structural analyses provide insights into the mechanism by which COBRA HAs induce enhanced antibody breadth.

Methods

Sequence comparisons of the NG2 HA to wild-type HAs

MUSCLE alignment of the NG2 HA sequence was performed to HAs from years 1968 to 2019 using Geneious 2023.2.1 (Invitrogen). Alignment visualization was performed in JalView.

Enzyme-linked immunosorbent assay (ELISA)

To determine #1664 mAb binding to Y2 and NG2 COBRAs, 384-well plates (Greiner Bio-One) were coated with these antigens diluted to 2 μg/mL in phosphate-buffered saline (PBS) at 4°C overnight. The plates were washed once with water and then blocked with 2% blocking buffer (PBS + 2% nonfat dry milk [Bio-Rad] + 2% goat serum + 0.05% Tween 20) for 1 h at room temperature. The plates were washed three times with water, and 25 μL of mAb dilutions were added. MAbs were serially diluted three-fold in PBS from a 20 μg/mL initial dilution for 12 total dilutions. The plates were incubated at 25°C for 1 h, then washed three times with water. 25 μL of goat anti-human IgG Fc-AP secondary antibody (Southern Biotech), diluted 1:4000 in 1% blocking buffer (1:1 dilution of PBS and 2% blocking buffer), were added, and the plates were incubated at 25°C for 1 h. The plates were then washed five times with PBS-T (PBS + 0.05% Tween 20). p-Nitrophenyl phosphate (PNPP) substrate, diluted in substrate buffer (1.0 M Tris + 0.5 mM MgCl2, pH 9.8) to 1 mg/mL, was added, and the plates were incubated for 1 h and read

at 405 nm on a BioTek plate reader. Curves were fit using GraphPad Prism software using four-parameter nonlinear regression.

H3 virus hemagglutination inhibition (HAI) assay

#1664 was tested for the ability to mediate receptor blocking against a panel of H3N2 viruses. Influenza viruses were titered to eight HAUs. 50 μL of #1664 at 2.5 μg/mL were added to the first well of a 96-well V-bottom plate (VWR) and diluted two-fold in PBS. Eight HAUs of virus with 40 nM oseltamivir were added in a 1:1 ratio to each serum dilution, and each well was mixed and incubated for 30 min at room temperature. Following this, 50 μL of 0.8% guinea pig red blood cells (Lampire) were added per well. The plates were read 1 h after the addition of 0.8% guinea pig red blood cells.

Cryo-electron microscopy (cryo-EM) analysis of Fab:NG2 complexes

MAbs TJ5-1, TJ5-13, and #1664 were previously isolated from human subjects receiving the seasonal inactivated influenza vaccine. TJ5-1 and TJ5-13 mAbs were isolated from recipients of the 2016-2017, 2017-2018, 2019-2020, and 2020-2021 Fluzone inactivated vaccine using B cell electrofusion with a myeloma cell line for hybridoma generation, whereas the #1664 mAb was isolated from a recipient of the 2016-2017 seasonal vaccine [162,186].

For TJ5-1:NG2, TJ5-13:NG2, and #1664:NG2 structure determination, the Fab was mixed in a two-fold molar excess to NG2, then incubated at 4°C overnight. The mixture was then subjected to size exclusion chromatography (SEC) on a Superdex 200 column (GE Healthcare) to isolate the Fab:NG2 complex from excess Fab. Sample was then applied to glow-discharged carbon/copper grids for grid plunging and data collection. Motion-corrected movies were processed in CryoSPARC for particle picking, followed by two-dimensional class averaging. Following successive rounds of class averaging, selected particles were used for *ab-initio*

reconstruction and heterogeneous refinements. Homogeneous refinement with C3 symmetry was used for TJ5-1:NG2, TJ5-13:NG2, and #1664:NG2. Refined maps were then used for structure building of TJ5-1:NG2, TJ5-13:NG2, and #1664:NG2 in COOT followed by refinement in PHENIX [181,182].

Trypsin cleavage inhibition assay

Stem-binding mAb TJ5-1 was assessed for its ability to prevent proteolytic cleavage and maturation of the NG2 HA0 precursor protein into the HA1/HA2 subunits using an adapted protocol [46]. 40 μg of the mAb or 40 μL of PBS was added to 4 μg of the NG2 HA0 protein. The mAb:NG2 mixture was then incubated at 37°C for 1 h, then a 1:1 volume ratio of PBS (for the no mAb control) or TPCK-trypsin at 5 μg/mL (for the mAb treatment) was added. The mixture was then either not incubated for the untreated control, or incubated at 37°C for 5, 20, 40, or 60 min. The sample was then run under reducing conditions on SDS-PAGE and stained with Coomassie blue to visualize the extent of NG2 HA0 cleavage. The NG2 HA0 band was expected at ~100 kDa, ~70 kDa for the HA1 subunit, and ~30 kDa subunit. Inhibition of proteolytic cleavage was assessed as the retention of the ~100 kDa NG2 HA0 band at all time points, whereas active cleavage is visualized as a decrease in HA0 band density across the time points.

Results

The NG2 COBRA HA captures sequence and epitope features of wild-type H3 HAs

The NG2 COBRA HA design period spans from 2016 to 2018 for H3 viruses. To determine the sequence similarity of this HA to wild-type HAs from years before, including, and after this design period, we performed a MUSCLE alignment of the NG2 full-length HA sequence to those of wild-type H3 HAs from strains A/Aichi/2/1968 (AI68), A/New York/55/2004 (NY04),

A/Wisconsin/67/2005 (WI05), A/Brisbane/10/2007 (BR07), A/Victoria/361/2011 (VI11), A/Switzerland/9715293/2013 (SW13), A/Hong Kong/4801/2014 (HK14), A/Kansas/14/2017 (KA17), and A/Hong Kong/45/2019 (HK19) **(Figures 7.1A, 7.1B)**. The highly variable antigenic sites A, B, and C were, in general, extensively mutated between NG2 and the wild-type H3 HAs. In contrast, the antigenic sites D and E were much more conserved except for eight residues in antigenic site D and four residues in antigenic site E for this panel of H3 HAs. 3 of 7 intratrimer epitope residues were also mutated in wild-type HAs relative to NG2 but only for strains from 2007 and before. The central stem epitope was highly conserved between NG2 and all wild-type viruses, even for the AI68 HA which otherwise possessed only 88% identity at the amino acid level with NG2 **(Figure 7.1C)**. Comparisons of the full amino acid sequence of the HAs from these strains and COBRAs revealed that AI68 was the most divergent relative to NG2, whereas more recent strains from 2004 onward were much more similar, possessing 95% or higher identity. This illustrated that significant antigenic drift has occurred in the H3 subtype HA since the 1968 H3N2 pandemic, leading to head-focused mutations localized primarily to the antigenic sites over the past 50 years.

The NG2 COBRA HA possesses an intact RBS epitope

Noting that NG2 possessed sequence features of both historic and recent H3 HAs, and also that this COBRA HA could cross-react with broadly reactive human antibody TJ5-13 [162], we sought to determine the structural basis for antibody binding and breadth **(Figure 7.2)**. We determined the cryo-EM structure of the Fab fragment of this mAb with the NG2 COBRA HA to verify its epitope **(Figure 7.2A)**. The structure, solved to 2.8 Å, showed that the Fab bound to the top of the HA head domain at a site that overlapped with the highly conserved RBS epitope. This finding was in line with several pieces of data published previously. For instance, this mAb

possessed HAI activity against several H3N2 viruses from 2005 to 2019, preventing viral attachment **(Figure 7.2B)**. In addition, TJ5-13 also competed with other RBS mAbs C05 [190] and F045-92 [194] in an epitope binning assay [162]. The ability for TJ5-13 to bind this wide range of H3 HAs and prevent HA-receptor binding supported the broadly conserved nature of its epitope within the RBS.

We also determined the structure of another broadly reactive human mAb, #1664, which was also previously characterized [186]. This mAb was found to possess reactivity to several H3 HAs from 1999 to 2012, as well as to more recent strains from 2014, 2016, and 2017 [186]. It also did not bind the cH7/3 chimeric HA (cHA), which possesses an exotic H7 subtype head domain fused to an H3 subtype stem domain, suggesting that its binding epitope was most likely on the head of the H3 HA [186]. We further verified #1664 binding to the NG2 COBRA HA by ELISA **(Figure 7.2C)**. By cryo-EM, we determined the structure of its Fab fragment also bound to NG2 to a resolution of 3.4 Å **(Figure 7.2D)**. The structure again confirmed that it bound to the head domain of NG2 at an epitope overlapping the RBS, similar to TJ5-13. We found that the apparent binding angles of TJ5-13 and #1664 were similar to each other, with the major difference in the interactions appearing to be a more heavy chain-dominated interaction for #1664, in contrast to contributions from both the heavy and light chains of TJ5-13 to bind their epitopes. We also found that #1664 could mediate HAI activity against several H3 viruses from 1999 to 2019, similar to TJ5-13 **(Figure 7.2E)**. This finding supported that the RBS epitope was again intact on the NG2 head domain in a manner that could bind broadly reactive, receptor-blocking antibodies.

NG2 possesses an intact membrane-proximal stem domain epitope and can bind a maturation-inhibiting bNAb

The stem domain of HAs are more highly conserved than the head domain. Moreover, this domain has been shown to be conformationally intact on the H1 COBRA HA X6, as discussed in the previous chapter. To assess whether this was also the case with the NG2 COBRA, we complexed it with the Fab fragment of a bNAb, TJ5-1, which could neutralize several H3N2 viruses based on previously published data **(Figure 7.3A)**. This mAb, however, lacked any HAI activity against the same viruses, suggesting that its epitope did not involve the RBS based on a previous report [162]. We then determined its epitope by cryo-EM **(Figure 7.3B)**. This structure was solved to 3.3 Å and confirmed that the mAb bound to the stem domain of the HA, consistent with previous epitope binning data that showed competition with the group 2 bNAb CR8020 [162]. We also determined its epitope, and found heavy chain- and light chain-derived interactions with the residues that spanned across the R329 HA1/HA2 cleavage site and the highly conserved fusion peptide. We further compared the binding orientations of TJ5-1 to NG2 relative to two group 2 stem bNAbs CR8020 and CR8043 to the A/Hong Kong/1/1968 (HK68) HA **(Figure 7.3C)**. Whereas CR8020 and CR8043 bound at a side-on angle to their epitopes, TJ5-1 appeared to bind its epitope from the front of the HA instead at a unique orientation. We also aligned the epitope residues of TJ5-1 to those of CR8020 and CR8043 to compare the interacting HA residues **(Figure 7.3D)**. We observed that TJ5-1 bound to G345 of the NG2 HA (G378 of the HK68 HA), a residue that was also involved in binding to both CR8020 and CR8043. However, other interactions of TJ5-1 with the NG2 HA involved residues that were upstream in the fusion peptide relative to those of CR8020 and CR8043.

After finding that TJ5-1 bound residues upstream and downstream of the R329 HA1/HA2 cleavage site, we sought to assess whether it could inhibit the HA maturation step from the HA0 precursor. This was found to be the case for the bNAb CR8020 [192], and we reasoned that the proximity of the TJ5-1 epitope to that of CR8020 might enable a similar inhibitory role. Therefore, we used a qualitative trypsin-based proteolytic cleavage inhibition assay to examine this possibility **(Figure 7.4A)**. We found that TJ5-1 could indeed inhibit proteolytic cleavage of the NG2 HA0 precursor similar to CR8020, as shown as the retention of the ~100 kDa HA0 band at all time points up to 1 h after exposure to trypsin **(Figure 7.4B)**. In contrast, the negative control head-directed mAb TJ5-13 could not inhibit cleavage which led to the disappearance of the HA0 band after 5 min of trypsin treatment. This result confirmed that TJ5-1, similar to previously characterized bNAbs, also bound proximal to the HA0 cleavage site and suggested a potential neutralization mechanism, preventing HA maturation.

Discussion

In this work, we structurally assessed the antibody epitopes on the lead H3 COBRA vaccine candidate NG2 [159]. We found through cryo-EM analyses that both the head and stem domains were intact on this HA construct through complexing with broadly reactive RBS- and stem-directed mAbs from human subjects receiving the seasonal vaccine. These results corroborate the possibility that COBRA HAs may trigger a broadened antibody response through targeting of conserved epitopes by broadly reactive antibody clones.

NG2 possessed sequence features of both historic and recent H3 HAs, with mutations relative to wild-type HAs found predominantly in the antigenic sites **(Figure 7.1A)**. Furthermore, the percent identity of NG2 to wild-type H3 HAs spanned from 88 to 99 percent for the historic

AI68 and the recent HK19 HAs at the amino acid level. This variability in percent identity reflected the gradual accumulation of mutations over the past 50 years within the H3 HA despite the absence of any significant antigenic shift events.

Many seasonal vaccine-directed antibodies target residues surrounding the conserved RBS, targeting the variable and strain-specific antigenic sites. However, a number of antibodies that bind only this conserved region of the HA head domain have been isolated, such as C05 [190] and F045-92 [194]. These interactions are often mediated through key interactions from CDR loops that are analogous to the binding of sialic acid to the HA protein in a mechanism called receptor mimicry [141,194]. In this work, we found that two seasonal vaccine-derived mAbs, #1664 and TJ5-13, also targeted the RBS epitope on the NG2 HA **(Figure 7.2)**. Both mAbs possessed broad HAI activity and reactivity against H3 viruses and HAs, and bound to their epitopes using a similar angle of approach, although the heavy and light chains were flipped relative to each other in their Fab:NG2 complex structures. That the NG2 COBRA HA could bind both mAbs verified the integrity of the RBS epitope on this immunogen, similar to results observed with the X6 H1 COBRA HA in the previous chapter.

We also found a novel bNAb, TJ5-1, derived from seasonal vaccination that could bind the NG2 HA based on previous studies [162]. This mAb neutralized virtually all H3N2 viruses tested from 1968 to 2019 **(Figure 7.3A)** and bound the bottom of the NG2 HA stem **(Figure 7.3B)**. Its epitope involved residues in the conserved fusion peptide as well as those spanning across the R329 cleavage site. Comparing this epitope to those of group 2 bNAbs CR8020 and CR8043 showed that TJ5-1 bound slightly upstream of these previously characterized mAbs at a novel epitope. This mAb could also prevent trypsin-mediated cleavage of the NG2 protein into the

HA1/HA2 form **(Figure 7.4)**, suggesting that this may be a potential neutralization mechanism to prevent virus maturation and to inhibit subsequent rounds of viral infection.

Structural analysis of this COBRA HA revealed a consistent overall trend in the COBRA HAs. For both the H1 and H3 HAs, it appears that the methodology captures broadly conserved epitopes in the head and stem domains that might mediate neutralization through two mechanisms. The fact that the RBS epitope is captured with the COBRA methodology suggests that immunization with this HA immunogen could elicit receptor-blocking, HAI-active antibodies like #1664 and TJ5-13 that altogether inhibit the attachment step of viral entry. The integrity of the stem domain in COBRA HA constructs like X6 from the previous chapter also suggests that the membrane fusion step might be inhibited, as this is likely the predominant neutralization mechanism for group 1 stem bNAbs such as CR6261 [195]. Alternatively, as in this study, bNAbs such as TJ5-1 might also be elicited to prevent the HA maturation step in subsequent viral replication cycles. Future efforts will also focus on evaluating whether fusion inhibition might also be a significant neutralizing mechanism for the TJ5-1 mAb. In conclusion, we found that NG2 captures the antigenic features of several H3 HAs, recapitulating the importance of these epitopes in this vaccine design.

Figures

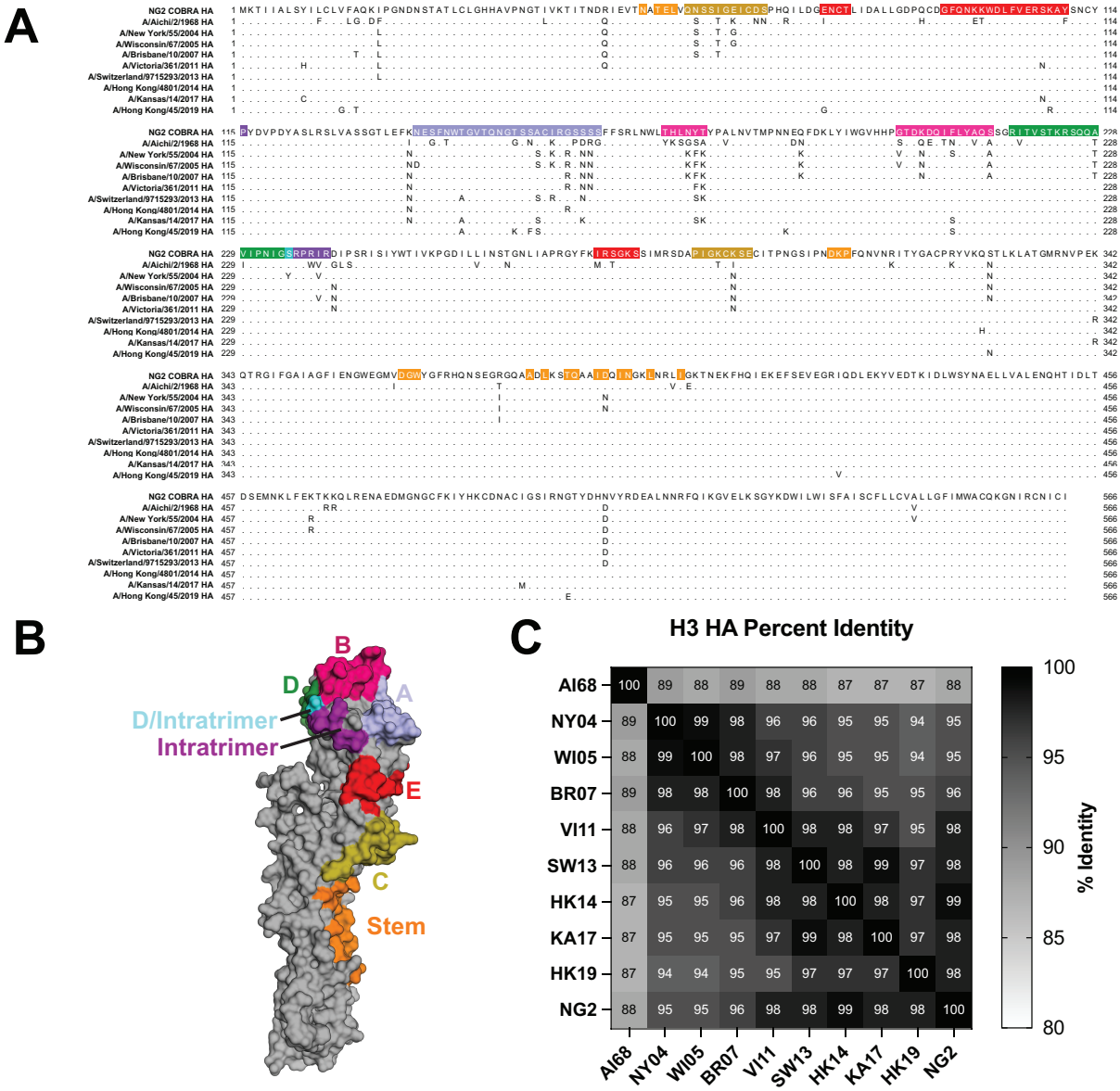

Figure 7.1. Sequence comparison of the NG2 COBRA HA to wild-type H3 HAs. (A) MUSCLE alignment of H3 HAs from 1968 to 2019 to each other and to NG2 were performed. Antibody epitopes are colored as in (B) for the NG2 COBRA, for which the antigenic sites A, B, C, D, and E, as well as the intratrimer and the stem epitopes are shown. (C) Percent identity between wild-type HAs, including the NG2 COBRA, shown as a heat map.

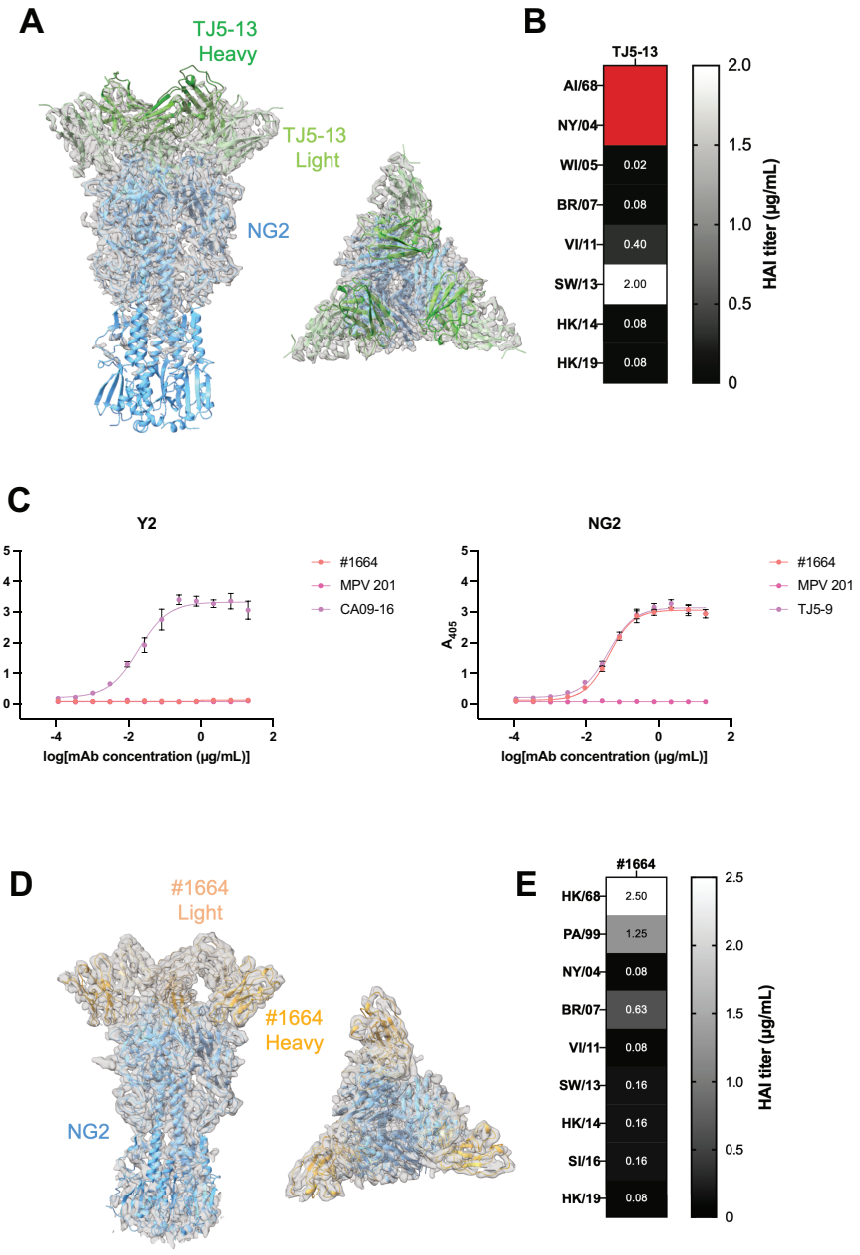

Figure 7.2. Cryo-EM structures of broadly HAI-active antibody Fabs with COBRA NG2 reveal an intact RBS. (A) The fit of the TJ5-13 Fab with NG2, shown in the cryo-EM density. (B) Hemagglutination inhibition (HAI) titers of TJ5-13 against the indicated H3 viruses. Red color indicates no activity at 2 µg/mL. (C) ELISA of #1664 against H1 COBRA Y2 and H3 COBRA NG2. CA09-16 is a positive control for Y2, and TJ5-9 is a positive control for NG2. MPV 201 is

a negative control. (D) Structure and fit of the #1664 Fab bound to NG2 in the cryo-EM map. (E) HAI activity of #1664 to the indicated H3 virus strains.

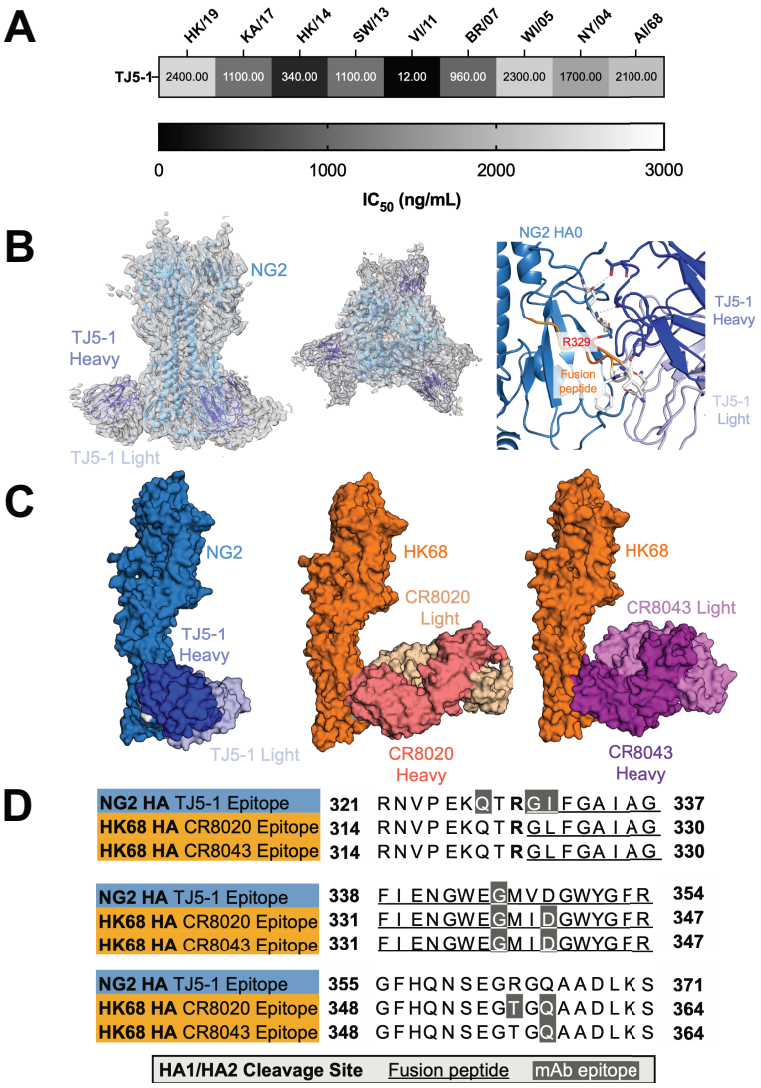

Figure 7.3. Cryo-EM structure of broadly reactive antibody TJ5-1 with NG2 reveals an intact stem. (A) The neutralization IC_{50}s against the indicated H3 viruses for stem-binding mAb TJ5-1. (B) The fit of TJ5-1:NG2 to the cryo-EM map is shown. The epitope of TJ5-1, in white, is shown on NG2 on the right. The epitope includes the fusion peptide and spans across the R329 HA1/HA2 cleavage site. (C) Comparison of the binding orientations of previously characterized bNAbs CR8020 and CR8043 to the A/Hong Kong/1/1968 (HK68) HA compared to TJ5-1 with NG2. (D) Sequence alignment of the NG2 and HK68 HAs with mAb epitopes shown in gray.

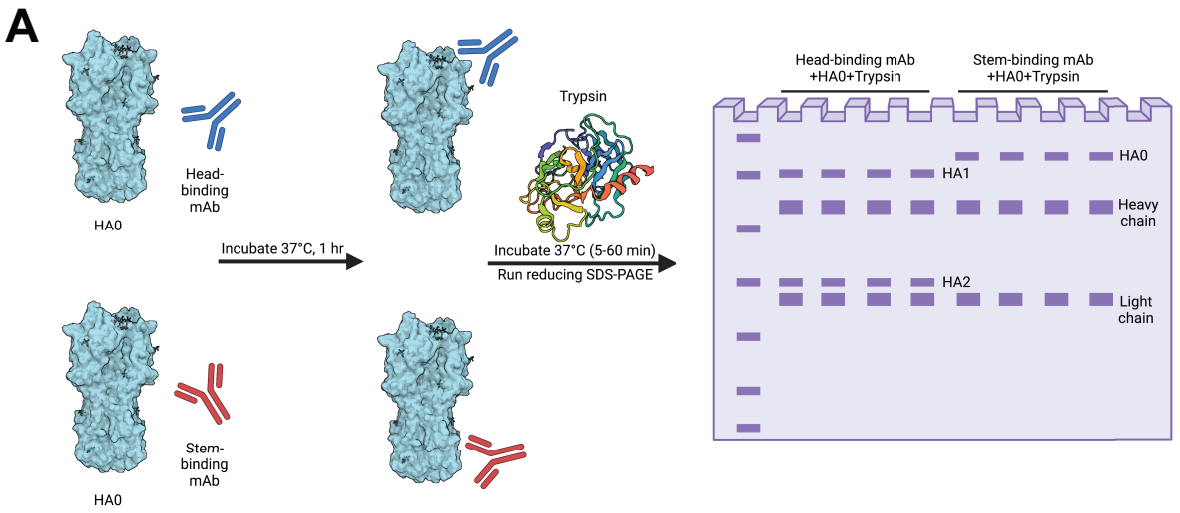
A
HA0
Head-binding mAb
Incubate 37°C, 1 hr
Trypsin
Incubate 37°C (5-60 min)
Run reducing SDS-PAGE
Stem-binding mAb
HA0
Head-binding mAb +HA0+Trypsin
Stem-binding mAb +HA0+Trypsin
HA0
HA1
Heavy chain
HA2
Light chain

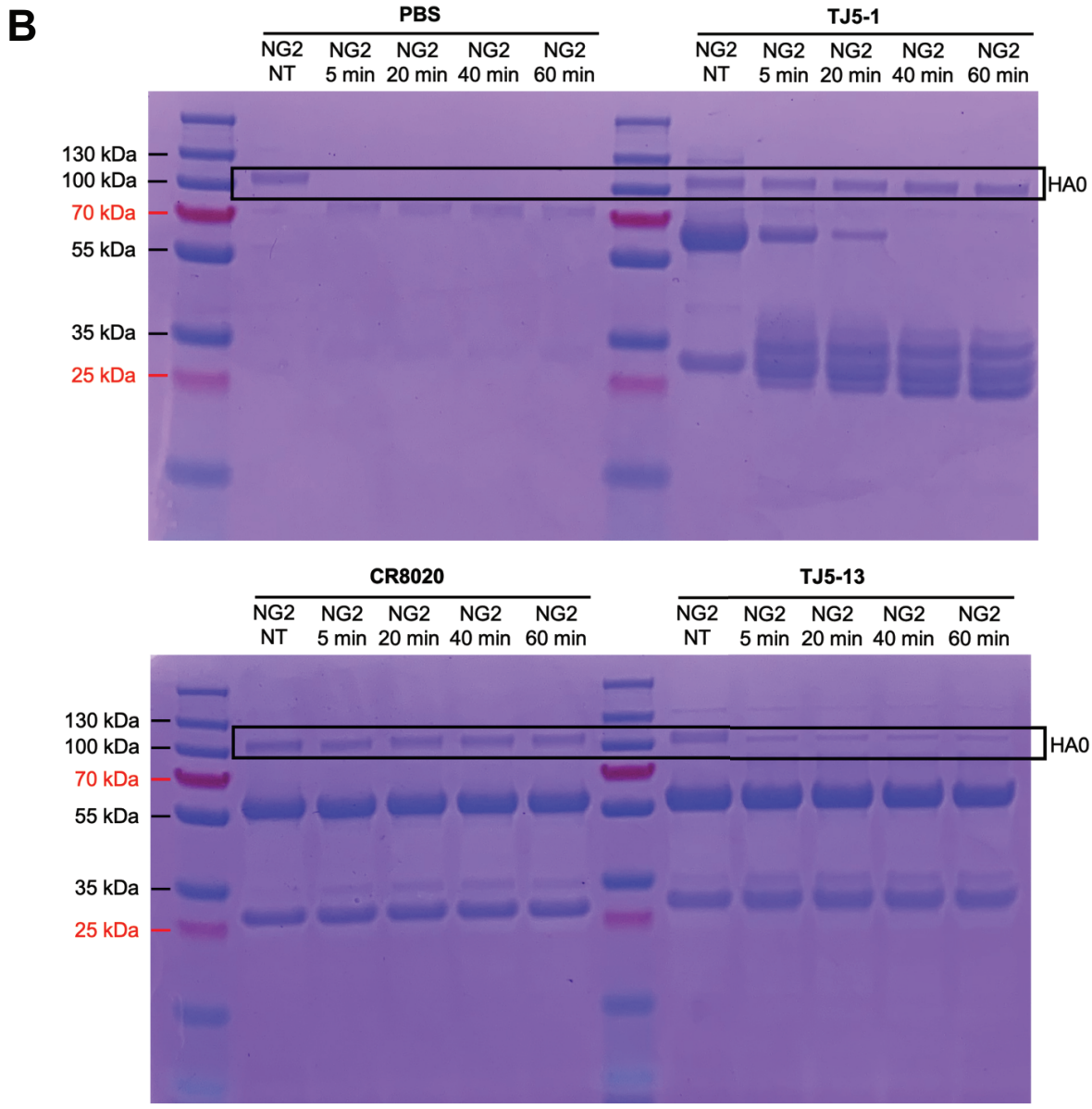
B
PBS
TJ5-1
NG2 NT
NG2 5 min
NG2 20 min
NG2 40 min
NG2 60 min
130 kDa
100 kDa
70 kDa
55 kDa
35 kDa
25 kDa
HA0
CR8020
TJ5-13

Figure 7.4. TJ5-1 can inhibit cleavage of NG2 HA0 as assessed by SDS-PAGE. (A) Schematic of a trypsin-based HA0 cleavage inhibition assay. The HA0 precursor is incubated with antibody, then exposed to trypsin for cleavage. The extent of HA0 cleavage is then assessed by the presence or absence of the HA0 band across multiple time points after incubation with trypsin. (B) Results of the cleavage inhibition assay with stem-binding mAb TJ5-1, stem-binding bNAb CR8020, and head-binding mAb TJ5-13. Uncleaved HA0 is visualized as a band at ~100 kDa at time points from 5 to 60 minutes.

CHAPTER 8

SUMMARY

Influenza remains as a major health burden worldwide. The current seasonal vaccine provides variable protection and does not effectively account for antigenic variation. The COBRA vaccine has shown promise in several animal models, demonstrating expanded antibody breadth to several strains of the virus. However, knowledge of the precise epitopes that are targeted by this vaccine approach was limited. The information about the characteristics of the pre-existing human B cell response to COBRA HA immunogens has been lacking, and whether the COBRA vaccine could be further optimized to elicit widely reactive antibodies was not fully investigated. Here, we discovered epitopes on COBRA HA immunogens that were associated with enhanced breadth against several IAVs and assessed whether such epitopes could be targeted using novel vaccine approaches.

Specific Aim 1: Determine the extent of pre-existing, functional antibody immunity to H1 subtype COBRA immunogens from seasonal vaccination. B cells were expanded from peripheral blood mononuclear cells (PBMCs) from human subjects receiving the 2017-2018 seasonal inactivated vaccine. We evaluated B cell reactivity against the H1 subtype COBRA HAs P1 and X6, finding that reactivity at the oligoclonal level was increased after seasonal vaccination relative to baseline. This confirmed that antibody epitopes between the seasonal vaccine and the COBRA HA vaccine were indeed conserved to some extent. We also isolated individual monoclonal antibodies (mAbs) to COBRAs Y2, P1, and X6 and evaluated their epitopes through an epitope binning assay, finding that they bound to the head and stem domains of the HA at

conserved sites like the RBS, the lateral patch, and the novel anchor epitope on the bottom of the HA stem. We also found that for a cohort who received the 2019-2020 seasonal vaccine, similar, Y2 COBRA-reactive antibodies could be isolated.

Specific Aim 2: Determine the role of adjuvant and antigen formulation on the breadth of COBRA-elicited antibodies. To assess the role of adjuvant on the COBRA HA antibody response, we paired the Y2 COBRA HA with four adjuvants for vaccination in BALB/c mice: (1) AddaVax, an MF59 oil-in-water emulsion analog, (2) AddaS03, an AS03 oil-in-water emulsion analog, (3) CpG, a TLR9 agonist, and (4) Alhydrogel, an alum analog. We found that the AddaS03 adjuvant elicited the highest binding and hemagglutination inhibition (HAI) titers against a panel of recent pandemic-like H1N1 viruses of all adjuvants tested. In addition, in contrast to our expectations, similar epitopes were targeted across adjuvant groups, specifically at the conserved RBS and anchor epitopes.

To evaluate whether nanoparticle (NP) formulation of COBRA HAs in a multimeric array could enhance antibody breadth, we used a two-component HA-I53_dn5B/I53_dn5A system to present the H1 COBRA Y2 or the H3 COBRA NG2 in Y2 NP and NG2 NP constructs. After structural and antigenic validation of these nanoparticles by negative-stain electron microscopy and ELISA, we used these NPs to immunize DBA/2J mice in a prime-boost-boost regimen. We evaluated serum reactivity against the H1 and H3 Y2 and NG2 COBRAs, finding virtually no expansion of antibody breadth to H3 HAs even with the use of this NP system with the Y2 COBRA. In contrast, detectable, enhanced breadth to the Y2 H1 COBRA was elicited after vaccination with the NG2 NP. Moreover, expanded, cross-group HAI breadth to H1 viruses was detected with the use of the NG2 NP, whereas expanded breadth to H3 viruses was not detected Y2 NP vaccination. These results suggested that the NP platform can enhance antibody breadth to

the H1 subtype following H3 COBRA NP vaccination, likely through inducing antibodies against conserved epitopes on the HA head domain and the RBS.

Specific Aim 3: Determine the structural correlates of COBRA-induced antibody breadth. Through X-ray crystallography and cryo-electron microscopy (cryo-EM) analyses, we determined the structure of the H1 COBRA X6, which has a design period from 1999 to 2012, to evaluate its glycosylation profile and its antibody epitopes. We compared the structures of X6 to the pre-2009 HA from A/New Caledonia/20/1999 (NC99) and the post-2009 HA from A/Michigan/45/2015 (MI15). We found that this COBRA possessed glycans of both types of HAs, consistent with its design period spanning across the 2009 H1N1 swine influenza pandemic. In addition, it also bound broadly neutralizing antibodies (bNAbs) CA09-26 (isolated from a seasonally vaccinated human subject in Specific Aim 1) and #58 at the RBS, as well as the CR6261 central stem-binding bNAb, verifying the structural integrity of these conserved epitopes. It also bound a murine mAb, BE1, elicited by X6 vaccination, with pre-2009 but not post-2009 H1 HA reactivity, suggesting that the X6 was more skewed towards pre-2009 than post-2009 HAs in terms of its overall antigenic structure.

We also performed cryo-EM analysis of the lead H3 vaccine candidate COBRA NG2 in complex with broadly reactive antibodies from seasonal vaccination. These mAbs, TJ5-13, #1664, and TJ5-1, bound to the conserved RBS and membrane-proximal stem epitopes. Interestingly, the TJ5-1 mAb bound across the HA1/HA2 cleavage site and to the fusion peptide, similar to previously characterized bNAbs CR8020 and CR8043. This mAb could also inhibit NG2 cleavage into the HA1 and HA2 subunits. These cryo-EM structures therefore verified the antigenicity of this COBRA HA in these sites, suggesting that receptor-blocking and maturation-blocking monoclonal antibodies might be elicited after vaccination with this H3 COBRA.

In summary, we characterized the pre-existing B cell features to the COBRA HA after seasonal vaccination and also found the positive immunological effects of adjuvant and COBRA HA multimerization on COBRA-directed antibody breadth. We finally also verified that COBRA HAs of both the H1 and H3 subtypes of IAVs possess epitope features of wild-type HAs of their design periods that can likely elicit broadly reactive mAbs after vaccination. The results presented here can inform future vaccine design efforts with this next-generation methodology to expand antibody breadth and reduce the burden of influenza.

REFERENCES

1. Krammer, F. The human antibody response to influenza A virus infection and vaccination. *Nat. Rev. Immunol.* **2019**, *19*, 383–397, doi:10.1038/s41577-019-0143-6.
2. Chen, J.R.; Liu, Y.M.; Tseng, Y.C.; Ma, C. Better influenza vaccines: An industry perspective. *J. Biomed. Sci.* **2020**, *27*, 1–11, doi:10.1186/s12929-020-0626-6.
3. Centers for Disease Control and Prevention. Selecting Viruses for the Seasonal Influenza Vaccine Available online: https://www.cdc.gov/flu/prevent/vaccine-selection.htm (accessed on Feb 23, 2020).
4. Crevar, C.J.; Carter, D.M.; Lee, K.Y.J.; Ross, T.M. Cocktail of H5N1 COBRA HA vaccines elicit protective antibodies against H5N1 viruses from multiple clades. *Hum. Vaccines Immunother.* **2015**, *11*, 572–583, doi:10.1080/21645515.2015.1012013.
5. Khurana, S.; Verma, N.; Yewdell, J.W.; Hilbert, A.K.; Castellino, F.; Lattanzi, M.; Del Giudice, G.; Rappuoli, R.; Golding, H. MF59 adjuvant enhances diversity and affinity of antibody-mediated immune response to pandemic influenza vaccines. *Sci. Transl. Med.* **2011**, *3*, 1–10, doi:10.1126/scitranslmed.3002336.
6. Boyoglu-Barnum, S.; Ellis, D.; Gillespie, R.A.; Hutchinson, G.B.; Park, Y.-J.; Moin, S.M.; Acton, O.J.; Ravichandran, R.; Murphy, M.; Pettie, D.; et al. Quadrivalent influenza nanoparticle vaccines induce broad protection. *Nature* **2021**, *592*, 623–628, doi:10.1038/s41586-021-03365-x.
7. Centers for Disease Control and Prevention. Influenza (Flu), Past Seasons. Available online: https://www.cdc.gov/flu/about/burden/past-seasons.html (accessed on Apr 25,

2022).

8. Olsen, S.J.; Azziz-Baumgartner, E.; Budd, A.P.; Brammer, L.; Sullivan, S.; Pineda, R.F.; Cohen, C.; Fry, A.M. Decreased Influenza Activity During the COVID-19 Pandemic — United States, Australia, Chile, and South Africa, 2020. *MMWR. Morb. Mortal. Wkly. Rep.* **2020**, *69*, 1305–1309, doi:10.15585/mmwr.mm6937a6.

9. Krammer, F.; Smith, G.J.D.; Fouchier, R.A.M.; Peiris, M.; Kedzierska, K.; Doherty, P.C.; Palese, P.; Shaw, M.L.; Treanor, J.; Webster, R.G.; et al. Influenza. *Nat. Rev. Dis. Prim.* **2018**, *4*, 1–21, doi:10.1038/s41572-018-0002-y.

10. Jang, Y.H.; Seong, B.L. The Quest for a Truly Universal Influenza Vaccine. *Front. Cell. Infect. Microbiol.* **2019**, *9*, 1–24, doi:10.3389/fcimb.2019.00344.

11. Virk, R.K.; Jayakumar, J.; Mendenhall, I.H.; Moorthy, M.; Lam, P.; Linster, M.; Lim, J.; Lin, C.; Oon, L.L.E.; Lee, H.K.; et al. Divergent evolutionary trajectories of influenza B viruses underlie their contemporaneous epidemic activity. *Proc. Natl. Acad. Sci. U. S. A.* **2020**, *117*, 619–628, doi:10.1073/pnas.1916585116.

12. Gilbert, P.B.; Fong, Y.; Juraska, M.; Carpp, L.N.; Monto, A.S.; Martin, E.T.; Petrie, J.G. HAI and NAI titer correlates of inactivated and live attenuated influenza vaccine efficacy. *BMC Infect. Dis.* **2019**, *19*, 1–12, doi:10.1186/s12879-019-4049-5.

13. Sriwilaijaroen, N.; Suzuki, Y. Molecular basis of the structure and function of H1 hemagglutinin of influenza virus. *Proc. Japan Acad. Ser. B Phys. Biol. Sci.* **2012**, *88*, 226–249, doi:10.2183/pjab.88.226.

14. Kimble, B.; Nieto, G.R.; Perez, D.R. Characterization of influenza virus sialic acid receptors in minor poultry species. *Virol. J.* **2010**, *7*, 1–10, doi:10.1186/1743-422X-7-365.

15. Teng, Q.; Xu, D.; Shen, W.; Liu, Q.; Rong, G.; Li, X.; Yan, L.; Yang, J.; Chen, H.; Yu,

H.; et al. A Single Mutation at Position 190 in Hemagglutinin Enhances Binding Affinity for Human Type Sialic Acid Receptor and Replication of H9N2 Avian Influenza Virus in Mice. *J. Virol.* **2016**, *90*, 9806–9825, doi:10.1128/jvi.01141-16.

16. Russell, C.J.; Hu, M.; Okda, F.A. Influenza Hemagglutinin Protein Stability, Activation, and Pandemic Risk. *Trends Microbiol.* **2018**, *26*, 841–853, doi:10.1016/j.tim.2018.03.005.
17. Carr, C.M.; Kim, P.S. A spring-loaded mechanism for the conformational change of influenza hemagglutinin. *Cell* **1993**, *73*, 823–832, doi:10.1016/0092-8674(93)90260-W.
18. Koel, B.F.; Burke, D.F.; Bestebroer, T.M.; Van Der Vliet, S.; Zondag, G.C.M.; Vervaet, G.; Skepner, E.; Lewis, N.S.; Spronken, M.I.J.; Russell, C.A.; et al. Substitutions near the receptor binding site determine major antigenic change during influenza virus evolution. *Science (80-.).* **2013**, *342*, 976–979, doi:10.1126/science.1244730.
19. Zost, S.J.; Wu, N.C.; Hensley, S.E.; Wilson, I.A. Immunodominance and Antigenic Variation of Influenza Virus Hemagglutinin: Implications for Design of Universal Vaccine Immunogens. *J. Infect. Dis.* **2019**, *219*, S38–S45, doi:10.1093/infdis/jiy696.
20. Caton, A.J.; Brownlee, G.G.; Yewdell, J.W.; Gerhard, W. The antigenic structure of the influenza virus A/PR/8/34 hemagglutinin (H1 subtype). *Cell* **1982**, *31*, 417–427, doi:10.1016/0092-8674(82)90135-0.
21. Wiley, D.C.; Wilson, I.A.; Skehel, J.J. Structural identification of the antibody-binding sites of Hong Kong influenza haemagglutinin and their involvement in antigenic variation. *Nature* **1981**, *289*, 373–378, doi:10.1038/289373a0.
22. Skehel, J.J.; Stevens, D.J.; Daniels, R.S.; Douglas, A.R.; Knossow, M.; Wilson, I.A.; Wiley, D.C. A carbohydrate side chain on hemagglutinins of Hong Kong influenza viruses inhibits recognition by a monoclonal antibody. *Proc. Natl. Acad. Sci. U. S. A.* **1984**, *81*,

1779–1783, doi:10.1073/pnas.81.6.1779.

23. Broecker, F.; Liu, S.T.H.; Sun, W.; Krammer, F.; Simon, V.; Palese, P. Immunodominance of Antigenic Site B in the Hemagglutinin of the Current H3N2 Influenza Virus in Humans and Mice. *J. Virol.* **2018**, *92*, 1–13, doi:10.1128/jvi.01100-18.

24. Monto, A.S.; Malosh, R.E.; Petrie, J.G.; Martin, E.T. The Doctrine of Original Antigenic Sin: Separating Good from Evil. *J. Infect. Dis.* **2017**, *215*, 1782–1788, doi:10.1093/infdis/jix173.

25. Ranjeva, S.; Subramanian, R.; Fang, V.J.; Leung, G.M.; Ip, D.K.M.; Perera, R.A.P.M.; Peiris, J.S.M.; Cowling, B.J.; Cobey, S. Age-specific differences in the dynamics of protective immunity to influenza. *Nat. Commun.* **2019**, *10*, 1–11, doi:10.1038/s41467-019-09652-6.

26. Lee, J.; Paparoditis, P.; Horton, A.P.; Frühwirth, A.; McDaniel, J.R.; Jung, J.; Boutz, D.R.; Hussein, D.A.; Tanno, Y.; Pappas, L.; et al. Persistent Antibody Clonotypes Dominate the Serum Response to Influenza over Multiple Years and Repeated Vaccinations. *Cell Host Microbe* **2019**, *25*, 367-376.e5, doi:10.1016/j.chom.2019.01.010.

27. Noh, J.Y.; Song, J.Y.; Choi, W.S.; Lee, J.; Seo, Y. Bin; Kwon, Y.J.; Ko, G.J.; Cha, D.R.; Kang, Y.S.; Lee, Y.K.; et al. Immunogenicity of trivalent influenza vaccines in patients with chronic kidney disease undergoing hemodialysis: MF59-adjuvanted versus non-adjuvanted vaccines. *Hum. Vaccines Immunother.* **2016**, *12*, 2902–2908, doi:10.1080/21645515.2016.1191717.

28. Monto, A.S. Seasonal influenza and vaccination coverage. *Vaccine* **2010**, *28*, 33–45, doi:10.1016/j.vaccine.2010.08.027.

29. Soema, P.C.; Kompier, R.; Amorij, J.P.; Kersten, G.F.A. Current and next generation

influenza vaccines: Formulation and production strategies. *Eur. J. Pharm. Biopharm.* **2015**, *94*, 251–263, doi:10.1016/j.ejpb.2015.05.023.

30. Zost, S.J.; Parkhouse, K.; Gumina, M.E.; Kim, K.; Perez, S.D.; Wilson, P.C.; Treanor, J.J.; Sant, A.J.; Cobey, S.; Hensley, S.E. Contemporary H3N2 influenza viruses have a glycosylation site that alters binding of antibodies elicited by egg-adapted vaccine strains. *Proc. Natl. Acad. Sci. U. S. A.* **2017**, *114*, 12578–12583, doi:10.1073/pnas.1712377114.
31. Chang, D.; Zaia, J. Why glycosylation matters in building a better flu vaccine. *Mol. Cell. Proteomics* **2019**, *18*, 2348–2358, doi:10.1074/mcp.R119.001491.
32. Webby, R.J.; Webster, R.G. Emergence of influenza A viruses. *Philos. Trans. R. Soc. London. Ser. B Biol. Sci.* **2001**, *356*, 1817–1828, doi:10.1098/rstb.2001.0997.
33. Both, G.W.; Sleigh, M.J.; Cox, N.J.; Kendal, A.P. Antigenic drift in influenza virus H3 hemagglutinin from 1968 to 1980: multiple evolutionary pathways and sequential amino acid changes at key antigenic sites. *J. Virol.* **1983**, *48*, 52–60, doi:10.1128/JVI.48.1.52-60.1983.
34. Klein, E.Y.; Serohijos, A.W.R.; Choi, J.-M.; Shakhnovich, E.I.; Pekosz, A. Influenza A H1N1 Pandemic Strain Evolution – Divergence and the Potential for Antigenic Drift Variants. *PLoS One* **2014**, *9*, e93632, doi:10.1371/journal.pone.0093632.
35. Smith, D.J.; Lapedes, A.S.; De Jong, J.C.; Bestebroer, T.M.; Rimmelzwaan, G.F.; Osterhaus, A.D.M.E.; Fouchier, R.A.M. Mapping the antigenic and genetic evolution of influenza virus. *Science (80-.).* **2004**, *305*, 371–376, doi:10.1126/science.1097211.
36. Khiabanian, H.; Trifonov, V.; Rabadan, R. Reassortment Patterns in Swine Influenza Viruses. *PLoS One* **2009**, *4*, e7366, doi:10.1371/journal.pone.0007366.
37. Block, S.L.; Ruiz-Palacios, G.M.; Guerrero, M.L.; Beygo, J.; Sales, V.; Holmes, S.J.

Dose-range Study of MF59-adjuvanted Versus Nonadjuvanted Monovalent A/H1N1 Pandemic Influenza Vaccine in Six- to Less Than Thirty-Six-month-old Children. *Pediatr. Infect. Dis. J.* **2012**, *31*, e92–e98, doi:10.1097/INF.0b013e318257644f.

38. Hervé, P.L.; Lorin, V.; Jouvion, G.; Da Costa, B.; Escriou, N. Addition of N-glycosylation sites on the globular head of the H5 hemagglutinin induces the escape of highly pathogenic avian influenza A H5N1 viruses from vaccine-induced immunity. *Virology* **2015**, *486*, 134–145, doi:10.1016/j.virol.2015.08.033.

39. Medina, R.A.; Stertz, S.; Manicassamy, B.; Zimmermann, P.; Sun, X.; Albrecht, R.A.; Uusi-Kerttula, H.; Zagordi, O.; Belshe, R.B.; Frey, S.E.; et al. Glycosylations in the globular head of the hemagglutinin protein modulate the virulence and antigenic properties of the H1N1 influenza viruses. *Sci. Transl. Med.* **2013**, *5*, doi:10.1126/scitranslmed.3005996.

40. Richards, K.A.; Moritzky, S.; Shannon, I.; Fitzgerald, T.; Yang, H.; Branche, A.; Topham, D.J.; Treanor, J.J.; Nayak, J.; Sant, A.J. Recombinant HA-based vaccine outperforms split and subunit vaccines in elicitation of influenza-specific CD4 T cells and CD4 T cell-dependent antibody responses in humans. *npj Vaccines* **2020**, *5*, 1–10, doi:10.1038/s41541-020-00227-x.

41. Chen, J.R.; Yu, Y.H.; Tseng, Y.C.; Chiang, W.L.; Chiang, M.F.; Ko, Y.A.; Chiu, Y.K.; Ma, H.H.; Wu, C.Y.; Jan, J.T.; et al. Vaccination of monoglycosylated hemagglutinin induces cross-strain protection against influenza virus infections. *Proc. Natl. Acad. Sci. U. S. A.* **2014**, *111*, 2476–2481, doi:10.1073/pnas.1323954111.

42. Tseng, Y.C.; Wu, C.Y.; Liu, M.L.; Chen, T.H.; Chiang, W.L.; Yu, Y.H.; Jan, J.T.; Lin, K.I.; Wong, C.H.; Ma, C. Egg-based influenza split virus vaccine with monoglycosylation

induces cross-strain protection against influenza virus infections. *Proc. Natl. Acad. Sci. U. S. A.* **2019**, *116*, 4200–4205, doi:10.1073/pnas.1819197116.

43. Boyoglu-Barnum, S.; Hutchinson, G.B.; Boyington, J.C.; Moin, S.M.; Gillespie, R.A.; Tsybovsky, Y.; Stephens, T.; Vaile, J.R.; Lederhofer, J.; Corbett, K.S.; et al. Glycan repositioning of influenza hemagglutinin stem facilitates the elicitation of protective cross-group antibody responses. *Nat. Commun.* **2020**, *11*, 1–12, doi:10.1038/s41467-020-14579-4.

44. Ren, H.; Zhou, P. Epitope-focused vaccine design against influenza A and B viruses. *Curr. Opin. Immunol.* **2016**, *42*, 83–90, doi:10.1016/j.coi.2016.06.002.

45. Raymond, D.D.; Bajic, G.; Ferdman, J.; Suphaphiphat, P.; Settembre, E.C.; Moody, M.A.; Schmidt, A.G.; Harrison, S.C. Conserved epitope on influenza-virus hemagglutinin head defined by a vaccine-induced antibody. *Proc. Natl. Acad. Sci. U. S. A.* **2018**, *115*, 168–173, doi:10.1073/pnas.1715471115.

46. Bangaru, S.; Lang, S.; Schotsaert, M.; Vanderven, H.A.; Zhu, X.; Kose, N.; Bombardi, R.; Finn, J.A.; Kent, S.J.; Gilchuk, P.; et al. A Site of Vulnerability on the Influenza Virus Hemagglutinin Head Domain Trimer Interface. *Cell* **2019**, *177*, 1136-1152.e18, doi:10.1016/j.cell.2019.04.011.

47. Dong, J.; Gilchuk, I.; Li, S.; Irving, R.; Goff, M.T.; Turner, H.L.; Ward, A.B.; Carnahan, R.H.; Crowe, J.E. Anti–influenza H7 human antibody targets antigenic site in hemagglutinin head domain interface. *J. Clin. Invest.* **2020**, *130*, 4734–4739, doi:10.1172/JCI136032.

48. Bajic, G.; Maron, M.J.; Adachi, Y.; Onodera, T.; McCarthy, K.R.; McGee, C.E.; Sempowski, G.D.; Takahashi, Y.; Kelsoe, G.; Kuraoka, M.; et al. Influenza Antigen

Engineering Focuses Immune Responses to a Subdominant but Broadly Protective Viral Epitope. *Cell Host Microbe* **2019**, *25*, 827-835.e6, doi:10.1016/j.chom.2019.04.003.

49. Watanabe, A.; McCarthy, K.R.; Kuraoka, M.; Schmidt, A.G.; Adachi, Y.; Onodera, T.; Tonouchi, K.; Caradonna, T.M.; Bajic, G.; Song, S.; et al. Antibodies to a Conserved Influenza Head Interface Epitope Protect by an IgG Subtype-Dependent Mechanism. *Cell* **2019**, *177*, 1124-1135.e16, doi:10.1016/j.cell.2019.03.048.

50. Huang, J.; Diaz, D.; Mousa, J.J. Antibody recognition of the pneumovirus fusion protein trimer interface. *PLoS Pathog.* **2020**, *16*, 1–22, doi:10.1371/journal.ppat.1008942.

51. Krammer, F. Emerging influenza viruses and the prospect of a universal influenza virus vaccine. *Biotechnol. J.* **2015**, *10*, 690–701, doi:10.1002/biot.201400393.

52. Darricarrère, N.; Pougatcheva, S.; Duan, X.; Rudicell, R.S.; Chou, T.; DiNapoli, J.; Ross, T.M.; Alefantis, T.; Vogel, T.U.; Kleanthous, H.; et al. Development of a Pan-H1 Influenza Vaccine. *J. Virol.* **2018**, *92*, 1–14, doi:10.1128/jvi.01349-18.

53. Wong, T.M.; Allen, J.D.; Bebin-Blackwell, A.-G.; Carter, D.M.; Alefantis, T.; DiNapoli, J.; Kleanthous, H.; Ross, T.M. Computationally Optimized Broadly Reactive Hemagglutinin Elicits Hemagglutination Inhibition Antibodies against a Panel of H3N2 Influenza Virus Cocirculating Variants. *J. Virol.* **2017**, *91*, 1–18, doi:10.1128/jvi.01581-17.

54. Allen, J.D.; Ray, S.; Ross, T.M. Split inactivated COBRA vaccine elicits protective antibodies against H1N1 and H3N2 influenza viruses. *PLoS One* **2018**, *13*, 1–15, doi:10.1371/journal.pone.0204284.

55. Bar-Peled, Y.; Huang, J.; Nuñez, I.A.; Pierce, S.R.; Ecker, J.W.; Ross, T.M.; Mousa, J.J. Structural and antigenic characterization of a computationally-optimized H5

hemagglutinin influenza vaccine. *Vaccine* **2019**, *37*, 6022–6029, doi:10.1016/j.vaccine.2019.08.062.

56. Carter, D.M.; Darby, C.A.; Johnson, S.K.; Carlock, M.A.; Kirchenbaum, G.A.; Allen, J.D.; Vogel, T.U.; Delagrave, S.; DiNapoli, J.; Kleanthous, H.; et al. Elicitation of Protective Antibodies against a Broad Panel of H1N1 Viruses in Ferrets Preimmune to Historical H1N1 Influenza Viruses. *J. Virol.* **2017**, *91*, 1–16, doi:10.1128/jvi.01283-17.

57. Yassine, H.M.; McTamney, P.M.; Boyington, J.C.; Ruckwardt, T.J.; Crank, M.C.; Smatti, M.K.; Ledgerwood, J.E.; Graham, B.S. Use of hemagglutinin stem probes demonstrate prevalence of broadly reactive group 1 influenza antibodies in human sera. *Sci. Rep.* **2018**, *8*, 1–11, doi:10.1038/s41598-018-26538-7.

58. Boyoglu-Barnum, S.; Ellis, D.; Gillespie, R.; Hutchinson, G.; Park, Y.-J.; Moin, S.; Acton, O.; Ravichandran, R.; Murphy, M.; Pettie, D.; et al. Elicitation of broadly protective immunity to influenza by multivalent hemagglutinin nanoparticle vaccines. *bioRxiv* **2020**, 1–29, doi:10.1101/2020.05.30.125179.

59. Ekiert, D.C.; Bhabha, G.; Elsliger, M.A.; Friesen, R.H.E.; Jongeneelen, M.; Throsby, M.; Goudsmit, J.; Wilson, I.A. Antibody recognition of a highly conserved influenza virus epitope. *Science (80-.).* **2009**, *324*, 246–251, doi:10.1126/science.1171491.

60. Wu, N.C.; Yamayoshi, S.; Ito, M.; Uraki, R.; Kawaoka, Y.; Wilson, I.A. Recurring and Adaptable Binding Motifs in Broadly Neutralizing Antibodies to Influenza Virus Are Encoded on the D3-9 Segment of the Ig Gene. *Cell Host Microbe* **2018**, *24*, 569-578.e4, doi:10.1016/j.chom.2018.09.010.

61. Sagawa, H.; Ohshima, A.; Kato, I.; Okuno, Y.; Isegawa, Y. The immunological activity of a deletion mutant of influenza virus haemagglutinin lacking the globular region. *J. Gen.*

Virol. **1996**, *77*, 1483–1487, doi:10.1099/0022-1317-77-7-1483.

62. Steel, J.; Lowen, A.C.; Wang, T.T.; Yondola, M.; Gao, Q.; Haye, K.; García-Sastre, A.; Palese, P. Influenza virus vaccine based on the conserved hemagglutinin stalk domain. *MBio* **2010**, *1*, 1–9, doi:10.1128/mBio.00018-10.

63. Gao, D.; Chen, Y.; Han, D.; Qi, Q.; Sun, X.; Zhang, H.; Feng, H.; Wang, M. Membrane-anchored stalk domain of influenza HA enhanced immune responses in mice. *Microb. Pathog.* **2017**, *113*, 421–426, doi:10.1016/j.micpath.2017.11.025.

64. Margine, I.; Hai, R.; Albrecht, R.A.; Obermoser, G.; Harrod, A.C.; Banchereau, J.; Palucka, K.; Garcia-Sastre, A.; Palese, P.; Treanor, J.J.; et al. H3N2 Influenza Virus Infection Induces Broadly Reactive Hemagglutinin Stalk Antibodies in Humans and Mice. *J. Virol.* **2013**, *87*, 4728–4737, doi:10.1128/jvi.03509-12.

65. Margine, I.; Krammer, F.; Hai, R.; Heaton, N.S.; Tan, G.S.; Andrews, S.A.; Runstadler, J.A.; Wilson, P.C.; Albrecht, R.A.; Garcia-Sastre, A.; et al. Hemagglutinin Stalk-Based Universal Vaccine Constructs Protect against Group 2 Influenza A Viruses. *J. Virol.* **2013**, *87*, 10435–10446, doi:10.1128/jvi.01715-13.

66. Krammer, F.; Hai, R.; Yondola, M.; Tan, G.S.; Leyva-Grado, V.H.; Ryder, A.B.; Miller, M.S.; Rose, J.K.; Palese, P.; Garcia-Sastre, A.; et al. Assessment of Influenza Virus Hemagglutinin Stalk-Based Immunity in Ferrets. *J. Virol.* **2014**, *88*, 3432–3442, doi:10.1128/jvi.03004-13.

67. Nachbagauer, R.; Feser, J.; Naficy, A.; Bernstein, D.I.; Guptill, J.; Walter, E.B.; Berlanda-Scorza, F.; Stadlbauer, D.; Wilson, P.C.; Aydillo, T.; et al. A chimeric hemagglutinin-based universal influenza virus vaccine approach induces broad and long-lasting immunity in a randomized, placebo-controlled phase I trial. *Nat. Med.* **2021**, *27*, 106–114,

doi:10.1038/s41591-020-1118-7.

68. Tran, E.E.H.; Podolsky, K.A.; Bartesaghi, A.; Kuybeda, O.; Grandinetti, G.; Wohlbold, T.J.; Tan, G.S.; Nachbagauer, R.; Palese, P.; Krammer, F.; et al. Cryo-electron Microscopy Structures of Chimeric Hemagglutinin Displayed on a Universal Influenza Vaccine Candidate. *MBio* **2016**, *7*, 1–9, doi:10.1128/mBio.00257-16.

69. Wohlbold, T.J.; Nachbagauer, R.; Margine, I.; Tan, G.S.; Hirsh, A.; Krammer, F. Vaccination with soluble headless hemagglutinin protects mice from challenge with divergent influenza viruses. *Vaccine* **2015**, *33*, 3314–3321, doi:10.1016/j.vaccine.2015.05.038.

70. Impagliazzo, A.; Milder, F.; Kuipers, H.; Wagner, M. V.; Zhu, X.; Hoffman, R.M.B.; Van Meersbergen, R.; Huizingh, J.; Wanningen, P.; Verspuij, J.; et al. A stable trimeric influenza hemagglutinin stem as a broadly protective immunogen. *Science (80-.).* **2015**, *349*, 1301–1306, doi:10.1126/science.aac7263.

71. Yassine, H.M.; Boyington, J.C.; McTamney, P.M.; Wei, C.J.; Kanekiyo, M.; Kong, W.P.; Gallagher, J.R.; Wang, L.; Zhang, Y.; Joyce, M.G.; et al. Hemagglutinin-stem nanoparticles generate heterosubtypic influenza protection. *Nat. Med.* **2015**, *21*, 1065–1070, doi:10.1038/nm.3927.

72. Broecker, F.; Liu, S.T.H.; Suntronwong, N.; Sun, W.; Bailey, M.J.; Nachbagauer, R.; Krammer, F.; Palese, P. A mosaic hemagglutinin-based influenza virus vaccine candidate protects mice from challenge with divergent H3N2 strains. *NPJ Vaccines* **2019**, *4*, 1–9, doi:10.1038/s41541-019-0126-4.

73. Sun, W.; Kirkpatrick, E.; Ermler, M.; Nachbagauer, R.; Broecker, F.; Krammer, F.; Palese, P. Development of Influenza B Universal Vaccine Candidates Using the “Mosaic”

Hemagglutinin Approach. *J. Virol.* **2019**, *93*, e00333-19, doi:10.1128/JVI.00333-19.

74. Corder, B.N.; Bullard, B.L.; DeBeauchamp, J.L.; Ilyushina, N.A.; Webby, R.J.; Weaver, E.A. Influenza H1 Mosaic Hemagglutinin Vaccine Induces Broad Immunity and Protection in Mice. *Vaccines* **2019**, *7*, 195, doi:10.3390/vaccines7040195.

75. Barouch, D.H.; O'Brien, K.L.; Simmons, N.L.; King, S.L.; Abbink, P.; Maxfield, L.F.; Sun, Y.H.; La Porte, A.; Riggs, A.M.; Lynch, D.M.; et al. Mosaic HIV-1 vaccines expand the breadth and depth of cellular immune responses in rhesus monkeys. *Nat. Med.* **2010**, *16*, 319–323, doi:10.1038/nm.2089.

76. Kamlangdee, A.; Kingstad-Bakke, B.; Osorio, J.E. Mosaic H5 Hemagglutinin Provides Broad Humoral and Cellular Immune Responses against Influenza Viruses. *J. Virol.* **2016**, *90*, 6771–6783, doi:10.1128/JVI.00730-16.

77. Kamlangdee, A.; Kingstad-Bakke, B.; Anderson, T.K.; Goldberg, T.L.; Osorio, J.E. Broad Protection against Avian Influenza Virus by Using a Modified Vaccinia Ankara Virus Expressing a Mosaic Hemagglutinin Gene. *J. Virol.* **2014**, *88*, 13300–13309, doi:10.1128/JVI.01532-14.

78. Vajo, Z.; Balaton, G.; Vajo, P.; Kalabay, L.; Erdman, A.; Torzsa, P. Dose sparing and the lack of a dose–response relationship with an influenza vaccine in adult and elderly patients – a randomized, double-blind clinical trial. *Br. J. Clin. Pharmacol.* **2017**, *83*, 1912–1920, doi:10.1111/bcp.13289.

79. Tregoning, J.S.; Russell, R.F.; Kinnear, E. Adjuvanted influenza vaccines. *Hum. Vaccines Immunother.* **2018**, *14*, 550–564, doi:10.1080/21645515.2017.1415684.

80. Del Giudice, G.; Rappuoli, R.; Didierlaurent, A.M. Correlates of adjuvanticity: A review on adjuvants in licensed vaccines. *Semin. Immunol.* **2018**, *39*, 14–21,

doi:10.1016/j.smim.2018.05.001.

81. Centers for Disease Control and Prevention. Adjuvants Available online: https://www.cdc.gov/vaccinesafety/concerns/adjuvants.html (accessed on Feb 23, 2020).

82. Knudsen, N.P.H.; Olsen, A.; Buonsanti, C.; Follmann, F.; Zhang, Y.; Coler, R.N.; Fox, C.B.; Meinke, A.; Dóro, U.; Casini, D.; et al. Different human vaccine adjuvants promote distinct antigen-independent immunological signatures tailored to different pathogens. *Sci. Rep.* **2016**, *6*, 1–13, doi:10.1038/srep19570.

83. Bungener, L.; Geeraedts, F.; ter Veer, W.; Medema, J.; Wilschut, J.; Huckriede, A. Alum boosts TH2-type antibody responses to whole-inactivated virus influenza vaccine in mice but does not confer superior protection. *Vaccine* **2008**, *26*, 2350–2359, doi:10.1016/j.vaccine.2008.02.063.

84. Galli, G.; Hancock, K.; Hoschler, K.; DeVos, J.; Praus, M.; Bardelli, M.; Malzone, C.; Castellino, F.; Gentile, C.; McNally, T.; et al. Fast rise of broadly cross-reactive antibodies after boosting long-lived human memory B cells primed by an MF59 adjuvanted prepandemic vaccine. *Proc. Natl. Acad. Sci. U. S. A.* **2009**, *106*, 7962–7967, doi:10.1073/pnas.0903181106.

85. O'Hagan, D.T.; Rappuoli, R.; De Gregorio, E.; Tsai, T.; Del Giudice, G. MF59 adjuvant: The best insurance against influenza strain diversity. *Expert Rev. Vaccines* **2011**, *10*, 447–462, doi:10.1586/erv.11.23.

86. Ou, H.; Yao, H.; Yao, W.; Wu, N.; Wu, X.; Han, C.; Cheng, L.; Chen, K.; Chen, H.; Li, L. Analysis of the immunogenicity and bioactivities of a split influenza A/H7N9 vaccine mixed with MF59 adjuvant in BALB/c mice. *Vaccine* **2016**, *34*, 2362–2370, doi:10.1016/j.vaccine.2016.03.037.

87. Patel, S.S.; Bizjajeva, S.; Heijnen, E.; Oberye, J. MF59-adjuvanted seasonal trivalent inactivated influenza vaccine: Safety and immunogenicity in young children at risk of influenza complications. *Int. J. Infect. Dis.* **2019**, *85*, S18–S25, doi:10.1016/j.ijid.2019.04.023.

88. Vesikari, T.; Groth, N.; Karvonen, A.; Borkowski, A.; Pellegrini, M. MF59®-adjuvanted influenza vaccine (FLUAD®) in children: Safety and immunogenicity following a second year seasonal vaccination. *Vaccine* **2009**, *27*, 6291–6295, doi:10.1016/j.vaccine.2009.02.004.

89. Hatz, C.; Von Sonnenburg, F.; Casula, D.; Lattanzi, M.; Leroux-Roels, G. A randomized clinical trial to identify the optimal antigen and MF59 ® adjuvant dose of a monovalent A/H1N1 pandemic influenza vaccine in healthy adult and elderly subjects. *Vaccine* **2012**, *30*, 3470–3477, doi:10.1016/j.vaccine.2012.03.017.

90. Khurana, S.; Verma, N.; Yewdell, J.W.; Hilbert, A.K.; Castellino, F.; Lattanzi, M.; Del Giudice, G.; Rappuoli, R.; Golding, H. MF59 adjuvant enhances diversity and affinity of antibody-mediated immune response to pandemic influenza vaccines. *Sci. Transl. Med.* **2011**, *3*, 1–10, doi:10.1126/scitranslmed.3002336.

91. Boudreau, C.M.; Yu, W.H.; Suscovich, T.J.; Talbot, H.K.; Edwards, K.M.; Alter, G. Selective induction of antibody effector functional responses using MF59-adjuvanted vaccination. *J. Clin. Invest.* **2020**, *130*, 662–672, doi:10.1172/JCI129520.

92. Garçon, N.; Vaughn, D.W.; Didierlaurent, A.M. Development and evaluation of AS03, an Adjuvant System containing α-tocopherol and squalene in an oil-in-water emulsion. *Expert Rev. Vaccines* **2012**, *11*, 349–366, doi:10.1586/erv.11.192.

93. Baras, B.; Stittelaar, K.J.; Simon, J.H.; Thoolen, R.J.M.M.; Mossman, S.P.; Pistoor,

F.H.M.; van Amerongen, G.; Wettendorff, M.A.; Hanon, E.; Osterhaus, A.D.M.E. Cross-protection against lethal H5N1 challenge ferrets with an adjuvanted pandemic influenza vaccine. *PLoS One* **2008**, *3*, 5–8, doi:10.1371/journal.pone.0001401.

94. Galson, J.D.; Trück, J.; Kelly, D.F.; Van Der Most, R. Investigating the effect of AS03 adjuvant on the plasma cell repertoire following pH1N1 influenza vaccination. *Sci. Rep.* **2016**, *6*, 1–11, doi:10.1038/srep37229.

95. Friel, D.; Co, M.; Ollinger, T.; Salaun, B.; Schuind, A.; Li, P.; Walravens, K.; Ennis, F.A.; Vaughn, D.W. Non-neutralizing antibody responses following A(H1N1)pdm09 influenza vaccination with or without AS03 adjuvant system. *Influenza Other Respi. Viruses* **2021**, *15*, 110–120, doi:10.1111/irv.12780.

96. Duthie, M.S.; Windish, H.P.; Fox, C.B.; Reed, S.G. Use of defined TLR ligands as adjuvants within human vaccines. *Immunol. Rev.* **2011**, *239*, 178–196, doi:10.1111/j.1600-065X.2010.00978.x.

97. Van Hoeven, N.; Fox, C.B.; Granger, B.; Evers, T.; Joshi, S.W.; Nana, G.I.; Evans, S.C.; Lin, S.; Liang, H.; Liang, L.; et al. A Formulated TLR7/8 agonist is a flexible, highly potent and effective adjuvant for pandemic influenza vaccines. *Sci. Rep.* **2017**, *7*, 1–15, doi:10.1038/srep46426.

98. Taylor, D.N.; Treanor, J.J.; Sheldon, E.A.; Johnson, C.; Umlauf, S.; Song, L.; Kavita, U.; Liu, G.; Tussey, L.; Ozer, K.; et al. Development of VAX128, a recombinant hemagglutinin (HA) influenza-flagellin fusion vaccine with improved safety and immune response. *Vaccine* **2012**, *30*, 5761–5769, doi:10.1016/j.vaccine.2012.06.086.

99. Rudicell, R.S.; Garinot, M.; Kanekiyo, M.; Kamp, H.D.; Swanson, K.; Chou, T.; Dai, S.; Bedel, O.; Simard, D.; Gillespie, R.A.; et al. Comparison of adjuvants to optimize

influenza neutralizing antibody responses. *Vaccine* **2019**, *37*, 6208–6220, doi:10.1016/j.vaccine.2019.08.030.

100. Kuo, T.Y.; Lin, M.Y.; Coffman, R.L.; Campbell, J.D.; Traquina, P.; Lin, Y.J.; Liu, L.T.C.; Cheng, J.; Wu, Y.C.; Wu, C.C.; et al. Development of CpG-adjuvanted stable prefusion SARS-CoV-2 spike antigen as a subunit vaccine against COVID-19. *bioRxiv* **2020**, 1–11, doi:10.1101/2020.08.11.245704.

101. Gordon, D.L.; Sajkov, D.; Woodman, R.J.; Honda-Okubo, Y.; Cox, M.M.J.; Heinzel, S.; Petrovsky, N. Randomized clinical trial of immunogenicity and safety of a recombinant H1N1/2009 pandemic influenza vaccine containing Advax™ polysaccharide adjuvant. *Vaccine* **2012**, *30*, 5407–5416, doi:10.1016/j.vaccine.2012.06.009.

102. Layton, R.C.; Petrovsky, N.; Gigliotti, A.P.; Pollock, Z.; Knight, J.; Donart, N.; Pyles, J.; Harrod, K.S.; Gao, P.; Koster, F. Delta inulin polysaccharide adjuvant enhances the ability of split-virion H5N1 vaccine to protect against lethal challenge in ferrets. *Vaccine* **2011**, *29*, 6242–6251, doi:10.1016/j.vaccine.2011.06.078.

103. Tomar, J.; Patil, H.P.; Bracho, G.; Tonnis, W.F.; Frijlink, H.W.; Petrovsky, N.; Vanbever, R.; Huckriede, A.; Hinrichs, W.L.J. Advax augments B and T cell responses upon influenza vaccination via the respiratory tract and enables complete protection of mice against lethal influenza virus challenge. *J. Control. Release* **2018**, *288*, 199–211, doi:10.1016/j.jconrel.2018.09.006.

104. Honda-Okubo, Y.; Ong, C.H.; Petrovsky, N. Advax delta inulin adjuvant overcomes immune immaturity in neonatal mice thereby allowing single-dose influenza vaccine protection. *Vaccine* **2015**, *33*, 4892–4900, doi:10.1016/j.vaccine.2015.07.051.

105. Hayashi, M.; Aoshi, T.; Haseda, Y.; Kobiyama, K.; Wijaya, E.; Nakatsu, N.; Igarashi, Y.;

Standley, D.M.; Yamada, H.; Honda-Okubo, Y.; et al. Advax, a Delta Inulin Microparticle, Potentiates In-built Adjuvant Property of Co-administered Vaccines. *EBioMedicine* **2017**, *15*, 127–136, doi:10.1016/j.ebiom.2016.11.015.

106. Maraskovsky, E.; Schnurr, M.; Wilson, N.S.; Robson, N.C.; Boyle, J.; Drane, D. Development of prophylactic and therapeutic vaccines using the ISCOMATRIX adjuvant. *Immunol. Cell Biol.* **2009**, *87*, 371–376, doi:10.1038/icb.2009.21.

107. Smith, G.E.; Flyer, D.C.; Raghunandan, R.; Liu, Y.; Wei, Z.; Wu, Y.; Kpamegan, E.; Courbron, D.; Fries, L.F.; Glenn, G.M. Development of influenza H7N9 virus like particle (VLP) vaccine: Homologous A/Anhui/1/2013 (H7N9) protection and heterologous A/chicken/Jalisco/CPA1/2012 (H7N3) cross-protection in vaccinated mice challenged with H7N9 virus. *Vaccine* **2013**, *31*, 4305–4313, doi:10.1016/j.vaccine.2013.07.043.

108. Chung, K.Y.; Coyle, E.M.; Jani, D.; King, L.R.; Bhardwaj, R.; Fries, L.; Smith, G.; Glenn, G.; Golding, H.; Khurana, S. ISCOMATRIX™ adjuvant promotes epitope spreading and antibody affinity maturation of influenza A H7N9 virus like particle vaccine that correlate with virus neutralization in humans. *Vaccine* **2015**, *33*, 3953–3962, doi:10.1016/j.vaccine.2015.06.047.

109. Ryder, A.B.; Buonocore, L.; Vogel, L.; Nachbagauer, R.; Krammer, F.; Rose, J.K. A Viable Recombinant Rhabdovirus Lacking Its Glycoprotein Gene and Expressing Influenza Virus Hemagglutinin and Neuraminidase Is a Potent Influenza Vaccine. *J. Virol.* **2015**, *89*, 2820–2830, doi:10.1128/jvi.03246-14.

110. Piepenbrink, M.S.; Nogales, A.; Basu, M.; Fucile, C.F.; Liesveld, J.L.; Keefer, M.C.; Rosenberg, A.F.; Martinez-Sobrido, L.; Kobie, J.J. Broad and protective influenza B virus neuraminidase antibodies in humans after vaccination and their clonal persistence as

plasma cells. *MBio* **2019**, *10*, 1–17, doi:10.1128/MBIO.00066-19.

111. Job, E.R.; Ysenbaert, T.; Smet, A.; Christopoulou, I.; Strugnell, T.; Oloo, E.O.; Oomen, R.P.; Kleanthous, H.; Vogel, T.U.; Saelens, X. Broadened immunity against influenza by vaccination with computationally designed influenza virus N1 neuraminidase constructs. *npj Vaccines* **2018**, *3*, 1–11, doi:10.1038/s41541-018-0093-1.

112. Iuliano, A.D.; Roguski, K.M.; Chang, H.H.; Muscatello, D.J.; Palekar, R.; Tempia, S.; Cohen, C.; Gran, J.M.; Schanzer, D.; Cowling, B.J.; et al. Estimates of global seasonal influenza-associated respiratory mortality: a modelling study. *Lancet* **2018**, *391*, 1285–1300, doi:https://doi.org/10.1016/S0140-6736(17)33293-2.

113. Flerlage, T.; Boyd, D.F.; Meliopoulos, V.; Thomas, P.G.; Schultz-Cherry, S. Influenza virus and SARS-CoV-2: pathogenesis and host responses in the respiratory tract. *Nat. Rev. Microbiol.* **2021**, *19*, 425–441, doi:10.1038/s41579-021-00542-7.

114. Jester, B.J.; Uyeki, T.M.; Jernigan, D.B. Fifty Years of Influenza A(H3N2) Following the Pandemic of 1968. *Am. J. Public Health* **2020**, *110*, 669–676, doi:10.2105/AJPH.2019.305557.

115. LaRussa, P. Pandemic novel 2009 H1N1 influenza: what have we learned? *Semin. Respir. Crit. Care Med.* **2011**, *32*, 393–399, doi:10.1055/s-0031-1283279.

116. Webster, R.G.; Govorkova, E.A. Continuing challenges in influenza. *Ann. N. Y. Acad. Sci.* **2014**, *1323*, 115–139, doi:10.1111/nyas.12462.

117. Nagashima, K.A.; Mousa, J.J. Next-Generation Influenza HA Immunogens and Adjuvants in Pursuit of a Broadly Protective Vaccine. *Viruses* **2021**, *13*, 546, doi:10.3390/v13040546.

118. Saunders-Hastings, P.R.; Krewski, D. Reviewing the History of Pandemic Influenza:

Understanding Patterns of Emergence and Transmission. *Pathog. (Basel, Switzerland)* **2016**, *5*, 66, doi:10.3390/pathogens5040066.

119. Krause, J.C.; Tsibane, T.; Tumpey, T.M.; Huffman, C.J.; Basler, C.F.; Crowe, J.E. A Broadly Neutralizing Human Monoclonal Antibody That Recognizes a Conserved, Novel Epitope on the Globular Head of the Influenza H1N1 Virus Hemagglutinin. *J. Virol.* **2011**, *85*, 10905–10908, doi:10.1128/JVI.00700-11.

120. Sautto, G.A.; Kirchenbaum, G.A.; Abreu, R.B.; Ecker, J.W.; Pierce, S.R.; Kleanthous, H.; Ross, T.M. A Computationally Optimized Broadly Reactive Antigen Subtype–Specific Influenza Vaccine Strategy Elicits Unique Potent Broadly Neutralizing Antibodies against Hemagglutinin. *J. Immunol.* **2020**, *204*, 375–385, doi:10.4049/jimmunol.1900379.

121. Carter, D.M.; Darby, C.A.; Lefoley, B.C.; Crevar, C.J.; Alefantis, T.; Oomen, R.; Anderson, S.F.; Strugnell, T.; Cortés-Garcia, G.; Vogel, T.U.; et al. Design and Characterization of a Computationally Optimized Broadly Reactive Hemagglutinin Vaccine for H1N1 Influenza Viruses. *J. Virol.* **2016**, *90*, 4720–4734, doi:10.1128/JVI.03152-15.

122. Huang, Y.; França, M.S.; Allen, J.D.; Shi, H.; Ross, T.M. Next Generation of Computationally Optimized Broadly Reactive HA Vaccines Elicited Cross-Reactive Immune Responses and Provided Protection against H1N1 Virus Infection. *Vaccines* **2021**, *9*, 793, doi:10.3390/vaccines9070793.

123. Bar-Peled, Y.; Diaz, D.; Pena-Briseno, A.; Murray, J.; Huang, J.; Tripp, R.A.; Mousa, J.J. A Potent Neutralizing Site III-Specific Human Antibody Neutralizes Human Metapneumovirus In Vivo . *J. Virol.* **2019**, *93*, doi:10.1128/jvi.00342-19.

124. Ecker, J.W.; Kirchenbaum, G.A.; Pierce, S.R.; Skarlupka, A.L.; Abreu, R.B.; Cooper,

R.E.; Taylor-Mulneix, D.; Ross, T.M.; Sautto, G.A. High-Yield Expression and Purification of Recombinant Influenza Virus Proteins from Stably-Transfected Mammalian Cell Lines. *Vaccines* **2020**, *8*, 462, doi:10.3390/vaccines8030462.

125. Guthmiller, J.J.; Dugan, H.L.; Neu, K.E.; Lan, L.Y.; Wilson, P.C. *Human Monoclonal Antibodies*; Steinitz, M., Ed.; Methods in Molecular Biology; 2nd ed.; Springer New York: New York, NY, 2019; Vol. 1904; ISBN 978-1-4939-8957-7.

126. Brochet, X.; Lefranc, M.-P.; Giudicelli, V. IMGT/V-QUEST: the highly customized and integrated system for IG and TR standardized V-J and V-D-J sequence analysis. *Nucleic Acids Res.* **2008**, *36*, W503–W508, doi:10.1093/nar/gkn316.

127. O'Rourke, S.M.; Byrne, G.; Tatsuno, G.; Wright, M.; Yu, B.; Mesa, K.A.; Doran, R.C.; Alexander, D.; Berman, P.W. Robotic selection for the rapid development of stable CHO cell lines for HIV vaccine production. *PLoS One* **2018**, *13*, e0197656, doi:10.1371/journal.pone.0197656.

128. Voss, N.R.; Yoshioka, C.K.; Radermacher, M.; Potter, C.S.; Carragher, B. DoG Picker and TiltPicker: Software tools to facilitate particle selection in single particle electron microscopy. *J. Struct. Biol.* **2009**, *166*, 205–213, doi:10.1016/J.JSB.2009.01.004.

129. Lander, G.C.; Stagg, S.M.; Voss, N.R.; Cheng, A.; Fellmann, D.; Pulokas, J.; Yoshioka, C.; Irving, C.; Mulder, A.; Lau, P.W.; et al. Appion: An integrated, database-driven pipeline to facilitate EM image processing. *J. Struct. Biol.* **2009**, *166*, 95–102, doi:10.1016/j.jsb.2009.01.002.

130. Suloway, C.; Pulokas, J.; Fellmann, D.; Cheng, A.; Guerra, F.; Quispe, J.; Stagg, S.; Potter, C.S.; Carragher, B. Automated molecular microscopy: The new Leginon system. *J. Struct. Biol.* **2005**, *151*, 41–60, doi:10.1016/j.jsb.2005.03.010.

131. Zivanov, J.; Nakane, T.; Forsberg, B.O.; Kimanius, D.; Hagen, W.J.H.; Lindahl, E.; Scheres, S.H.W. New tools for automated high-resolution cryo-EM structure determination in RELION-3. *Elife* **2018**, *7*, 1–22, doi:10.7554/eLife.42166.

132. Punjani, A.; Rubinstein, J.L.; Fleet, D.J.; Brubaker, M.A. cryoSPARC: algorithms for rapid unsupervised cryo-EM structure determination. *Nat. Methods* **2017**, *14*, 290–296, doi:10.1038/nmeth.4169.

133. Pettersen, E.F.; Goddard, T.D.; Huang, C.C.; Couch, G.S.; Greenblatt, D.M.; Meng, E.C.; Ferrin, T.E. UCSF Chimera - A visualization system for exploratory research and analysis. *J. Comput. Chem.* **2004**, *25*, 1605–1612, doi:10.1002/jcc.20084.

134. Boudreau, C.M.; Yu, W.H.; Suscovich, T.J.; Talbot, H.K.; Edwards, K.M.; Alter, G. Selective induction of antibody effector functional responses using MF59-adjuvanted vaccination. *J. Clin. Invest.* **2020**, *130*, 662–672, doi:10.1172/JCI129520.

135. Huang, J.; Diaz, D.; Mousa, J.J. Antibody recognition of the Pneumovirus fusion protein trimer interface. *PLOS Pathog.* **2020**, *16*, e1008942, doi:10.1371/journal.ppat.1008942.

136. Guthmiller, J.J.; Han, J.; Li, L.; Freyn, A.W.; Liu, S.T.H.; Stovicek, O.; Stamper, C.T.; Dugan, H.L.; Tepora, M.E.; Utset, H.A.; et al. First exposure to the pandemic H1N1 virus induced broadly neutralizing antibodies targeting hemagglutinin head epitopes. *Sci. Transl. Med.* **2021**, *13*, doi:10.1126/scitranslmed.abg4535.

137. Benton, D.J.; Nans, A.; Calder, L.J.; Turner, J.; Neu, U.; Lin, Y.P.; Ketelaars, E.; Kallewaard, N.L.; Corti, D.; Lanzavecchia, A.; et al. Influenza hemagglutinin membrane anchor. *Proc. Natl. Acad. Sci.* **2018**, *115*, 10112 LP – 10117, doi:10.1073/pnas.1810927115.

138. Guthmiller, J.J.; Han, J.; Utset, H.A.; Li, L.; Lan, L.Y.-L.; Henry, C.; Stamper, C.T.;

McMahon, M.; O'Dell, G.; Fernández-Quintero, M.L.; et al. Broadly neutralizing antibodies target a haemagglutinin anchor epitope. *Nature* **2022**, *602*, 314–320, doi:10.1038/s41586-021-04356-8.

139. Skarlupka, A.L.; Bebin-Blackwell, A.-G.; Sumner, S.F.; Ross, T.M. Universal Influenza Virus Neuraminidase Vaccine Elicits Protective Immune Responses against Human Seasonal and Pre-pandemic Strains. *J. Virol.* **2021**, *95*, doi:10.1128/JVI.00759-21.

140. Zanobini, P.; Bonaccorsi, G.; Lorini, C.; Haag, M.; McGovern, I.; Paget, J.; Caini, S. Global patterns of seasonal influenza activity, duration of activity and virus (sub)type circulation from 2010 to 2020. *Influenza Other Respi. Viruses* **2022**, *16*, 696–706, doi:10.1111/irv.12969.

141. Hong, M.; Lee, P.S.; Hoffman, R.M.B.; Zhu, X.; Krause, J.C.; Laursen, N.S.; Yoon, S. -i.; Song, L.; Tussey, L.; Crowe, J.E.; et al. Antibody Recognition of the Pandemic H1N1 Influenza Virus Hemagglutinin Receptor Binding Site. *J. Virol.* **2013**, *87*, 12471–12480, doi:10.1128/jvi.01388-13.

142. Nagashima, K.; Dzimianski, J. V; Han, J.; Abbadi, N.; Gingerich, A.D.; Royer, F.; O'Rourke, S.; Sautto, G.A.; Ross, T.M.; Ward, A.B.; et al. The Pre-Existing Human Antibody Repertoire to Computationally Optimized Influenza H1 Hemagglutinin Vaccines. *J. Immunol.* **2022**, *209*, 5–15, doi:10.4049/jimmunol.2101171.

143. Jang, J.; Bae, S.-E. Comparative Co-Evolution Analysis Between the HA and NA Genes of Influenza A Virus. *Virol. Res. Treat.* **2018**, *9*, 1178122X1878832, doi:10.1177/1178122X18788328.

144. Monto, A.S.; Petrie, J.G.; Cross, R.T.; Johnson, E.; Liu, M.; Zhong, W.; Levine, M.; Katz, J.M.; Ohmit, S.E. Antibody to Influenza Virus Neuraminidase: An Independent Correlate

of Protection. *J. Infect. Dis.* **2015**, *212*, 1191–1199, doi:10.1093/infdis/jiv195.

145. Memoli, M.J.; Shaw, P.A.; Han, A.; Czajkowski, L.; Reed, S.; Athota, R.; Bristol, T.; Fargis, S.; Risos, K.; Powers, J.H.; et al. Evaluation of Antihemagglutinin and Antineuraminidase Antibodies as Correlates of Protection in an Influenza A/H1N1 Virus Healthy Human Challenge Model. *MBio* **2016**, *7*, doi:10.1128/mBio.00417-16.

146. Pulendran, B.; S. Arunachalam, P.; O'Hagan, D.T. Emerging concepts in the science of vaccine adjuvants. *Nat. Rev. Drug Discov.* **2021**, *20*, 454–475, doi:10.1038/s41573-021-00163-y.

147. Khurana, S.; Verma, N.; Yewdell, J.W.; Hilbert, A.K.; Castellino, F.; Lattanzi, M.; Del Giudice, G.; Rappuoli, R.; Golding, H. MF59 Adjuvant Enhances Diversity and Affinity of Antibody-Mediated Immune Response to Pandemic Influenza Vaccines. *Sci. Transl. Med.* **2011**, *3*, 85ra48-85ra48, doi:10.1126/scitranslmed.3002336.

148. He, W.; Mullarkey, C.E.; Duty, J.A.; Moran, T.M.; Palese, P.; Miller, M.S. Broadly Neutralizing Anti-Influenza Virus Antibodies: Enhancement of Neutralizing Potency in Polyclonal Mixtures and IgA Backbones. *J. Virol.* **2015**, *89*, 3610–3618, doi:10.1128/JVI.03099-14.

149. Committee for Medicinal Products for Human Use *Guideline on Influenza Vaccines – Non-clinical and Clinical Module*; 2016; Vol. 44;.

150. Sautto, G.A.; Kirchenbaum, G.A.; Ecker, J.W.; Bebin-Blackwell, A.-G.; Pierce, S.R.; Ross, T.M. Elicitation of Broadly Protective Antibodies following Infection with Influenza Viruses Expressing H1N1 Computationally Optimized Broadly Reactive Hemagglutinin Antigens. *ImmunoHorizons* **2018**, *2*, 226–237, doi:10.4049/immunohorizons.1800044.

151. Creytens, S.; Pascha, M.N.; Ballegeer, M.; Saelens, X.; de Haan, C.A.M. Influenza Neuraminidase Characteristics and Potential as a Vaccine Target. *Front. Immunol.* **2021**, *12*, 1–19, doi:10.3389/fimmu.2021.786617.

152. Shi, S.; Zhu, H.; Xia, X.; Liang, Z.; Ma, X.; Sun, B. Vaccine adjuvants: Understanding the structure and mechanism of adjuvanticity. *Vaccine* **2019**, *37*, 3167–3178, doi:10.1016/j.vaccine.2019.04.055.

153. Ellebedy, A.H.; Nachbagauer, R.; Jackson, K.J.L.; Dai, Y.-N.; Han, J.; Alsoussi, W.B.; Davis, C.W.; Stadlbauer, D.; Rouphael, N.; Chromikova, V.; et al. Adjuvanted H5N1 influenza vaccine enhances both cross-reactive memory B cell and strain-specific naive B cell responses in humans. *Proc. Natl. Acad. Sci.* **2020**, *117*, 17957–17964, doi:10.1073/pnas.1906613117.

154. Hong, M.; Lee, P.S.; Hoffman, R.M.B.; Zhu, X.; Krause, J.C.; Laursen, N.S.; Yoon, S.; Song, L.; Tussey, L.; Crowe, J.E.; et al. Antibody Recognition of the Pandemic H1N1 Influenza Virus Hemagglutinin Receptor Binding Site. *J. Virol.* **2013**, *87*, 12471–12480, doi:10.1128/JVI.01388-13.

155. Nagashima, K.; Dzimianski, J. V.; Han, J.; Abbadi, N.; Gingerich, A.D.; Royer, F.; O'Rourke, S.; Sautto, G.A.; Ross, T.M.; Ward, A.B.; et al. The Pre-Existing Human Antibody Repertoire to Computationally Optimized Influenza H1 Hemagglutinin Vaccines. *J. Immunol.* **2022**, *209*, 5–15, doi:10.4049/jimmunol.2101171.

156. Kanekiyo, M.; Wei, C.J.; Yassine, H.M.; McTamney, P.M.; Boyington, J.C.; Whittle, J.R.R.; Rao, S.S.; Kong, W.P.; Wang, L.; Nabel, G.J. Self-assembling influenza nanoparticle vaccines elicit broadly neutralizing H1N1 antibodies. *Nature* **2013**, *499*, 102–106, doi:10.1038/nature12202.

157. Houser, K. V.; Chen, G.L.; Carter, C.; Crank, M.C.; Nguyen, T.A.; Burgos Florez, M.C.; Berkowitz, N.M.; Mendoza, F.; Hendel, C.S.; Gordon, I.J.; et al. Safety and immunogenicity of a ferritin nanoparticle H2 influenza vaccine in healthy adults: a phase 1 trial. *Nat. Med.* **2022**, *28*, 383–391, doi:10.1038/s41591-021-01660-8.

158. Cohen, A.A.; Yang, Z.; Gnanapragasam, P.N.P.; Ou, S.; Dam, K.M.A.; Wang, H.; Bjorkman, P.J. Construction, characterization, and immunization of nanoparticles that display a diverse array of influenza HA trimers. *PLoS One* **2021**, *16*, 1–24, doi:10.1371/journal.pone.0247963.

159. Allen, J.D.; Ross, T.M. Bivalent H1 and H3 COBRA Recombinant Hemagglutinin Vaccines Elicit Seroprotective Antibodies against H1N1 and H3N2 Influenza Viruses from 2009 to 2019. *J. Virol.* **2022**, *96*, doi:10.1128/jvi.01652-21.

160. Nagashima, K.; Abbadi, N.; Vyas, V.; Roegner, A.; Ross, T.M.; Mousa, J.J. Adjuvant-Mediated Differences in Antibody Responses to Computationally Optimized Hemagglutinin and Neuraminidase Vaccines. *Viruses* **2023**, *15*, 347, doi:10.3390/v15020347.

161. Kraft, J.C.; Pham, M.N.; Shehata, L.; Brinkkemper, M.; Boyoglu-Barnum, S.; Sprouse, K.R.; Walls, A.C.; Cheng, S.; Murphy, M.; Pettie, D.; et al. Antigen- and scaffold-specific antibody responses to protein nanoparticle immunogens. *Cell Reports Med.* **2022**, *3*, 100780, doi:10.1016/j.xcrm.2022.100780.

162. Abbadi, N.; Nagashima, K.; Pena-Briseno, A.; Ross, T.M.; Mousa, J.J. Differential Recognition of Computationally Optimized H3 Hemagglutinin Influenza Vaccine Candidates by Human Antibodies. *J. Virol.* **2022**, 2022.02.24.481830, doi:10.1128/jvi.00896-22.

163. Allen, J.D.; Owino, S.O.; Carter, D.M.; Crevar, C.J.; Reese, V.A.; Fox, C.B.; Coler, R.N.; Reed, S.G.; Baldwin, S.L.; Ross, T.M. Broadened immunity and protective responses with emulsion-adjuvanted H5 COBRA-VLP vaccines. *Vaccine* **2017**, *35*, 5209–5216, doi:10.1016/j.vaccine.2017.07.107.

164. Nagashima, K.; Dzimianski, J. V; Han, J.; Abbadi, N.; Gingerich, A.D.; Royer, F.; O'Rourke, S.; Sautto, G.A.; Ross, T.M.; Ward, A.B.; et al. The pre-existing human antibody repertoire to computationally optimized influenza H1 hemagglutinin vaccines. *bioRxiv* **2021**, 2021.10.25.465669, doi:https://doi.org/10.1101/2021.10.25.465669.

165. Abbadi, N.; Nagashima, K.; Pena-Briseno, A.; Ross, T.M.; Mousa, J.J. Differential recognition of computationally optimized H3 hemagglutinin influenza vaccine candidates by human antibodies. **2022**, doi:https://doi.org/10.1101/2022.02.24.481830.

166. Mena, I.; Nelson, M.I.; Quezada-monroy, F.; Dutta, J.; Lara-puente, J.H.; Castro-peralta, F.; Lozano-dubernard, B.; Cunha, L.F.; Trova, S.; Rambaut, A. Origins of the 2009 H1N1 influenza pandemic in swine in Mexico. **2016**, 1–21, doi:10.7554/eLife.16777.

167. Pica, N.; Hai, R.; Krammer, F.; Wang, T.T.; Maamary, J.; Eggink, D.; Tan, G.S.; Krause, J.C.; Moran, T.; Stein, C.R.; et al. Hemagglutinin stalk antibodies elicited by the 2009 pandemic influenza virus as a mechanism for the extinction of seasonal H1N1 viruses. *Proc. Natl. Acad. Sci. U. S. A.* **2012**, *109*, 2573–2578, doi:10.1073/pnas.1200039109.

168. Carter, D.M.; Darby, C.A.; Lefoley, B.C.; Crevar, C.J.; Alefantis, T.; Oomen, R.; Anderson, S.F.; Strugnell, T.; Cortés-Garcia, G.; Vogel, T.U.; et al. Design and Characterization of a Computationally Optimized Broadly Reactive Hemagglutinin Vaccine for H1N1 Influenza Viruses. *J. Virol.* **2016**, *90*, 4720–4734, doi:10.1128/JVI.03152-15.

169. Gupta, R.; Brunak, S. Prediction of glycosylation across the human proteome and the correlation to protein function. In Proceedings of the Biocomputing 2002; WORLD SCIENTIFIC, 2001; Vol. 7, pp. 310–322.

170. Pulit-Penaloza, J.A.; Jones, J.; Sun, X.; Jang, Y.; Thor, S.; Belser, J.A.; Zanders, N.; Creager, H.M.; Ridenour, C.; Wang, L.; et al. Antigenically Diverse Swine Origin H1N1 Variant Influenza Viruses Exhibit Differential Ferret Pathogenesis and Transmission Phenotypes. *J. Virol.* **2018**, *92*, doi:10.1128/jvi.00095-18.

171. Dzimianski, J. V; Han, J.; Sautto, G.A.; O'Rourke, S.M.; Cruz, J.M.; Pierce, S.R.; Ecker, J.W.; Carlock, M.A.; Nagashima, K.A.; Mousa, J.J.; et al. Structural insights into the broad protection against H1 influenza viruses by a computationally optimized hemagglutinin vaccine. *Commun. Biol.* **2023**, *6*, 454, doi:10.1038/s42003-023-04793-3.

172. Sautto, G.A.; Kirchenbaum, G.A.; Ecker, J.W.; Bebin-Blackwell, A.-G.; Pierce, S.R.; Ross, T.M. Elicitation of Broadly Protective Antibodies following Infection with Influenza Viruses Expressing H1N1 Computationally Optimized Broadly Reactive Hemagglutinin Antigens. *ImmunoHorizons* **2018**, *2*, 226–237, doi:10.4049/immunohorizons.1800044.

173. Ecker, J.W.; Kirchenbaum, G.A.; Pierce, S.R.; Skarlupka, A.L.; Abreu, R.B.; Ethan Cooper, R.; Taylor-Mulneix, D.; Ross, T.M.; Sautto, G.A. High-yield expression and purification of recombinant influenza virus proteins from stably-transfected mammalian cell lines. *Vaccines* **2020**, *8*, 1–20, doi:10.3390/vaccines8030462.

174. Whittle, J.R.R.; Wheatley, A.K.; Wu, L.; Lingwood, D.; Kanekiyo, M.; Ma, S.S.; Narpala, S.R.; Yassine, H.M.; Frank, G.M.; Yewdell, J.W.; et al. Flow Cytometry Reveals that H5N1 Vaccination Elicits Cross-Reactive Stem-Directed Antibodies from Multiple Ig

Heavy-Chain Lineages. *J. Virol.* **2014**, *88*, 4047–4057, doi:10.1128/jvi.03422-13.

175. Kabsch, W. XDS. *Acta Crystallogr. D. Biol. Crystallogr.* **2010**, *66*, 125–32, doi:10.1107/S0907444909047337.

176. Kabsch, W. Integration, scaling, space-group assignment and post-refinement. *Acta Crystallogr. D. Biol. Crystallogr.* **2010**, *66*, 133–44, doi:10.1107/S0907444909047374.

177. Evans, P.R.; Murshudov, G.N. How good are my data and what is the resolution? *Acta Crystallogr. D. Biol. Crystallogr.* **2013**, *69*, 1204–14, doi:10.1107/S0907444913000061.

178. Winn, M.D.; Ballard, C.C.; Cowtan, K.D.; Dodson, E.J.; Emsley, P.; Evans, P.R.; Keegan, R.M.; Krissinel, E.B.; Leslie, A.G.W.; McCoy, A.; et al. Overview of the CCP4 suite and current developments. *Acta Crystallogr. Sect. D Biol. Crystallogr.* **2011**, *67*, 235–242, doi:10.1107/S0907444910045749.

179. McCoy, A.J.; Grosse-Kunstleve, R.W.; Adams, P.D.; Winn, M.D.; Storoni, L.C.; Read, R.J. Phaser crystallographic software. *J. Appl. Crystallogr.* **2007**, *40*, 658–674, doi:10.1107/S0021889807021206.

180. Waterhouse, A.; Bertoni, M.; Bienert, S.; Studer, G.; Tauriello, G.; Gumienny, R.; Heer, F.T.; de Beer, T.A.P.; Rempfer, C.; Bordoli, L.; et al. SWISS-MODEL: homology modelling of protein structures and complexes. *Nucleic Acids Res.* **2018**, *46*, W296–W303, doi:10.1093/nar/gky427.

181. Afonine, P. V; Grosse-Kunstleve, R.W.; Echols, N.; Headd, J.J.; Moriarty, N.W.; Mustyakimov, M.; Terwilliger, T.C.; Urzhumtsev, A.; Zwart, P.H.; Adams, P.D. Towards automated crystallographic structure refinement with phenix.refine. *Acta Crystallogr. D. Biol. Crystallogr.* **2012**, *68*, 352–67, doi:10.1107/S0907444912001308.

182. Emsley, P.; Lohkamp, B.; Scott, W.G.; Cowtan, K. Features and development of Coot.

Acta Crystallogr. Sect. D Biol. Crystallogr. **2010**, *66*, 486–501, doi:10.1107/S0907444910007493.

183. Williams, C.J.; Headd, J.J.; Moriarty, N.W.; Prisant, M.G.; Videau, L.L.; Deis, L.N.; Verma, V.; Keedy, D.A.; Hintze, B.J.; Chen, V.B.; et al. MolProbity: More and better reference data for improved all-atom structure validation. *Protein Sci.* **2018**, *27*, 293–315, doi:10.1002/pro.3330.

184. Agirre, J.; Iglesias-Fernández, J.; Rovira, C.; Davies, G.J.; Wilson, K.S.; Cowtan, K.D. Privateer: software for the conformational validation of carbohydrate structures. *Nat. Struct. Mol. Biol.* **2015**, *22*, 833–4, doi:10.1038/nsmb.3115.

185. Nuñez, I.A.; Carlock, M.A.; Allen, J.D.; Owino, S.O.; Moehling, K.K.; Nowalk, P.; Susick, M.; Diagle, K.; Sweeney, K.; Mundle, S.; et al. Impact of age and pre-existing influenza immune responses in humans receiving split inactivated influenza vaccine on the induction of the breadth of antibodies to influenza A strains. *PLoS One* **2017**, *12*, e0185666, doi:10.1371/journal.pone.0185666.

186. Forgacs, D.; Abreu, R.B.; Sautto, G.A.; Kirchenbaum, G.A.; Drabek, E.; Williamson, K.S.; Kim, D.; Emerling, D.E.; Ross, T.M. Convergent antibody evolution and clonotype expansion following influenza virus vaccination. *PLoS One* **2021**, *16*, e0247253, doi:10.1371/journal.pone.0247253.

187. Gadush, M. V.; Sautto, G.A.; Chandrasekaran, H.; Bensussan, A.; Ross, T.M.; Ippolito, G.C.; Person, M.D. Template-Assisted De Novo Sequencing of SARS-CoV-2 and Influenza Monoclonal Antibodies by Mass Spectrometry. *J. Proteome Res.* **2022**, *21*, 1616–1627, doi:10.1021/acs.jproteome.1c00913.

188. Centers for Disease Control and Prevention Disease Burden of Flu Available online:

https://www.cdc.gov/flu/about/burden/index.html (accessed on Jun 14, 2023).

189. Koutsakos, M.; Wheatley, A.K.; Laurie, K.; Kent, S.J.; Rockman, S. Influenza lineage extinction during the COVID-19 pandemic? *Nat. Rev. Microbiol.* **2021**, *19*, 741–742, doi:10.1038/s41579-021-00642-4.

190. Ekiert, D.C.; Kashyap, A.K.; Steel, J.; Rubrum, A.; Bhabha, G.; Khayat, R.; Lee, J.H.; Dillon, M.A.; O'Neil, R.E.; Faynboym, A.M.; et al. Cross-neutralization of influenza A viruses mediated by a single antibody loop. *Nature* **2012**, *489*, 526–532, doi:10.1038/nature11414.

191. Dreyfus, C.; Laursen, N.S.; Kwaks, T.; Zuijdgeest, D.; Khayat, R.; Ekiert, D.C.; Lee, J.H.; Metlagel, Z.; Bujny, M. V.; Jongeneelen, M.; et al. Highly conserved protective epitopes on influenza B viruses. *Science (80-.).* **2012**, *337*, 1343–1348, doi:10.1126/science.1222908.

192. Ekiert, D.C.; Friesen, R.H.E.; Bhabha, G.; Kwaks, T.; Jongeneelen, M.; Yu, W.; Ophorst, C.; Cox, F.; Korse, H.J.W.M.; Brandenburg, B.; et al. A Highly Conserved Neutralizing Epitope on Group 2 Influenza A Viruses. *Science (80-.).* **2011**, *333*, 843–850, doi:10.1126/science.1204839.

193. Friesen, R.H.E.; Lee, P.S.; Stoop, E.J.M.; Hoffman, R.M.B.; Ekiert, D.C.; Bhabha, G.; Yu, W.; Juraszek, J.; Koudstaal, W.; Jongeneelen, M.; et al. A common solution to group 2 influenza virus neutralization. *Proc. Natl. Acad. Sci. U. S. A.* **2014**, *111*, 445–450, doi:10.1073/pnas.1319058110.

194. Lee, P.S.; Ohshima, N.; Stanfield, R.L.; Yu, W.; Iba, Y.; Okuno, Y.; Kurosawa, Y.; Wilson, I.A. Receptor mimicry by antibody F045-092 facilitates universal binding to the H3 subtype of influenza virus. *Nat. Commun.* **2014**, *5*, doi:10.1038/ncomms4614.

195. Ekiert, D.C.; Bhabha, G.; Elsliger, M.-A.; Friesen, R.H.E.; Jongeneelen, M.; Throsby, M.; Goudsmit, J.; Wilson, I.A. Antibody Recognition of a Highly Conserved Influenza Virus Epitope. *Science (80-.).* **2009**, *324*, 246–251, doi:10.1126/science.1171491.